Determination of the precision and reliability parameters of terrestrial laser scanners

by creating a practical experiment set-up

Graduation research

Geomatics

Master thesis

November 2006

Jane Margaret van Ree
E-mail: janevanree81@hotmail.com

Delft Institute of Earth Observation and Space Systems
Faculty of Aerospace engineering
Delft University of Technology

Graduation research by order of:
Fugro–Inpark B.V.
Geo-information Services,
In Breda, the Netherlands

Graduation professor:	prof. dr. ir. P.J.G. Teunissen
Supervisor TU Delft:	dr. R.C. Lindenbergh
Supervisor TU Delft:	A. Bucksch MSc
Supervisor Fugro–Inpark:	ir. E.P. Claassen

Preface

This thesis is the result of my graduation research and is entitled '*Determination of precision and reliability parameters of different terrestrial laser scanners; by creating a practical experiment set-up*'. The thesis is the final stage of my Master studies in Geomatics at Delft University of Technology, the Netherlands. The research is done by order of Fugro-Inpark B.V. (FINP), Geo-information Services.

This report contains nine chapters. The first chapter is an introduction to the research. Chapter two gives background information about laser scanning and introduces the two laser scanners to be tested: the IMAGER 5003 and the FARO LS 880. The error sources known that have an influence on measurements obtained by means of terrestrial laser scanners are discussed in chapter three as well as existing experiment set-ups. Chapter four discusses the methods of analyses implemented and relevant background theories.

The following four chapters each discuss one experiment created by first giving a motivation followed by a description of the experiment set-up, the expected results and results really obtained. First the scan angle experiment will be discussed in chapter five. Chapter six describes the colour experiment, chapter seven the reflectivity experiment and chapter eight discusses the range experiment. This thesis ends with the conclusions and recommendations for further research in chapter nine.

The first four chapters of this thesis contain general information on different subjects relevant for the research. People who are interested in the experiments created, the measurements and the results obtained are advised to read from chapter 5 onwards as these chapters contain the full descriptions of the experiments and their results.

As I mentioned before, this research is done by order of FINP. They gave me the opportunity to do something new in the relatively young field of laser scanning. I would like to thank Ron Rozema, FINP manager of Geo-Information Services Breda, to make my master research possible. Furthermore I would like to thank my supervisor on behalf of FINP, Erik Claassen. Thanks for being open to discussion and willing to help me whenever I had questions.

During this research I needed to test different scanners and these scanners cannot always be arranged easily. Therefore I would like to thank Eric Bergholz of FARO EUROPE for coming to the Netherlands on a free day to scan my test set-up and making it possible to visit the FARO factory in Germany.

I would also like to thank the Dutch forensic institute in the person of Paul Lucas for allowing me to use their scanner and taking me to the Zoller + Fröhlich factory in Wangen, Germany.

For the total station measurements that were done as ground truth data, I needed some help. Therefore, I want to thank Jasper Hellemons, Steven Sablerolle and Niels van der Zon for holding the prism and helping me carry all the heavy equipment.

My supervisors on behalf of Delft University of Technology were Professor Peter Teunissen, Roderik Lindenbergh and Alexander Bucksch. I would like to thank Professor Teunissen for being very interested in my research and giving me some valuable tips during my research. Roderik and Alexander, thank you very much for being patient with me and for being very enthusiastic about my research and my results. Your enthusiastic approach made the research a pleasure to work on.

Last, but certainly not least, I would like to thank my parents for making it possible for me to study and supporting me all the way through my studies. Mum and Dad, you are great!

Delft, November 2006
Jane van Ree

Summary

Fugro-Inpark B.V. (FINP) currently uses terrestrial laser scanning for surveying purposes. After emitting a laser signal in a defined direction, laser scanning measures the distance between scanner and object in order to create a 3D scan of the surroundings. At the moment FINP is in possession of a pulse laser scanner, the *Leica HDS 2500* that measures the distance by means of the time of flight principle.

But as laser scanning is a relatively new way of collecting data, it is going through a big development at the moment. One of the main developments concerns the method of distance determination. FINP uses the scans obtained mainly for modelling industrial plants and for architectural purposes. In these situations the scanned objects are relatively close to the scanner. Therefore the most profitable thing for FINP to do is to examine the possibilities of a laser scanner that uses the phase shift method to determine distances, because these scanners scan with high accuracies on short distances and have a relatively short scanning time.

The wish of FINP to get an insight into the reliability and precision features of two different phase shift laser scanners resulted in the research described in this thesis, which is entitled:

Determination of the precision and reliability parameters of different terrestrial laser scanners by creating a practical experiment set-up

The two phase shift scanners that are examined are the IMAGER 5003 of Zoller und Fröhlich (also known as the HDS 4500 by Leica Geosystems) and the FARO LS 880.

First an inventory of the features of the two selected phase shift laser scanners is made, followed by an investigation into the error sources known that influence measurements done with terrestrial laser scanners in general. Because the reliability and precision parameters will be examined by creating a practical experiment set-up, test areas that exist already are examined as well.

This information is used to create a practical set-up in which different experiments are implemented. The purpose of each experiment is to test one or two features that may influence the performance of the laser scanners and to eliminate other effects. The following four experiments are created and done:

1. A scan angle experiment, in which the influence of an increasing scan angle is examined.
2. A colour experiment, in which the influence of different colours and their absorption characteristics are examined.
3. A reflectivity experiment, in which the influence of different reflectivity characteristics is examined.
4. A range experiment, in which the influence of an increasing scan range is determined.

After executing these four experiments the results are analysed, in order to gain an insight into the precision and the reliability parameters of the scans obtained with the two laser scanners. The results of these analyses are used to compute the performances of the two laser scanners in general and to compare them with each other. This will eventually result in an advice to FINP on which scanner is the better for them to use in their areas of interest. For the data processing the available laser scanner software and the calculation program Matlab are used.

Before analyses are carried out, the interiors of the objects of interest are selected from the scans obtained in order to reduce the calculation time and to eliminate edge effects. In all experiments the objects of interest are planar and therefore it is easy to select the interior of the objects automatically.

After the interior selection, the object is represented by a planar model that is estimated through the scan points by performing a Least Square (LSQ) adjustment. This model is used in order to determine the performances of the laser scanners with respect to the features that are examined in the experiments. The analysis of the results of each of the four experiments is based on the same principles, i.e. by determining the following four parameters:

1. *The number of points scanned*; the real number of points measured per [cm^2] is compared to the expected number of points per [cm^2] based on the specifications. This is done to gain an insight into the truthfulness of the specifications.
2. *The mean intensity values;* this analysis is done to gain an insight into the influence of the feature of interest on the intensity values measured. If the intensity values of two different scanners have to be compared a histogram equalization is used to make the results comparable.
3. *The precision test;* subtracting the scan points from the LSQ-model results in the residuals. These residuals determine whether the model fits the scan points closely or not. The standard deviation of the residuals is used to express the precision.
4. *The reliability test;* the reliability of the obtained results can be researched by comparing the model features with the true features. The difference between the true values and the measured values determine the reliability of the scan and therefore the laser scanner.

The analyses have shown that there is not a large difference between the two scanners with respect to the number of points scanned and the intensity values measured. The performances of the IMAGER 5003 are slightly better with respect to the number of points scanned.

A few exceptions to this statement are achieved on extreme objects like a black velvet patch with a remission of only 0.5% and a blue patch. The FARO LS 880 loses almost no points on these difficult objects, whereas scans obtained by the IMAGER 5003 show a lot of gaps on these objects.

However, there is a big difference when it concerns the precision parameters of both scanners. The precision of the IMAGER 5003 is in almost all situations two or more times better then the precision of the FARO LS 880. Further research showed that the IMAGER 5003 filters the data before an output file is created whereas the FARO LS 880 software allows manual filtering and does not filter the data beforehand. The difference in the filtering approach explains the difference in the precision. However, this knowledge was gained after all the analyses were done which means that the results of the two scanners are not really comparable.

In general it can be said that the precision of a green object obtained with the two scanners is relatively low in comparison with other colours. This is as expected because green is the complementary colour of red so the green patch absorbs most of the incoming laser light because this is close to red light.

Furthermore, it was found out that the precision of the FARO LS 880 does not significantly changes with the scan range. This precision parameter is in the order of 2 – 4.5[mm] up to a distance of 29[m].

The reliability of the scans of both scanners is not significantly different. The reliability of the scans made by the IMAGER 5003 is in most situations slightly better. This can be explained by the difference in the filtering of both scanners.

Further research is recommended on the difference in precision and reliability parameters after filtering the scans obtained of the FARO LS 880. After this filtering, it is possible to compare the scans of both scanners and clarify which scanner is more precise and reliable.

Samenvatting

Fugro-Inpark B.V. (FINP) gebruikt de techniek terrestrische laserscanning voor het meten van een omgeving in de vorm van een 3D puntenwolk. Hiervoor wordt in de laserscanner een afstands- en een richtingsmeting uitgevoerd. FINP is momenteel in het bezit van een terrestrische laserscanner, de *Leica HDS 2500*. Deze laserscanner meet de afstand tussen scanner en object door het tijdsverschil te bepalen tussen een uitgezonden laser puls en zijn gereflecteerde echo.

Maar omdat laserscanning een relatieve nieuwe manier van data inwinnen is, is deze inwinningstechniek onderhevig aan grote ontwikkelingen. Een van de belangrijkste ontwikkeling binnen het gebied van de terrestrische laserscanners heeft betrekking op de methode die gebruikt voor wordt voor de afstandsmetingen. FINP zet laserscanners voornamelijk in bij het inwinnen van gegevens over industriële ruimten en architectuur. In deze situaties is de afstand tussen de scanner en de te scannen objecten vaak klein en kunnen fasescanners efficiënt gebruikt worden. Het wordt namelijk gezegd dat deze scanners relatief nauwkeurig meten op korte afstanden. Verder is de tijd die het maken van één scan duurt relatief kort ten opzichte van de pulsscanner.

De wens van FINP om meer inzicht te verkrijgen in de precisie en nauwkeurigheid van twee fasescanners, heeft geresulteerd in dit onderzoek. De titel van het onderzoek is daarom dan ook:

Het bepalen van de precisie en nauwkeurigheid parameters voor verschillende laserscanners, door middel van het creëren van een aantal praktische experimenten

De volgende twee fasescanners zijn gebruikt in dit onderzoek: de IMAGER 5003 van Zoller und Fröhlich (ook bekend als de HDS 4500 van Leica Geosystems) en de FARO LS 880.

In het onderzoek zijn eerst de eigenschappen van beide scanners onderzocht. Ten tweede is onderzoek gedaan naar de bekende foutenbronnen die de metingen met behulp van laserscanners beïnvloeden. Vervolgens is gekeken naar bestaande testopstellingen en experimenten omdat het opbouwen van zo´n test ruimte ook het uiteindelijke doel van dit onderzoek is.

De opgedane kennis is gebruikt om zelf een praktische testopstelling te creëren waarin een aantal experimenten geïmplementeerd is. Het doel van ieder uitgevoerd experiment is om de invloeden van één of twee variabelen te bepalen en de andere factoren te elimineren uit de opstelling. Dit om te voorkomen dat ze de resultaten beïnvloeden. De volgende vier experimenten zijn gecreëerd:

1. Een experiment dat de invloed van een toenemende scanhoek bepaald.
2. Een experiment dat de invloed van de absorptie eigenschappen van verschillende kleuren bepaald.
3. Een experiment dat kijkt naar de invloed van verschillende reflectiekenmerken.
4. Een experiment dat de invloed van een toenemende afstand tussen scanner en object bepaald.

Na het scannen van deze vier experimenten is een aantal analysemethoden gecreëerd die het mogelijk maken inzicht te verkrijgen in de precisie- en nauwkeurigheidsparameters van beide scanners. De resultaten van deze analyses zijn gebruikt om het algemene gedrag van de twee laserscanners te bepalen en om de resultaten van de twee laserscanners met elkaar te kunnen vergelijken. Voor de dataverwerking is gebruik gemaakt van de beschikbare sofware behorend bij de laserscanners en van de mogelijkheden van het rekenprogramma Matlab.

Voordat echter aan de analyse begonnen kan worden is het binnenste gedeelte van het object geselecteerd om zo de rekentijd te verkorten en om de randeffecten uit de scan te verwijderen. Alle experimenten zijn uitgevoerd op vlakke objecten of in andere woorden, objecten die gerepresenteerd kunnen worden door een vlak.

Deze representatie is tot stand gekomen door het uitvoeren van een kleinste-kwadraten vereffening op de scanpunten. Op deze manier zijn de scanpunten gerepresenteerd door een vlak en dit vlak is gebruikt in de analysefase van dit onderzoek. De analysefase van ieder experiment is gebaseerd op hetzelfde principe, namelijk door het bepalen van de volgende parameters:

1. *De hoeveelheid gescande punten;* hier wordt de werkelijke hoeveelheid gescande punten per [cm^2] vergeleken met het verwachte aantal gescande punten per [cm^2]. De laatste is gebaseerd op gegevens uit de specificaties van de scanners en op deze manier wordt dus gekeken of deze kloppen.
2. *De gemiddelde intensiteit;* de invloed van het gescande object op de gemeten intensiteit wordt bekeken in deze analyse. Als de uitkomsten van de gemeten intensiteit van twee laserscanners vergeleken moeten worden, moet eerst een histogram-egalisatie uitgevoerd worden, alvorens de vergelijking plaats kan vinden.
3. *De precisie test;* door de scanpunten uit de scan af te trekken van het model ontstaan de residuen. De standaarddeviaties van de residuen worden gebruikt als maat om de precisie in uit te drukken.
4. *De betrouwbaarheidstest;* de nauwkeurigheid van de scans wordt bepaald door eigenschappen van het model te vergelijken met 'ground truth' waarden. Het verschil tussen de 'ground truth' en het model bepalen de mate van nauwkeurigheid van de scan.

De analysefase van dit onderzoek heeft laten zien dat er geen groot verschil is tussen beide laserscanners ten opzichte van het gescande aantal punten en de gemeten intensiteit. Het verschil tussen het verwachte aantal punten en het werkelijke aantal punten is over het algemeen net iets kleiner voor de IMAGER 5003.

Enige uitzonderingen op deze stelling gelden voor de behaalde resultaten op extreme objecten. Voorbeelden van deze objecten zijn een stukje zwart vilt met een uitstraling van minder dan 0.5% van het inkomende signaal en een blauw gekleurd object. De FARO LS 880 verliest relatief veel minder punten op deze objecten terwijl de IMAGER 5003 nauwelijks punten scant op deze objecten, hier ontstaan dus scans met grote gaten.

Een groot verschil is aanwezig tussen de precisieparameters van beide scanners. De precisie van de scans verkregen met de IMAGER 5003 is in bijna alle gevallen twee keer beter dan de precisie van de scans verkregen met de FARO LS 880. Verder onderzoek heeft uitgewezen dat de IMAGER 5003 de data filtert voordat een uitvoerfile is gemaakt terwijl de software van de FARO LS 880 handmatige filtering mogelijk maakt. Dit verschil verklaart zeer waarschijnlijk het verschil in precisie. Echter, kennis in dit verschil is pas verkregen na het analyseren van de data en daarom zijn de resultaten van beide scanners eigenlijk niet eerlijk vergelijkbaar.

In het algemeen kan gezegd worden dat de precisie van een groen gekleurd object relatief laag is in vergelijking met objecten van andere kleuren. Dit resultaat is behaald met beide scanners en was ook verwacht omdat groen de complementaire kleur van rood is.

Verder verandert de precisie van de FARO LS 880 niet significant met de afstand. De precisie parameters zijn in de order van 2 – 4.5[mm] voor een maximale afstand van 29[m].

Het verschil in de nauwkeurigheid van beide scanners is niet significant te noemen, hoewel de nauwkeurigheid van de IMAGER 5003 net iets beter is. Dit kan ook verklaard worden door het verschil in filtering.

Verder onderzoek is aanbevolen ten opzichte van de filtering. Het is te verwachten dat de precisie en de nauwkeurigheid parameters van de FARO LS 880 beter zullen zijn nadat de scan gefilterd is. Pas na deze filtering is vergelijking tussen beide scanners mogelijk en kan er gezegd worden welke scanner nauwkeuriger is.

List of symbols

3D	=	three dimensional
a, b, c	=	plane coefficients/parameters
c	=	velocity of a laser pulse in air
$d^{\perp}$	=	the orthogonal scan distance at which the *fpr* specifications are given
$\hat{e}$	=	estimating of the residuals
e_i	=	residual of the *i*-th measurement
$\bar{e}$	=	mean of all residuals = 0
fpr	=	diameter of the footprint [mm] given in the specifications
l	=	length in [m] between two scan points in one scan
m	=	number of observations
n	=	number of unknown parameters
n	=	normal vector of a plane
p_{xy}	=	position of the XY-mirror inside a laser scanner
p_{zy}	=	position of the ZY-mirror inside a laser scanner
q	=	redundancy
t_{fl}	=	time of flight
x	=	vector of unknown parameters
$\hat{x}$	=	estimating of the unknown parameters
y	=	vector of observations
$\hat{y}$	=	estimating of the observations
x_L, y_L, z_L	=	3D coordinates of a laser point in the local coordinate system of the laser scanner
A	=	A-matrix; this matrix gives the relation between the unknown parameters and the observations
C	=	colour value of the surface of the object
D(.)	=	dispersion
$D^{\perp}$	=	the orthogonal scan distance between the scanner and the object
D_i	=	distance between scanner and corner point *i* of the interior selection
E(.)	=	expectation
F	=	the diameter of the footprint [mm] at a scan distance
F_{α}	=	central F-distribution
I	=	identity matrix
I_D	=	intensity of the diffusely reflected light
I_{fpr}	=	the percentage of lost energy due to an increasing footprint
I_L	=	intensity of the incoming light/energy at the surface
L	=	normal vector of the laser signal to the object
L	=	length of the laser signal to the object
L_1	=	the length of the interior selection [m]
L_2	=	the width of the interior selection [m]
N	=	normal vector of the object
N	=	length of the normal vector

Num	=	the number of expected points to be scanned
P	=	vector from point P on the plane
Q	=	vector from point Q
$Q_{\hat{e}}$	=	variance-covariance matrix of the estimated residuals
$Q_{\hat{x}}$	=	variance-covariance matrix of the estimated unknown parameters
Q_y	=	variance-covariance matrix of the observations
$Q_{\hat{y}}$	=	variance-covariance matrix of the estimated observations
R	=	distance between scanner and a scanned point on the object
α	=	scan angle
$\alpha_{h\ incr}$	=	horizontal increment following from the specifications
α_s	=	level of significance
$\alpha_{v\ incr}$	=	vertical increment following from the specifications
β	=	vertical angle between corner point 1 – scanner – corner point 2 of an object
γ_z	=	rotation angle around the z-axis
γ_y	=	rotation angle around the y-axis
θ	=	horizontal angle in a spherical coordinate system
θ_i	=	angle of incidence
θ_r	=	angle of reflection
λ	=	wavelength
σ	=	standard deviation
$\hat{\sigma}$	=	SD of the overall model
σ^2	=	variance of the measurements
σ_R	=	accuracy of the distance between scanner and object
φ	=	vertical angle in a spherical coordinate system
χ^2	=	Chi-square distribution
ψ	=	horizontal angle between corner point 1 – scanner – corner point 2 of an object

Table of contents

1 Introduction

Fugro-Inpark B.V. (FINP) currently uses terrestrial laser scanning for surveying purposes. After emitting a laser signal in a defined direction, a laser scanner measures the distance between scanner and object in order to create a 3D scan of the surroundings. The direction in which a laser signal is emitted is determined by the position of one or two mirrors inside the laser scanner. The distance between scanner and object can be measured in three different ways, i.e.:

1. triangulation,
2. time of flight of one laser pulse,
3. phase shift between the incoming and outgoing signal.

FINP is in the possession of a terrestrial laser scanner: the *Leica HDS 2500*. This is a laser scanner that measures the distance between scanner and object by means of the time of flight principle.

Laser scanning is a relatively new way of collecting data and is going through a big development at the moment. One of the main developments concerns the method of distance determination. FINP uses scans obtained with a laser scanner mainly for modelling industrial plants and for architectural purposes. In these situations the objects scanned are relatively close to the scanner. Therefore it is interesting for FINP to use in a laser scanner that uses the phase shift method to determine distances because these scanners scan with high accuracies on short distances. But before focussing on a certain scanner, FINP wants to investigate the features of the different phase scanners on the market. Especially the accuracy of the laser scanners is important as FINP wants to provide their customers with models as accurate as possible. Their wish to have an insight into the features of different phase shift laser scanners has resulted in the research described in this thesis. The subject of this thesis therefore is as follows:

> *Determination of the precision and reliability parameters of different terrestrial laser scanners by creating a practical experiment set-up*

Because of the time limit, only two phase shift scanners are selected to be researched. The two selected scanners are the IMAGER 5003 of Zoller und Fröhlich (also known as the HDS 4500 by Leica Geosystems) and the FARO LS 880. They are assumed to be the most interesting phase shift scanners for FINP at the moment.

The research described in this thesis is consists of three steps, i.e.:

1. Making an inventory of:
   - the specifications of the two selected phase shift laser scanners,
   - the known error sources influencing the results of laser scanners,
   - existing test areas used to test and compare different terrestrial laser scanners;
2. The creation of a practical set-up in which different experiments are done in order to test and compare different features of the selected laser scanners;
3. Creation of methods to analyse the scans obtained, in order to gain insight into the precision and the reliability parameters of both laser scanners.

The first research step is carried out because little is known about testing laser scanners and the tests that have already been done. Therefore an inventory of known error sources is made during this step as well. Obviously insight into the error sources of terrestrial laser scanning and the way to determine them is important as they will be researched in the experiments.

The knowledge gained from the first research step is used to create a practical set-up in which different experiments will be implemented. The purpose of each experiment is to test one or two features that can influence the performance of a laser scanner. The features that are researched are:

1. the influence of the scan angle,
2. the influence of the colour of a surface,
3. the influence of the reflectivity of a surface,
4. the influence of the distance between scanner and object.

The third and last step will result in different methods to analyse the scan data. All experiments will be analyzed following the same procedure, resulting in different Matlab programs. These Matlab programs can be used in the future to test scanners in the same test area and get insight in their performance with respect to other tested scanners.

In order to be able to determine an advice for FINP on which scanner is best for them to use in their areas of interest, a comparison of both scanners and their performances will be done in this step as well.

This report consists of nine chapters. Chapter two describes the measuring principles of terrestrial laser scanning in general and gives some information on the two selected phase scanners. This chapter is followed by a description of the main error sources that influence terrestrial laser scanning and a description of existing experiment set-ups. Chapter four discusses the methods of analysis implemented and relevant background theories.

The following four chapters each discuss one experiment by first giving a motivation for the experiment followed by a description of the experiment set-up used, the results expected and the results obtained. First the scan angle experiment will be discussed in chapter five. Chapter six describes the colour experiment, chapter seven the reflectivity experiment and chapter eight discusses the range experiment. This thesis ends with conclusions and recommendations for further research in chapter nine.

2 Terrestrial Laser Scanning

Terrestrial laser scanning is the central focus of the research described in this thesis. Therefore it is important to understand the principle of terrestrial laser scanning as a way of collecting data.

Paragraph 1 of this chapter gives an overview of the positioning measuring technique used by laser scanners. Paragraph 2 will discusses the two selected laser scanners used in this research: the *Imager 5003* of Zoller + Fröhlich (also known as the *HDS 4500* of Leica Geosystems) and the *Faro LS 880 HE series (FARO LS 880)*.

2.1 The principle of terrestrial laser scanning

A terrestrial laser scanner sets two *angles* in which the laser signal is emitted and measures the *distance* between the scanner and a point on the object using the laser signal. These measurements are done in rapid order which results in many scanned points on an object in a short time interval. The 3D coordinates of each scanned point are determined in a coordinate system local to the scanner. This paragraph will discuss the measuring principle of laser scanning.

Inside the scanner a laser beam is deflected in a certain direction using *one* or *two rotating mirrors*. The emitted laser signal is reflected on an object and a part of this reflected signal is received back at the scanner (see figure 2.1). To determine whether the received signal is indeed the echo of the emitted signal, the *intensity* of the echo is measured. In order to be detected as an echo, the intensity of a signal has to extent a certain threshold, which is a percentage of the emitted signal strength. This threshold is implemented in the measurements to be sure the incoming intensity belongs to the emitted laser signal and not to external light sources like the sun or artificial light sources.

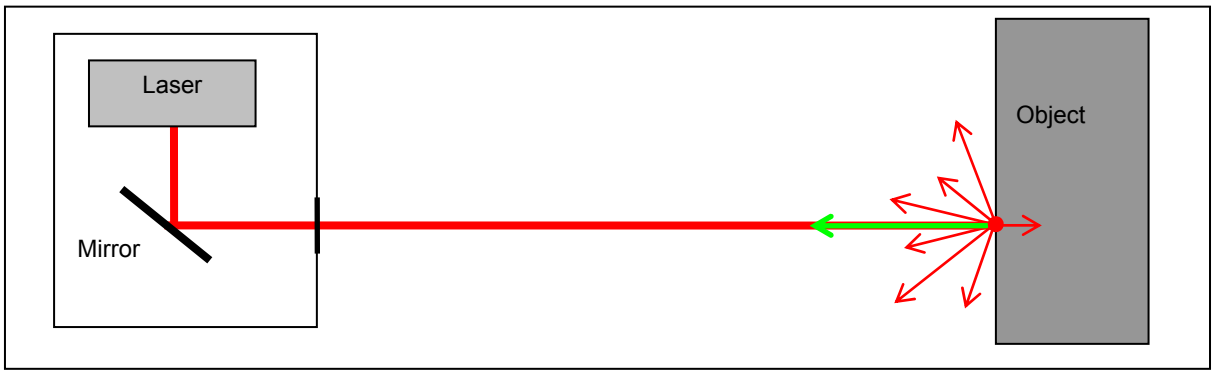

Figure 2.1: Measuring principle of a terrestrial laser scanner with left; the mirror, inside the laser scanner, which deflects the laser signal in a certain direction, right; the measured object on which the signal is reflected; the green arrow is the echo returning to the laser scanner (source: Claassen, 2003).

In order to create a 3D scan the *horizontal angle* and the *vertical angle* in which the laser signal is deflected is set within in the laser scanner followed by the determination of the *distance* between the scanner and the object. These measuring techniques will be discussed in the next subparagraphs.

2.1.1 Horizontal and vertical angles of deflection

There are two ways to change the direction in which a laser signal is emitted, i.e.:

1. by determining the positions of two rotating mirrors inside the scanner,
2. by determining the position of one rotating mirror inside the scanner and the position of the entire measuring device.

The interior of a laser scanner that determines the direction of the emitted laser signal using two mirrors is different than the interior of a laser scanner that consist of 1 mirror and a rotating device. The two different interiors are shown in figure 2.2.

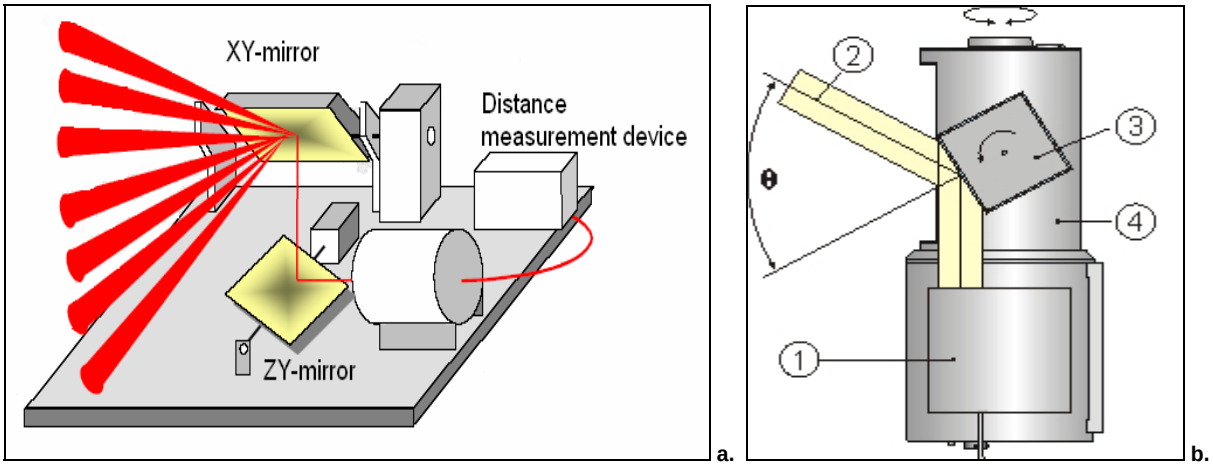

Figure 2.2: Two different interiors of laser scanners, **a.**; the interior of a laser scanner with two rotating mirrors, **b.**; the interior of a laser scanner with one rotating mirror and a rotating measuring device; 1. The laser signal is sent from here, 2. The deflection of the laser signal caused by the mirror, 3. The rotating mirror, 4. The rotating measuring device (source: Riegl, 2006).

Two rotating mirrors

By changing the position of the mirrors, the direction of the emitted signal changes as well (see figure 2.2). The ZY-mirror sets the horizontal angle (θ) and the XY-mirror sets the vertical angle (φ) in which the laser signal is emitted. Because the distance between the laser scanner and the scanned object is determined next (see section 2.1.2), the coordinates of the scan point are known in *a spherical coordinate system* (see section 4.2.2) [Mathworld, 2006c]. Therefore, the x,y,z-coordinates of each laser point can now be determined using the following formulas (2.1):

$$\begin{aligned} x_L &= R \cdot \cos(\theta) \cdot \sin(\varphi) \\ y_L &= R \cdot \sin(\theta) \cdot \sin(\varphi) \\ z_L &= R \cdot \cos(\varphi) \end{aligned} \qquad (2.1)$$

with:

x_L, y_L, z_L	= 3D coordinates of the laser point
θ	= horizontal angle in which the laser signal is emitted
φ	= vertical angle in which the laser signal is emitted
R	= distance between scanner and object (see paragraph 2.1.2)

One rotating mirror and a rotating measuring device

In a laser scanner that consists of only one mirror, the mirror determines the vertical angle in which the laser signal is emitted. The scanner device rotates around the vertical axis in order to determine the horizontal angle (see figure 2.2b). The 3D-coordinates of each scanned point can be determined in the same way as mentioned in the previous section (see formula 2.1). The angle of the scanner with respect to its vertical axis is θ and the angle of the mirror inside the scanner corresponds to φ.

2.1.2 Distance measurements

The distance between an object and the laser scanner can be determined by three different principles, which are the following:

1. triangulation,
2. time of flight determination,
3. phase shift determination.

Triangulation

As the name already does suspect, a triangulation scanner uses a triangulation to determine the distance between the scanner and the object (see figure 2.3a). It can be seen in this figure that the length of one side of a triangle (the base) and two angles of the triangle, formed by the mirror, the CCD camera and the object, are used to determine the distance between scanner and object.

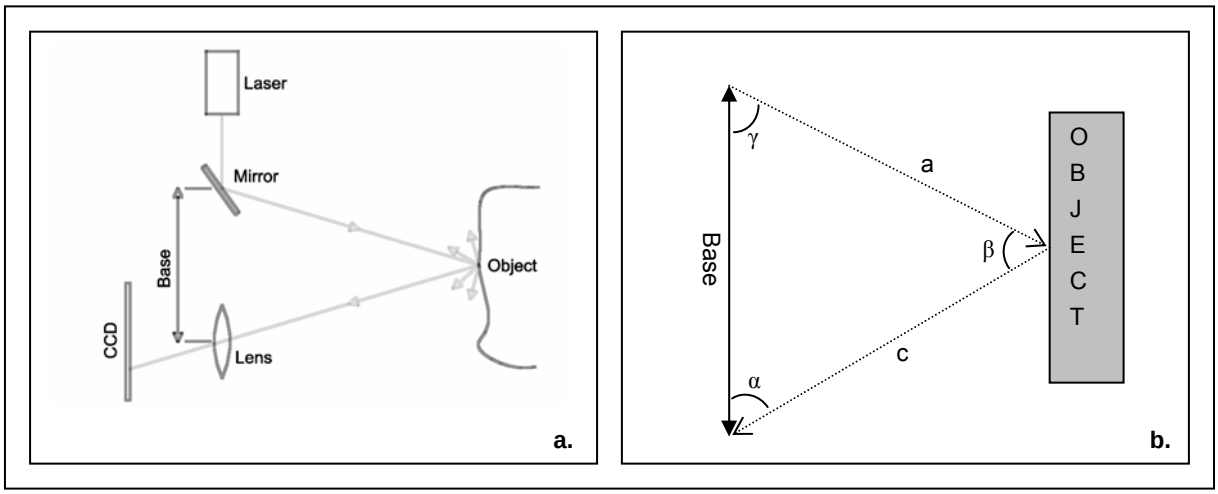

Figure 2.3: **a.**: the triangulation principle of laser scanners (source: Boehler and Marbs, 2000), **b.**: the schematic triangle that is used in the triangulation and the law of sine.

The incrementally changed angle of the mirror determines in which direction the laser signal is emitted and the CCD detects the reflected laser signal. The 3D position of the reflecting surface can be derived from the resulting triangle and the law of sine (2.2) [Boeler and Marbs, 2002].

The law of sine

The sine rule is used to determine the length of a triangle edge/side when either two angles and one side are given or when two sides and a non-included angle are given. In case of the triangulation scanner, the angles α

and γ are the same and known just like the base (see figure 2.3b). The other unknown angle and sides of the triangle can be determined with the law of sine (2.2).

$$\frac{a}{\sin\alpha} = \frac{Base}{\sin\beta} = \frac{c}{\sin\gamma} \qquad with:\ \alpha+\beta+\gamma = 180[°] \tag{2.2}$$

As the base length between mirror and CCD cannot be increased at will, it is known that the accuracy of the determined distance between instrument and object decreases with the square of the distance (formula 2.3). Therefore, these scanners are used mainly to scan short distances (up to 10 [m]) and small objects because in this case they are more accurate than other ranging laser scanners [Boeler and Marbs, 2002].

$$\sigma_R \approx R^2 \tag{2.3}$$

with:

σ_R = accuracy of the distance between scanner and object
R = distance between scanner and object

Examples of commercially used triangulation scanners are the *Mensi S series* (currently Trimble) and the *Minolta Vivid series*.

Time of flight

This type of scanner sends a pulse in a certain direction to an object and ´waits´ for the returning echo. The distance between object and scanner can now be determined by using the time of flight (t_{fl}) of the pulse. Therefore, the scanner measures the time difference between emitting the signal and receiving it back. Figure 2.4 visualizes the principle of a pulse scanner.

The velocity of a laser pulse in the air[1] (c) is known so formula 2.4 can be used to determine the distance between the scanner and the object (R) [Wehr and Lohr, 1999].

$$R = c \cdot \frac{t_{fl}}{2} \tag{2.4}$$

with:

R = distance scanner and object
c = velocity of a laser pulse in the air
t_{fl} = time of flight

It can be seen in figure 2.4 that the emitted signal losses intensity during the flight. Therefore, it is important that the emitted pulse has a high intensity value because the bigger the strength of the emitted signal, the higher the reflected intensity of the echo so the more accurate the time difference can be determined. It can be assumed that this results in a more accurate distance determination. The loss of intensity is partly due to the travelling through the air. For example, dust and water vapour in the air absorb or reflect the emitted signal diffusely. These effects cause loss of intensity because less energy of the signal is returning to the scanner. They are called *atmospheric errors*.

[1] c = 299.792.458 [m/s]

It is said that the quality of the distance measurements is independent of the distance between the scanner and object [Boeler and Marbs, 2002]. However, it is recommended to emit stronger pulses when long distances have to be measured due to the atmospheric errors; this to make sure that enough energy is received back at the scanner. Currently pulse scanners can measure distances over 100[m].

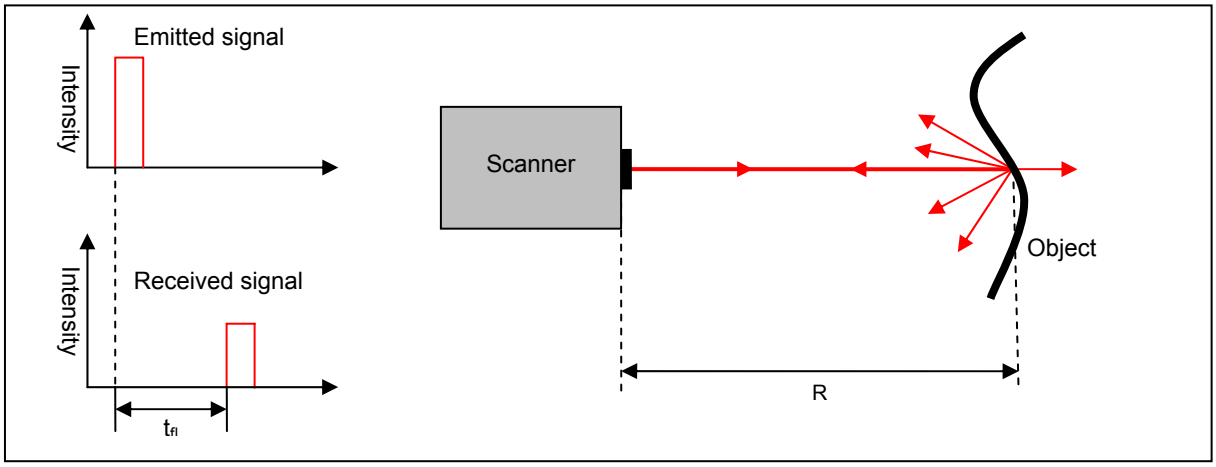

Figure 2.4: The principle of a time of flight laser scanner, t_{fl} is the time of flight of the pulse and R is the distance between scanner and object (source: Claassen, 2003).

Examples of commercial used time of flight scanners are the *Leica HDS2500*, *Leica HDS3000*, *Trimble GS200*, *Trimble GX* and the *Riegl LMS series*.

Phase shift

The basic principle of a phase shift laser scanner is the determination of the phase difference between the emitted and the received signal. This is done in order to determine the distance between scanner and object. To be able to determine the phase difference the laser signal is modulated[2] with a harmonic wave[3]. In the current phase scanners, a bi- or tri-modulation is being used. This means that the carrier wave is being modulated with 2 or 3 different harmonic waves. Figure 2.5 visualizes the principle of a tri-modulation.

The blue wave of figure 2.5 is the harmonic wave with the highest frequency and therefore determines the accuracy in which the laser scanner can measure the distances. The purple line is the harmonic wave with the longest wave length. This wave defines the maximum distance that can be measured because this is equal to half the wave length of the longest wave. The reason for this limitation in the distance is that no ambiguities are determined. The maximum distance that can be measured with the current phase shift laser scanners is approximately 50[m]. The red wave shown in figure 2.5 is the result of the modulation and will be used in the laser signal to determine the phase shifts.

The phase shift laser scanner now emits the modulated laser signal with a certain phase angle that varies in time. At the moment a reflected signal returns to the scanner, the difference in the phase angle between the emitted signal and the received signal can be determined. Because the wave lengths of the signal are known, the distance between object and scanner can now be calculated. Figure 2.6 shows the measuring principle of a phase shift laser scanner and a calculation example of the distance determination.

[2] Modulation means that a carrier wave is being changed with respect to its source signal
[3] A harmonic wave is a wave that can be described by a (co-)sine function with a constant amplitude and period

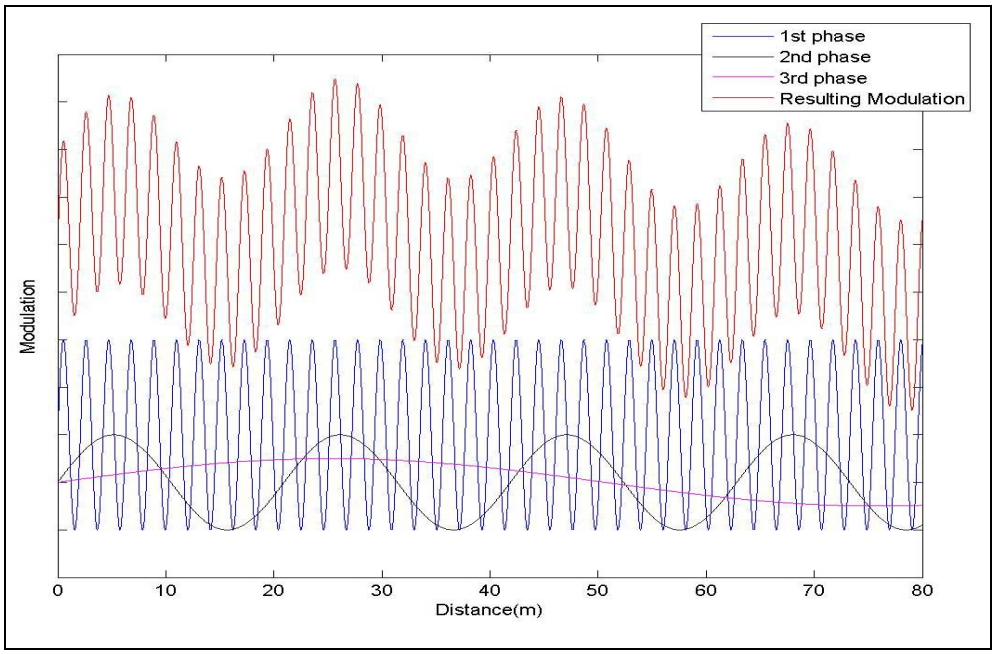

Figure 2.5: an example of a tri-modulation of a laser signal using 3 harmonic waves (source: Van Gosliga, 2005).

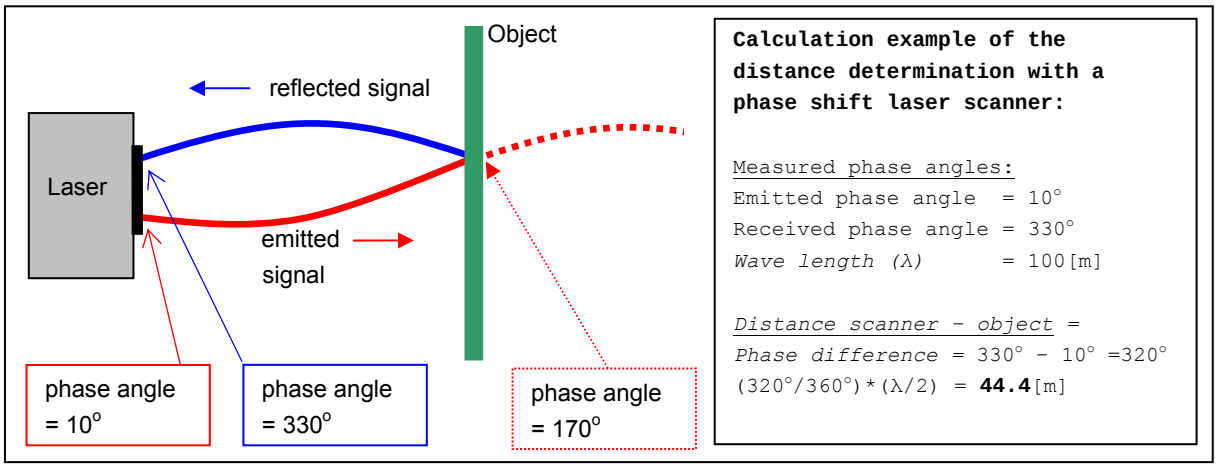

Figure 2.6: the principle of distance determination with a phase shift laser scanner and an example of the distance calculation on the right (source: Pfeifer, 2005).

Because the phase angles of both the received and emitted signal differ continuously, the scanner can determine the distances continuously as well. In contrast with the pulse scanner, the phase scanner does not have to wait until an echo of a signal is received back. This makes the phase scanner much faster than the pulse scanner.

Examples of commercial used scanners using phase differences are the *Z+F Imager 5003* (equal to the *Leica HDS4500*) and the *FARO LS series*.

2.2 The selected laser scanners

One of the main topics of this thesis is to compare two different phase laser scanners, the *IMAGER 5003* of Zoller + Fröhlich and the *FARO LS 880*. This paragraph will give a short overview of the features and specifications of both laser scanners.

2.2.1 IMAGER 5003

The German company *Zoller + Fröhlich* (Z+F) developed the phase scanner *'IMAGER 5003'* [Zoller und Fröhlich, 2006]. In 2003 Z+F made a cooperation agreement with *Leica Geosystems* (Leica). Leica could sell the *Leica HDS 4500* which is identical to the IMAGER 5003. The specifications of the two systems therefore can be assumed equal. A list of the specifications is shown in table 2.1 at the end of this paragraph. This section will continue to discuss the IMAGER 5003 but all commends are also valid for the HDS 4500 [Leica Geosystems, 2006].

The *result* of the measurements done with the IMAGER 5003 is an output file with the x-, y-, z-coordinates and the measured relative intensity value for each scan point.

The sizes of the IMAGER 5003 are 30 x 18 x 35[cm] (respectively. length, width and height) and its weight is 16[kg]. The system is connected to a 24[V] battery of the sizes 24 x 26 x 30[cm] and a weight of also 16[kg]. Both a laptop and a battery need to be connected to the scanner. The 2 cables are connected to the rotating part of the scanner so they will rotate around the instrument while scanning. Figure 2.7a shows a picture of the IMAGER 5003 complete with tripod, laptop and battery. Figure 2.7b shows the HDS 4500 used during one of the experiments for this research. It can be seen in this figure that both systems look identical apart from the colour of the cover.

As mentioned in paragraph 2.1, the wave length of the modulated wave limits a phase scanner in its maximum measurement range. Implemented in the IMAGER 5003 is a range measuring system called LARA. There are two different types of LARA systems available and they are both implemented in the IMAGER 5003; the LARA 25200 and the LARA 53500. The difference both LARA systems is the length of the longest wave length of the modulated wave. Therefore, the maximum distance that can be measured with each system differs; 25.2[m] for the LARA 25200 and 53.5[m] for the LARA 53500. Selecting or deselecting the close range option in the IMAGER 5003 software makes it possible to switch between both distance measurements devices.

a. **b.** **c.**

Figure 2.7: the IMAGER 5003 (**a.**), the HDS 4500 (**b.**) and the FARO LS 880 HE 80 (**c.**) ready to scan.
(sources: (**a.**) Zoller und Fröhlich, 2006, (**b.**) picture: Van Ree, 29-03-2006, (**c.**) picture: Van Ree, 01-05-2006)

2.2.2 FARO LS 880

The German company *FARO* took over the German company *iQvolution* and its phase shift laser scanner; the *iQsun 880*. The laser scanner is now being sold as *FARO LS 880 series* [Faro, 2006].

Like the IMAGER 5003 the result of the measurements with this scanner is an output file with the x-, y-, z-coordinates and the measured relative intensity value for each scan point.

The FARO LS 880 is constructed of three exchangeable modules (see figure 2.7c):

1. the module containing the distance sensor,
2. the mirror module,
3. the PC module.

This makes it possible to exchange a module if it is broken or purchase a new module after new developments are done. This feature makes it possible to buy cheaper parts instead of a whole new scanner when new technologies become available [Faro, 2006].

The sizes of the FARO LS 880 are 40 x 16 x 28[cm] (resp. length, width and height) and its weight is 14.5[kg]. The system is connected to a 24 V battery of the sizes 15 x 7 x 3.5[cm] and a weight of 0.6[kg]. The scanner is connected to both the laptop and battery with only one cable of 15[m]. This makes it possible to move the scanner and leave the laptop and battery at the original place.

The FARO LS 880 is also available in two different versions that determine the maximum scan distance. The FARO LS 880 HE 40 can measure distances up to 40[m] and the FARO LS 880 HE 80 can measure distances up to 80[m].

Table 2.1: an overview of the specifications of the IMAGER 5003 and the FARO LS 880 (sources: Zoller und Fröhlich, 2006 and Faro, 2006).

	IMAGER 5003		**FARO LS 880**	
FEATURES	LARA25200	LARA53500	HE40	HE80
Laser measurement system				
Range [m]	25.2	53.3	40	80
Resolution Range [Bit]	16	16	17	17
Measurement rate [pps]	625000	500000	120000	120000
Position accuracy [mm]	7 on 25.5 [m]	≤ 6 on 10 [m]	3.5 on 10 [m]	3.5 on 10 [m]
Angle accuracy [º]	0.01	0.01	0.007	0.007
Range accuracy [mm]	<3 on 0.4-25.5 [m]	<6 on 0.4-53.5 [m]	3 on 10 [m]	3 on 10 [m]
Optical transceiver				
Laser output power (CW) [mW]	23	32	10.5	22
Beam divergence [mrad]	0.22	0.22	0.25	0.25
Footprint diameter ([mm] circular)	3.5 on 1 [m]	3.5 on 1 [m]	3 on 0 [m]	3 on 0 [m]
Laser wavelength [nm]	780	780	782	782
Deflection unit				
Vertical field of view	310°		320°	
Horizontal field of view	360°		360°	
Vertical resolution	0.018°		0.009°	
Horizontal resolution	0.01°		0.00076°	
Vertical maximum scanning speed [rpm]	2000		3000	
Max. # points vertical (per 360 deg)	20000		16384	
Max. # points horizontal (per 360 deg)	20000		470000	
Middle resolution [pps]	125000		240000	
Scanning time at middle resolution [sec]	100		233	
Dimensions and weight				
Scanner (w x d x h) [mm]	300 x 180 x 500		400 x 160 x 280	
weight scanner [kg]	16		14.5	
accu size (w x d x h) [mm]	240 x 260 x 300		150 x 70 x 35	
weight accu [kg]	16		0.6	
number of cables	2, rotation part of the scanner		1, non rotating part of the scanner	
Separate components (yes/no)	No		yes (4)	

3 Known error sources and existing test set-ups

This thesis discusses the creation of four experiments that will be implemented in a practical set-up. But before the creation of the experiments will be discussed, some known error sources that influence the measurements with terrestrial laser scanners are selected. These might be interesting to research in the different experiments. The selection of the error sources is done together with FINP. Furthermore, existing experiments with respect to terrestrial laser scanners are investigated and used to create ideas for the experiments that will be self created in the practical set-up.

Paragraph 1 of this chapter discusses the selected error sources. An overview of existing test set-ups and their results will be discussed in paragraph 2.

3.1 Known error sources in laser scanning

FINP mentioned a few known error source that influence the measurements done with a terrestrial laser scanner. They created the list with error sources using their experience with their pulse scanner (the Cyrex 2500/HDS2500). It is expected that the same error sources influence the measurements done with a phase shift scanner and therefore, their influences are interesting to test during one of the experiments. The following error sources are mentioned and will be discussed in this section:

1. specifications of the laser scanners,
2. intensity,
3. scan angle,
4. resolution,
5. range.

Ad 1.
The specifications of the laser scanners are not actual error sources but they are implemented in this section because currently they are the only information available on laser scanners and therefore they are used to decide which laser scanner is best for to use for a company. In practise however, the specifications of different laser scanners are not comparable so the companies base their procurement on the wrong information without knowing.

3.1.1 The specifications of the laser scanners

Most producers publish ‘the most positive parameters’ of their scanner. For example, this means that the accuracy specifications are based on a scan obtained with the highest point density so the highest resolution. Scanning with a high resolution obviously means a lot of measurements per scan, so a high reliability, but it is also time consuming.

On the other hand, the scan time values that are given in the specifications mostly refer to the average resolution of the scanner. This means that the individual specifications of one scanner are not always comparable with each other.

This also counts for the comparison of two different scanners using the specifications only, see table 2.1. The individual specifications of the scanners are valid for different resolutions or for different ranges. This makes it impossible to compare two scanners based on their specifications. However, it is the only information that is known about the scanners by forehand so people do use them to make the choice which scanner to use or purchase.

During this research it is therefore tried to create results based on the same experiments in the same room with the same circumstances. This makes the results obtained with different laser scanners comparable. The results of the experiments will also be used to test the given specifications of the individual scanners to see whether the specifications of each laser scanner hold true in the tested situations.

3.1.2 Intensity

Besides the calculated x, y, z coordinates per scan point, a laser scanner also gives an output value for the intensity of the received signal. The *intensity* is the strength of the incoming signal after it is reflected and is dependent on both *absorption* and *dispersion,* so these effects need to be taken into account because it is expected that the higher the intensity of a point, the higher the precision and accuracy of the distance determination.

Absorption

While measuring with a laser scanner the effects of absorption are always present. Absorption means that an object absorbs an amount of the energy of the emitted laser signal that hits the surface of that object. This direct result is that an echo with less energy that returns to the scanner. It is known that light coloured bodies absorb less energy and dark bodies absorb a lot of energy [Longhurst, 1957].

Dispersion

In most situations the emitted signal will be reflected in different directions when it 'hits' the surface of an object. This phenomenon is called dispersion and causes that only a small part of the emitted signal is reflected back to the scanner. The remaining part of the energy is reflected in other directions or absorbed. Obviously this results in a decreasing intensity of the echo. The amount of dispersion depends on the surface/ material of the object. It is known that smooth objects cause less dispersion than rough objects [Longhurst, 1957].

On the other hand, dispersion is important because it makes the principle of laser scanning possible. As mentioned before, a laser scanner needs an echo to be able to measure a distance. Dispersion reflects a signal in different directions causing different echoes which improves the chance that one of these echoes reaches the scanner. Figure 3.1a shows the effect of absorption and dispersion. Because the sizes of the arrows in figure 3.1a represent the amount of energy, it can be seen that the energy of the echo returning to the scanner is lower than the energy of the emitted signal. The energy of the echo is measured and is called the *intensity value* of that scan point.

The stored intensity value can be used to create an intensity image. If this image is a black and white image the points with a light colour are scan points on objects with a high reflectivity and points with a dark colour are situated on objects with a low reflectivity (see figure 3.1b).

FINP commonly uses laser scanning for industrial plants. In these plants a lot of different materials and colours are present. Therefore it is useful to know how the scanners react on certain materials and colours.

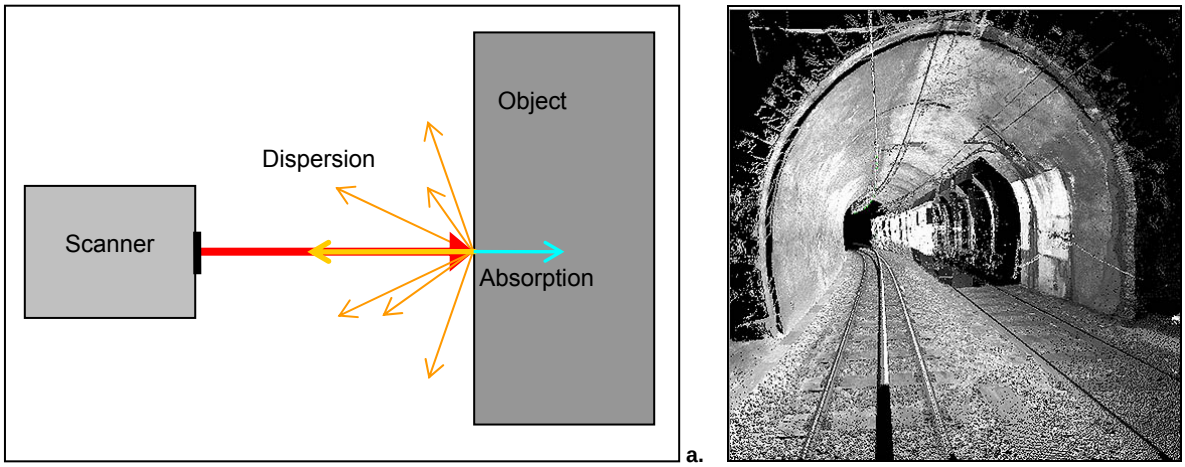

Figure 3.1 **a.**: the effect of absorption (blue arrow) and dispersion (orange arrows), the sizes and thickness of the arrows correspond to the energy level they represent, **b.**: an example of an intensity image made in a tunnel; the darker parts are objects with low reflectivity and the lighter parts are object with high reflectivity (source: Zoller + Fröhlich, 2006).

3.1.3 Scan angle and reflectivity

Closely connected to the intensity is the scan angle. The scan angle is the angle between the normal of the object[4] and the laser signal. Dispersion or the so-called surface scattering is also of importance while scanning objects with different scan angles. In this section two limiting cases of surface scattering will be discussed; *Specular reflection* and *Lambertian scattering*.

Specular reflection

Shiny objects like water, glass and mirrors do not reflect a signal back to the scanner when the angle of incidence on the scanned object is > 0[°]. This effect is called Specular reflection or Specular scattering and can be described by the law of reflection or by Snellius law (formula 3.1) [Rees, 2001].

$$\theta_i = \theta_r \tag{3.1}$$

with:

θ_i = angle of incidence
θ_r = angle of reflection

From this formula it can be seen that when Specular reflection occurs, the angle of incidence is equal to the angle of reflection (see figure 3.2). The result is that no signal will return to the scanner when the scan angle is > 0[°]. This makes it impossible to determine a distance and 'gapes' in the scan data will occur.

[4] The line perpendicular on the surface of the object where the laser signal 'hits' the surface

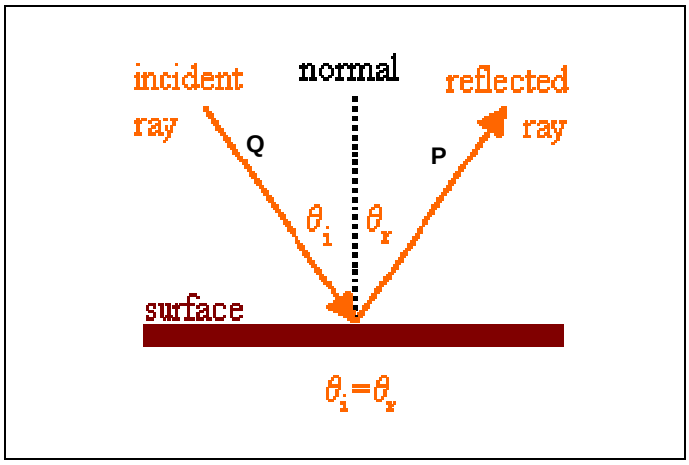

Figure 3.2: the effect of Specular reflection; if the scanner is located in point Q, no signal is returning to the scanner as the signal continues its route through point P (source: Optics, 2006).

Lambertian scattering

As mentioned above, specular reflection occurs when the surface of an object is smooth. The other limiting case of scattering is that of an ideally rough surface, giving *Lambertian scattering* [Rees, 2006]. This surface has the property that, for any illumination that is uniform across the surface, the scattered signal is distributed isotropic, which means that the laser signal will be scattered in all directions (see figure 3.4).

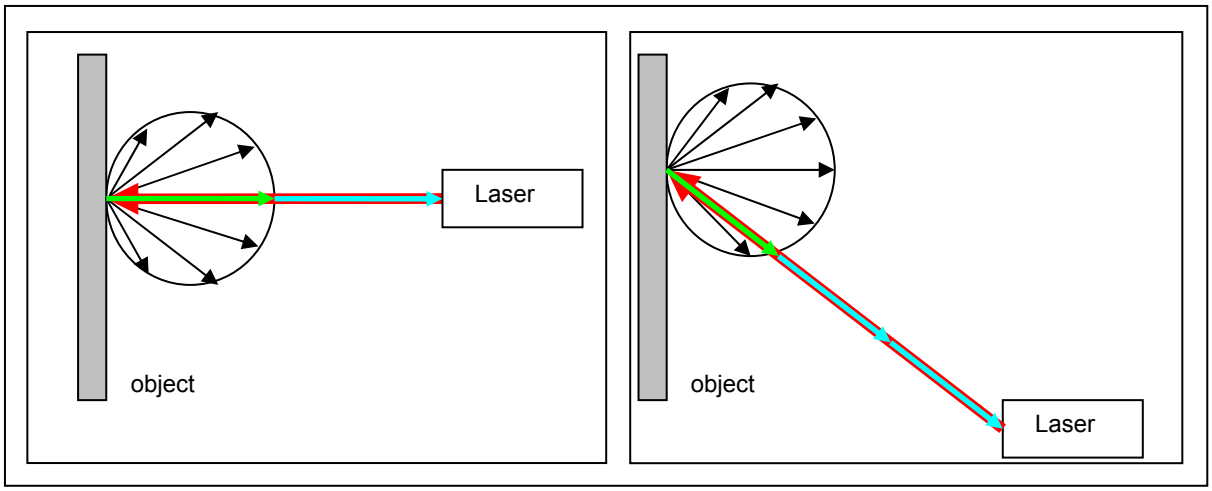

Figure 3.3: the effect of a perfect Lambertian body; after hitting the surface, the signal is scattered is isotropical, the green arrows represent the intensity of the echo, *left;* for a scan angle of 0[º], *right;* for a scan angle of 0[º] < α < 90[º].

Remark: Figure 3.3 shows the isotropic backscattering of a perfect Lambertian body by means of the black and green arrows but in fact the number of echoes is infinite, the black arrows are only a few examples of echoes.

The intensity of all echoes caused by Lambertian scattering is calculated by taking the dot product of the normalized normal vector of the surface (*N*) and a normalized vector pointing from the scanner to the object (*L*). This product is multiplied by the colour value of the surface of the object (*C*) and the intensity of the laser signal when it hits the surface (*I*) (formula 3.2).

$$I_D = \mathbf{L} \cdot \mathbf{N} * C * I_L \tag{3.2}$$

with:

I_D = Intensity of the diffusely reflected light
L = The normalized vector of the laser signal to the object
N = The objects normalized normal vector
C = Colour of the object's surface
I_L = Intensity of the incoming light at the surface

Furthermore it counts that:

$$\mathbf{L} \cdot \mathbf{N} = |N||L| \cos\alpha \tag{3.3}$$

with:

L = The normalized vector of the laser signal to the object
N = The objects normalized normal vector
N = Length of the normal vector
L = Length of the laser signal to the object
α = Angle between both vectors = the scan angle

The combination of formulas 3.2 and 3.3 proves that the intensity is the highest when the scan angle is 0[°]. Figure 3.4 confirms this as it shows that the intensity values at a scan angle (α) of 0[°] is the highest and when the scan angle (α) increases, the intensity values measured of the echoes decrease (with: 0[°] ≤ α ≤ 90[°]). The curve shown in figure 3.4 represents the relation between the intensity values measured and the scan angle (the scanned object has one colour of and the scan range is set constant).

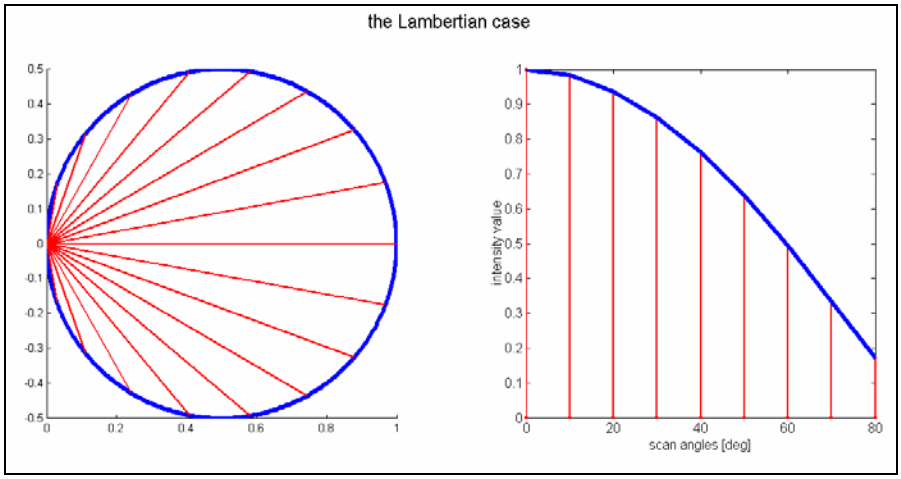

Figure 3.4: left: a perfect Lambertian scatter, the red lines are examples of the backscattered signals, *right;* a simulation of the *intensity-scan angle* curve, based on the formulas 3.2 and 3.3; for the simulation, the color characteristics and the scan range are set constant.

"Although the Lambertian model is simple and idealized, the scattering from many natural surfaces can often, to a first approximation at least, be described using it" [Rees, 2001, p. 50].

As mentioned at the beginning of this paragraph, the two discussed surface scatters are the most extreme cases of surface scattering. The expectation therefore is that the scatter pattern of a laser signal will be a combination of Lambertian scattering and Specular reflection (see figure 3.5).

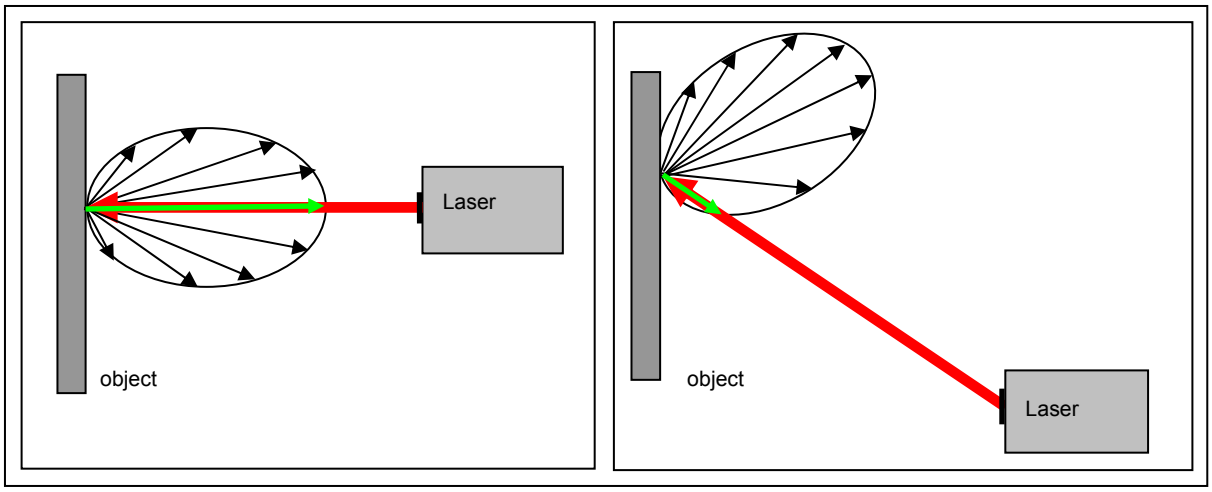

Figure 3.5: The expected scatter pattern which is a combination of specular reflection and Lambertian scattering.

It can be seen in the figure that the circular scatter pattern of the Lambertian theory is replaced by an ellipsoidal scatter pattern. The long axis of the ellipsoid is located in the direction of the angle of reflection based on the theory of specular scattering. This assumption results in the expectation that most of the signal strength will be reflected in a specular way and the rest of the signal strength will be scattered by means of an ellipsoid pattern. The surface characteristics of the object determine the shape of the ellipsoid. When the scanner object is smooth the ellipsoid will be long and small and when the surface is rough it is expected that the ellipsoid will be close to circular.

To test the effects of the scan angle on an object, an experiment will be created in which an object will be scanned with a number of different angles. The angles will be determined using an angle measurement device. Another way to test the effect of scan angles is to scan different cylinders; because of the roundness of a cylinder all scan angles are included.

3.1.4 Resolution

The resolution of a laser scanner is mostly defined as the number of points per scan and is dependent on both the *angle resolution* and the *footprint resolution*. The resolution determines the minimal size of the objects (or object parts) that can be detected and which objects are too small to be detected in a scan.

Angle resolution

The angle resolution defines how many points can be scanned in horizontal and vertical direction and can therefore be defined as the angle increment between two emitted signals. The highest resolution of a scanner is determined by the smallest possible rotation steps of the mirrors and/or the scan device (see chapter 3.2). This means; the higher the resolution of a scan, the more points will be present in the scan, so the smaller the angle increment that is used (see figure 3.6a).

The total number of points in a scan is important as the points are the observations and they will be used to create a 3D-model. If the *random errors* are dominant it can be said that more observations will most likely results in a more accurate model because there are more points to fit the model through. This does not hold true when *systematic errors* are dominant.

A disadvantage of scanning with a high resolution is that it is time consuming and in practice this can be a problem. Furthermore, the file sizes of high resolution scans increase significantly. The processing capabilities of computers might reduce this problem in the future, but at the moment this is fact has to be taken into account.

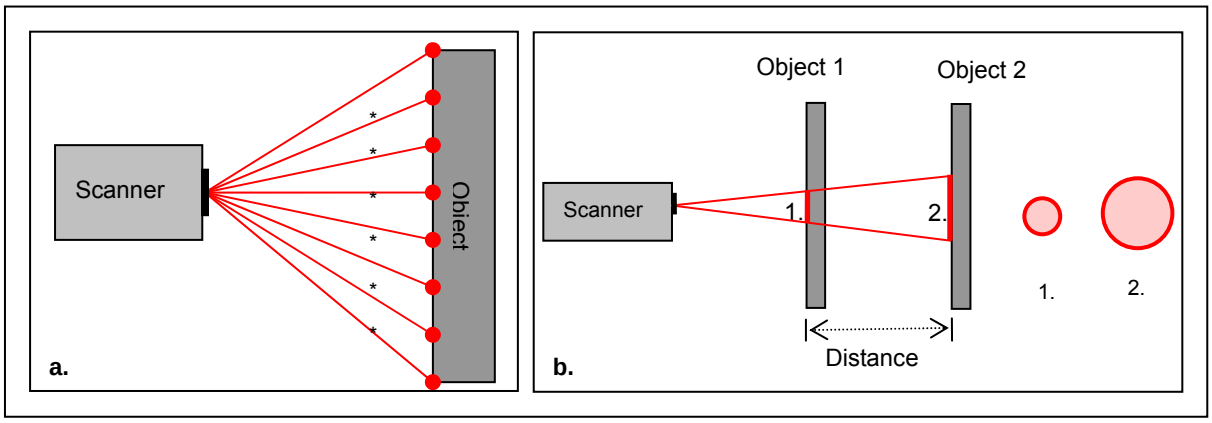

Figure 3.6: schematic visualization of both angle and footprint resolution, **a;** a top-view of a scan set-up, showing the constant horizontal increments (*) between two emitted laser signals, **b;** the effect of the distance on the footprint of the laser signal; the footprint on an object closer to the scanner is smaller (1.) than the footprint on an object further away from the scanner (2.).

Footprint resolution

If two similar objects are scanned with the same scanner and they are placed perpendicular to the scanner, the diameter of the laser signal on an object that is located further away from the scanner is larger than the diameter of the laser signal on the object close to the scanner (see figure 3.6b). A smaller footprint results in the possibility to detect more details within the scan and in a higher resolution. When certain accuracy is required, the footprint resolution is one of the main parameters that determine the maximum distance between scanner and object.

At the moment, an indication of the footprint resolution follows from the specifications of the scanners. These specifications give a diameter on a certain distance, therefore the footprint as function of the range can be determined with formula (3.4).

$$F_i = \frac{D_i^{\perp} \cdot fpr}{d^{\perp}} \tag{3.4}$$

with:

F_i = Diameter of the footprint [mm] at scan distance *i*
fpr = Diameter of the footprint given in the specifications
$D_i^{\perp}$ = The orthogonal scan distance *i* between object and scanner
$d^{\perp}$ = The orthogonal scan distance at which the fpr specifications are given

Whether these specifications are reliable is not known. Furthermore, the specifications do not mention the effect of the scan angle on the shape of the footprint. This shape becomes an ellipse when an object is scanned with an angle and obviously this effects the footprint resolution as well.

3.1.5 Range

The range is defined as the distance between the laser scanner and the scanned object. It is claimed that the accuracy of a pulse scanner is constant over the range [Boehler et al., 2003]. But it is hard to accept that the accuracy of the scanned points will be the same on a range of 5[m] and 50[m]. Therefore it is expected that it decreases with the distance (see figure 3.7), but the exact behaviour of the accuracy line is not known.

Furthermore, it is said that the accuracy of a phase scanner decreases exponentially with the distance but this exact curve is also not known [Claassen, 2006] and is not given by the producers of these types of scanners. Most producers give an accuracy of *x*[mm] on a range of 10[m]. This means that if a phase scanner is being used one can only guess that the accuracy of the scanned object within a range of 0 – 10[m] is less than *x*[mm] and when the range between scanner and object is larger than 10[m] the accuracy will decrease very fast. Knowledge of the exact curves is important for FINP so they are able to decide whether the pulse scanner or a phase scanner is best to use in a certain situation. If the choice between the two types of scanners is not possible, the knowledge of the curves will give insight in expected errors of a certain scan set-up.

To be able to formulate the accuracy curves of the tested scanners, an object will be scanned over a number of distances. These distances will also be measured with a total station because the accuracy of this instrument is known. Now it is possible to find the accuracy-range curves.

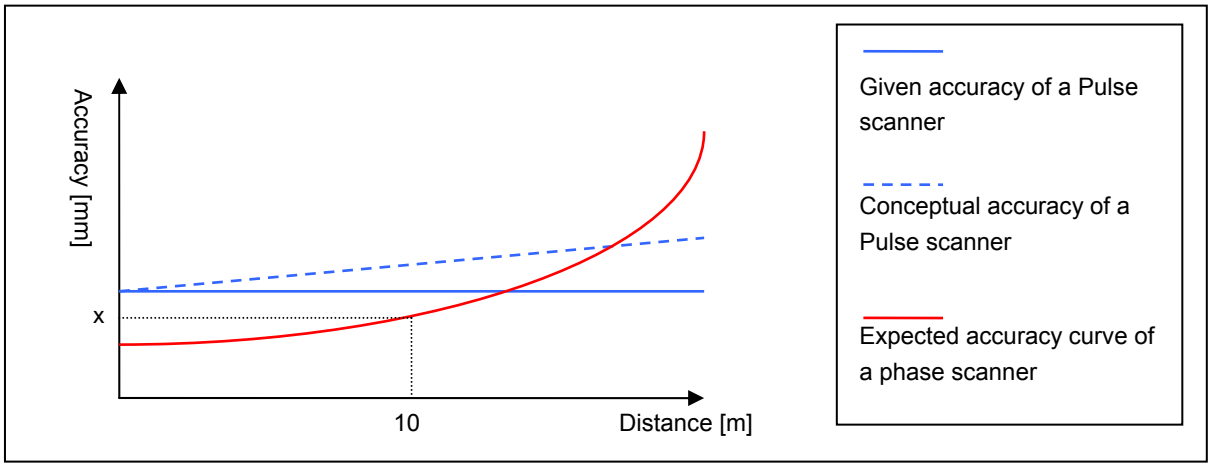

Figure 3.7: the expected accuracy curves of phase and pulse scanners.

3.1.6 Environmental conditions

Like all surveying instruments laser scanners are also sensitive for the environmental conditions like *temperature*, *atmosphere* and *sunshine.* These conditions can have negative influences on the measurements [Boehler et al, 2003].

Temperature

Any scanner will only function properly when it is used in a certain temperature range. Within this range however deviations may be observed, especially in distance measurement. It should be noted that the temperature inside the scanner might be much higher than the temperature of the surroundings, due to internal heating.

Atmosphere

In general only short distances are measured with the two selected laser scanners. The change of the propagation speed of the signal in the atmosphere will therefore not seriously be affecting the results. However, users mentioned that measuring in surroundings with dust and/or steam led to effects similar to the edge effects (see section 3.2.4) [Boehler et al, 2003].

Interfering radiation

Lasers operate in a very limited frequency band. Therefore filters can be applied in the receiving unit allowing only this frequency to reach the receiver. If the radiation of the illumination source (sunlight, lamps) is strong compared to the laser signal, enough of this external radiation will pass the filter and influence the accuracy or prevent any measurements at all.

As this section shows, the environmental conditions can have a negative influence on the test results. Therefore, the influences of these conditions must be eliminated by creating similar conditions during each experiment. This was achieved by performing the experiment in the cellar of a building with climate control, meaning the temperature was approximately 20[°C] in all situations. The interfering radiation of the lights was of no influence because the frequencies of the light and the laser scanner are different. Furthermore, the atmospheric conditions in the cellar are similar to the conditions in closed industrial plants which make the results of the experiments useful for FINP as well.

3.2 Existing experiments

The previous paragraph mentioned a number of known error sources that are interesting to investigate or need to be eliminated from the experiments. Even though not a lot is known about testing laser scanners by means of experiments, a few sources are found that discuss an experiment. In most of these experiments other laser scanners are used then the scanner used in this research (see chapter 2). But to gather some insight in creating experiments, this paragraph will discuss a few of the experiments which are found to be most relevant. Every section of this paragraph contains one experiment and is subdivided into the goal of the experiment, the experiment set-up, the results and a discussion.

The text in the coming 5 sections is based on [Boehler, et al, 2003]. This article evaluates the results of a research project at i3meinz - Institute for Spatial Information and Surveying Technology of the University of Applied Sciences in Mainz, Germany. In this project a number of different experiments were installed that allowed an investigation in the quality of points recorded by laser scanners and the geometric models derived from the scans. The reason for the creation of this test area was to be able to compare the results of different laser scanners with each other as the specifications of the scanners does not make this possible. Table 3.1 shows the list of used laser scanners at i3Meinz[5].

[5] Remark: the test set up does not exist anymore.

Table 3.1: List of tested laser scanners at the test area at i3meinz

Manufacturer	Type	Ranging principle	Range [m]
Callidus Precission Systems	Callidus	Triangulation	1 – 180
Cyra Technologies	Cyrax 2500[(1)]	Time of fight	1.5 – 100
Mensi	S25	Triangulation	1 – 25
Mensi	GS100	Time of flight	2 – 100
Riegl	LMS-Z210	Time of flight	2 – 350
Riegl	LMS-Z420i	Time of flight	2 – 1000
Zoller + Frohlich	IMAGER 5003[(2)]	Phase difference	1 – 53

[(1)] Now known as the LEICA HDS2500

[(2)] Identical to the LEICA HDS4500

3.2.1 Accuracy of the horizontal and vertical angles

As mentioned in paragraph 2.1, a laser scanner sets the direction in which a laser signal is emitted by positioning one or two rotating mirrors. The positions of the mirrors are set inside the scanner and determine the horizontal angle (θ) and the vertical angle (φ) in which the signal is emitted. These angles are used for the computation of the 3D point coordinates in the local coordinate system of the laser scanner.

Goal of the experiment

Any deviation in setting the angles of the mirrors inside the scanner will result in errors perpendicular to the propagation path. Therefore it is important to get insight in the accuracy in which the horizontal and vertical angles are set. This accuracy is now referred to as the angular accuracy of the different scanners.

The experiment set-up

Errors in the setting the angles can be detected by measuring short horizontal and vertical distances between objects which are located at the same distance from the scanner and comparing those two measurements with measurements derived from other surveying methods of which the accuracy is known. The two set-ups that were created will be discussed next.

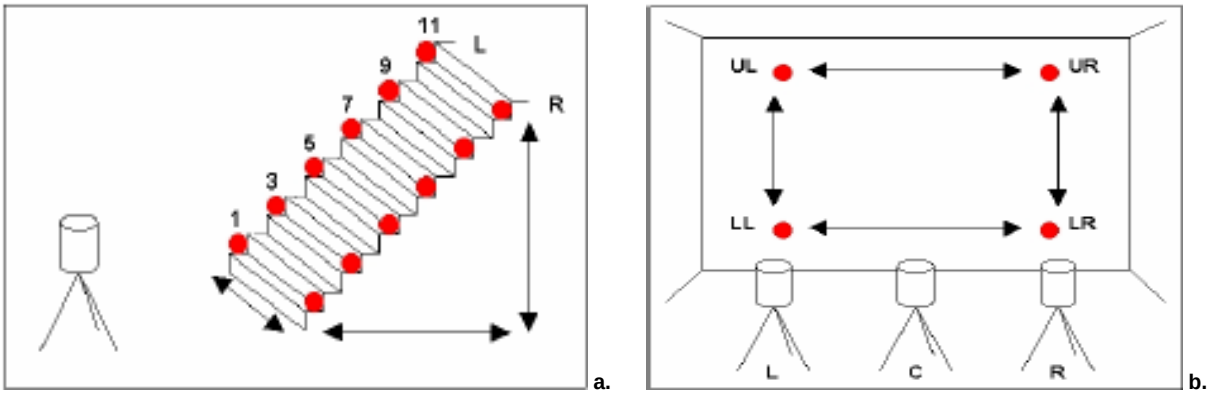

a. **b.**

Figure 3.8: 2 experiment set ups to determine the angular accuracy; **a.** a staircase with 6 spherical objects on each side; **b.** a vertical wall with 4 spherical objects on each corner of a rectangle of 3.5 [m] by 5 [m].

In the first experiment, spherical objects are positioned at either side of six steps of a staircase (see figure 3.8a). This set-up makes it possible to determine six independent short distances in vertical and horizontal direction.

The second test contains four spheres located on a vertical wall on the corners of a rectangle of 3.5[m] by 5[m] (see figure 3.8b). The original positions of the spheres are determined with a total station. The rectangle is scanned from 3 positions, up to a distance of 15 [m]. This again yields in six independent distances in horizontal and vertical direction.

Table 3.2: The results of the angle accuracy experiment done at i3Meinz; standard deviations [mm] of at least 12 independent vertical and 12 independent horizontal distances between two spheres.

Manufacturer	Type	Vert dist.	Horz dist.	Max dist.
Callidus Precision Syst.	Callidus (1)	5.6[a]	4.3[a]	12.2[a]
Callidus Precision Syst.	Callidus (2)	9.9[a]	2.5[a]	18.3[a]
Cyra Technologies	Cyrax2500 (1)	0.8	0.8	1.6
Cyra Technologies	Cyrax2500 (2)	0.5	0.5	1.1
Mensi	S25	3.8[b]	3.4[b]	9.2[b]
Mensi	GS100	1.9	2.3	3.3
Riegl	LMS-Z420i	10.2[a]	16.8[a]	27.1[a]
Riegl	LMS-Z420i	1.7	2.1	4.1
Zoller+Fröhlich	Imager 5003	2.9	7.5	11.1

[a] Because of coarse grid tested for short ranges only!

[b] Influenced by low range accuracy due to triangulation principle at far range.

Results

Each individual distance between the targets is determined by a total station and set as a reference. Next all distances between the targets are determined using the different laser scanners. The determined distances are compared with the reference data which results in the residuals. These residuals are used to obtain the standard deviation of each scanner belonging to the horizontal and vertical distance determination. It can be said that the smaller the standard deviation, the better the angle accuracy of the scanner or in other words, the better the internal 'reading' of the positions of the mirrors. Table 3.2 shows the results of this experiment.

Discussion

The introduction of the experiment set-up mentions that the angular accuracy can be determined when the scan range between two scanned objects is equal. In the set-up that is discussed however, these ranges are not constant.

The vertical distances in the staircase set-up are determined between two objects located on two different stairs of the stair case. This indicates that one object is located in front of the other which means that the scan range between these two objects can never be equal. The horizontal distances can be determined between the two objects of equal range from the scanner if the scanner is located exactly in the middle of the staircase but this is not mentioned in the article.

The distance differences in the second set-up are also dependent on the distance for the situations in which the scanner is located in position L and R. The ranges to the four points on the wall are only equal when the scanner is located exactly perpendicular to the middle point of the created rectangle. Whether this is done for scanner position C is also not mentioned in the article.

It can be concluded that the results as shown in table 3.2 are not independent of the range and therefore they do not only give information on the angular accuracy primarily.

A better method to test the angular accuracy is to locate the scanner perpendicular to the middle point of a rectangle on a wall which is the middle point of other rectangles as well. Figure 3.9 shows this set-up. In this situation three different horizontal and vertical distances can be determined.

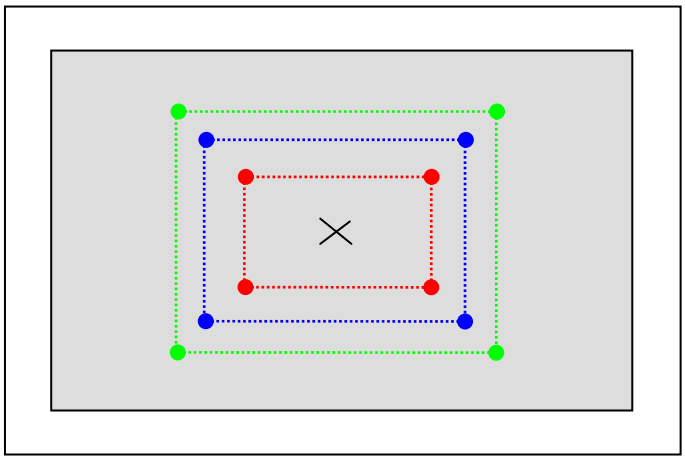

Figure 3.9: An alternative for the angular accuracy determination of different scanners. By locating the scanner perpendicular to middle point of the rectangles (the cross on the wall) the distance between all the points can be determined, resulting is range independent distances.

3.2.2 Range accuracy measurements

The range between the scanner and object is either determined by a triangulation, by the time of flight of a laser pulse or by comparing the phase shift between the emitted and the received signal (see paragraph 2.1). These different ways of determining ranges are suitable in different situations but the exact performances of the different kind of scanners are not known.

Goal of the experiment

In general, the specifications of a scanner do not give the range accuracy as a function of the range/distance. In most specifications, the accuracy of the scanner at one specific distance is given. But because the shape of the accuracy-range curve is unknown, this value does not give any insight in the accuracy of the scanner on other ranges. Therefore and because a lot of different scan ranges are present in a normal scan set-up, it is important to gather insight in the accuracy-range curve. For example: to be able to predict the quality of the measurements in certain situation.

The experiment set-up

Ranging errors can be observed when known distances are measured with a scanner and compared with an instrument of which the accuracy is known. But as the examined scanners are not equipped with a defined reference point, such as forced centring, it is only possible to measure range differences between targets or objects. The advantage of working with the range differences is that systematic errors will be eliminated.

The following three experiments are combined in one set up with the eventual goal to compare the obtained range differences with the ground truth data, determined with a total station.

1. In a long corridor the long-range performance of the scanners will be determined by using the staircase set-up shown in figure 3.8a of the previous section. This staircase will be scanned from a range up to 50[m]. The horizontal components in range direction are used to form six independent distances.
2. To determine the middle-range performance of the scanners spheres are placed on well known locations in the same corridor. This will result in four independent range differences at distances of 10 – 40[m].
3. The close range (3 – 8[m]) performance will be examined by using a sphere placed on an interferometric comparator. The sphere was moved into six positions with spacing of 1[m]. This resulted in another three independent range differences.

Besides the above mentioned experiment, an experiment is created to measure the noise of the scanned data at different ranges. The noise (= random error) can easily be checked by calculating the average plane through the scan of a scanned planar object, followed by the determination of the standard deviation of the residuals.

For the creation of this experiment, three different plates are used and these are scanned at different ranges. The plates that are used are:

- a white plate with a reflectivity of 80%;
- a grey plate with a reflectivity of 40%;
- a black plate with a reflectivity of 8%.

Results

Each individual range difference between two targets is determined by a total station and set as a reference. Next, all range differences are determined with the different laser scanners. The comparison of the scanned ranges with the total station ranges will result in the residuals per scan difference. These residuals will be used to obtain the standard deviation of each scanner of at least 12 independent distances in short range and 14 independent distances in the far range. Table 3.3 shows the results of this experiment.

The results shown in figure 3.10 belong to the noise determination and the curves represent the standard deviations of the single points based on the grey surface (reflectivity 40%).

Table 3.3: Standard deviations [mm] of differences between known and scanned range differences.

Manufacturer	Type	Close (<10 [m])	Far (10 – 50 [m])	Max. diff
Callidus Precision Syst.	Callidus (1)	1.5	- [a]	2.6
Callidus Precision Syst.	Callidus (2)	2.8	- [a]	5.9
Cyra Technologies	Cyrax2500 (1)	0.6	1.1	2.3
Cyra Technologies	Cyrax2500 (2)	0.4	0.5	0.9
Mensi	S25	1.4 [b]	4.6 [c]	7.7
Mensi	GS100	2.6	2.0	8.2
Riegl	LMS-Z420i	19.7	- [a]	40.4
Riegl	LMS-Z420i	2.6	2.7 [d]	5.9
Zoller+Fröhlich	Imager 5003	1.6	0.7 [e]	12.3

[a] Modeling of spheres not possible for far ranges due to coarse grid
[b] But 0.2 [mm] at 4 [m] range and 0.5 [mm] at 6 [m] range
[c] at 22 [m] range
[d] only 4 measurements in far range
[e] only 2 measurements in far range

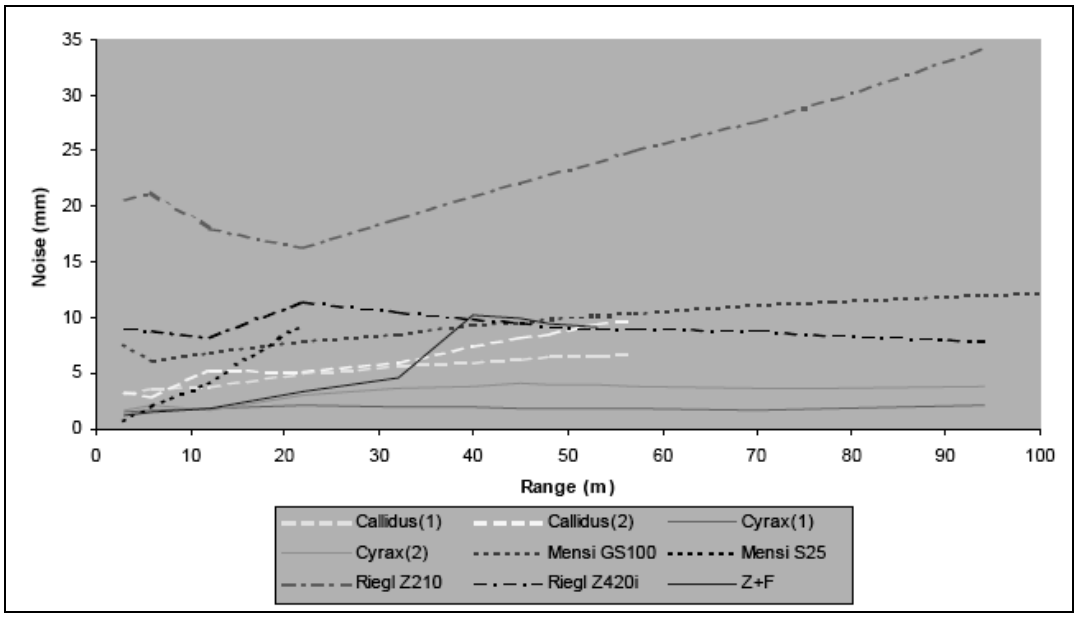

Figure 3.10: Results for measuring the noise in range direction (std. dev. for a single point) for different scanners on a grey surface with a reflectivity of 40%.

Discussion

The idea behind this experiment is understandable and the set-up is correct but the question is whether it is valid to compare the different kind of laser scanners with each other. It is known that triangulation scanners perform best on ranges between 0 – 10[m]. Therefore it is not valid to compare them with a pulse scanner on larger distances as the last one will perform much better in this situation.

It is better to make a comparison of the results of the same kind of scanners, so it can easily be seen which pulse scanner, triangulation scanner or phase shift scanner is best in their class with respect to the scan range.

However, the experiments at i3-Meinz are done with a practical point of view. This means that the results must give information on which scanner is best to use in a certain situation. In other words, when someone has an application in mind, the results will be used to find the 'best' scanner for this application. The experiment described in this section can indeed be used for this purpose.

3.2.3 Resolution determination

The resolution describes the ability to detect small objects or object parts in the scans. As mentioned in paragraph 3.1.3 two different laser scanner parameters contribute to this ability: the smallest possible increment between two successive scanned points and the size of the laser spot on the object.

Goal of the experiment

Since values for increments and spot sizes in the specifications do not give much indication about the ability of a scanner to reach a certain resolution, the practical experiment discussed in this section is created in order to achieve comparable resolution information for each scanner.

Experiment set-up

A box of 300[mm] x 300[mm] which consists of two panels is used to determine the resolution (see figure 3.11). The front panel has slots of about 30[mm] wide at the outside and becoming smaller towards the centre of the panel. The second panel is placed 55[mm] behind the first panel.

If a scanner has a high resolution there must be reflections from both the front and the back of the panel. The higher the resolution the closer the measured points on the back panel reach the centre of the box. The target is used to detect the resolution information from different scan ranges.

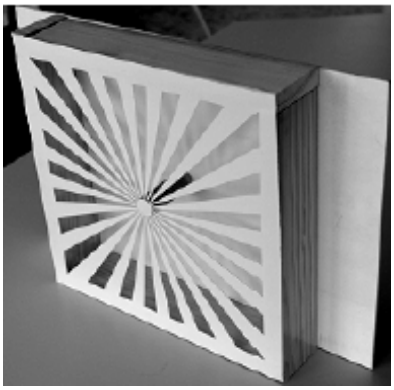

Figure 3.11: Box with slots varying in width towards the center, used to determine the resolution of different scanners.

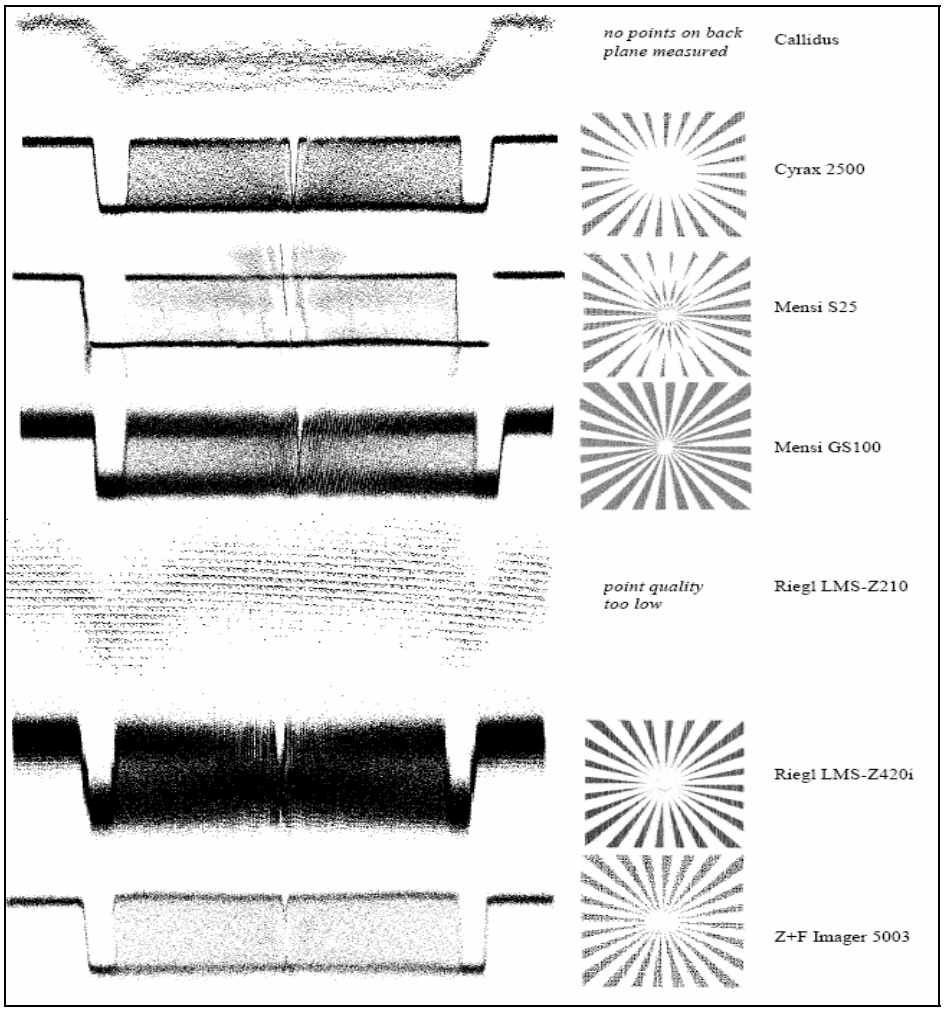

Figure 3.12: The results of the resolution test using the target shown in figure 3.9, left a cross section of the scan is shown; right the scanner points on the back panel are shown.

Results

Figure 3.12 shows the results of scanning the above mentioned box at a scan range of 6[m]. From this figure it follows that the scans obtained with the Mensi GS100 shows the best results with respect to the resolution test at a scan range of 6[m]. The test is also done with a scan range of 22[m] and here the scans obtained with the Cyrex 2500 show the best results with respect to the resolution test [Boehler, et al, 2003].

Discussion

The object used in this experiment indeed allows investigation in the resolution features of the laser scanners. However, it only makes a comparison of the resolution features possible. This means that no absolute value for the resolution (footprint size or angles of increment) is determined. In the future it is therefore only possible to compare the resolution features of other laser scanners with these laser scanners if they also scanned the object of figure 3.11.

3.2.4 Edge effect measurements

While hitting an edge of a surface, only a part of the laser signal will be reflected on the edge of the surface. The rest of the signal continues and will be reflected on the object behind the first object, or if there is no object behind the first object it will not be reflected at all. This effect is caused by the size of the footprint of a laser signal. A schematic overview of this situation is shown in figure 3.13.

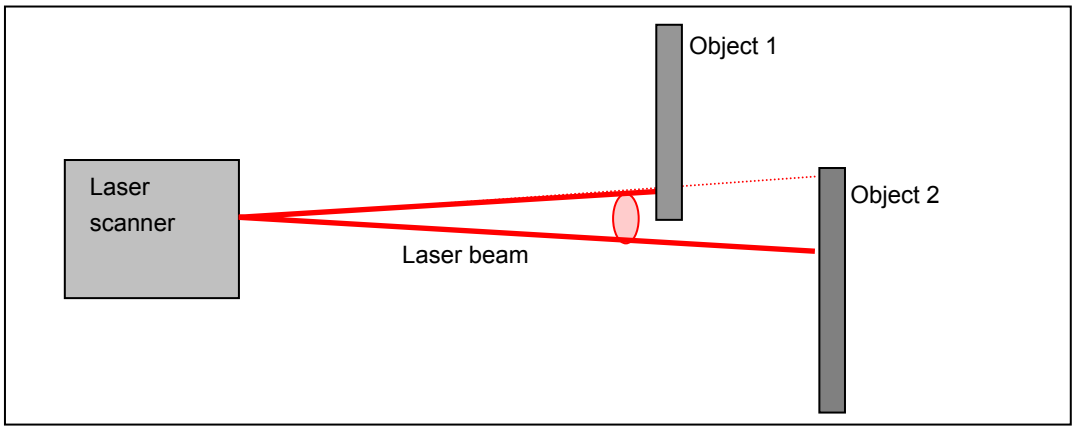

Figure 3.13: The edge effect that can occur by using a laser scanner, the laser signal will be reflected on both the first and the second object due to the footprint size of the laser signal.

Goal of the experiment

Since a laser signal cannot be focused to one point exactly, edge effects will always occur; no matter with scanner is used. However, it can be assumed that the influences of the edge effects will be less significant when a better focused laser scanner is used. Goal of this test is to see how well focused the laser signals of the different scanners are. This result can help a user to decide which scanner is best to use if a scan area contains a lot of (small) objects that are standing in front of each other.

Experiment set-up

Figure 3.14a shows the object that is used in this experiment. This board is placed at a sky background so the measurement of the outer edges will not be influenced by any objects behind the board. The small plate in front of the board is used to simulate the effects that occur when two objects are located in front of each other.

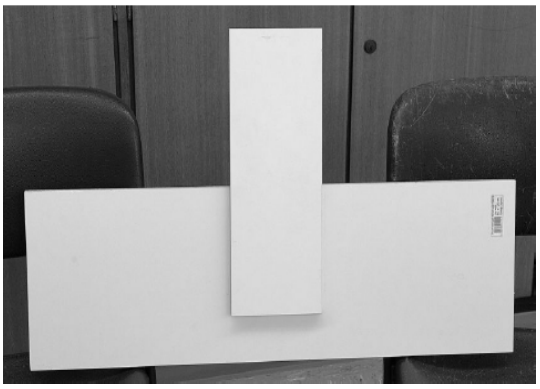
a.

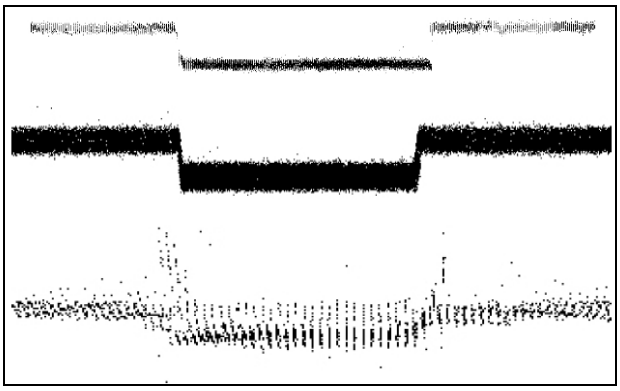
b.

Figure 3.14: **a.;** The plate used at i3meinz to research the edge effects. **b.;** examples of possible edge qualities with at the top the highest quality (not achieved with any tested scanner), in the middle the average quality and on the bottom an example of a low quality.

Results

Figure 3.14b shows three examples of scans that can be obtained with the different scanners. These three examples are set as possible edge qualities. The top scan from this figure will be achieved if the edge quality inside the scan is high. This situation is not achieved with any of the tested scanners. The middle and lower scans show situations of average and low quality respectively. The results achieved with the test are shown in Table 3.4. Note: the distance between scanner and the board belonging with the shown results is not mentioned in the article.

Table 3.4: results after evaluation of the edge quality of the different scanners.

Manufacturer	**Type**	**Edge quality**
Callidus Precision Syst.	Callidus (1)	low
Cyra Technologies	Cyrax2500 (1)	average
Mensi	S25	average
Mensi	GS100	average
Riegl	LMS-Z420i	low
Riegl	LMS-Z420i	average
Zoller+Fröhlich	Imager 5003	low

Discussion

This experiment also only allows a relative comparison of the results. However, the results of this experiment do show that the edge effects are present in all scans obtained and do effect the quality of the scans. Therefore, it is wise to eliminate the edge effects from the object of interest in experiments that research other features because they will influence the results of other experiments.

The article does not show the scans obtained during this experiment. However, these scans might be interesting in order to find out which part of the returning waveform is used as a measurement. Examples are: the first received echo, the last received echo or the mean of all received echoes. Insight in which part is used for the

distance measurements is important because it can be assumed that these measurements determine the influence of the edge effects in the scans. Further research on this topic can be recommended.

3.2.5 Testing the influence of the surface reflectivity

The measured intensity is influenced (among other facts like distance, atmospheric conditions, angle of incidence) by the reflectivity features of the scanned surface. For example, white surfaces will yield in stronger reflection than black objects. The effects of coloured surfaces depend on the wavelength of the laser light (green, red, near infra red).

Goal of the experiment

Experience has shown that scanning surfaces of different reflectivity characteristics result in systematic range errors. This can lead to serious errors if objects consisting of different materials and/or different colours are scanned. The only way to avoid these problems is to coat the object with a unique material, but this is almost never possible. Gathering insight in the performance of different laser scanners on different materials and/or different colours can be used to determine which errors can be expected in a scan area and whether coating is necessary.

Experiment set-up

The board shown in figure 3.15 is used for this experiment. It contains of a wide white frame and two square parts in which coatings from different materials and colours can be placed.

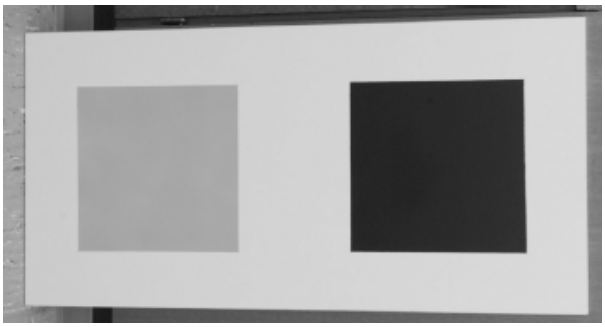

Figure 3.15: the board used for reflectivity testing containing of a white frame and different surface coatings.

After scanning the board, separate planes will be modelled through the coatings and the white plate. The edges are excluded in order to eliminate the edge effects. The computed range differences between the planes are used to indicate the error that can be expected in similar situations. The following colours and materials are used in this experiment:

- White dull spray paint, reflectivity of 90%
- White dull spray paint, reflectivity of 80%,
- Grey dull spray paint, reflectivity 40%,
- Black dull spray paint, reflectivity 8%,
- Spray paint with metallic appearance,
- Polished aluminium foil,
- Blue retro foil, used as Cyrax targets.

Results

The results of this experiment are shown in table 3.5. The white frame of the plate is set as a reference. Table 3.5 shows the difference between the computed ranges of the different coatings and the reference plane. If the sign in the table is positive this means that the distance to the coating is determined too short compared to the white surface.

Discussion

The experiment discussed in this section is assumed to be a representative experiment for the examination of the effect of different reflectivity features on the performance of laser scanners. Additional information on the accuracy in which the reference white frame is scanned will make the computed results absolute and that will increase the quality of the experiment.

Table 3.5: distance corrections in [mm] due to different surface materials.

Type	White 90%	White 80%	Grey 40%	Black 8%	Metal paint	Aluminium foil	Blue foil
Callidus (1)	0	0	0	0	0	0..-100	+7
Callidus (2)	0	0	+4	+3	0..-10	0..-15	+5
Cyrax2500 (1)	0	0	0	0	0	0..+10	+22
Cyrax2500 (2)	0	0	0	0	0	0	+17
S25	0	0	0	0	0	0	0
GS100	0	0	0	+8	0	0	n.a.[a]
LMS-Z420i	0	0	+13	+3	0..-100	0..-250	0
LMS-Z420i	0	0	0	0	0	0	0
Imager 5003	0	0	0	0	0	0..+30	-18 [m]

[a] Scanner did not record any points on this surface

3.2.6 Testing laser scanners on surfaces with a known colour

The text in this section is based on [Clark and Robson, 2004]. This article discusses accuracy measurements made with a Cyrax 2500 scanner against surfaces of known colours. The Cyrax 2500 is a pulse scanner and currently known as the HDS 2500 by Leica Geosystems.

Goal of the experiment

Experience has shown that materials with different colours and textures produce scans of varying quality. The quality of the scan with respect to the colour of a surface is tested using a GretagMacbeth ColourChecker chart (see figure 3.16b). Normally this chart is manufactured to provide a standard set of colour patches with known spectral reflectance for the photographic industry. For the test purposes of this experiment the chart is adhered to a planar surface to provide a planar object suitable for scanning.

The key aims of this experiment are the following:

- to investigate any variation in data distribution and noise for each colour patch
- to investigate any variation in data distribution and noise after rotating the patch
- to investigate any changes in range for each colour patch and to attempt to link these to the scanner output giving a measure of the intensity of the return signal.

The test set-up

The experiments are divided into three groups, i.e.:

1. a close range set where chart rotation and translation are carefully controlled,
2. a near range set where only the translation is varied, and
3. a long range set scanned outside.

For the close and near range sets, the scanner was mounted on an optical rail. Figure 3.16a shows a sketch of the experiment.

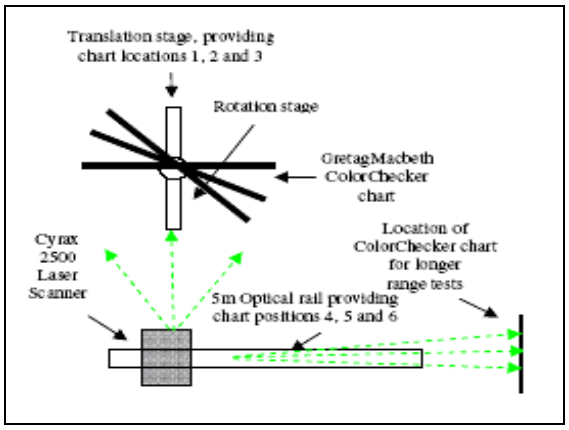

a.

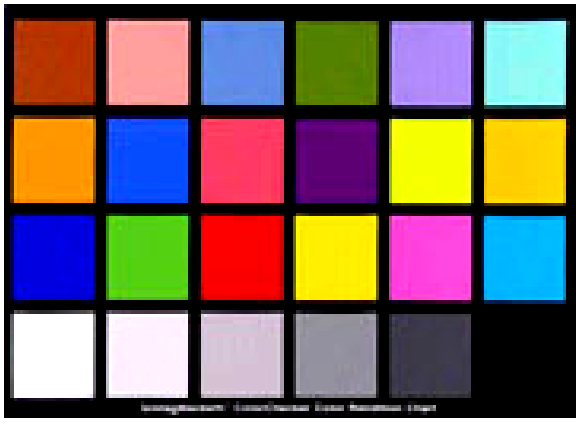

b.

Figure 3.16: a sketch of the experiment set-up (**a.**) used for testing laser scanners on a surface with a known colour. **b.;** the GretagMacbeth ColourChecker chart that is used during this experiment (source: GretagMacbeth, 2006).

During the experiment in the close range set, the distance between the scanner and colour chart are varied (positions 1 – 3). On each position scans are made with the scanner perpendicular to the colour chart and with a rotation of the chart with known scan angles of 20, 40 and 60[°]. During the near range measurements, the scanner itself is rotated by 90[°] and the colour chart is scanned at three more distances (positions: 4 – 6). Rotation measurements are not done in this step.

The long range measurements are done outside so these scans are not made in such stable conditions as the previous discussed scans. Still the results of scanning on a longer distance (positions 7 – 8) are considered valuable.

After scanning, each scan of the ColourChecker chart is divided into small point sets representing one colour patch each. Next the central area of the colour patches is selected to eliminate the boundary points because these points might contain mixed information of both the colour patch and the surroundings. By eliminating the edges, the test concentrates on the colour information only and this is the goal of the experiment.

Next, a Least Squares adjustment is applied to determine the best fitting plane (LSQ-plane) through the points of each patch. This LSQ-plane is used to determine the distance between the scanner and the colour patch and the residuals. The residuals are computed by subtracting the original points from the LSQ-plane. These residuals are used to create a series of histograms that indicate the distribution and the quality of the points in one single chart. This process is done for all the patches from the bottom two rows of the ColourChecker chart (figure 3.16b) and all eight scan ranges.

Results

The computed standard deviation of each individual colour patch is found out to be in the order of 2 – 3[mm]. But the distance between each colour patch and the scanner is also determined, using the LSQ-plane per colour

patch. These distances are compared with the LSQ-plane through the entire chart (which is set as a reference). The result is shown in figure 3.17. This figure shows that the computed scan range between the scanner to the LSQ-plane of the white chart (lower left corner) is smaller than the computed scan range to the LSQ-plane of the black chart (lower right corner).

The maximum observed difference in range between the black and white patch is 12[mm]. These 12[mm] are beyond the accuracies the manufacturer gives for single point, linear and range measurements. Therefore it can be concluded that the surface reflectivity might have significant implications for the precision of scanning projects.

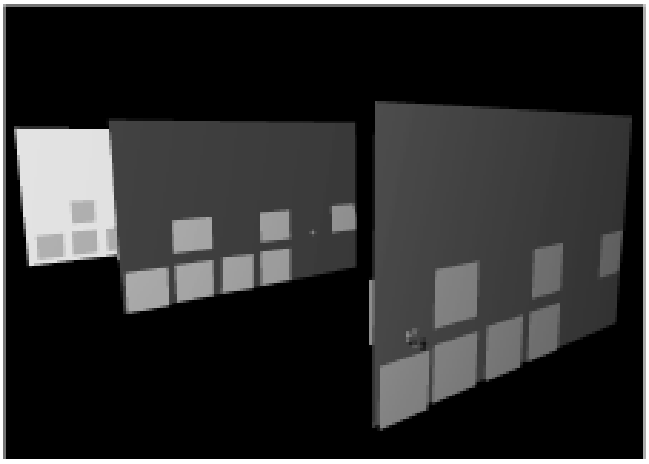

Figure 3.17: the determined scan ranges of the mean chart and the small colour patches at the scan position 1 – 3.

The residuals are used to create histograms of all colour patches. These histograms give an indication of the spread of the data and therefore allow any discrepancies in the data between experimental conditions to be detected. All histograms of the patches scanned with the chart oriented perpendicular to the scanner showed very little variation. The standard deviation in all cases is between 2 – 3[mm], with minima and maxima of up to 12[mm] for each individual colour patch.

LSQ-planes and residuals are also created for the scans that represent the rotated colour patches. The created histograms show that the area under the curve decreases if the scan angle is increased. This means that less data points are collected when the object is scanned with an angle, this is as expected. The histograms also show that the normal distributions become narrower when the angle increases, which means that the standard deviations decrease. However it should be noted that although the histograms for the chart scanned at 60[°] exhibit the narrowest distribution, the density of points captured is noticeable reduced. Therefore it is concluded that the best scan angle to scan a matt surface with is an angle between 20 and 40[°]. These scan angle produce the optimal scan with a reduced proportion of noise compared to an object scanned with a scan angle of [°].

Discussion

The experiment described in this section combines different kind of features that can influence a laser measurement. The features that are tested are:

1. the influence of the scan angle,
2. the influence of the scan range,
3. the influence of the surface reflectivity and colours.

However, it might be better not to combine all these features in one experiment but create three or four different experiments that examine one or two of these features each. The main advantage is that it keeps the influences of the different features separate and this makes them easier to investigate. However, the general idea behind this experiment is assumed to be one of the most interesting and it contains information on un-investigated influences in terrestrial laser scanning. Therefore the main principles will be used in the experiments done for this research.

4 Methods of analysis

One of the main goals of this thesis is to create a practical set-up in which different experiments can and will be implemented. Eventually, each experiment will result in a number of scans which will be used to analyze and compare the performances of two laser scanners; the IMAGER 5003 and the FARO LS 880. Four experiments are implemented in the practical set-up and they will be discussed in the chapters 5 – 8 of this thesis. It concerns the following four experiments; (1) a scan angle experiment, (2) a colour experiment, (3) a reflectivity experiment and (4) a range experiment.

But before these experiments will be discussed, this chapter describes the chosen practical set-up that is set as the base for the experiments (paragraph 1). This paragraph also outlines the chosen settings of the laser scanner and the general characteristics an experiment set-up should fulfil. In order to eliminate the external effects, the object of interest needs to be selected from the scans. This will be discussed in paragraph 2 of this chapter.

Paragraphs 3 – 7 of this chapter outline the methods of analysis that are used in order to make the results of both scanners comparable. The following analysing features are discussed:

1. the resolution of the scan,
2. the intensity values,
3. the reliability and precision of the scans obtained.

First an explanation is given on how to compare the resolution in which an object is scanned to the resolution that can be expected from the specifications in paragraph 4.3. Paragraph 4.4 describes the method used to determine the mean intensity values of the scanned objects and how these values can be compared between two scans obtained with the different laser scanners.

Because all experiments contain an object of interest that is planar, a least square plane (LSQ-plane) is fitted through the points of the scans obtained. Therefore, paragraph 4.5 will discuss the theory of the Least Squares and paragraph 4.6 handles the theory of plane equations and the resulting model of observation equations for the LSQ-plane. In order to determine the reliability and precision parameters of the scans obtained, the LSQ-plane will be used. The method of analysis with respect to the precision and the reliability will be discussed in paragraph 4.7.

4.1 The created practical set-up

A laser scanner in general allows different settings. Most of these settings are closely connected to the resolution of the scans obtained. Because of the different possibilities in settings, it is impossible to compare the performances of the two laser scanners using all possible combinations of settings. Therefore, a selection of tested settings is made by forehand. Section 4.1.1 of this paragraph will give a summation of the *general laser scanner settings* used in the experiments.

Besides limiting the possible settings of the scanner, some other standards are chosen as well. To limit the possible experiments that can be created, a practical set-up is designed. This set-up is used as a base for most of the preformed experiments. Section 4.1.2 discusses the *practical set-up.*

Laser scanning in general is used to retrieve scans of the full 360[°] around the scanner. But the experiments discussed in this thesis only focus on one object. Therefore, it will save a lot of scan time if only the

surroundings of the object of interest will be scanned instead of the full 360[º]. Section 4.1.3 will discuss the settings with respect to the *selected scan areas*.

4.1.1 Chosen settings of the laser scanners

It is found out that changing the resolution setting is most common in laser scanning. Therefore, the only setting that will be changed during this research is with respect to the resolution. The following two resolution settings are chosen and used in all the performed experiments:

1. the standard resolution according to the manufacturer,
2. the second highest resolution.

The standard resolution is chosen because the manufacturers promise that scanning with this resolution will result in a scan of which the accuracy is high enough in most common situations. The main advantages of working with the standard resolution are that the scan time is relatively short and the file sizes of the scans are reasonably small.

However, when a project demands a more accurate result, a higher scan resolution is required. During this research the second highest resolution will be examined as well. The reason for not taking the highest resolution into account is because scanning with this resolution is very time consuming and the file sizes (scans) are too big to process on an average computer. Because of these disadvantages, it would be non-representative to select and use this resolution as no company will use these settings for a full 360[°] scan.

The highest resolution is common to scan the targets which are used for registering multiple scans. It can be assumed that more scan points result in a more accurate position determination of the targets. However, registering is not a part of this research which is another reason for not including the highest resolution in this thesis.

The above mentioned resolution settings of the two selected phase shift scanners differ from each other. Table 4.1 gives an overview of these settings and their main differences.

Table 4.1: a list of chosen settings of the IMAGER 5003 and FARO LS 880 (sources: FARO, 2006 and Zoller + Fröhlich, 2006).

	IMAGER 5003		**FARO LS 880 HE 80**	
Resolution	**Middle**	**Second highest**	**Middle**	**Second highest**
Name Resolution Manufacturer	*Medium*	*High*	*1/5*	*1/2*
# points per 360[º]	5,000	10,000	8,000	20,000
Horz. and vert. angle increments	0.072º	0.036º	0.045º	0.018º
Expected file size full scan (MB)	327	1191	104	652

4.1.2 The created practical basis set-up

Besides the possibility to change the settings of a laser scanner, it is also possible to create al lot of interesting experiments to test the laser scanner. To reduce the number of possibilities, a basis set-up is formed. This set-up needs to fulfil at least the following three demands:

1. it needs to be easy to create,
2. it needs to be re-creatable,
3. it needs to eliminate parameters that are not examined in that particular experiment.

Ad 3.
Elimination of these parameters is necessary to prevent them from influencing the results.

Figure 4.1a gives a schematic top view of the created practical basis set-up and 4.1b shows a picture of the set-up taken during one of the experiments. It can be seen in this figure that the basis set-up consists of a position of the scanner and a position for the object, about 4[m] from the scanner. The distance between the scanner and the object cannot be set at 4[m] exactly because the two scanners do not allow forced centring and the middle points of the scanners are not exactly known either. Therefore it is not possible to centre the scanners above a known point.

The object is an 800[mm] x 400[mm] x 90[mm] (length x width x height) wooden white plate. This plate is used in all experiments as object of interest or as background plate. A white plate is chosen because white has a high reflectivity.

The plate is pinched inside an angle measurement device which is mounted on a tripod. The plate can now be rotated if this is required in the experiment.

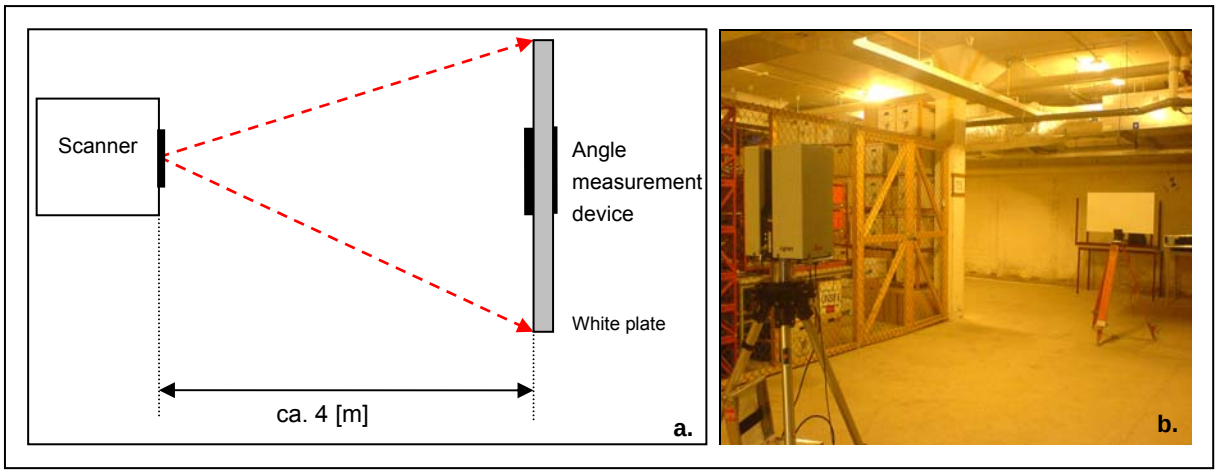

Figure 4.1: the basis set-up used for the experiments, **a.**; the schematic top view of the basis set-up. **b.**; a picture of the basis set-up taken during the experiments with the HDS 4500 (photo: Van Ree, 29-03-2006).

The basis set-up as shown in figure 4.1 eliminates the influences of the *range* because the distance between scanner and object is set constant. The *influence of the environment/surroundings* is also eliminated in this set-up because the room in which all the experiments are done is the same and the environmental conditions in this room are constant as well, because of climate control.

4.1.3 Selected scan area

It can be seen in figure 4.1 that during most of the experiments the scanner will be placed approximately 4[m] from the object of interest. Furthermore, the scanner will not be moved during an experiment. Therefore, it can be assumed that the basis situation of the experiment will not change, apart from the rotation of the plate in the measurement device if this is required during that experiment. With this assumption and the possibility to select a smaller scan area in the software of the laser scanners, it is possible to scan only the part of the scan area in which the object of interest is located instead of the entire 360[°]. This will save a lot of time and will also result in smaller file sizes that are easier to process on a computer.

To control whether the scanner does not move, five paper targets are placed in the surroundings of the position of the scanner. These five targets need to be visible in the first scan and the last scan obtained during one experiment. By registering these two scans, a change in the position of the scanner can be noticed. If a change in the position of the scanner occurs, the experiment needs to be repeated as the scans obtained, refer to different and unknown positions of the scanner which makes comparison of them impossible.

This was done for all experiments and no significant movements of the scanner and the plate were detected between the first and last scan. This means that the scans obtained can be used in the analysing phase of this research.

4.2 Interior selection of the object from the scan

Only the surroundings containing the object of interest are scanned during the experiments because this result in reduction of both the scan time and the file sizes. But scanning only a part of the entire 360[°] still results in a lot of redundant information in the scans obtained. To eliminate this redundant information, the object of interest is 'cut' from the original scan. Section 4.2.1 of this paragraph discusses the selection of the object from the obtained scan.

The resulting scan points represent the object of interest only. But in this 'new' scan external information like edge effects are still present. Furthermore, over 150 scans are obtained during this research. By making an *interior selection* of the object the external influences of the edge effects will be eliminated and the calculation time for the analysis will be reduced significantly. Section 4.2.2 discusses the automatic interior selection. Remark: all objects of interest in this research are plates so the interior selection is based on this feature.

4.2.1 Selection of the object of interest

Each created experiment is focusing on one object and all objects of interest in the experiments are plates. It is required to cut these planar objects from the scans in order to make it possible and easier to analyze the data. Figure 4.2a shows a part of the scan before selecting the object.

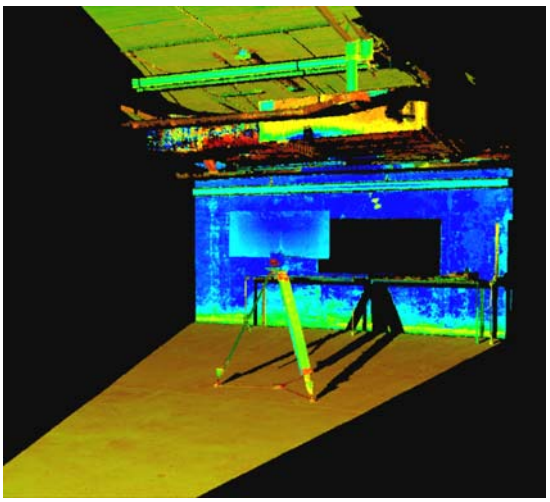
a.

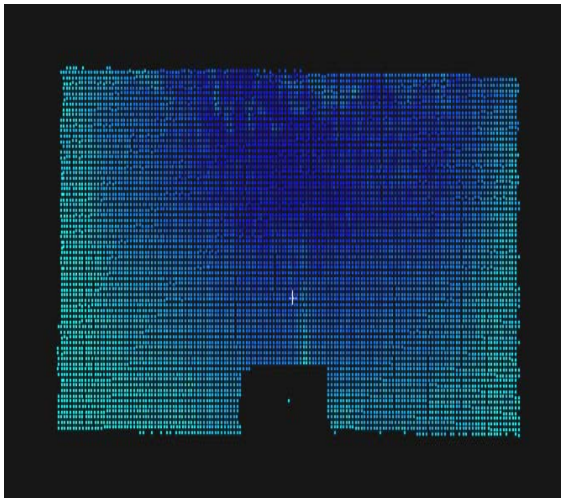
b.

Figure 4.2: an obtained scan during the scan angle experiment with the IMAGER 5003. **a.**; the original scan, before selecting the object, **b.**; the resulting scan after selecting the object from the original dataset and deleting all the surrounding points.

It can be seen that the object of interest is easy to identify in the scan. The object is selected manually using the possibilities of the software package "Cyclone". Selecting the objects in this software program is easy and quick and the resulting scan of the white plate is shown in figure 4.2b.

4.2.2 Selection of the interior of the object

Because over 150 scans are obtained during this research and because the edge effects are still present in the scans, even after the selection of the object (see section 4.2.1) from the original scan, the interior of the object is selected and used for the analysis.

The influence of edge effects is discussed in section 3.2.4 of this thesis and they can be avoided by selecting the interior of the object. But the main advantage of selecting the interior is the decreasing file sizes because this results in shorter processing times during the analysing phase of this research, which is of importance because of the amount of scans obtained.

A Matlab program is created to automatically select the interior of the object of interest (see Appendix VI). In order to find the interior, the dataset needs to be transformed into spherical coordinates first.

Transformation from Cartesian to spherical coordinates

The output file retrieved with both laser scanners consists of x, y, z-coordinates and an intensity value per scanned point. This means that the locations of the points are represented by a Cartesian coordinate system. However, the x, y, z-values are not determined by the laser scanner itself.

As section 2.1.1 already mentioned, the laser scanner emits laser signals by defined angles of increments. Every emitted laser signal is used to determine the distance between scanner and object. This means that the direction in which the laser signal is emitted and the measured distance determine the position of the scanned point. In other words: the position is determined in a spherical coordinate system. After scanning the points, the laser scanner or its software transforms the measured spherical coordinates into Cartesian coordinates.

Cartesian coordinate system

A Cartesian coordinate system is an orthogonal coordinate system. This means that every dimension is represented by an axis and all the axes are orthogonal to each other. The scale factor of each axis is constant over the entire system. Cartesian coordinate systems are the most commonly used systems because they describe geometric shapes such as curves the best.

In this thesis only 3D coordinate systems are used, they consist of 3 orthogonal axes and provide the 3 physical dimensions of space; length (x), width (y) and height (z). Figure 4.3a shows a point P in a Cartesian coordinate system [Mathworld, 2006a].

Spherical coordinate system

Spherical coordinates, also called spherical polar coordinates, are a system of curvilinear coordinates that are natural for describing positions on a sphere or spheroid. The first coordinate is the distance between the systems origin and point P. The second and third coordinates are the two angles (θ, φ). The angle θ is used to express the angle between line OP and the x-axis of a Cartesian coordinate system and the angle φ is used to express the angle between line OP and the z-axis of a Cartesian coordinate system (see figure 4.3b) [Mathworld, 2006c].

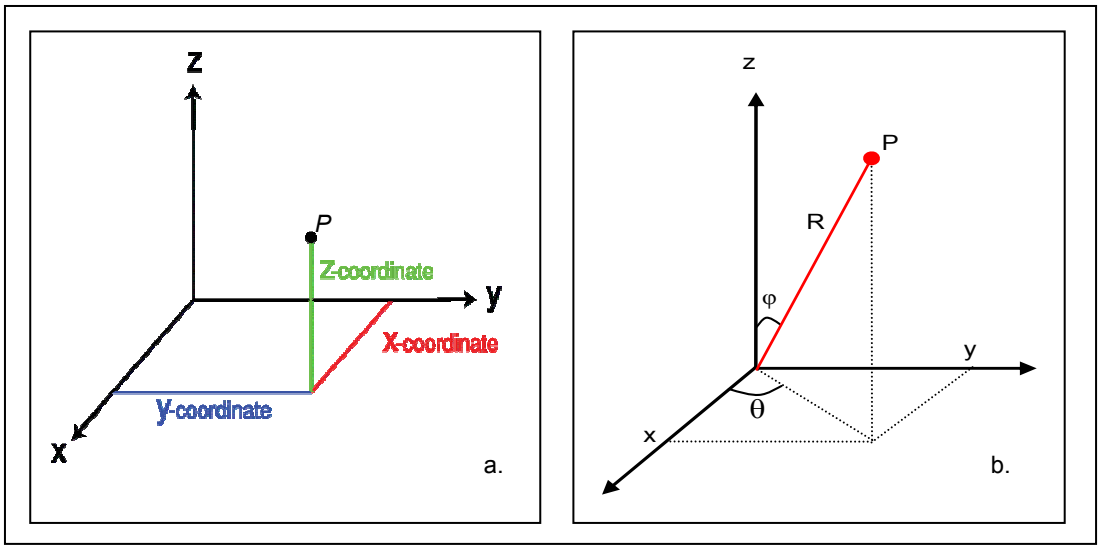

Figure 4.3: representations of a Cartesian coordinate system (**a.**) and a spherical coordinate system (**b.**).

Transformation formulas

The relation between Cartesian and spherical coordinates can be seen in figure 4.3b. The following formulas can be used to transform a Cartesian dataset (x,y,z) to a spherical coordinate system (R,θ,φ) and the other way around [Mathworld, 2006c].

From Cartesian to spherical coordinates:

$$R = \sqrt{x^2 + y^2 + z^2}$$
$$\theta = \arctan(\frac{y}{x}) \qquad (4.1)$$
$$\varphi = \arctan(\frac{\sqrt{x^2 + y^2}}{z})$$

From spherical to Cartesian coordinates:

$$x = R \cdot \cos(\theta) \cdot \sin(\varphi)$$
$$y = R \cdot \sin(\theta) \cdot \sin(\varphi) \qquad (4.2)$$
$$z = R \cdot \cos(\varphi)$$

Transferring the 3D-coordinates of the scans obtained to the spherical coordinates (θ, φ, R) using the formulas of 4.1 results in a matrix shaped dataset which consists of lines and columns of approximate equal spacing (see figure 4.4). This is the desired result that will be used in the following step to select the interior of the scanned object.

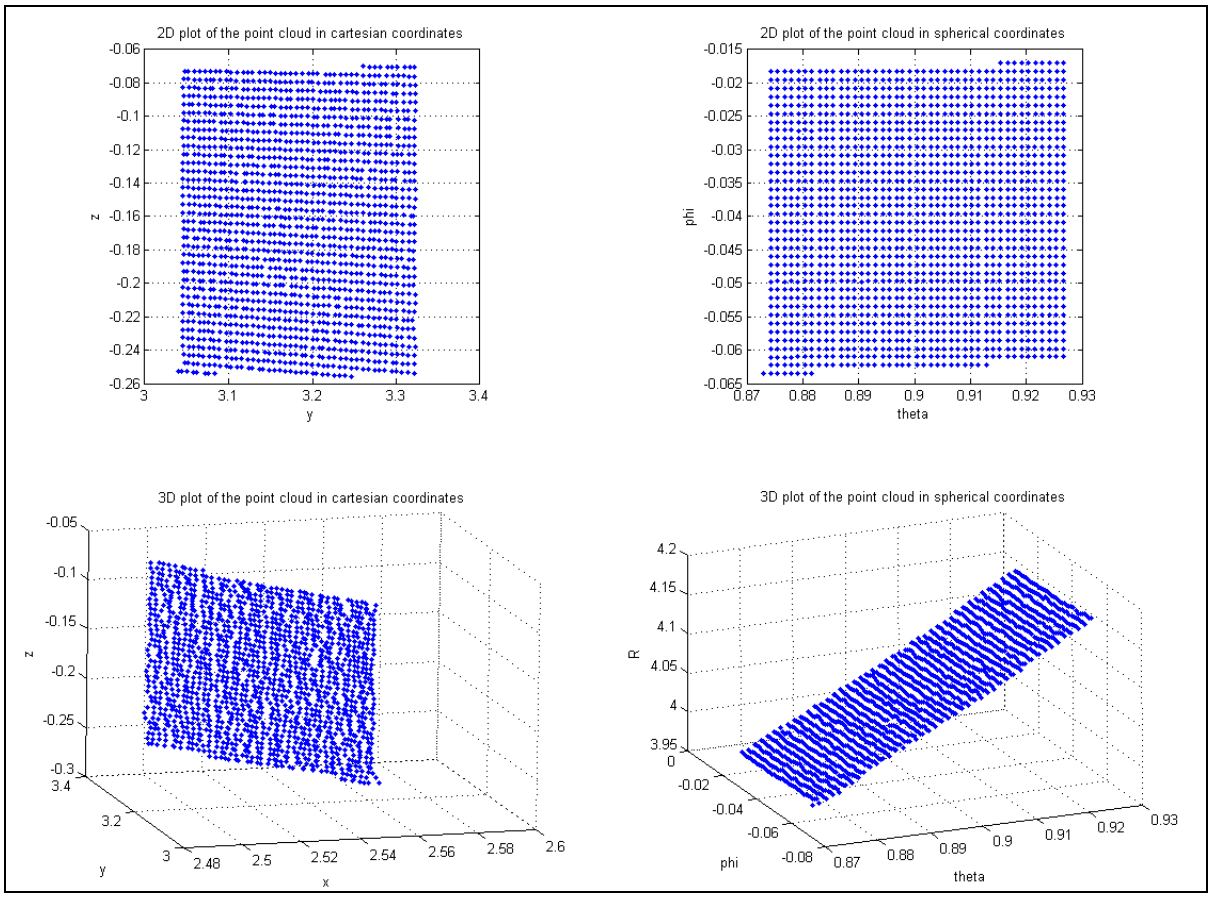

Figure 4.4: 4 plots of the same scan, *upper left;* a 2D plot of the obtained scan in Cartesian coordinates, *upper right;* the 2D result after transforming the scan from a Cartesian coordinate to a spherical coordinate system, *lower left;* 3D visualization of the scan in an Cartesian coordinate system and at the *lower right;* the 3D visualization of the obtained scan in the spherical coordinate system after transformation.

Automatic interior selection

After the manual selection of the object of interest and the transformation to spherical coordinates, the scans of both the IMAGER 5003 and the FARO LS 880 are represented by a number of scan points that are close to a regular grid. However, small variations are still present and this makes it impossible to use the scan for the interior selection immediately (see figure 4.4).

The following steps are done in order to create an automatic interior selection of the object of interest from the scans obtained:

1. A regular grid is fitted through the scan points.
2. The coordinates of the middle points of the grid cells are determined => grid points.
3. The matrix coordinates (row, column) of the grid points are determined next.
4. The nearest neighbour algorithm is used to assign the scan points to the nearest grid point.
5. The middle point of the entire grid is determined.
6. The size and shape of the interior selection is determined manually by choosing the maximum number of grid cells horizontal and vertical.
7. The last step is to transform the selected grid points to the original scan points using the nearest neighbours of step 4.

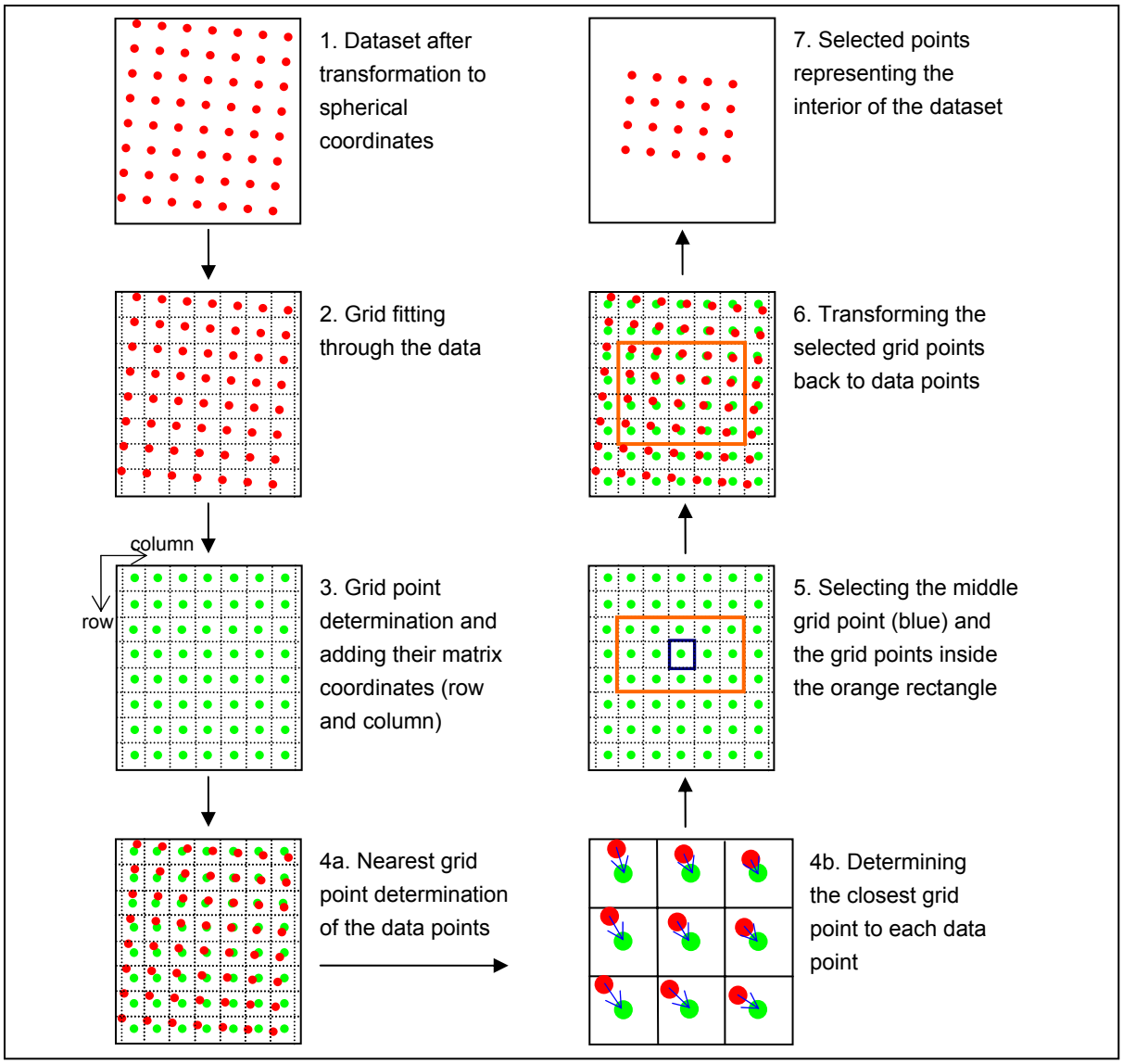

Figure 4.5: a schematic overview of the automatic interior selection. Following the arrows from the top left, each mentioned step is visualised. This eventually results in the interior selection of the object of interest from the scans obtained at the top right.

These steps can also be identified in the interior selection program that is created in Matlab (Appendix VI). Figure 4.5 visualizes the steps schematically. After the selection, the data points will be transferred back to Cartesian coordinates.

Ad 4.
There will be an error when two or more data points are assigned to one grid point. To solve this problem, step 1 is done again but now a smaller grid will be created. This process will be repeated until all data points are represented by one grid cell and each grid cell will represent not more than one data point.

The main disadvantage of this approach is that it is time consuming, especially when the high resolutions scans are examined. If the original scan consists of k scan points and the number of grid points is l, the distances between the scan points and the grid points are determined k x l times.

Whenever this thesis mentions a ‘scan’ or a ‘point cloud’ from now on, the interior selection of the object of interest is meant.

4.3 The resolution of the scans obtained

The percentage of lost point in a scan is one of the parameters used for the analysis and it is computed by determining the difference between the number of points scanned (= the scan resolution) and the number of expected points (= the expected resolution) on an object in particular circumstances. It is used to compare the performances of the two laser scanners with each other. The expected resolution follows from the specifications of the scanner. The percentage of lost points is achieved by performing the following four steps:

1. determining the surface area of the scan,
2. counting of the number of points inside the surface area,
3. determining the expected resolution of the surface area,
4. comparing the results of the previous steps in order to compute a percentage of lost points.

Determination of the surface area of the scan

All objects scanned in the experiments are planar and the automatic selection of the interior results in scan points that represent a rectangular part of the object. This means that the surface area of the scan points can simply be determined by multiplying the length and width of the sides of the rectangle.

Therefore, the length and width of the rectangle need to be determined. This is done by selecting the corner points of the scan, using the same grid fitting principle as discussed in section 4.2.2. The four possible combinations of the minimum and maximum matrix coordinates of the grid points result in the corner points of the interior selection (see figure 4.6).

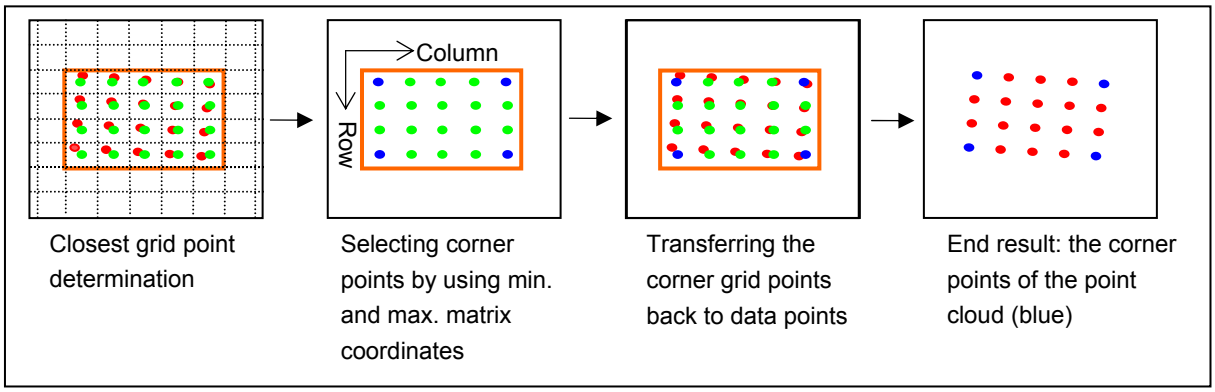

Figure 4.6: the procedure of selecting the corner points of a scan, the end result consists of the 4 corner points of the interior as visualized on the far right of this figure.

Now, the corner scan points are identified and their x, y, and z values are known, the length of the sides can be determined using formula (4.3).

$$L = \sqrt{(x_2 - x_1)^2 + (y_2 - y_1)^2 + (z_2 - z_1)^2} \tag{4.3}$$

with:

L	= the length [m]
x_1,y_1,z_1	= coordinates of corner point 1
x_2,y_2,z_2	= coordinates of corner point 2

Counting the number of points in the area

The number of scan points inside the scan is counted next. This number represents the scanned resolution on an object with a surface area of x[m^2]. To be able to compare the results obtained with both laser scanners, the number of points per [m^2] is determined.

Determining the expected resolution of the surface area

The next step is to determine the expected resolution based on the specifications of the laser scanners. The specifications are used to determine the horizontal and vertical angle increments. Figure 4.7 shows an example of the calculation of the angles of increments for the IMAGER 5003 at the middle resolution.

Example: **Determination of the horizontal and vertical angle increments**
For: **Middle Resolution IMAGER 5003**

Used specifications:
Typ. Data acquisition rate : 125,000 [px/sec]
Scanning time middle resolution : 100 [sec]
Typical vertical scanning speed : 1500 [rpm]
Vertical field of view : 155 [°]
Horizontal field of view : 360 [°]

Calculation:
125,000 [px/sec] * 100 [sec] = 12,500,000 [px/scan]
1500 [rows/min] * 100 [sec] = 2500 [rows/scan]
12,500,000 [px/scan] / 2500 [rows/scan] = 5000 [px/row]

Vertical angle increment = 2500 [rows] : 155 [°] = 1 [px] : *0.062 [°]*
Horizontal angle increment = 5000 [px] : 360 [°] = 1 [px] : *0.072 [°]*

Figure 4.7: an example of the determination of the angles of increment for the IMAGER 5003 by using its specifications.

A laser scanner always assumes its own location to be in the origin of the local coordinate system. This knowledge is used in order to determine the distances from the laser scanner to the selected corner points using formula 4.3. These distances and the law of cosine are both used to determine the angles (ψ and β). Angle ψ represents the horizontal angle between the corner points of the object and the scanner and angle β represents the vertical angle between the corner points of the object and scanner. Figure 4.8 shows the horizontal triangle used to determine ψ.

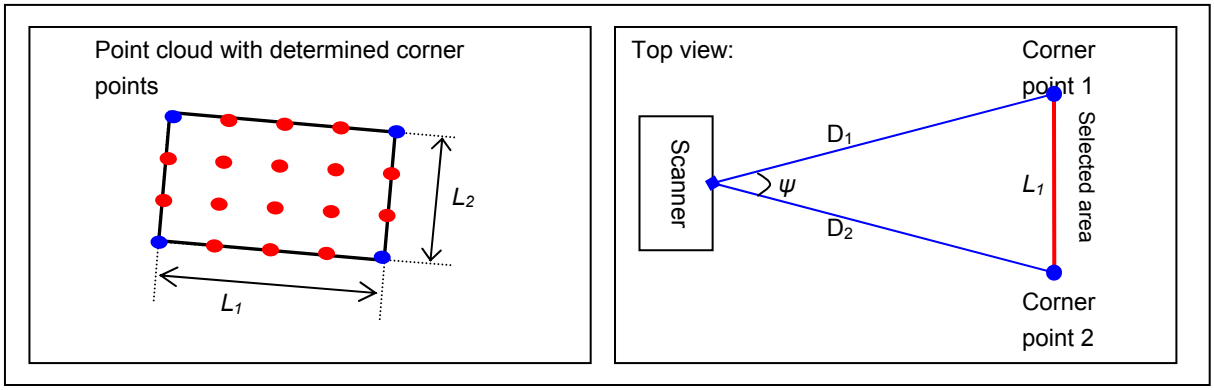

Figure 4.8: the determination of the angle between corner point-scanner-corner point, this angle is used to calculate the expected resolution on the selected area; the side view looks the same only ψ would be replaced by β, D_2 by D_3 and L_1 by L_2.

Law of Cosine

Figure 4.8 shows the situation with the triangle *corner point-scanner-corner point*. The angle ψ needs to be determined. The cosine rule can be used when either three sides or two sides and the included angle are given. In this situation, the distance between scanner and corner points (D_i) and the length of the selected area (L_1 or L_2) are the 3 known lengths of the triangle as they can be determined with formula (4.3). The cosine rule (4.4) needs to be transformed to be able to determine angle ψ (see function 4.5):

$$L_1^2 = D_1^2 + D_2^2 - 2 \cdot D_1 \cdot D_2 \cos\psi \tag{4.4}$$

$$\psi = \arccos\left(\frac{D_1^2 + D_2^2 - L_i^2}{2 \cdot D_1 \cdot D_2}\right) \tag{4.5}$$

with:

L_i = the length or width of the selected area [m]
D_i = distance between scanner and corner point *i*
ψ = angle between corner point-scanner-corner point

Dividing the angles (ψ and β) by the calculated angle increments, results in the expected number of points or the expected resolution of the surface area. In order to find the expected number of points per [m^2], the expected number of points is divided by the surface area of the scan. Figure 4.9 shows an example of the calculation of the expected number of points for the IMAGER 5003 at the middle resolution.

This method for the computation of the number of expected points in a scan can also be described by the following formula (4.6):

$$Num = \frac{\left[\frac{1}{\alpha_{h\,incr}} \cdot \left(\arccos\left[\frac{D_2^2 + D_1^2 - L_1^2}{2 \cdot D_2 \cdot D_1}\right]\right) + 1\right] \cdot \left[\frac{1}{\alpha_{v\,incr}} \cdot \left(\arccos\left[\frac{D_3^2 + D_1^2 - L_2^2}{2 \cdot D_3 \cdot D_1}\right]\right) + 1\right]}{(L_1 \cdot L_2)} \tag{4.6}$$

with:

Num = the number of expected points per [m^2]
$\alpha_{h\,incr}$ = horizontal increment following from the specifications
$\alpha_{v\,incr}$ = vertical increment following from the specifications
D_i = distance between scanner and corner point *i*
L_1 = length of the interior selection [m]
L_2 = width of the interior selection [m]

The variables of L_1, L_2 and D_i can be determined using formula (4.3).

Comparing the results

The last step that is done in order to compare the results of both scanners is to express the number of points scanned per [m^2] as a percentage of the number of expected points per [m^2]. In other words, the results are *normalized.* This is done because the hardware settings of both laser scanners are not equal.

Example: **Determination of the expected number of points / expected resolution**
For: **Middle Resolution IMAGER 5003**

Angles:
Horizontal angle increment : 0.072 [°]
Vertical angle increment : 0.062 [°]
Horiz Corner-scanner-corner angle : ψ [°]
Vert Corner-scanner-corner angle : β [°]

Calculation:
Expected #points horizontal = eph = (ψ [°]/0.072 [°])+1
Expected #points vertical = epv = (β [°]/0.062 [°])+1

Expected #points scan = ep = eph*epv
Expected #points per [m^2] = ep/area [m^2]

Figure 4.9: calculation example of the expected points per [m^2] for the IMAGER 5003 at the middle resolution.

Appendix VI of this thesis contains the Matlab program in which all four previous discussed steps are implemented. This program can be used for all scans that contain an interior selection of a planar object. The output of this program is the surface area of the interior selection, the scanned resolution, the expected resolution and most importantly the percentage of lost points.

4.4 Intensity determination

Besides 3D coordinates, a laser scanner also determines the intensity values of a scanned point. The measured intensity value is identical to the strength of the returning signal and is dependent on both the colour and the roughness of the scanned object (see section 3.1.2). The objects scanned in the experiments are scanned with both scanners. Therefore, it is possible to compare the intensity values measured in the scans obtained of both scanners. The comparison will result in a relation of the obtained intensity values per scanner with a feature like the scan angle or the range.

Note: it is assumed that the intensity values measured of the echoes are independent of the resolution that is used for scanning because the strength of an echo is not influenced by the angle of increment between two emitted laser signals.

The specifications of the IMAGER 5003 claim that they use a 16[bit] storage for the intensity. This means that the intensity values measured are spread over a range of 0 - 65,535. In reality however, the intensity values of the IMAGER 5003 show variations between -2048 and 2048 which means an 11[bit] storage is used. The FARO LS 880 claims that they use an 8[bit] storage for the intensity values.

To be able to compare the laser scanners, the intensity values of the FARO LS 880 are spread over the same domain as the intensity values of the IMAGER 5003 obtained under the same circumstances. This spreading is done using the theory of greyscale histogram equalisation (see appendix III).

After the equalisation, the spreading of the intensity values for both laser scanners will be in the same domain. The next step is to determine the mean intensity values in the scans obtained and compare them. The spreading of the intensity is represented by the shape of the intensity histograms. This feature gives insight in the variation of the intensity values measured.

Appendix VI of this thesis contains the Matlab program which is created to compare the intensity values measured of both laser scanners. The program can be used for all scans that contain an interior selection of a planar object. The output of this program is the mean intensity value of all points inside the scan and a histogram which shows the spreading features of the intensity values measured of the points inside this scan.

4.5 Least square adjustment

As mentioned before, a best fitting plate is estimated through the scan points in order to gather insight in the reliability and precision parameters of the different laser scanners. The theory of the Least Square adjustment is used to compute the best fitting plane (LSQ-plane). This paragraph highlights the main principles of this theory for *linear situations* only because the objects of interest in this research are always planar and therefore linear, see also [Teunissen, 2000a] and [Teunissen, 2000b].

4.5.1 Creating the model of observation equations

The Least Square principle is a mathematical optimization technique which attempts to find a linear function *f(x)* which closely approximates the series of measured data (*y*) (4.7).

$$f(x_i) \approx y_i \qquad \textit{with: } i = 1, 2, \ldots, n \tag{4.7}$$

The approximation is based on minimizing the sum of the squares of the offsets - residuals (*e*) - between points generated by the function *f(x)* and the corresponding points in the data, the so-called observations (*y*).

$$D = \min_x \sum_i (y - f(x_i))^2 \qquad \textit{with: } i = 1, 2, \ldots, n \tag{4.8}$$

The model *f(x)* can be written as a model of observation equations. This model contains of the observations (*y*), the unknowns (*x*) and an A-matrix. This matrix describes the relation between the observations and unknowns. The accuracy of the observations is described in a stochastic model (4.9).

$$\begin{aligned} E(\underline{y}) &= Ax \\ D(\underline{y}) &= Q_y \end{aligned} \tag{4.9}$$

with:

$E(\underline{y})$	= the expectation vector of the observations
$D(\underline{y})$	= dispersion
Q_y	= variance-covariance matrix of the observations

4.5.2 Adjustment theory

Now the model of observation equations and the stochastic model are known, the least square adjustment can be applied. The adjustment estimates values for: *the unknown model parameters* $(\hat{x})$, *the adjusted observations* $(\hat{y})$ and *the residuals* $(\hat{e})$. Figure 4.10 visualizes the principle of an adjustment in 2D.

From the geometry of figure 4.10a it seems intuitive to estimate *x* such that *ax* is as close as possible to the given observation vector *y* [Teunissen, 2000a]. The model of observation equations can be written as (4.10):

$$y = Ax + e \tag{4.10}$$

From figure 4.10b it follows that the vector of the residuals (*e*) is closest to the observation vector *y* if this vector is orthogonal to *ax,* so in case of $\hat{e}$ and $a\hat{x}$. These two parameters are the estimated vectors for the residuals and the unknown model parameters respectively. They can be determined with the following formulas (4.11), (4.12) and (4.13):

$$\hat{x} = (A^T Q_y^{-1} A)^{-1} A^T Q_y^{-1} y \tag{4.11}$$

$$\hat{y} = A\hat{x} \tag{4.12}$$

$$\hat{e} = y - \hat{y} \tag{4.13}$$

The stochastic models for the estimated values are also determined with the least square adjustment. They are determined by the following formulas and give information on the quality of the adjustment (4.14), (4.15) and (4.16):

$$Q_{\hat{x}} = (A^T Q_y^{-1} A)^{-1} \tag{4.14}$$

$$Q_{\hat{y}} = A Q_{\hat{x}} A^T \tag{4.15}$$

$$Q_{\hat{e}} = Q_y - Q_{\hat{y}} \tag{4.16}$$

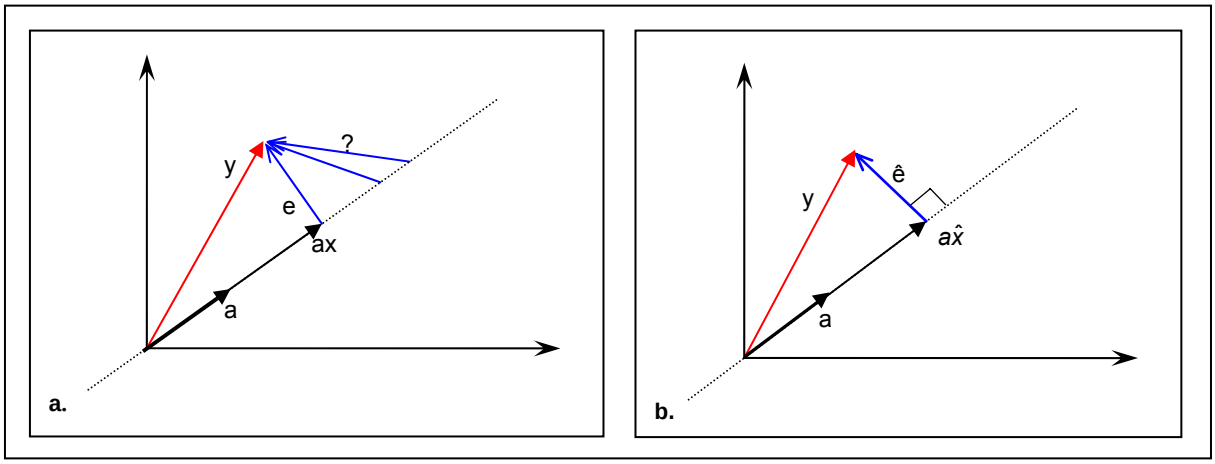

Figure 4.10: visualization of a simple least-square principle; **a,** visualization of formula 5.5 where y is the observations vector and x and e are the unknown vectors; **b,** optimized situation in which $\hat{e}$ and $\hat{x}$ are the estimated vectors for the unknowns x and the residuals e.

As mentioned in the beginning of this paragraph, only planar objects are scanned during this research. Therefore, only models of planes will be fitted through the scans obtained. The function of a plane is linear and therefore the model of observation equations of 4.9 holds true in all situations discussed in this thesis.

4.6 Least square plane fitting

In mathematics a plane can be imaged by a flat surface of infinite extent but no thickness [All refer, 2006]. An example of a plane, or more exactly of a bounded portion of a plane, is the surface forming one face, or side, of a cube. A plane can be determined or defined by any of the following: (1) a point in the plane and the normal vector of the plane; (2) the plane equation; (3) three points in the plane that are not in a straight line.

These representations of planes are found to be the three most common representations and they will be discussed in this paragraph. This paragraph ends with the model of observation equations that is used for the LSQ-adjustment.

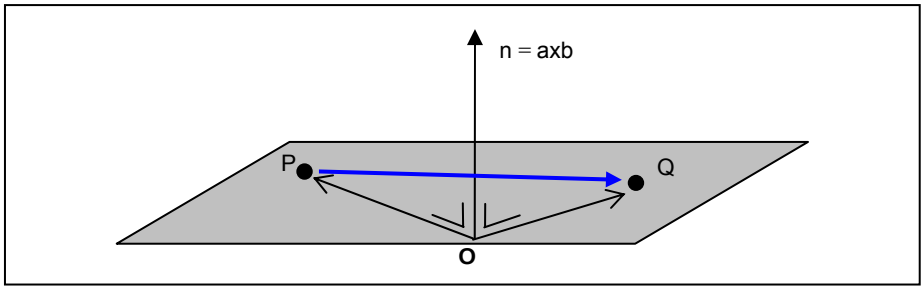

Figure 4.11: a representation of a plane by a normal vector *n* and a point *P* in the plane; point *Q* is in the plane if the dot product of the difference vector between point *P* and *Q* (blue vector) and the normal vector is zero, in this situation it is assumed that the normal vector starts in the origin of a coordinate system.

4.6.1 Point and normal vector

A plane can be fixed by a point P in the plane and a vector orthogonal to the plane. This vector is the normal vector n and determines the orientation of the plane. The plane consists of all points Q for which the dot product of the vector of differences between point P and point Q and the normal vector n is zero (4.17). When the dot product between two vectors is zero, this means that the two vectors are orthogonal to each other (Appendix II). Figure 4.11 visualizes this situation.

$$(Q - P) \bullet n = 0 \tag{4.17}$$

with:

Q = the vector from the origin to point Q
P = the vector from the origin to point P on the plane
n = the normal vector of the plane

In other words: If point P and the normal vector n in the 3D space are given by $P = (x_0, y_0, z_0)$ and $n = (a,b,c)$, the plane consists of the points $Q = (x_q, y_q, z_q)$ for which hold true (4.18):

$$\mathbf{a}x_q + \mathbf{b}y_q + \mathbf{c}z_q = \mathbf{a}x_0 + \mathbf{b}y_0 + \mathbf{c}z_0 \tag{4.18}$$

with:

a,b,c	= plane coefficients, (a,b,c) is the normal vector
x_q,y_q,z_q	= coordinates of point Q in the plane
x_0,y_0,z_0	= coordinates of known point P located in the plane

4.6.2 Plane equation

From the previous section it can be concluded that for all points in a plane formula (4.19) counts. This formula is known as the *general plane equation*.

$$\mathbf{a}x + \mathbf{b}y + \mathbf{c}z + \mathbf{d} = 0 \qquad \textit{with: } \mathbf{d} = -\mathbf{a}x_0 - \mathbf{b}y_0 - \mathbf{c}z_0 \tag{4.19}$$

with:

a,b,c	= plane coefficients, (a,b,c) is the normal vector
x,y,z	= coordinates of point Q in the plane
x_0,y_0,z_0	= coordinates of known point P located in the plane

4.6.3 Three points on the plane

Three points fix a plane when they are located in the plane and when they are not located on a straight line. Two sides of the triangle spanned by these three points are taken and set as direction vectors. Determination of the cross product of these vectors results in the normal vector of the plane (Appendix II). Figure 4.12 shows an example of this theory.

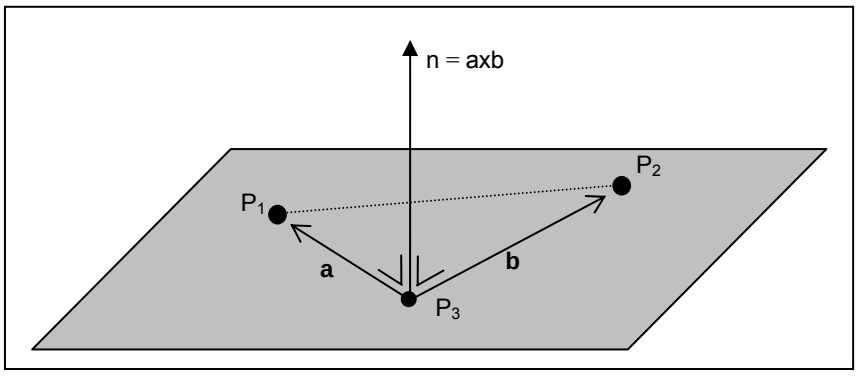

Figure 4.12: determination of a plane equation by using the three points (P_1,P_2,P_3) located on the plane, the normal vector *n* is determined by taking the cross product between the 2 direction vectors **a** and **b**.

With the calculated normal vector and one of the points on the plane, the previous discussed steps can be used to determine the plane equation of formula (4.19).

4.6.4 Implementation of a least squares adjustment

The function *f(x)* that is used in the LSQ-adjustment is a plane equation. The unknown parameters (*x*) of the model of observation equations are the plane coefficients; **a, b** and **c**. This section discusses the model of observation equations that is used for adjustment.

At first the scans, that are obtained during the experiments, are rotated so the planar object is located perpendicular to the x-axis of a coordinate system (see figure 4.13). In order to compute the rotation angles, the centre of gravity (CoG) point of all scan points together is determined by taking the mean of the x, y and z-coordinates of the dataset obtained. The rotation angles (γ_z and γ_y) are determined next by computing the angles that the CoG point makes with the x-axis in resp. the xy- and xz-plane. By rotating all the scan points around the z-axis with angle (γ_z) using the 3D rotation matrix R_z and around the y-axis with angle (γ_y) using the 3D rotation matrix R_y (4.20), the object will be located perpendicular to the x-axis (see figure 4.13b). And because the CoG point is positioned exactly in the centre of the dataset, the x-axis is now going exactly through the middle points of the dataset.

$$R_z = \begin{bmatrix} \cos(\gamma_z) & -\sin(\gamma_z) & 0 \\ \sin(\gamma_z) & \cos(\gamma_z) & 0 \\ 0 & 0 & 1 \end{bmatrix}, \quad R_y = \begin{bmatrix} \cos(\gamma_y) & 0 & \sin(\gamma_y) \\ 0 & 1 & 0 \\ -\sin(\gamma_y) & 0 & \cos(\gamma_y) \end{bmatrix} \tag{4.20}$$

In the following, the assumption is made that the y- and the z-values indicate the position of a laser point. The variable that remains is the x-value and they are the *observations* or the signal. This will result in the planar model of equations of (4.21) [Lindenbergh et al, 2005]:

$$ay + bz + c = x \tag{4.21}$$

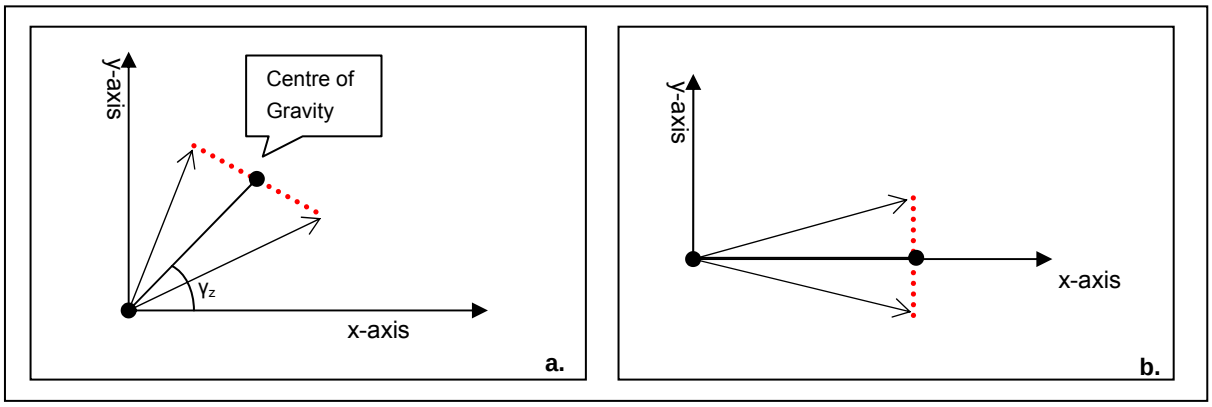

Figure 4.13: visualization of the rotation of the scan points around the z-axis with angle γ, **a.**; a schematic top view of the original situation, **b.**; a top view of the scan after a rotation by angle γ.

The unknown parameters $\hat{x} = (a,b,c)$ and the residuals $\hat{e}$ can be found by using the following linear model of observation equations (4.22):

$$A = \begin{bmatrix} y_1 & z_1 & 1 \\ \vdots & \vdots & \vdots \\ y_n & z_n & 1 \end{bmatrix}, \quad x = \begin{bmatrix} \mathrm{a} \\ \mathrm{b} \\ \mathrm{c} \end{bmatrix}, \quad y = \begin{bmatrix} x_1 \\ \vdots \\ x_n \end{bmatrix}, \quad Q_y = \sigma^2 I_n \tag{4.22}$$

with:

a, b, c = the unknown plane coefficients
$x_1 \ldots x_2$ = observations
σ^2 = variance of the measurements

In order to compute both the unknown model parameters and the residuals, the formulas (4.11), (4.12) and (4.13) are used.

It can be seen in formula 4.16 that the variance-covariance matrix of the observations (Q_y) is assumed to be an identity matrix multiplied with the variance σ^2. This assumption is done because the correlation between two different measurements is not known. The variance of the measurements follows from the given specifications of both laser scanners (see table 2.1).

Variance-covariance matrix of the unknown parameters

The variance-covariance matrix of the unknown parameters ($Q_{\hat{x}}$) is obtained with formula (4.11) which is also known as the propagation law. This matrix gives insight in the theoretical accuracy of the fitted model; the lower the values in this matrix, the better the LSQ-fit. If the model fits perfect, the residuals will be normally distributed which means they are only dependent on the random noise and no systematic errors are present.

In this research the $Q_{\hat{x}}$-matrix will be a 3x3-matrix because the three unknown plane parameters (**a**, **b**, **c**) are to be determined. The previous discussed rotation of the dataset placed the dataset perpendicular to the x-axis of a Cartesian coordinate system. The advantage of this approach is that the $Q_{\hat{x}}$-matrix will become a diagonal matrix in which the values on the diagonal represent the variances of the unknown plane parameters each. Prove for this is given in figure 4.14.

Because this research assumes the y- and z-values to indicate the position of a laser point, the most interesting variance is the variance that corresponds to the unknown plane parameter **c**. This parameter corresponds to the range between scanner and object. It can be seen in figure 4.14 that the theoretical variance of plane parameter **c** can approximately be determined by dividing the given variance (σ^2) by the number of observations (n).

With this knowledge it is expected that the variance of the unknown plane parameter **c** for the FARO LS 880 is higher then for the IMAGER 5003. Reason for this expectation is that the middle and high resolutions of the FARO LS 880 contain more observations (points scanned) then the IMAGER 5003 on these resolutions (see section 4.1.1). Furthermore, the specifications of the FARO LS 880 give a better accuracy for the scans obtained than the specifications of the IMAGER 5003 (see table 2.1) and therefore σ^2 of the FARO LS 880 is smaller as well.

Prove that the $Q_{\hat{x}}$-matrix is a diagonal matrix in all situations of this research:

$$Q_{\hat{x}} = (A^T Q_y^{-1} A)^{-1} \qquad with: A = \begin{bmatrix} y_1 & z_1 & 1 \\ y_2 & z_2 & 1 \\ \vdots & \vdots & \vdots \\ y_n & z_n & 1 \end{bmatrix} \quad and \quad Q_y = \sigma^2 I_n$$

The A-matrix can be written as three vectors: $\underline{x}$, $\underline{y}$, $\underline{o(nes)}$. This means that $Q_{\hat{x}}$ can be expressed as follows:

$$Q_{\hat{x}} = \sigma^2 (A^T A)^{-1} \qquad with: (A^T A) = \begin{bmatrix} \underline{y}^T\underline{y} & \underline{y}^T\underline{z} & \underline{y}^T\underline{o} \\ \underline{z}^T\underline{y} & \underline{z}^T\underline{z} & \underline{z}^T\underline{o} \\ \underline{o}^T\underline{y} & \underline{o}^T\underline{z} & \underline{o}^T\underline{o} \end{bmatrix}^{-1}$$

Due to the rotation of the entire point cloud, the CoG point of the point cloud is located exactly on the x-axis. This means this point has the coordinates (x_{CoG},0,0) and the y and z-values of the rest of the points in the point cloud are spread evenly around the CoG point. This means that the terms $\underline{y}^T\underline{z}$ and $\underline{z}^T\underline{y}$, $\underline{o}^T\underline{y}$, $\underline{y}^T\underline{o}$, $\underline{o}^T\underline{z}$ and $\underline{z}^T\underline{o}$ are all 0.

$Q_{\hat{x}}$ now becomes:

$$Q_{\hat{x}} = \sigma^2 \begin{bmatrix} \underline{y}^2 & 0 & 0 \\ 0 & \underline{z}^2 & 0 \\ 0 & 0 & n \end{bmatrix}^{-1} \qquad with: \begin{cases} \dfrac{\sigma^2}{\underline{y}^2} = \text{var}(\mathbf{a}) \\ \dfrac{\sigma^2}{\underline{z}^2} = \text{var}(\mathbf{b}) \\ \dfrac{\sigma^2}{n} = \text{var}(\mathbf{c}) \end{cases}$$

It can be seen above that the $Q_{\hat{x}}$-matrix indeed is in approximation a diagonal-matrix for all situations in this research with the variances of the unknown plane parameters on the diagonal.

Figure 4.14: Prove that the $Q_{\hat{x}}$ - matrix becomes a diagonal matrix with the variances of the unknown plane parameters (**a**, **b**, **c**) on the diagonal.

4.7 Determination of the precision and reliability parameters

The title of this research implies that the end result of this thesis gives insight in the precision and reliability parameters of both scanners. Although their meanings appear quite similar, they are not. A visualization of both terms is given in figure 4.15. The accuracy is the combination of both the precision and the reliability.

Figure 4.15a shows precise measurements as *precision* means: the nearness of one measurement to another or the mean value of a number of measurements, without regard to correctness of truth.

Figure 4.15b shows a number of reliable measurements as *reliability* means: the closeness of a measurement to the true or accepted value of the quantity being measured.

This paragraph discusses the methods that are used to determine the precision and reliability parameters, starting with the types of errors that can occur in a set of measurements, followed by the method to determine the

precision parameters in section 4.7.2 and the reliability parameters in section 4.7.3. At the end of this chapter the theory behind the overall model test is given. This test is used to check whether the plane equation (section 4.6.4) is valid or not. Furthermore this test makes it possible to determine the unbiased estimator of the variance which is used to compare the accuracy of the eventual models of the two scanners with each other.

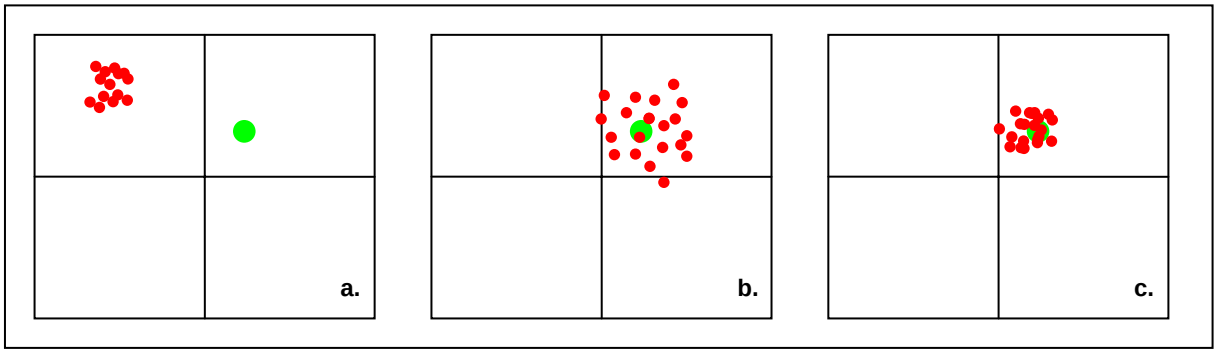

Figure 4.15: precision versus reliability with the true value (green dot) in upper right from the centre; **a.**: a precise set of measurements but not reliable; **b.**: a reliable set of measurements but not precise; **c.**: a set of both reliable and precise measurements, in other words: an accurate set of measurements.

4.7.1 Types of errors

Three common types of errors can occur in (laser) measurements and these will be discussed in this section. The types of errors are:

1. Blunders;
2. Systematic errors;
3. Random errors.

Blunders

Unlike the other errors, blunders are caused by humanity like inattention instead of equipment. Errors caused by blunders are usually large and need to be corrected or removed before adjustment because leaving the blunders in the measurements has an adverse effect on the adjustment. Figure 4.16a visualizes a blunder in a set of measurements.

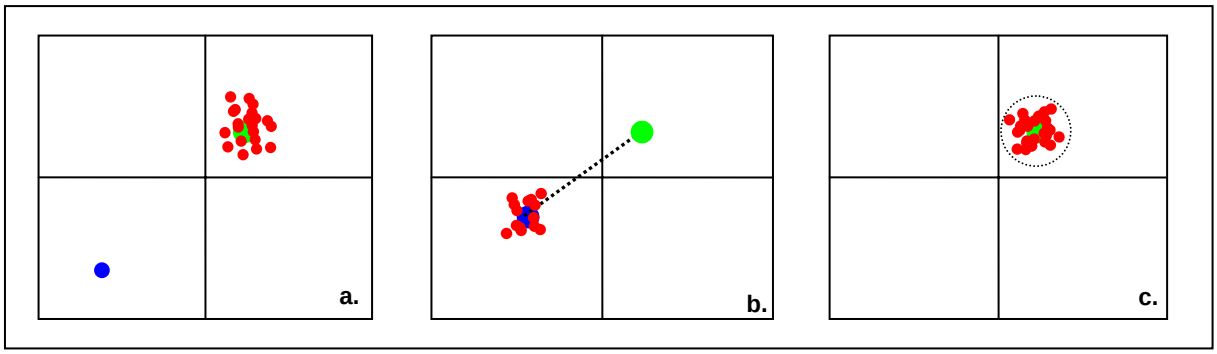

Figure 4.16: Visualization of the three types of errors that can occur on a set of measurements, the green dot represents the true value and the red dots are the measurements; **a.**: a blunder is visualized by the blue dot, located far from the true value, **b.**: the dashed black line represents the systematic error between the measured mean (blue dot) and the true value, it can be seen that the measurements are precise but not reliable in this situation; **c.**: the dashed circle represents the boundaries in which the random errors occur in the set of measurements, it can be seen that this set of measurements is precise and reliable.

Systematic errors

Systematic errors are constant and follow a physical law. They can be mathematically modelled if they are known. The errors for each observation usually have the same size and the same sign (+/-) under the same conditions. This causes the errors to accumulate as more measurements are made. Most of the systematic errors are introduced with improperly used or maintained survey equipment. These errors must also be modelled before completing an adjustment.

A simple example of this type of error is a cloth measurement tape. After repeated use, the tape will stretch. If one is aware of the magnitude of the tape stretch the error can be modelled. Figure 4.16b visualizes a set of measurements that contain a systematic error.

Systematic errors within a set of measurements done with a laser scanner are for example dependent on reading errors inside the laser scanner itself, or set-up errors like unexpected atmospheric influences. Lichti and Light [2006] discuss methods to find the systematic errors of the FARO LS 880.

However, the systematic errors are not known in the situations described in this thesis so they cannot be modelled. However, it can be assumed that the laser systems are calibrated occasionally so reading errors will most likely have no or little influence on the measurements. The atmospheric and set-up features will be the same during all experiments so they will have no influence on the comparison of both scanners.

Random errors

All measurements have some inherent error. These errors are random, typically small and mutually compensating. In other words, these errors are stochastic deviations and together they are denoted as the *noise* of a set of measurement. The random errors can never be completely known but only estimated as probable values. Figure 4.16c visualizes a set of measurements with random errors only.

4.7.2 Precision parameters

Noise represents random errors that are present in (laser) measurements. They can be represented by the residuals of a model. In this situation the residuals are formed by subtracting the LSQ-plane from the scan points and they are used to express the precision of the scans obtained.

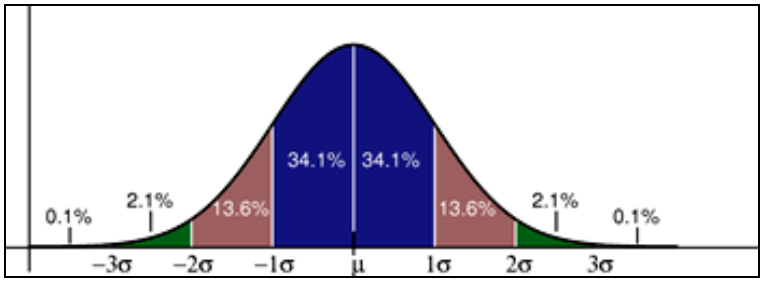

Figure 4.17: the visualization of a Gaussian normal distribution; the dark blue area represents measurements within less than one standard deviation (σ) from the mean (μ) which accounts for about 68% of the measurements, while 2σ from μ (blue and brown areas) account for about 95% and 3σ (blue, brown and green areas) account for about 99.7% (source: Sablerolle, 2006).

Once the residuals are known, they can be represented by a normally distributed histogram. The width of these histograms is used to express the noise factor. In other words, the noise is expressed by the standard deviations (SD) [mm] of the residuals per scan per scanner. Figure 4.17 shows an example of a normal distribution

including the definition of the SD. It can be seen in this figure that the SD represents the range in which approximately 68% of the residuals are located. The SD can be determined with the following formula (4.23):

$$\sigma = \sqrt{\frac{1}{m}\sum_{i=1}^{m}(\hat{e}_i - \bar{e})^2} \tag{4.23}$$

with:

σ	= SD of the residuals
m	= number of observations
e_i	= residual of the *i-th* measurement
$\bar{e}$	= mean of all residuals = 0

Because the LSQ-adjustment determines the best fitting plane through the data by minimizing the sum of the squares of the residuals between the model and the observations, the mean of all residuals ($\bar{e}$) is zero. Therefore, (4.23) can be written as follows:

$$\sigma = \sqrt{\frac{1}{m}\sum_{i=1}^{m}\hat{e}_i^2} = \sqrt{\frac{\hat{e}^T\,\hat{e}}{m}}, \quad with: \hat{e} = (\hat{e}_1, \ldots, \hat{e}_m)^T = vector\ of\ all\ residuals \tag{4.24}$$

Another feature that is examined in order to determine the precision parameters is the maximum and minimum residual. Within these two values 100% of the residuals are located.

Concluding; from each scan per scanner the SD and the minimum and maximum residual are computed in order to express the precision parameters. These precision parameters are among other things used to compare the two laser scanners with each other.

4.7.3 Reliability parameters

It can be seen in figure 4.15 that the reliability is the closeness of a measurement to the true or accepted value. In order to determine the reliability parameters of the scans, the computed model (the LSQ-plane) is compared with a ground truth value. The ground truth value is determined by using (surveying) instruments of which the reliability is known. Examples of instruments used for creating a ground truth in this research are a total station and the angle measurements device.

The eventual determined reliability parameters of the scans with respect to the angle measurement device represent the *relative reliability* parameters because the exact location of the plate can not be examined by this device. It compares whether the true scan angle, measured with this device, agrees the scan angle represented by the created model

The reliability parameters that are determined with respect to the ground truth set by the total station represent the *absolute reliability* parameters because the total station determines the exact location of the plate with a known reliability. If the difference between the model and the measurements shows a constant deviation this might indicate the presence of systematic errors in the data. However, as mentioned in section 4.7.1 it is expected that these errors are of no influence in this research.

The total station can also be used to determine the relative reliability parameters, if the range difference between two measurements is computed. The main advantage of this approach is that the unknown systematic errors are eliminated from the analysis.

4.7.4 Overall model test

In general an overall model test is done to test the null hypothesis (H_0). This means that the computed and assumed model is tested in order to see whether this model is valid or not. In the latter situation an alternative model, also known as an alternative hypothesis, needs to be created [Teunissen 2000b].

The overall model test opposes the null hypothesis to the most relaxed alternative hypothesis possible. This most relaxed alternative hypothesis is the one that leaves the observables completely free. Hence, under this alternative hypothesis no restrictions at all are imposed on the observables [Teunissen 2000b]. Therefore, the following situation occurs (4.25):

$$H_0 : E\{\underline{y}\} = Ax \qquad versus \qquad H_A : E\{\underline{y}\} \in \Re^m \tag{4.25}$$

In this case that the appropriate test statistic reads (4.26):

$$\underline{T}_{q=m-n} = \underline{\hat{e}}^T Q_y^{-1} \underline{\hat{e}} \tag{4.26}$$

This means that the appropriate test statistics of the null hypothesis against the most relaxed alternative hypothesis is equal to the weighted sum-of-squares of the residuals ($\hat{e}$). The null hypothesis will be rejected when (4.27) [Teunissen 2000b]:

$$T_{q=m-n} > \chi^2_\alpha(m-n,0) \tag{4.27}$$

with:

χ^2	= Chi-square distribution used for the computation of the critical value
α	= the chosen level of significance
m-n	= redundancy

The overall model test can be formulated in a different way as well. Therefore the factorization $D\{\underline{y}\} = Q_y = \sigma^2 Q$ is used. σ^2 is the variance factor of unit weight and Q is the corresponding cofactor matrix. It can be shown that (4.28):

$$\underline{\hat{\sigma}}^2 = \frac{\underline{\hat{e}}^T Q_y{}^{-1} \underline{\hat{e}}}{m-n} \tag{4.28}$$

This $\hat{\sigma}^2$ is an unbiased estimator for the variance σ^2, which means that it counts that (4.29):

$$E\{\underline{\hat{\sigma}}^2\} = \sigma^2 \tag{4.29}$$

Thus, the test of (4.27) can now be formulated as (4.30):

$$\frac{\hat{\sigma}^2}{\sigma^2} > \frac{\chi^2_\alpha(m-n,0)}{m-n} = F_\alpha(m-n,\infty,0) \tag{4.30}$$

with:

F_α	= central F-distribution with:
α	= the chosen level of significance
m-n	= degrees of freedom
∞	= degrees of freedom

The overall model test can be used to test whether the model of the fitted plane is indeed valid or not. Besides this validation test, the expression of (4.28) can be used for the comparison of the two laser scanners. The main advantage of using the unbiased estimator for the variance σ^2 for the comparison is that the redundancy is taken into account as well.

It follows from (4.28) that $\hat{\sigma}^2$ represents the weighted sum-of-squares of the residuals divided by the redundancy. This tells us that a situation with high residuals and a large redundancy can result in a $\hat{\sigma}^2$ that is as good or better compared to a situation with little redundancy and small residuals. This is especially of importance because the number of scanned points obtained with the selected resolutions settings of the two scanners is different (see section 4.1.1) and this test takes this difference into account as well.

However, the overall model test requires the variance information of the observations and as section 4.6.4 already mentioned, this variance is no known. Therefore, an assumption is made with respect to the variance (4.31).

$$Q_y = \sigma^2 I_m \tag{4.31}$$

The σ^2 in statement (4.31) is obtained from the specifications of the scanners. As can be seen in (4.28), the chosen σ^2 does influence the outcome positively if the manufacturer gives an opportunistic variance value and the other way around. In this research one of the main focuses is to be able to compare results obtained with different laser scanners. This means that in this research it is recommended not to use the given variance values but equal values for all scans. This means that the variance can be equalled out from formula (4.28), resulting in the following (4.32):

$$\hat{\sigma} = \sqrt{\frac{\hat{e}^T\hat{e}}{m-n}} \tag{4.32}$$

with:

$\hat{\sigma}$	= SD of the overall model
n	= number of unknown parameters
m	= number of observations
$\hat{e}$	= vector of residuals

The number of unknowns in this research is always three (representing the unknown plane parameters **a**, **b**, **c**) and the number of observations is large compared to the unknowns (see section 2.1.1). Therefore the nominator can be approximated by the number of observations *m* as well. Formula (4.32) now becomes (4.33):

$$\hat{\sigma} = \sqrt{\frac{\hat{e}^T \hat{e}}{m}} \tag{4.33}$$

This resulting formula is equal to the formula obtained for the SD of the residuals (4.24) therefore; computing the SD of the residuals gives the information that is necessary to compare the performances of the two laser scanners with each other. The overall model test is therefore not used when the performances of the two laser scanners are compared. However, when the performances of a laser scanner needs to be compared with the tachymetric data, the overall model test is used.

5 Scan angle experiment

The feature of interest discussed in this chapter is the scan angle. In other words: the influence of an increasing scan angle on the performances of the two selected scanners is examined in this chapter. First a motivation for the implementation of a scan angle experiment will be giving in paragraph 1 followed by the experiment set-up in paragraph 2. Paragraph 3 will discuss the expected results or hypotheses with respect to (1) the scanned resolution, (2) the intensity values and (3) the precision and reliability parameters of the scans obtained. Besides comparing the obtained results of both scanners with each other, they can now be compared with the expected results as well. The results of the experiment and their comparison will eventually be discussed in paragraph 4.

5.1 Motivation

Terrestrial laser scanning is often used to visualize an area like a room or even an entire building. To acquire a full visualization of the area of interest, a number of 360[°] scans will be made from different locations and coupled (registered). Overlap between the scans is needed for the registration. Placing targets in the overlapping parts may facilitate the registration. During a full 360[°] scan, the objects inside the area are hit under numerous of different angles. This is one of the reasons why it is important to gather insight in the performances of the laser scanners with respect to the scan angles.

5.2 Experiment set-up

A top view of the scan angle experiment is shown in figure 5.1a. This figure shows that the experiment is based on the practical basis set-up discussed in section 4.1.2. To test and to compare the performances of the two laser scanners with respect to increasing scan angles, the white plate is rotated with steps of 10[°], first clockwise and then anti-clockwise. The advantage of the clock and anti-clockwise rotation is that two independent scans per scan angle per resolution are created.

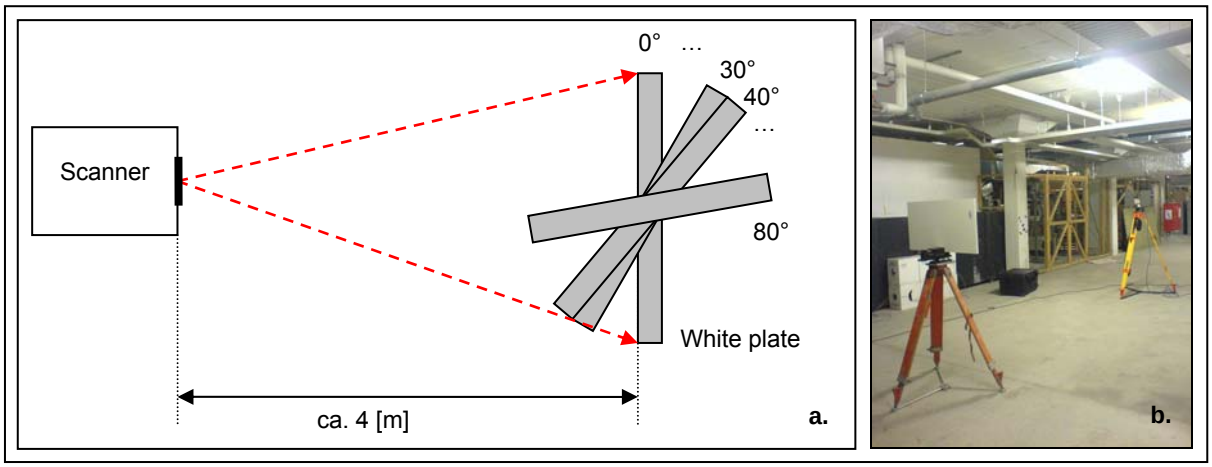

Figure 5.1: Schematic overview (top view) of the scan angle experiment (**a.**) and a picture of the set-up during the angle experiment with the FARO LS 880 (**b.**) (photo: Van Ree, 01-05-2006).

Scanning this set-up resulted in eighteen datasets of the white plate per resolution per scanner. This means that the experiment resulted in a total of 72 scans of the white plate.

As mentioned in the introduction of this chapter, external effects need to be eliminated from the experiment in order to be able to focus on the effect of changing the scan angle. By using the basis set-up, influences by range change or changing environmental conditions are eliminated. Furthermore, the effects of *different surface features* are eliminated as well because the object of interest that is used during the entire experiment is the white plate. And because the interior of the object of interest is selected as well before analysis, no edge effects have to be taken into account either.

5.3 Hypotheses

By using the specifications of the laser scanners and common sense, it is possible to create a number of hypotheses with respect to the scan angle. These hypotheses are also used to compare the results obtained from both scanners in order to check the specifications of the scanners.

This paragraph will discuss these expected results with respect to the following three parameters:

1. the number of points scanned or the scanned resolution,
2. the intensity values of the scanned points,
3. the precision and reliability parameters of the scans obtained.

5.3.1 Number of points scanned

It is possible with every scanner to choose on forehand the scanning resolution (see section 2.1.1). Within the chosen resolution the angle increment between two emitted laser signals is constant, horizontally and vertically. This feature is used to compute the number of points expected with respect to the scan angle.

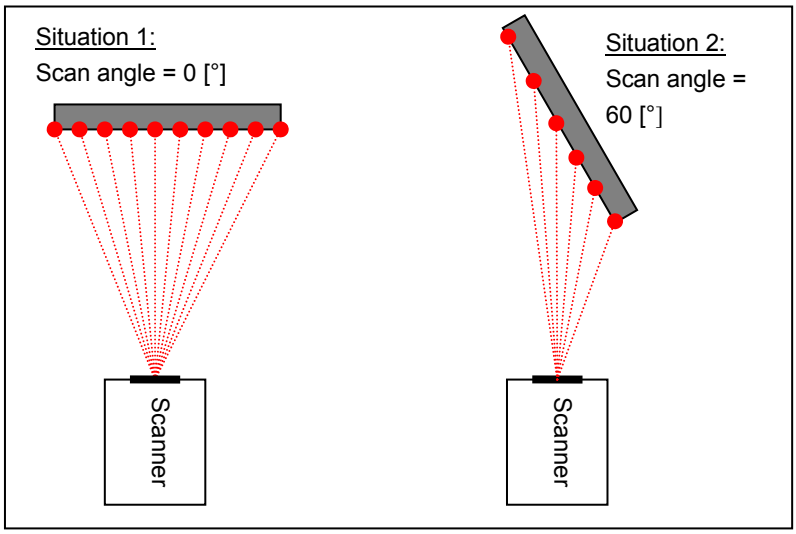

Figure 5.2: a schematic visualization of the influence of the scan angle on the number of points scanned; in situation 1 the scan angle is 0° and 10 points hit the object, in situation 2 the scan angle is 60° resulting in 6 points on the same but rotated object.

The number of points scanned on an object will decrease when the scan angle is increased. In figure 5.2 it can be seen that when an object is rotated, less points will hit the surface of the object.

The curve that is shown in figure 5.3 is an example of a *number of points scanned – scan angle* curve. The curve is created by a simulation that is based on the principle of the determination of the number of points scanned discussed in paragraph 4.3. The chosen variables for this simulation are: (1) an angle of increment of 0.0018[°], (2) an object of 2[m] by 2[m] and (3) a range of 4[m] (distance between the scanner and the object). Formula 4.4 is used to compute this curve.

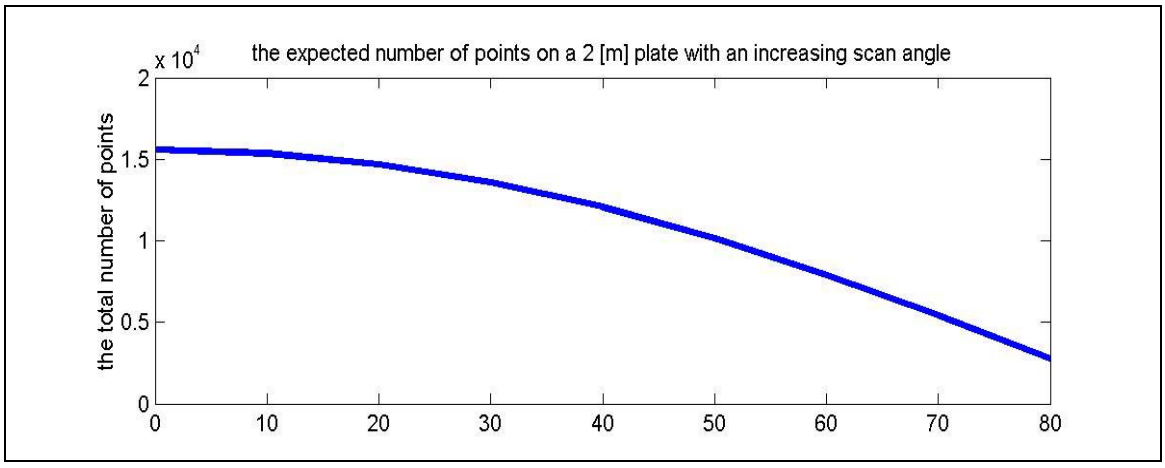

Figure 5.3: the expected *number of points-scan angle* curve determined for an object of 2 [m] with an angle increment of 0.0018 [°] and a range of 4 [m].

The curve visualizes the expected relation between the number of points scanned and the scan angles. It can be seen in this figure that the number of points scanned is indeed expected to decreases with the scan angle. Furthermore, it can be assumed that the shape of this curve will be the same for all laser scanners as it is only dependent on the angle of increment between two emitted laser signals. When the angle of increment is larger at a certain resolution, the trend will still be the same but the curve will be less steep. If the angle of increment is smaller however, more points will hit the surface of the object, which results in a steeper curve that starts higher on the y-axis then the curve shown in figure 5.3, but they will have the same trend.

The above mentioned theory is confirmed in [Clark and Robson, 2004] (see section 4.2). The article mentions that the number of points will decrease very fast when an object is scanned with different scan angles.

5.3.2 Intensity values

Section 3.1.3 of this thesis discusses the theories of Lambertian scattering, specular reflection and the assumed ellipsoid scatter pattern. The long axis of the ellipsoid will be pointing in the direction of the angle of reflection and its length is dependent on the surface characteristics of the scanned object.

Figure 5.4 shows the expected *intensity – scan angle* curves for three different surface features of objects:

1. a perfect Lambertian object, the relation between the long and sort axis is 1:1,
2. a combination of secular reflection and Lambertian scattering with a relation between both axis of 2:1 (resp. long and short axis),
3. an almost secular case, the relation between the two axes is 5:1 (resp. long and short axis).

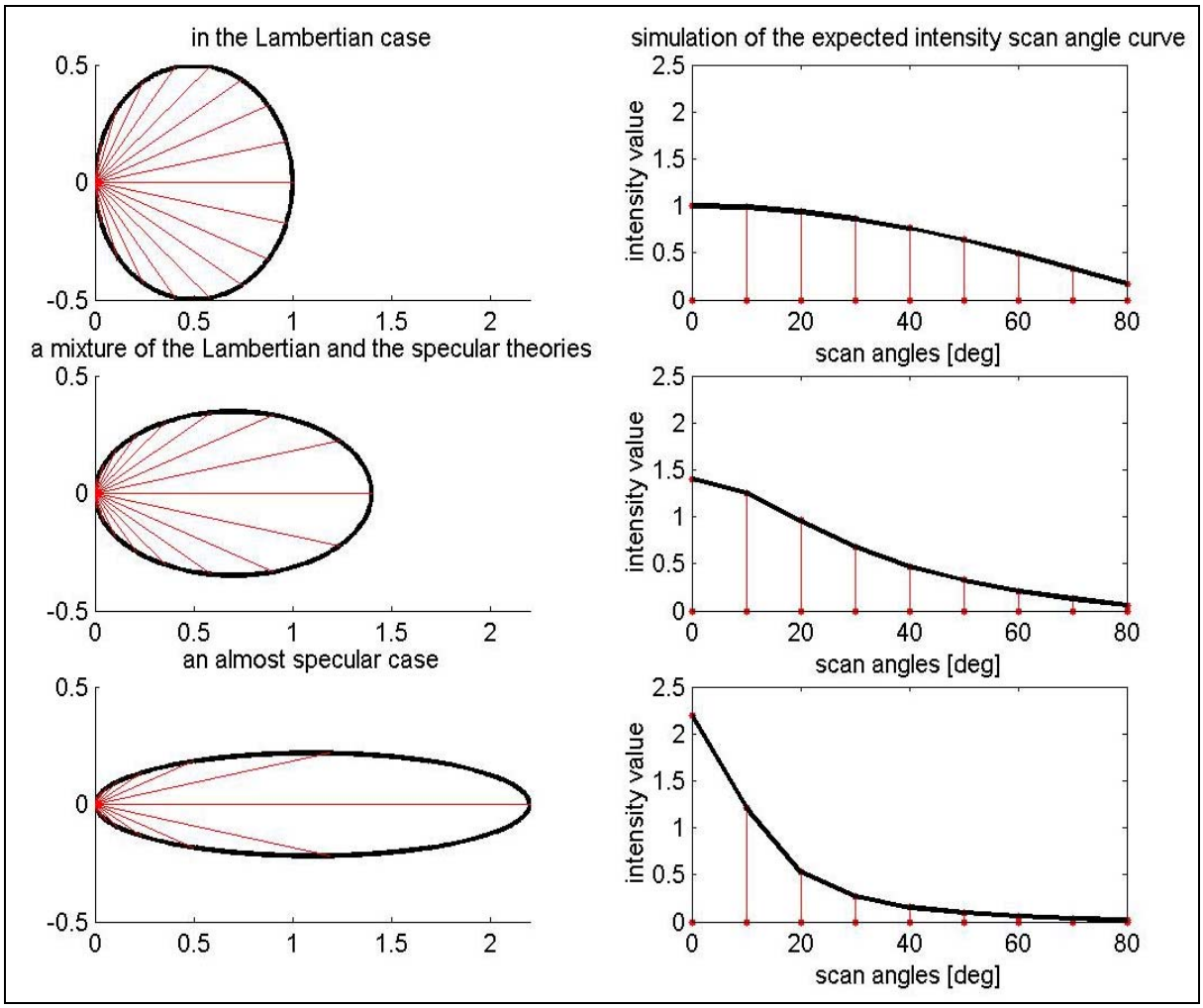

Figure 5.4: 3 different *intensity-scan angle* curves based on the combination of the Lambertian scattering and specular reflection theories. The length of the red lines represents the intensity value of the echo at the scan angles of 0 – 80 [°] with steps of 10 [°]. Top; the scatter behaviour of a perfect Lambertian body with its *intensity-scan angle* curve on the right, Middle; the scatter behaviour of a mixture between both theories, Bottom, the scatter characteristics of an almost specular reflection.

The area inside the ellipse represents the total amount of reflected energy. In figure 5.4 the areas of the ellipses are the same, which means that the sum of all the reflectivity vectors is constant in these three situations.

The curves on the right of the figure show that in all cases the highest intensity values will be achieved when an object is scanned with a scan angle of 0[°]. This is obvious when you look at the length of the red lines in the figures on the left, they represent the intensity values. It can also be seen that the intensity value belonging to a scan angle of 0[°] increases when the scatter pattern becomes less Lambertian and closer to specular reflection.

Furthermore, the three curves all look different. The expectation of the *intensity – scan angle* curve is dependent on the surface characteristics of the scanned object. As the used objects in the experiments are neither perfect Lambertian nor very smooth, the curve in the middle of figure 5.4 is expected to be the *intensity – scan angle* curve to appear during these experiments. Like the other curves, this curve shows a decreasing intensity but it also shows that the intensity decreases slowly at first, faster in the middle and slowly in the end.

5.3.3 Precision and reliability parameters of the scans

The best comparison between laser scanners can be made by comparing the precision and the reliability of the results gathered under the same environmental conditions. However, it is difficult to give the reliability and precision expectations in numbers. Therefore a more general approach is used in this section.

It is expected that the precision and the reliability in which an object is scanned is better when a lot of points are scanned on the object and when the returned intensity values are high as well. Therefore, a combination of the knowledge achieved with the literature research and the hypotheses discussed in the previous two sections is made in order to give an expectation of the precision and reliability parameters of the scans.

In order to compute the residuals, a LSQ-plane is fitted through the scan points of a 3D scan. The residuals are determined by subtracting this plane from the scanned points. From the experiment described in [Clark and Robson, 2004] it follows that the spreading of the residuals is normally distributed. The article also mentions that the normal distribution improves (the variance decreases) as the scan angle is increased although the decreasing number of points scanned can cause problems with the fit. It is said that this problem occurs for scan angles > 60[°] [Clark and Robson, 2006].

It can be concluded from this article that if the scan angle is 0[°] the scan contains more points but also more noise. The noise will be reduced when an object is scanned with an angle > 0[°]. But if the scan angle increases, the number of points on the object will decrease (see figure 5.2), resulting in less observations. Furthermore, it is expected that the intensity values of the observations will also decrease when the scan angle is increased (see figure 5.4). Combining all these statements results in the expectation that the reliability and the precision of the measurements are best when an object is scanned with a scan angle of: $0[°] > \alpha > 60[°]$.

5.4 Results

The experiment set-up as shown in figure 5.1 is scanned with both laser scanners which resulted in 72 scans of the white plate. These scans are the results of the scanning phase of this research and will be used for the analysis, based on the methods discussed in the previous chapter. This means that these analyses are divided into three parts: (1) number of points scanned, (2) the intensity values and (3) the reliability and precision of the scan. This paragraph will discuss the results of the analysis in the following sections.

All results discussed in this paragraph are achieved on the white plate (see paragraph 5.2), which is the object of interest, a scan range of approximately 4[m] and scans obtained at middle resolution.

5.4.1 Number of points scanned

As mentioned in paragraph 4.3, the actual number of points scanned per [m^2] is compared with the number of expected points. The number of points expected is determined using the specifications of the laser scanners and can be computed with formula (4.4). The results of the analysis based on the number of points scanned will be discussed in this section.

The top graph of figure 5.5 shows the curves corresponding to the number points scanned and expected per [m^2] of the two scanners at their middle resolutions. It can be seen that the *number of points - scan angle* curves of

both scanners have the same shape as expected (see section 5.3.1). However, it can also be seen that the number of points expected and scanned per scanner are different. This means that scanning with the middle resolution settings of the IMAGER 5003 less points are obtained than by scanning with the middle resolution settings of the FARO LS 880. This is due to the difference in the angle increments between two emitted laser signals. Table 4.1 of in the previous chapter understates this.

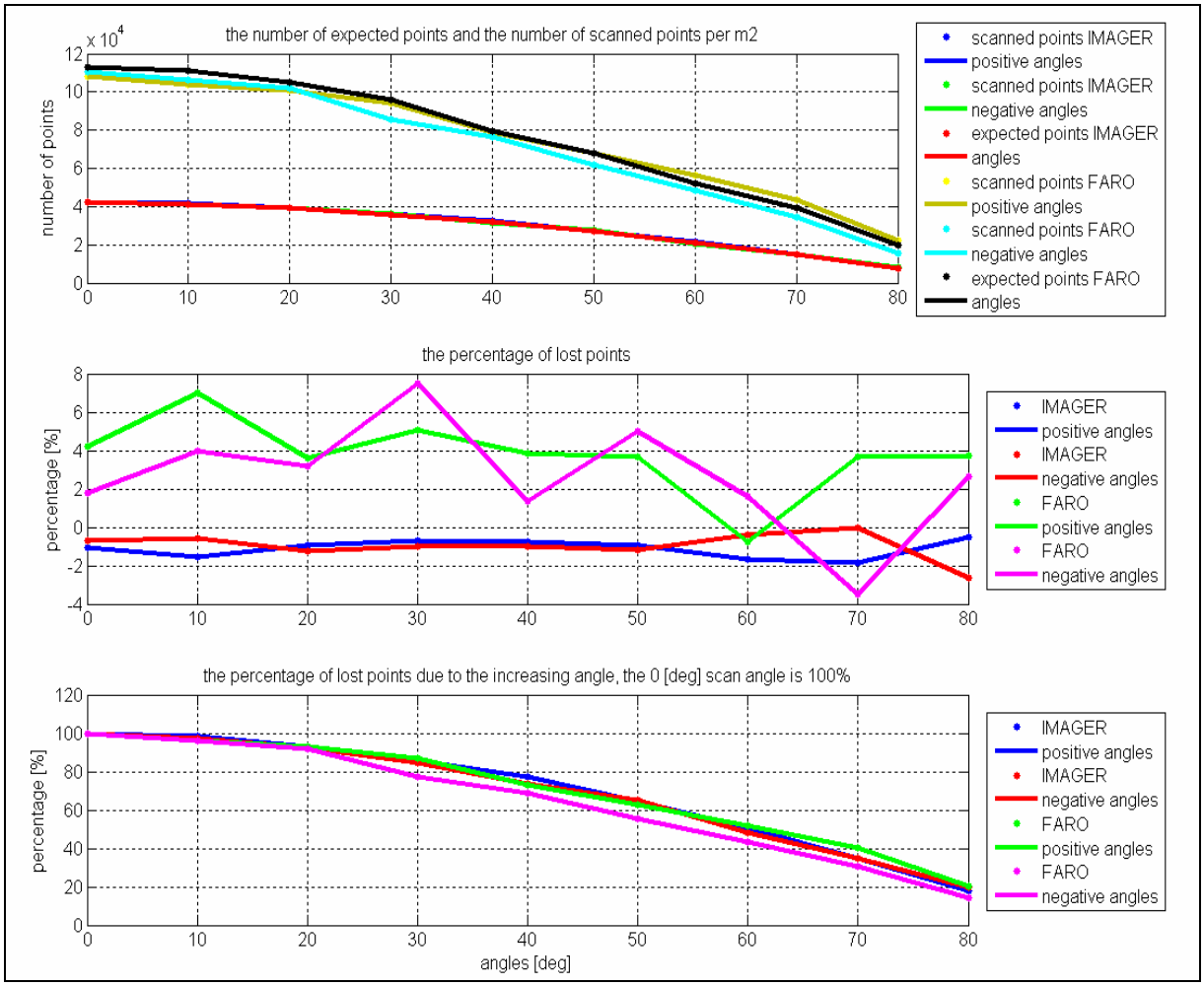

Figure 5.5: 3 curves showing the relation between the number of points scanned and the scan angle, *top:* the number of scanned and expected points per [m^2] for both the IMAGER 5003 and the FARO LS 880 at different scan angles, *middle:* the difference in percentages between the number of points scanned and the number of expected points per scanner, *bottom:* the relation between the scan angle and the number of points scanned, the number of points on an object scanned with a scan angle of 0 [°] is set as 100%.

As the curves are not based on the same number of points, they are not directly comparable. In order to make the results of both scanners comparable two different normalization approaches are used, i.e.:

1. computing the difference between the expected and the scanned points in percentages, and
2. computing the percentage of lost points per scan angle with respect to a scan angle of 0[°].

The difference between the scanned and the expected number of points

The curves shown in the middle graph of figure 5.5 represent the difference between the number of points scanned and the number of expected points. The last is set as 100% so a negative percentage in this graph means that more points are scanned than is expected. It can be seen that in case of the IMAGER 5003 all percentages

are negative so it can be assumed that a 'safety' range is present in the specifications. In other words: the IMAGER 5003 obtains a scan with at least the number of points on an object that can be expected from the specifications, but it is most likely that more points are obtained. This means that most likely the angle increment is smaller then expected, which results in more points. In order to find out whether this statement is true, 20 randomly chosen increments between different scan points are determined and their mean value is indeed lower then given in the specifications. The mean increment of these 20 determination is 0.055[°] in stead of the 0.072[°] that followed from the specifications.

On the other hand, the percentages of the FARO LS 880 differ between -3% and 7%. The percentages are positive in most cases, meaning fewer points are scanned than expected.

However, a variation in percentages is insuperable because of the interior selection of the object. Figure 5.6 shows a schematic overview of two possible situations. It can be seen that the number of points scanned located inside the selected part of the object depend on the selection criteria. These criteria influence the number of points selected at the boundaries. The situations shown in this figure is extreme but in reality it is found out that the effect due to selecting parts of a scan causes fluctuations between approximately -5% and 5% of the values expected.

With this knowledge, it can be said that both scanners obtain a certain number of points scanned within the bounds of what is expected.

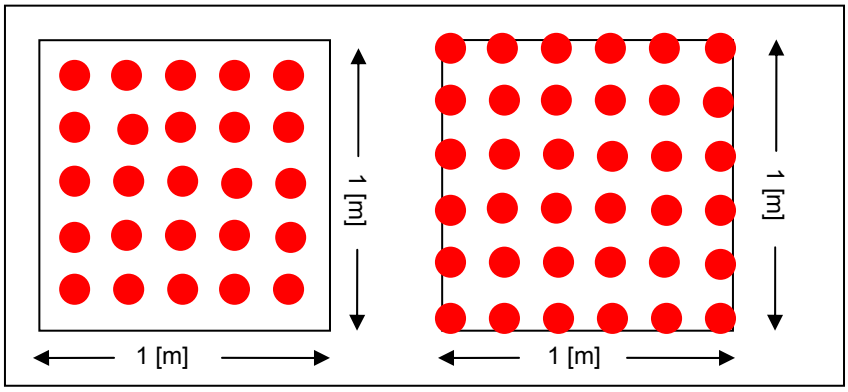

Figure 5.6: the effect of selecting a part of a scan on the number of points per 1 [m^2], *left:* the selection criteria is located between two scan points, *right:* the selection follows the points in the scan tightly resulting in more points per 1 [m^2] with respect to the situation shown on the left of this figure.

The percentage of lost points with respect to the scan angle of 0 [°]

Another method to compare the results of both scanners is to compute the relation between the number of points scanned and the increasing scan angle. In this situation the number of points scanned obtained at a scan angle of 0[°] is set as a reference (= 100%). The percentage of scanned points per angle ≠ 0[°] can now be computed with respect to this reference. The result is shown in the bottom graph of figure 5.5.

It can be seen in this graph that the shapes of all four curves are the same. This confirms the theory of the previous comparison that there are no large differences between the performances of the two scanners with respect to their number of points scanned. In all cases the curves have the shape as expected.

To make interpretation of this graph and its curves easier, figure 5.7 shows the inverse of the bottom graph of figure 5.5. This figure shows the percentage of lost points with respect to the scan angle of 0[°]. For example: it can be seen that approximately 85% less points will hit an object when this object is scanned with an angle of 80[°] instead of 0[°].

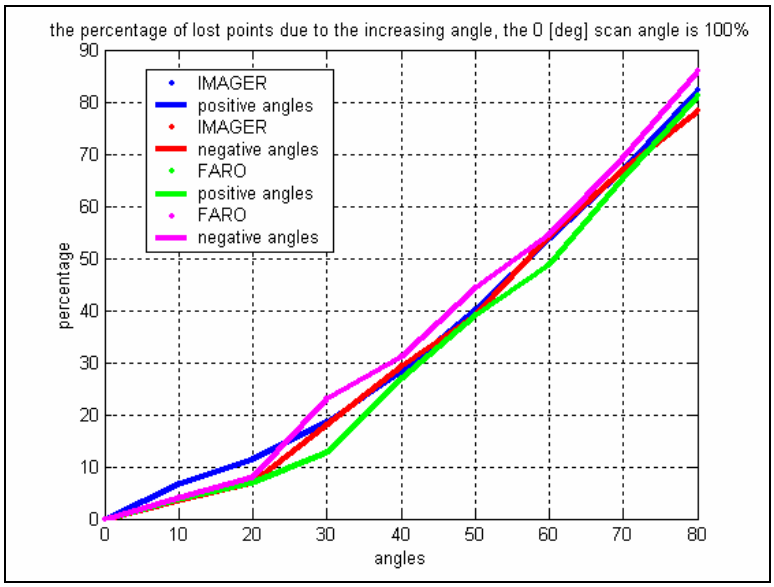

Figure 5.7: the inverse curve of the bottom graph shown in figure 5.5, it can be seen that the percentage of scanned points that hit an object decreases with the scan angle.

5.4.2 Intensity values

The intensity values are measured by both laser scanners and will be compared to be able to see a trend in the scatter features of the laser signal on the white plate. This comparison is based on the mean value of the intensity values measured. But as already mentioned in section 4.4, both laser scanners have different capacity ranges for the storage of the intensity values. Therefore, histogram equalization will be used before the intensity values will be compared. The resulting *intensity – scan angle* curves per scanner are shown in the upper left graph of figure 5.8.

It can be seen in this figure that the curves obtained for both scanners show the same relation between the scan angles and intensity values measured. However, the shape of the *intensity – scan angle* curves is not as expected, which means that the scatter pattern of the laser signal is not an ellipsoid. This can be seen by comparing the curves with the expected curve based on an ellipsoid backscatter pattern (the top-right graph of figure 5.8). The true scatter pattern can be computed by using the knowledge of the *intensity – scan angle* curve obtained. The results for both scanners are shown in figure 5.8 as well (the bottom figures). It can be seen that the scatter pattern is the same for both scanners but does not represent an ellipsoid but a more complex pattern.

Further research gave insight in other scatter patterns besides the Lambertian and specular scattering theories. The comparison of the knowledge on other scatter models with the computed scatter patterns resulted in the conclusion that the pattern obtained most likely represents a *Minnaert model* [Rees, 2001]. The shape of the scatter pattern computed is represented by the blue line in the figure on the bottom left of figure 5.8. This shape is clearly comparable with the Minnaert scatter model shown in figure 5.9c.

However, the computed scatter pattern differs from the Minneart model for the scan angles of 0 and 10[°]. The occurrence of the large peak at the scan angle of 0[°] can not be explained by this theory and neither are the scatter lines at 10[°]. Additional research for the scan angles between 0 and 10[°] is recommended in order to see if there is a trend in the scatter patterns of these angles. If the scatter pattern is relatively high for these angles as well, this part of the scatter pattern might be represented by a *Henyey-Greenstein model of forward scattering* or

by a *model close to specular scattering* because in both situation the shape of the scatter pattern will be close to an ellipsoid [Rees, 2001] (see figure 5.9d).

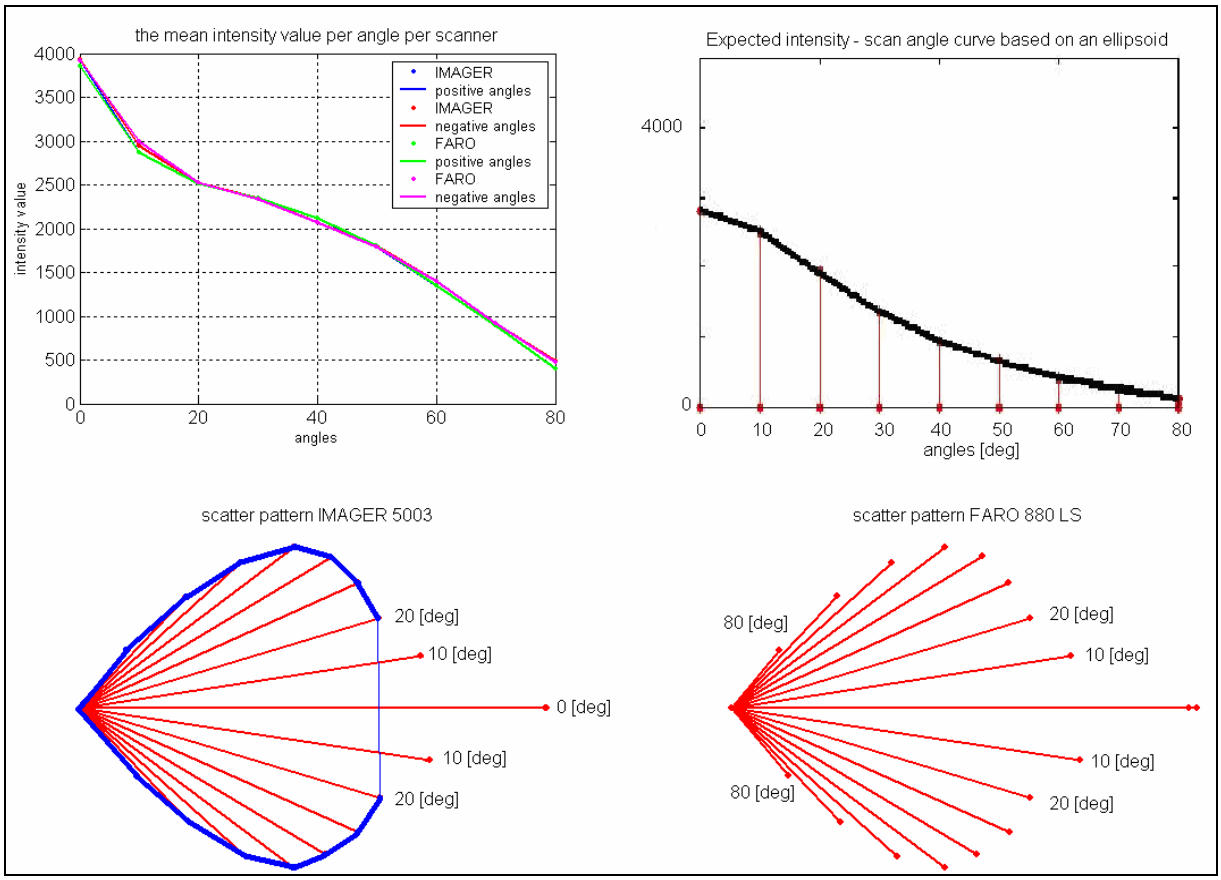

Figure 5.8: the results with respect to the *intensity – scan angle* curves, *top left:* the *intensity – scan angle* curve for both laser scanners after histogram equalization, *top right;* the expected *intensity – scan angle* curve, based in the expected theory of ellipsoid backscattering, *bottom left:* the true scatter pattern of the laser signal obtained on the surface of the white plate with the IMAGER 5003, *bottom right:* the true scatter pattern of the laser signal obtained on the white plate with the FARO LS 880.

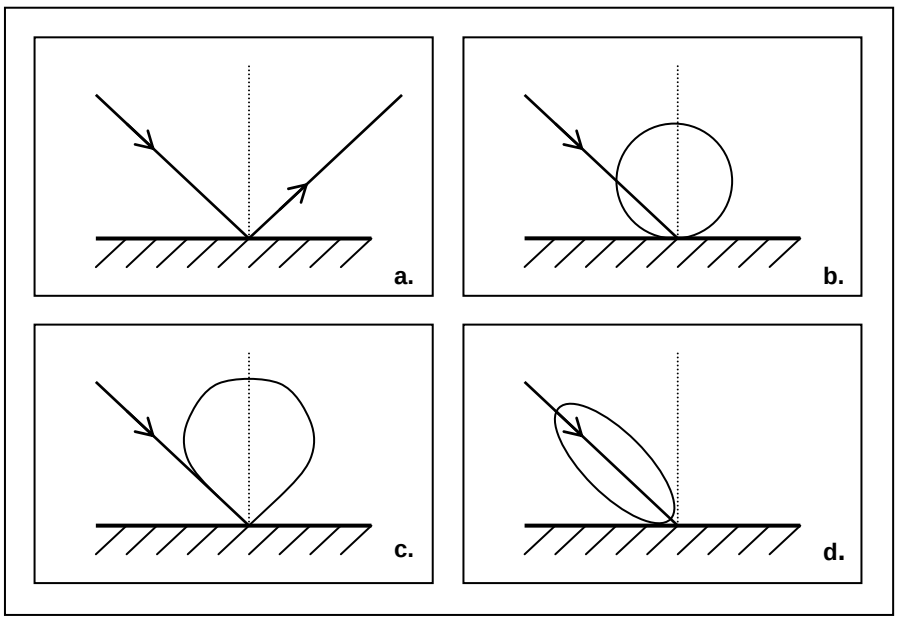

Figure 5.9: Different scatter models, **a.**: specular scattering, **b.**: Lambertian scattering, **c.**: Minnaert model of scattering, **d.**: Henyey-Greenstein model of forward scattering (source: Rees, 2001).

5.4.3 Precision and reliability parameters of the scans

As mentioned in chapter 4, the precision and reliability parameters of all scans obtained will eventually be examined followed by an overall model test. These three parameters will be discussed in this section.

The *precision* is examined by fitting a best fitting plane through the data points first, using the Least Square (LSQ) theory. Figure 5.10 shows the results of the LSQ-plane fitting through the scans obtained with the IMAGER 5003 at middle resolution and for the positive scan angles (clockwise rotation of the plate).

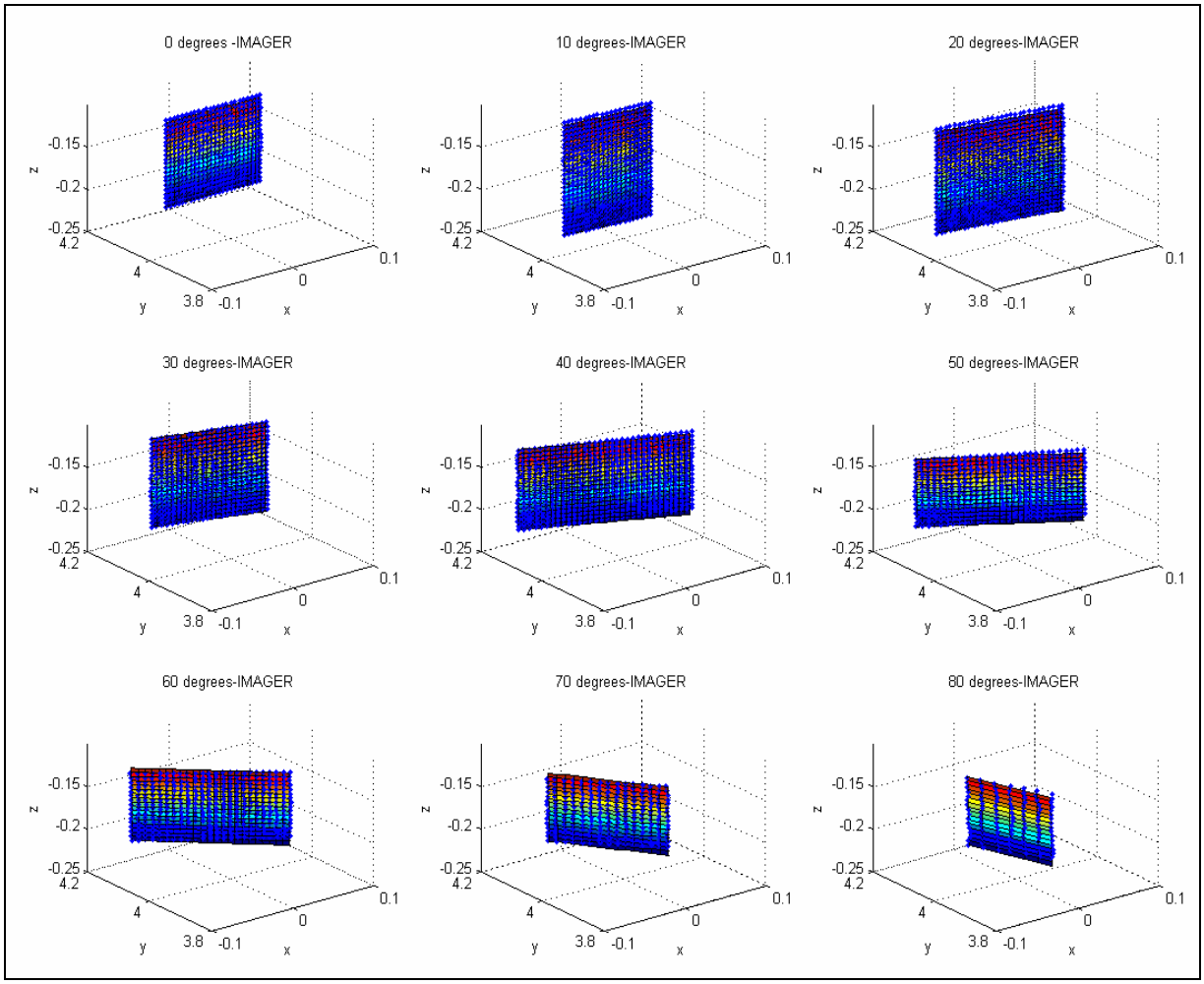

Figure 5.10: the results of fitting LSQ-planes through the scan points of the white plate, the scans in this figure are obtained with the IMAGER 5003 and for the positive (clockwise) scan angles; the blue dots represent the scan points and the surface through the points represents the LSQ-plane, the colours correspond to the z-values.

The residuals are obtained by subtracting the LSQ-plane from the points in the scans. In order to gather insight in the spreading of the residuals, histograms of these residuals are created. Figure 5.11 shows the resulting histograms for the scans obtained with the two scanners for the scan angles 0, 30, 40 and 70[°]. The SDs are shown in figure 5.11 as well.

By comparing the shapes of the histograms shown in figure 5.11 and the values in tables 5.1 and 5.2, two conclusions can be drawn:

1. one with respect to the performances of a phase laser scanner to an increasing scan angle in general,
2. one with respect to the comparison of the performances of both scanners.

First the resulting precision parameters of step 1 and 2 will be discussed, followed by the reliability parameters.

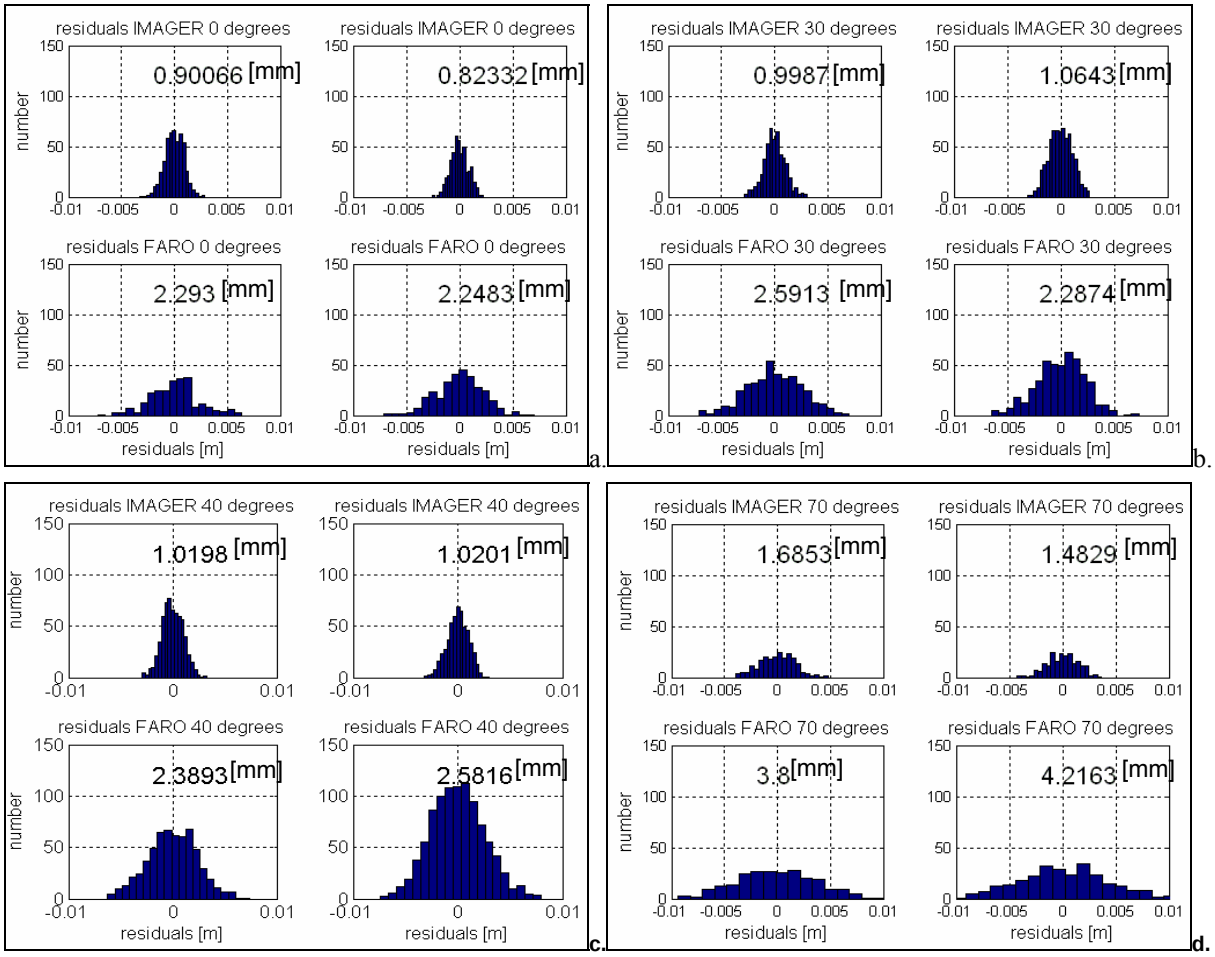

Figure 5.11: the resulting histograms of the residuals obtained for different scan angles, the black number above each histogram represents the standard deviation of that histogram in [mm], **a.**: the histograms belonging to a scan angle of 0 [°] for both the IMAGER 5003 (top two histograms) and the FARO LS 880 (bottom two histograms), **b.**: the histograms belonging to a scan angle of 30 [°], **c.**: the histograms belonging to a scan angle of 40 [°], **d.**: the histograms belonging to a scan angle of 70 [°].

Precision of a phase shift laser scanner with respect to the scan angle in general

By looking at the shape of the histograms shown in figure 5.11, it can be concluded that the width of the histograms increases with the scan angle, which means that the SD increases. This is also confirmed by looking at the SDs shown in table 5.1.

Table 5.1: standard deviations of the residuals after a LSQ-plane was fitted through the scan; per scanner per scan angle.

	IMAGER 5003		**FARO LS 880**	
Scan angle [°]	*SD residuals [mm] pos angles*	*SD residuals [mm] neg angles*	*SD residuals [mm] pos angles*	*SD residuals [mm] neg angles*
0	0.90	0.82	2.29	2.25
10	0.83	0.93	2.25	2.67
20	1.00	1.01	2.30	2.59
30	1.00	1.07	2.59	2.29
40	1.02	1.02	2.39	2.58
50	1.16	1.01	2.84	2.97
60	1.34	1.27	2.85	3.17
70	1.69	1.49	3.80	4.22
80	2.79	2.31	4.91	5.37

Figure 5.12 shows the curves of both scanners with two lines representing the SD of the residuals and two lines that represent the maximum and minimum residual values per scanner per scan angle. It can be seen in this figure that the SDs of the residuals all show an increasing trend and that the minimum and maximum residual values diverge further from the SDs when the scan angle increases.

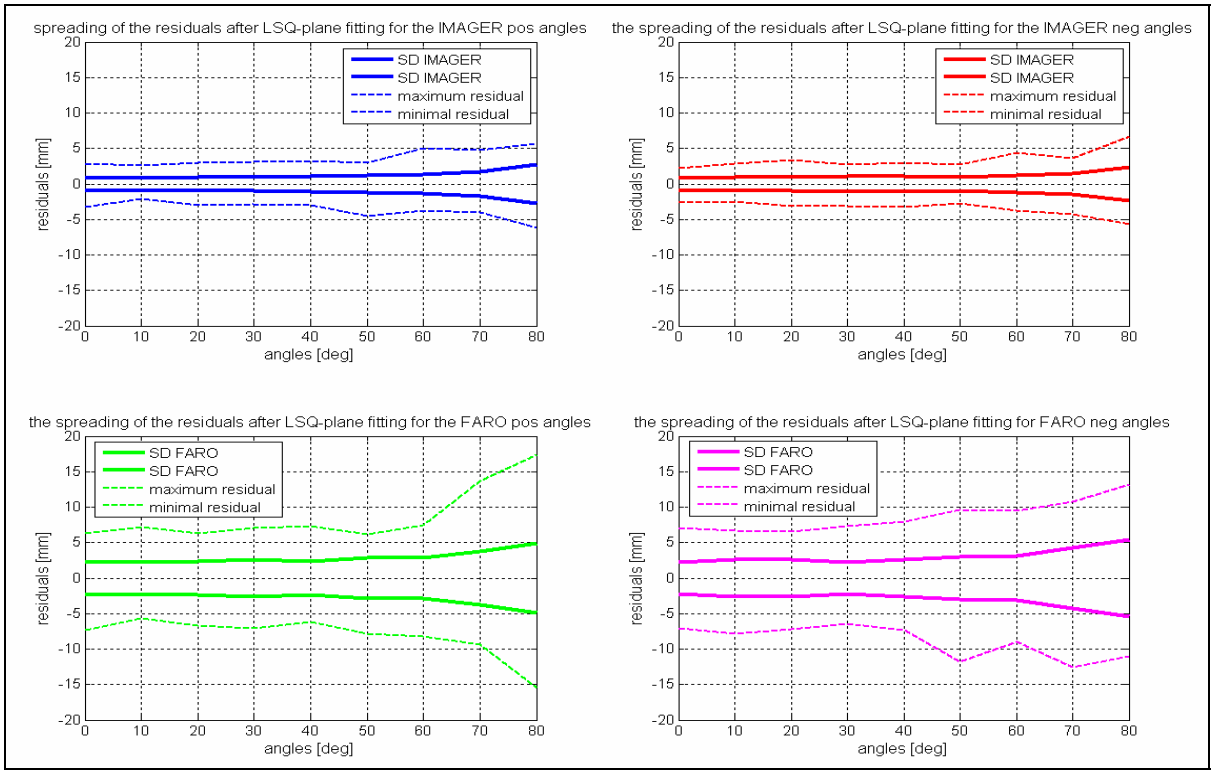

Figure 5.12: Visualization of the spreading features of the residuals by showing the trends of the standard deviations (SD), the minimum and the maximum residuals per scanner per scan angle, 68% of the residuals are located within the bold lines of the figures as they represent the SD and 100% of the residuals are located within the dashed lines, *top:* the visualization of the spreading of the residuals for the IMAGER 5003 (both negative and positive angles), *bottom:* the visualization of the spreading of the residuals for the FARO LS 880 (both negative and positive angles).

The approach discussed in this section confirms that the SD of the normal distribution indeed increases with the scan angle. In other words: all scans contain more noise when the scan angle is increased. It can therefore be concluded that the precision of the scans of both the IMAGER 5003 and the FARO LS 880 decreases with the scan angle.

Comparing the precision parameters of both laser scanners

Figures 5.11, 5.12 and 5.13 can also be used to compare the precision of both laser scanners. It follows from these figures that the scans obtained with the FARO LS 880 contain more noise than the scans obtained with the IMAGER 5003. This can be seen by looking at the spreading features shown in figure 5.12 and the widths of the histograms. The computed SDs confirm this conclusion (see table 5.1). The SDs of the FARO LS 880 are twice as high as the SDs of the IMAGER 5003 obtained under the same circumstances.

Concluding this means that the scans obtained with the IMAGER 5003 contain less noise with respect to the scans obtained with the FARO LS 880 and are therefore more precise.

Reliability of a phase shift laser scanner with respect to the scan angle in general

The reliability of a scan is determined by computing the measured scan angle from the LSQ-plane and compares it with the true scan angle. The true scan angles are determined with the angle measurement device that was implemented in the experiment set-up. Figure 5.13 shows two graphs in which the measured scan angles are compared with the true scan angles. The dashed lines in both graphs represent the assumed accuracy of the angle measurement device. When the computed scan angles are located within these two lines, the reliability of the laser scanner is assumed to be at least as reliable as the angle measurement device.

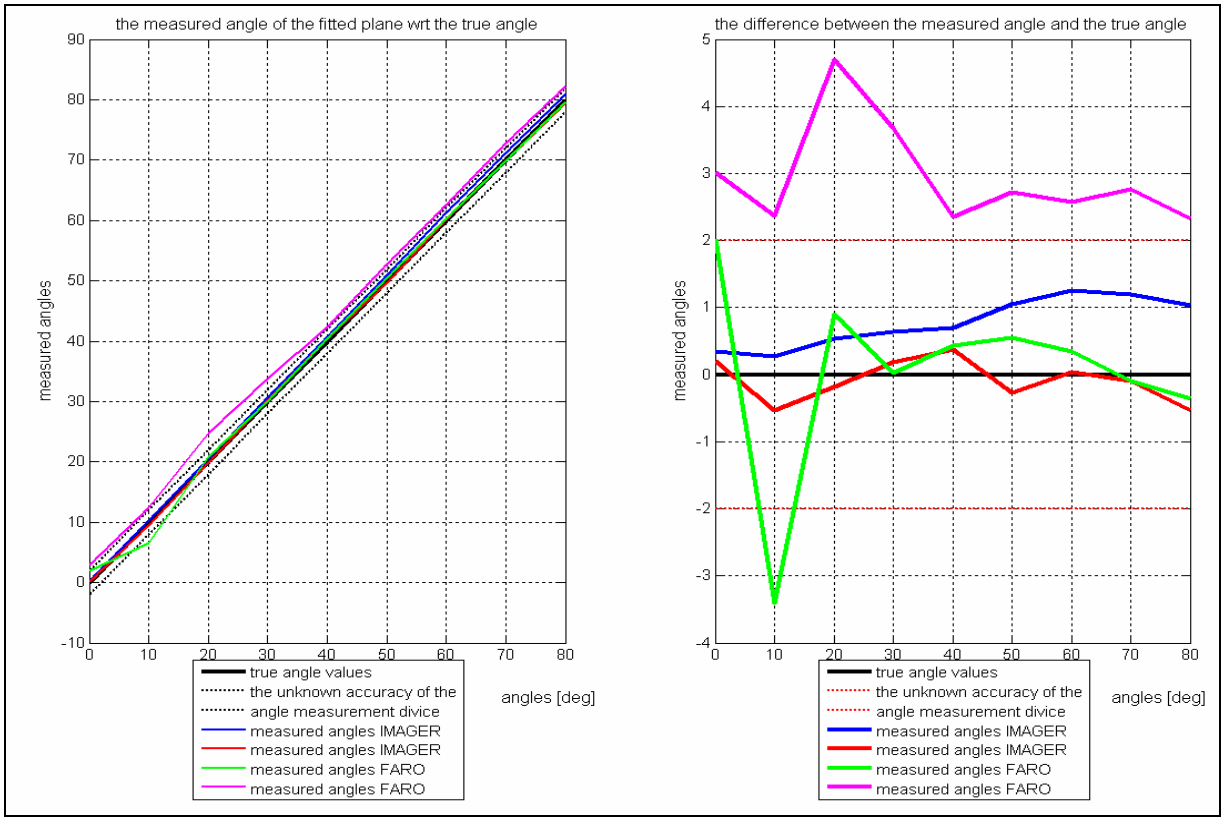

Figure 5.13: Visualization of the reliability of both the IMAGER 5003 and the FARO LS 880 by computing the scan angles from the scans obtained and their LSQ-plane and compare them with the true scan angles determined with the angle measurement device. The reliability of this device is assumed to be 2 [°]. *Left:* the measured *scan angle – true scan angle* curves for both laser scanners, *right:* the difference between the true and the computed scan angles for both laser scanners.

By looking at the lines shown in this figure, no general trend can be seen. This means that it is impossible to say something about the general behaviour of the reliability of the scans with respect to an increasing scan angle. It can be recommended to use a more accurate angle measurement device in order to be able to compute a better value for the reliability of the laser scanners.

Comparing the reliability parameters of both laser scanners

By comparing the results shown in figure 5.13, it can be concluded that the computed scan angles from a scan obtained with the IMAGER 5003 are more reliable than the computed scan angles from a scan obtained with the FARO LS 880. For one set of measurements the entire computed *scan angle* curve for the FARO LS 880 is located outside the accuracy of the angle measurement device meaning that this set of measurements is not reliable.

Comparing the results with respect to precision and reliability with the hypotheses

Section 5.4.3 mentioned that due to the decreasing number of points scanned, the decreasing intensity values and the literature research it is expected that the best results are obtained for a scan angle (α) of 0[°] < α < 60[°]. It is also expected that the noise factor at a scan angle of 0[°] is higher than for scan angles > 0[°].

By looking at the results discussed in this section it can be seen that this expectation does not hold true. In all situations it counts that, the noise factor for a scan angle of 0[°] is smaller or equal to the noise factor of scan angles > 0[°].

The results shown in figure 5.12 do show increasing SDs, maximum and minimum residuals after a scan angle of 60[°]. Therefore, the expected boundary of α < 60[°] indeed is correct.

Concluding: the 'best' scan angles to scan an object are located between 0 – 60[°] based on the results shown in figure 5.12.

Because the differences between the reliability and the precision of the scans obtained with the two scanners are large, the cause of these differences is researched. It is found out that the IMAGER 5003 or the build in software checks the data for noisy points and removes or filters the outliers before an output file is created. The FARO LS 880 on the other hand does not filter the data so the output file still contains all noisy points. The FARO software allows manual filtering of the output file by selecting a number of implemented filters. Both approaches have advantages and disadvantages which are shown in table 5.2.

Table 5.2: the advantages and disadvantages of manual and automatic filtering.

	Advantages	**Disadvantages**
Automatic filtering (IMAGER 5003)	No post-processing necessary, the scans obtained are precise and ready to use immediately	1. Noisy points are filtered out, resulting in gaps in the dataset on objects that are difficult to scan → These objects are not present in the scans obtained 2. The used filters are not known and a better result might be achieved when less or other filters are used
Manual filtering (FARO LS 880)	1. If a lot of 'difficult objects' are present in an area at least some points are scanned on these objects. And even though they are noisy, it is better than no points if the location of the object is required 2. Not all filters are necessary in all situations and now different choices can be made with respect to the filters	Post-processing is time consuming and delay the start of the modelling phase

As it is not 'fair' to compare the results of a non-filtered and a filtered scan, the conclusions drawn in this section are only valid for the performances of the two scanners with respect to their output files. The results of the FARO LS 880 will most likely improve after manual filtering is applied on the scans.

But as the research is done by order of Fugro-Inpark, a conclusion is drawn with respect to their interest. They prefer to start modelling the scans directly after the scanning phase, which means that they prefer to work with the output files without needing to post process them first. Therefore, it can be concluded that, based on the scan angle experiment, the IMAGER 5003 is best for FINP to use.

6 Colour experiment

The feature of interest that will be discussed in this chapter is the colour of an object. This feature is one of the main surface characteristics that can influence the performance of a laser scanner. This follows from [Clark and Robson, 2004]; they mention that experience on a variety of projects has shown that scanning materials with different colours and textures produces point clouds of varying quality.

First a motivation for the implementation of a colour experiment will be given in paragraph 1 of this chapter followed by some of the colour theories in paragraph 2. The experiment set-up that is used for this research is discussed in paragraph 3. The expected results or hypotheses with respect to (1) the number of points scanned, (2) the intensity values and (3) the precision and reliability of the scans obtained are handled in paragraph 4. In paragraph 5, the experiment results are compared to the expected results, while the results of both individual scanners are evaluated and compared as well.

6.1 Motivation

Like mentioned in the previous chapter, terrestrial laser scanning is often used to visualize an area like a room or an entire building. To acquire a full visualization of the area of interest, a number of 360[°] scans will be made from different locations and coupled (registered). Inside these areas numerous of different objects are present. These objects have different surface characteristics, like different colours and roughness features. Therefore, it is important to gather insight in the performance of both laser scanners on the different colours of the objects.

6.2 Colour theories

Section 3.1.2 already mentioned that a laser signal will be partly absorbed and partly reflected by the scanned object. The absorption characteristics of an object are due to the brightness and colour of the object and the reflection characteristics are dependent on the roughness of the surface of the object.

The behaviour of light can be explained by describing it as electromagnetic waves or as a collection of particles [Lester, 2005]. It this research the electromagnetic wave theory is used to explain the influence of different colours on the absorption characteristics of the scanned objects.

The complete electromagnetic spectrum contains of Gamma rays, X-rays, Ultraviolet, visible light, Infrared and Radio waves (see figure 6.1). Visible light is defined by the sensitivity of the human eye and is only a small part of the electromagnetic spectrum. This part of the spectrum has wavelengths between 380[nm] and 780[nm]. Each wavelength represents a unique colour as can be seen in figure 6.1a.

White light is a mixture of all wavelengths inside the visible spectrum. When the incoming light on an object is white, the object absorbs certain characteristic wavelengths of the light bundle. The absorption is typical for that colour. If one sees a red object, for example, this object will absorb all of the incoming blue and green light and reflects only red light. This red reflection reaches our eyes which results in the observation of a red object.

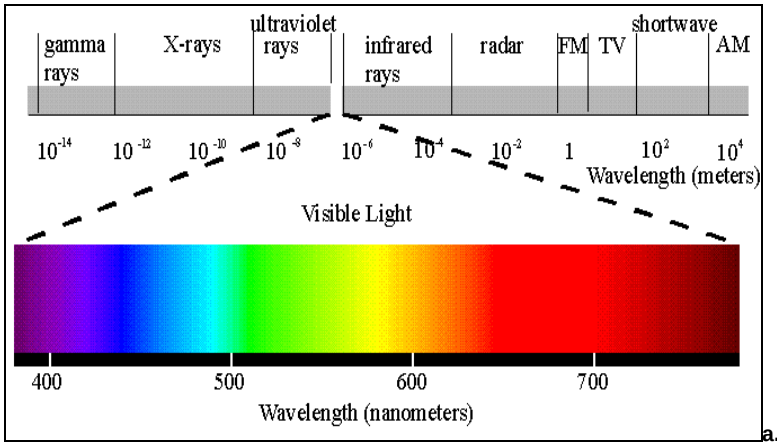

a.

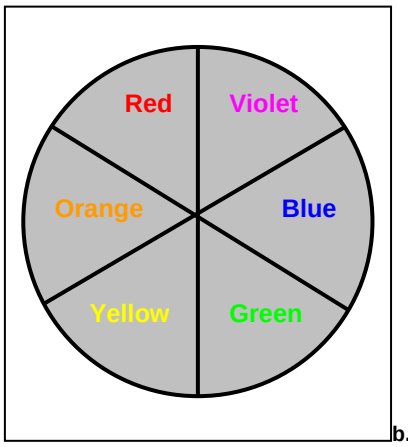

b.

Figure 6.1: **a.**: the electromagnetic spectrum with the visible light highlighted in the middle (source: Yorku, 2006), **b.**: the complementary colour circle in which complementary colours are located opposite from each other.

The researched laser scanners both use Near-Infra red (NIR) wavelengths to scan their objects (780[nm] < λ < 785[nm]). The NIR region of the electromagnetic spectrum lies just beyond the sensitivity of the human eye and covers a wavelength range of 780[nm] to 3000[nm]. As the laser scanners measure the intensity of an echo, the emitted NIR signal must be reflected from the surface of an object because no signal would return if the object absorbs the entire incoming signal. This means that the measurements done with a laser scanner determine the intensity values with respect to the NIR part of the spectrum of that object and not with respect to the visible light.

Complementary colours

However, the emitted wavelengths of both scanners are very close to the visible spectrum (780[nm] < λ < 785[nm]) so the laser signals might are comparable to visible red light. In this situation the complementary colour theory can be used to describe the performances of the laser scanners on different colours. A colour circle in which the complementary colours are located opposite from each other is shown in figure 6.1b.

The theory of complementary colours holds that an object with a certain colour absorbs its complementary colour the strongest. For example this means that if white light is shining on a green surface it will absorbs the red light. As this research is done with laser scanners, only red light is present. Therefore, the green and red part of the complementary colour circle will be of most interest in this research.

6.3 Experiment set-up

Section 3.2.6 mentioned an experiment in which colours are examined. In this experiment a ColourChecker chart is used containing both grey value and colour patches [Clark and Robson, 2004]. The general set-up used for the experiment is found representative and is therefore used to gather insight in the influence of colours of the surface of an object on the scans obtained.

In the created experiment set-up of this research, an ‘Esser test chart’ is used [Digitalkamera, 2006]. This plate is originally designed for evaluating the colour features of TV cameras [Bucksch, 2006]. The chart contains seven patches with different colours. These colours have the property that when they are lightened with a standard light (D65), the colours of the test chart have the coordinates in the CIE-xy-diagram as are shown in table 6.1. For the

comparison, this table also contains the standard values (EBU) of the corresponding colours. Appendix IV of this thesis discusses the CIE-diagram more into detail.

Table 6.1: The CIE based characteristics of the colour patches of the Esser test chart used for the colour experiment

	Colour	**EBU standard** *		**TE 106 K with D65 (=colour test plate)**	
		x	y	x	y
1.	White	0.31	0.33	0.31	0.33
2.	Yellow	0.41	0.50	0.43	0.49
3.	Cyan	0.22	0.33	0.24	0.32
4.	Green	0.29	0.60	0.30	0.53
5.	Purple	0.32	0.15	0.33	0.18
6.	Red	0.64	0.33	0.59	0.34
7.	Blue	0.15	0.06	0.18	0.15

* See Appendix IV for an explanation on EBU standards in the CIE-xy-diagram and how they are connected to spectral wavelengths

For this experiment again the basis set-up (see figure 4.1) is used. The test chart is placed in front of the white plate. The influence of the scan angle on the different colours is also taken into account during this experiment by rotating the plate with steps of 20[°] clockwise. A picture of the set-up is shown in figure 6.2.

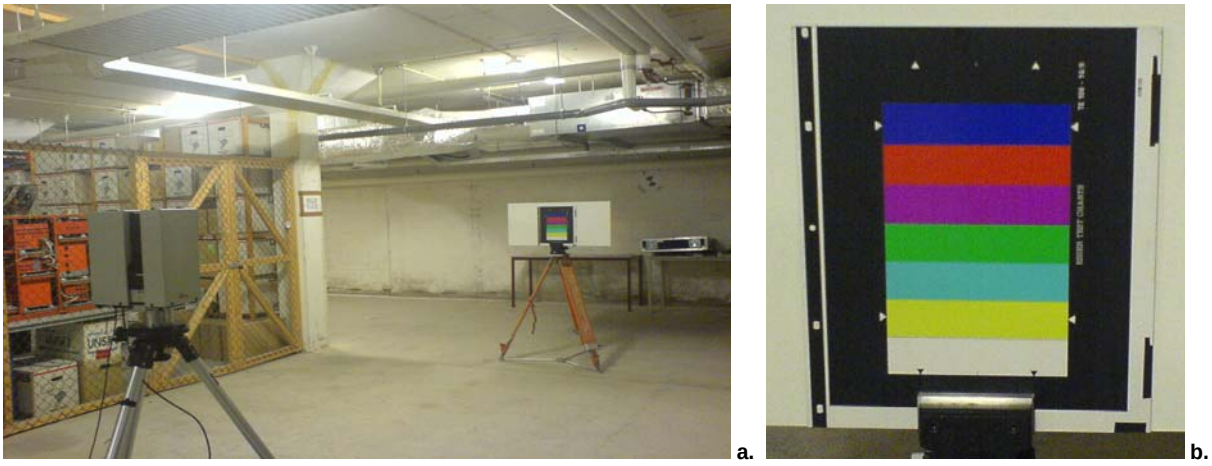

a. **b.**

Figure 6.2: **a.** The colour experiment set-up with left the Leica HDS4500 scanner and right in the picture the tripod with the white plate and the colourChart placed in front, **b.** a close up of the colourChart in the angle m. device (photos: Van Ree, 29-03-2006).

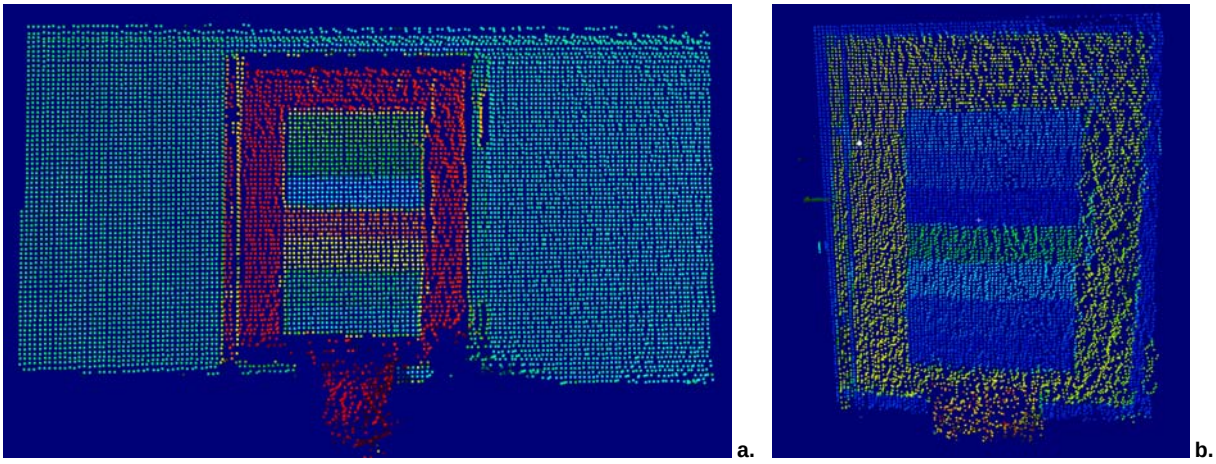

a. **b.**

Figure 6.3: Two scans achieved with the colour experiment set-up, both scanned at the middle resolution and with a scan angle of 20 [°], **a.**; the scan achieved with the Leica HDS 4500, **b.**; the scan achieved with the FARO LS 880.

After scanning this set-up four scans of the test chart per resolution per scanner are obtained. This means that the experiment will result in a total of sixteen scans of the chart. Two of the scans are shown in figure 6.3. These are obtained with both laser scanners for a scan angle of 20[°], left with the IMAGER 5003 and the right with the FARO LS 880. The colours in the scan represent the intensity values measured per point. It can be seen that different intensity values are measured for the colour patches in the test chart.

The set-up as shown in figure 6.2 eliminates the parameter *range* because the range is set at approximately 4[m] and will not change during the experiment. Furthermore, the effect of the *surface roughness* is eliminated because the reflection characteristics of the colour patches are assumed to be equal for all patches as their roughness characteristics are the same. Therefore it is possible to investigate the influence of the colours only.

6.4 Hypothesis

By using the colour theory discussed in paragraph 6.2, it is possible to create a number of hypotheses with respect to the influence of colours on the scans obtained. These hypotheses can also be used for the comparison of the computed results of both scanners.

This paragraph will discuss the expected results with respect to the following three features:

1. the number of points scanned,
2. the scanned intensity values,
3. the reliability and precision of the scans obtained.

6.4.1 Number of points scanned

The theories discussed in paragraph 6.2 show that different colours have different characteristics with respect to the absorption of the laser signal. But as the laser scanners used in this thesis both scan their objects in the NIR domain of the spectrum, the amount of reflected energy of the NIR signal determines the accuracy of the measurements done with the two laser scanners. The more NIR is reflected, the less NIR is absorbed so the higher the intensity of the echo. In general this also means a high number of points scanned on the objects. Unfortunately, NIR is not visible by the human eye and therefore it is not possible to give an indication on which patch will perform best or worse.

The performance of the laser scanner on green, which is the complementary colour of red, is expected to be bad. Because green is the complementary colour of red, it is expected that most of the energy of the incoming laser signal is absorbed by this patch. This results in less energy for the echo and/or less measurements. It can also be assumed that both scanners perform well on objects that are red because the laser signal will not be absorbed by this colour but reflected totally.

6.4.2 Intensity values

With the knowledge obtained from the previous chapter and paragraph 6.2 it is expected that the colour of an object does not influence the scatter pattern of the laser signal because this is linked to the roughness

characteristics. This means that the shape of the *intensity – scan angle* curve remains the same. However, the colour characteristics of the object have an influence on the amount of signal that is absorbed. This will influence steepness and the maximum intensity value of the *intensity – scan angle* curve. This is due to the fact that certain colours absorb more of the incoming energy of the signal so less energy is reflected back.

It is expected that low intensity values are measured on the green patch and high intensities on the red patch due to the complementary colour theory. The performances of the white patch are also assumed to results in high intensity values measured. Reason for this statement is that white is a combination of all visible colours. It will therefore always reflect the incoming signal independent of the colour of the incoming signal.

Because it is not known what the reflectivity and absorption characteristics of the colour patches is with respect to the incoming NIR signals, it is impossible to say something about the expected intensity values measured on the other colour patches.

6.4.3 Reliability and precision of the scans

The best comparison between laser scanners can be made by comparing the precision and the reliability of the results gathered in the same environmental conditions. However, it is difficult to express the reliability and precision expectations in numbers. Therefore a more general approach is used in this section.

It is expected that the precision and the reliability in which an object is scanned is better when a lot of points are scanned on the object and when the returned intensity values are high as well. Therefore, a combination of the knowledge of the literature research and the hypotheses of section 6.4.1 and 6.4.2 is made in order to give an expectation of the precision and reliability parameters of the scans.

Concluding this means that it is expected that the red and white patch are determined with a higher reliability and precision because it is assumed that there will be almost no difference between the expected and measured number of points and that the intensity values measured are expected to be high as well because a large amounts of the incoming laser light will be reflected. The opposite is expected for the green patch because almost all the incoming signal will be absorbed. The reliability and precision parameters of the other patches are hard to predict because their reflection and absorption features with respect to the NIR laser signal are not known.

6.5 Results

The sixteen scans obtained of the test chart are the results of the scanning phase of this experiment of the research and will be used for the analysis. The analyses are divided into three parts, i.e.: (1) number of points scanned, (2) the intensity values measured and (3) the reliability and precision of the scan and will be discussed in this paragraph.

Before the analyses are done, the interiors of the colour patches will be selected. Chapter 4 of this thesis mentioned that an interior selection of the object of interest will be made in order to reduce the calculation time and to eliminate the edge effects. The automatic method that is discussed in this chapter was valid for the white plate but can not be used in this situation because seven instead of one interior selection need to be created, for every colour patch is the scan one. By manually selecting the colour areas and implementing a couple of changes to the automatic interior program, the interiors of the patches can be selected. Two examples are shown in figure 6.4. The different colours of the points inside the selections represent the intensity values measured.

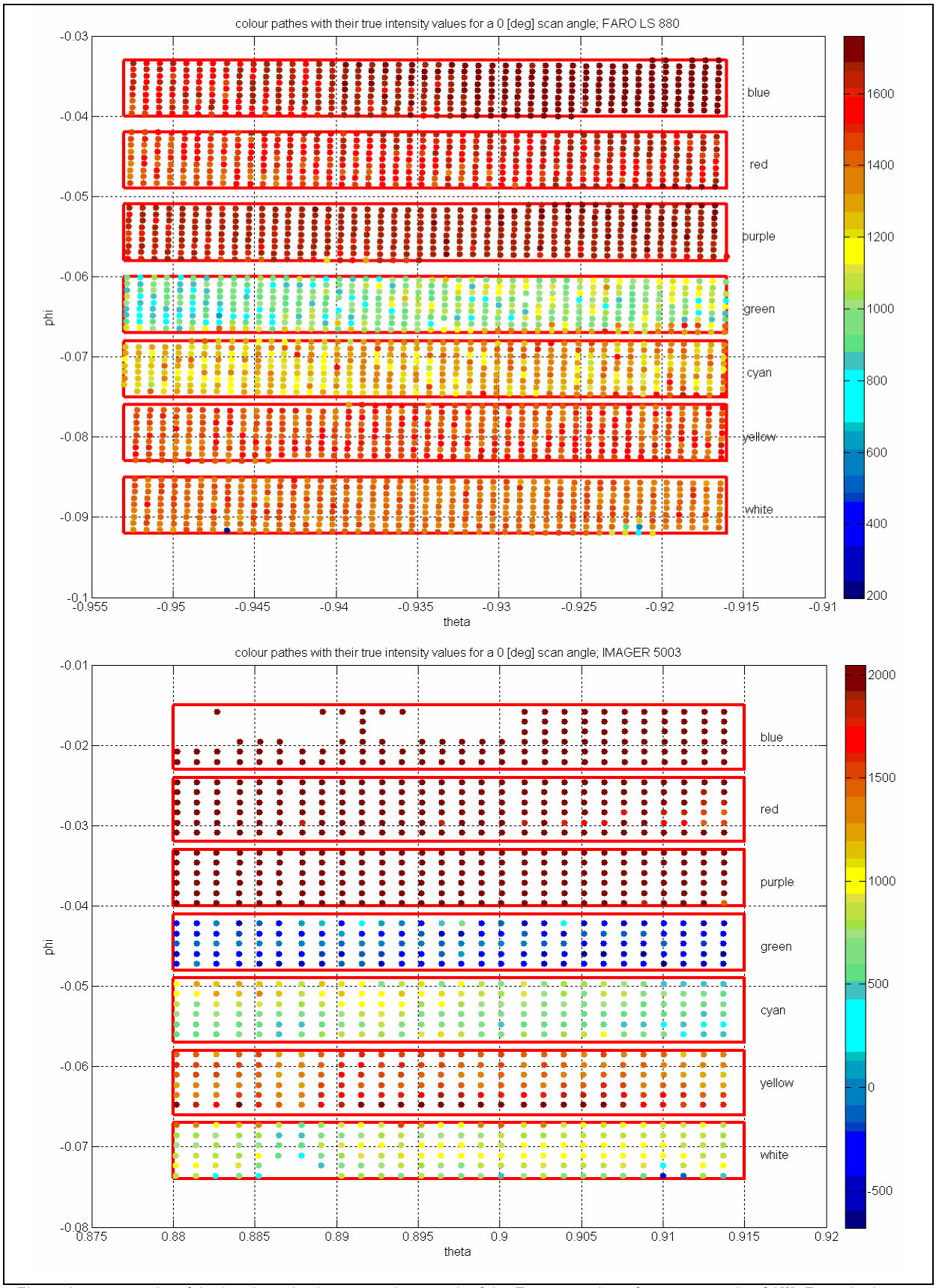

Figure 6.4: two results of the interior selections per colour patch of the Esser test chart; for a scan angle of 0[°]. From the bottom up the areas represent the colours: white, yellow, cyan, green, purple, red and blue. *Top figure*: the results of the interior selection of the scan obtained with the FARO LS 880 and *bottom figure*: the results of the interior selections of the scan obtained with the IMAGER 5003.

NOTE: all results that are discussed in this paragraph are achieved on the test chart, which is the object of interest; using a scan range of approximately 4[m] and the scans are obtained with the middle resolution of both scanners.

6.5.1 Number of points scanned

The number of points scanned per colour patch per [cm^2] is determined in order to be able to compare the results of both scanners with each other and to compare them with the number of points expected per [cm^2]. The number of points expected is determined using the constant angle increments between two emitted laser signals that follow from the specifications. The results of the analysis based on the number of points scanned will be discussed in this section.

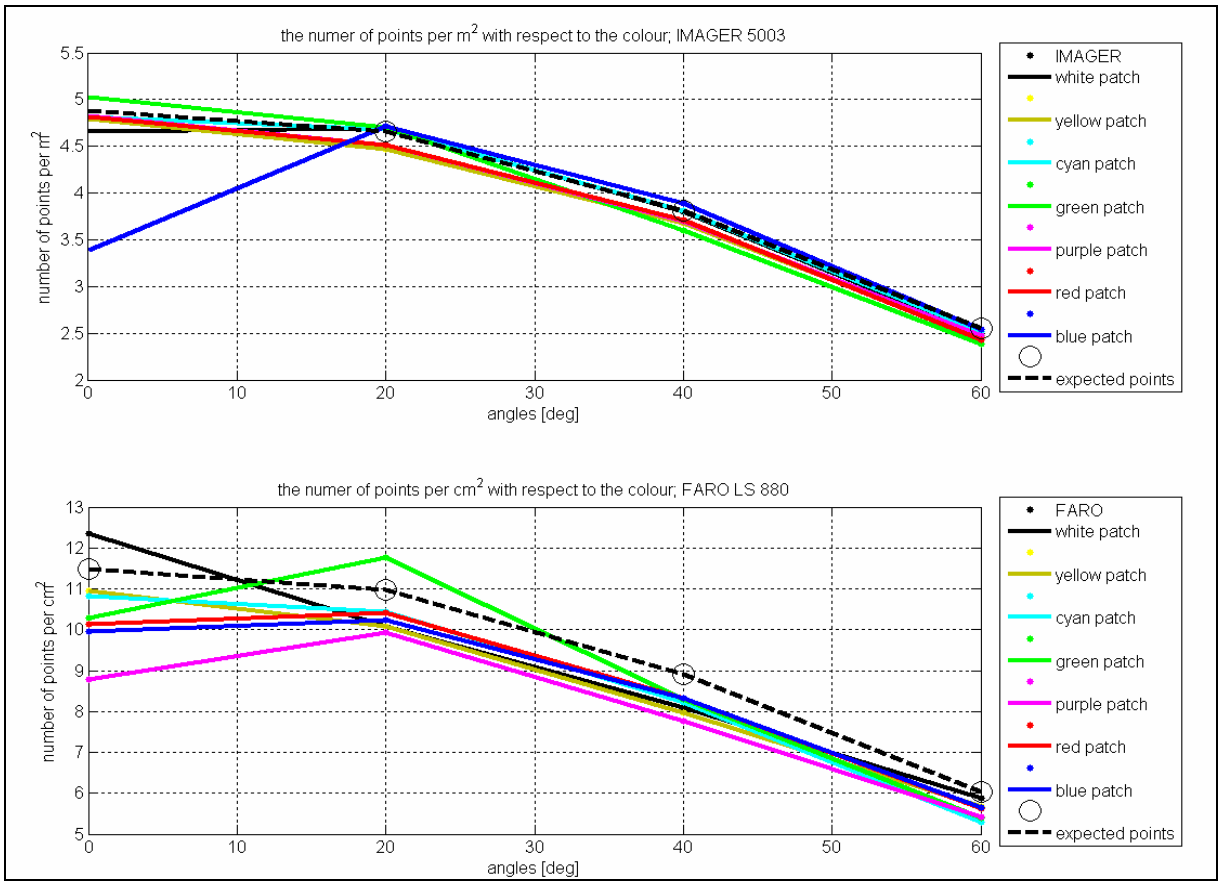

Figure 6.5: The number of *scanned and expected points – scan angle* curves per [cm^2] per scanner per colour patch. *Top:* the curves for the colour patches scanned with the IMAGER 5003, *Bottom:* the curves for the colour patches scanned with the FARO LS 880.

Eight *number of points scanned – scan angle* curves per laser scanner are computed. Seven of these curves represent the number of points obtained per [cm^2] per colour patch and one curve represents the number of points expected per [cm^2] (see figure 6.5). The curves are divided into two graphs in order to make them 'easier' to interpreted.

It can be seen that the curves computed for the IMAGER 5003 follow the expected *number of points – scan angle* curve closely with the blue patch as an exception. The number of points scanned on the blue curve at a scan angle of 0[º] is lower then expected. This can also be seen in figure 6.3b. The top point selection of this figure represents the blue patch of the test chart and a lot of points are absent here. At the other scan angles the

blue patch acts as expected. Combining this feature with the intensity measurements (see section 6.5.2), it is seen that the blue patch returns a very strong signal to the laser scanner while scanned with an angle of 0[º]. It looks like the echo overloads the scanner, making it impossible to measure accurate distances. And as the previous chapter already mentioned, the output scan obtained with the IMAGER 5003 is filtered automatically. The difference in filtering between the two scanners explains the fact that the loss of points on the blue patch does not occur in the scans obtained with the FARO LS 880.

It can also be seen in figure 6.5 that the colour patches scanned with the FARO LS 880 do not follow *the number of points expected – scan angle curve* very closely. In most situations fewer points are scanned than expected. On the other hand, most curves have the same shape as the expected number of points curve.

Because the curves of the different scanners are not based on the same number of points, they are not directly comparable. In order to make the results of both scanners comparable, the curves are normalized by computing the difference between the expected and the scanned points in percentages.

The difference between the scanned and the expected number of points

The curves shown in the figure 6.6 represent the difference between the number of points scanned and the number of points expected. The last is set as 100% so a negative percentage in this graph means that more points are scanned than is expected. As mentioned in the previous chapter, fluctuations between approximately -5% and 5% are insuperable due to the criteria used for the interior selections.

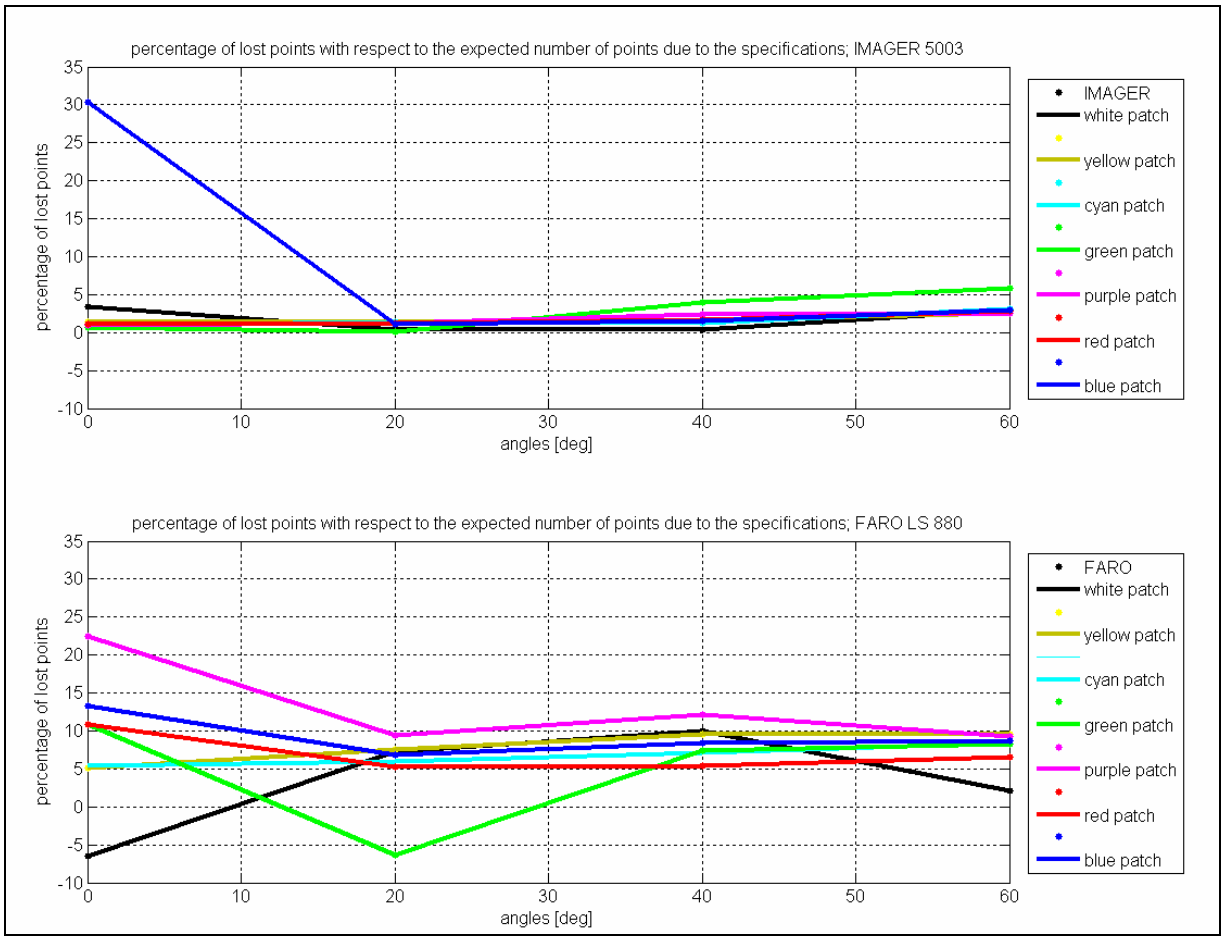

Figure 6.6: The curves showing the difference in percentages between the number of points scanned and the number of expected points for an increasing scan angle per colour patch of the 'Esser' test chart per scanner, *Top:* the curves obtained with the IMAGER 5003 and *bottom:* the curves obtained for the FARO LS 880.

With this knowledge it can be seen that, apart from the blue patch at a scan angle of 0[°], the number of points scanned per colour patch obtained with the IMAGER 5003 does not extent this 5% threshold. On the other hand, the number of points scanned with the FARO LS 880 extent the threshold in almost all situations. This means that fewer points are scanned with respect to the number of points expected with the FARO LS 880.

6.5.2 Intensity values measured

The intensity values measured give insight in the amount of absorbed and reflected energy per colour patch. The intensity values measured obtained with the two laser scanners are compared to be able to see a trend in the absorption and scatter features of the laser signal on different colours. In order to make the results comparable, histogram equalization is performed (see Appendix III). The resulting *intensity – scan angle* curves per colour patch per scanner are shown in figure 6.7.

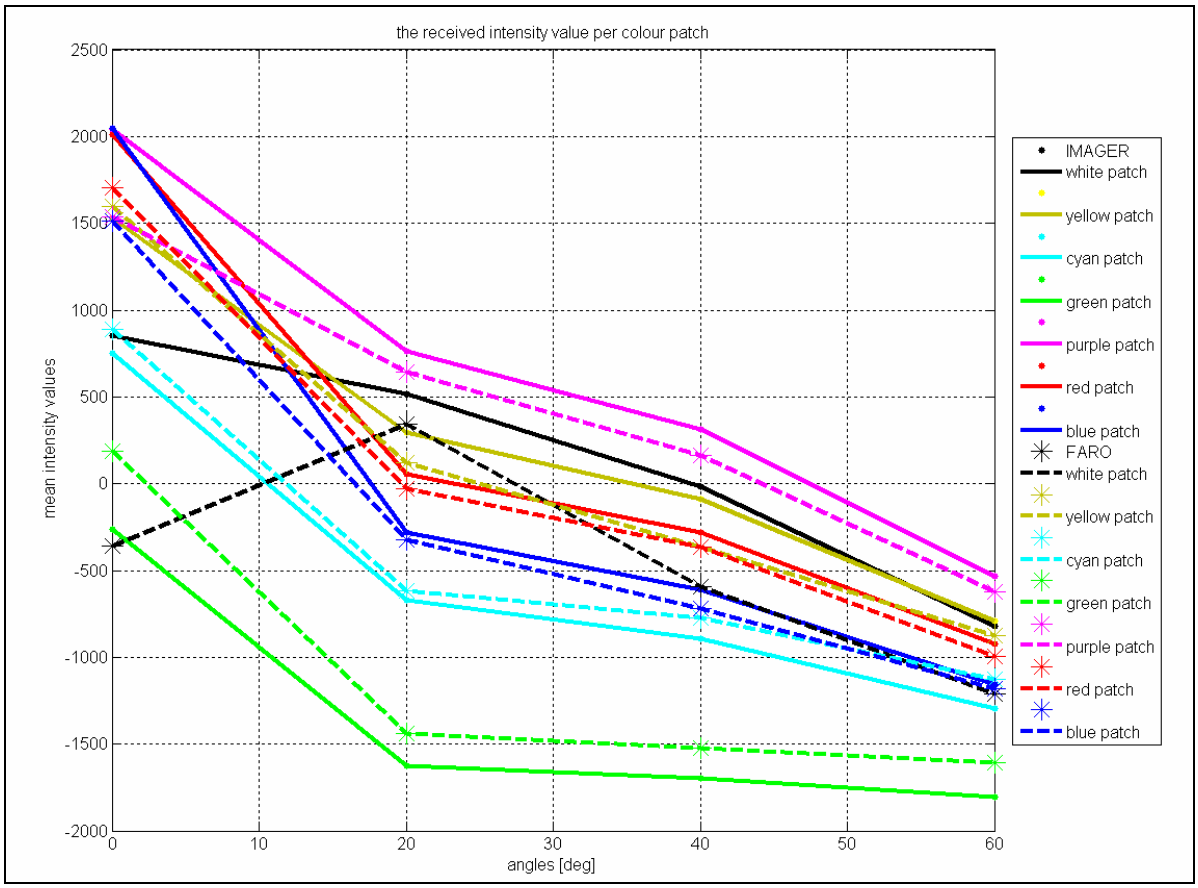

Figure 6.7: The resulting *intensity – scan angle* curves per colour patch per scanner.

Scatter patterns

It can be seen in this figure that for almost all colour patches, the *intensity – scan angle* curves have the same shape as the resulting *intensity – scan angle* curve obtained for the white plate discussed in the previous chapter. However, it must be noted that less scan angles are researched during this experiment which results in less smooth curves. Therefore, it can be concluded that the scatter patterns of most colour patches for the scan angles between 20[°] and 80[°] can be represented be a Minnaert model (see figure 5.9) as well. In order to be able to

find out the scatter patterns for the scan angles between 0[º] and 20[º] additional research is recommended just like mentioned in the previous chapter.

Comparison with scan angle experiment

Exceptions on the above discussed conclusions are the intensity values measured for the white patch at a scan angle of 0[º]. The computed *intensity – scan angle* curves for the white patch scanned with both the IMAGER 5003 and the FARO LS 880 differs from the curves obtained for the other patches. The behaviour with respect to the intensity of both scanners is different but comparable and completely different then the behaviour resulting from the scan angle experiment (chapter 5). This scan angle experiment is based on the white plate, so the colour features are similar. Therefore, the difference between the *intensity – scan angle* curves is most likely due to the roughness of the surfaces. In contrast with the smooth surface of the white patch, the white plate used in the scan angle experiment has a rough surface.

Another explanation can be that the white patch reflects less of the incoming NIR signals. This means that the reflection characteristics of a white object in the NIR domain of the spectrum are different with respect to the reflection characteristics a white object in the visible light domain of the spectrum. In the latter case, almost all incoming light will be reflected and none will be absorbed. It is possible however that a white object absorbs the NIR instead of reflecting it. Whether this is true can be researched by creating a NIR image of the test chart using a NIR filter on a photo camera. This image can clarify whether different patches indeed reflect more of the incoming NIR signal than other patches. It outcome can be used to explain the *intensity – scan angle* curves as well.

Absorption

The height of the curves on the y-axis (= mean intensity values) represents the strength of the returning signal. In this experiment the maximum intensity value that can be achieved is 2048 and the minimum intensity value is -2048. The IMAGER 5003 obtained the maximum intensity values for the purple, red and blue patches at a scan angle of 0[º]. These colour patches ‘score’ also high values with the FARO LS 880 at a scan angle of 0[º]. By looking at the overall heights of the curves, a list can be created which represents the colour with the highest intensity values measured to the colour with the lowest intensity values measured:

1. Purple;
2. Yellow;
3. Red;
4. Blue;
5. Cyan;
6. Green.

NOTE: The white patch is not mentioned in this list because the shape of the curve is different as mentioned in the previous section.

Unfortunately the results do not give insight in the reflection or absorption characteristics of the patches with respect to the NIR domain of the spectrum. However if the theory discussed in section 6.2 is true, NIR must be reflected by the colour patches. Additional research is requested on the NIR. Answers to this question will result in proving or rejecting the theory.

It can be seen that for both scanners the obtained intensity values for the green patch are much lower than the intensity values for the other patches. This is as expected because green is the complementary colour of red (see paragraph 6.2).

Further investigation in the list of intensity values measured did result in a confirmation of the theory that the laser light used for the scans is very close to the red domain of the spectrum and therefore can be assumed red. The six colour patches on the test chart represent the three primary colours in the light theory (red, green and blue) and the three secondary colours (magenta, cyan and yellow). The feature of the secondary colours is that they are a combination of two primary colours only [Brother, 2006]. Figure 6.8 shows three circles of the primary colours and the colour of their intersections. It can be seen that:

- Yellow is a combination of red and green,
- Magenta (purple in this research) is a combination of red and blue,
- Cyan is a combination of green and blue.

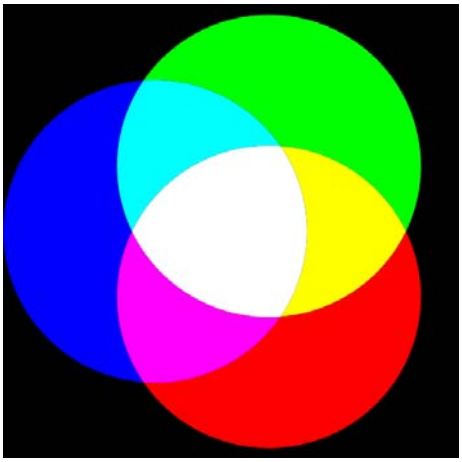

Figure 6.8: Visualization of the triad of primary light colours mixed additively to produce the secondary light triad. The intersection of all primary colours (green, red and blue) gives white light and the intersection of green and blue gives cyan, of red and blue gives magenta and of green and red gives yellow (source: michaelharding, 2006)

If this knowledge is compared to the list on the previous page, it can be seen that both yellow and purple (=magenta) score high with respect to the intensity values measured. Both colours are a combination of red and another colour and according to paragraph 6.2 this combination results in high reflections of the incoming red laser signal at the surface of the object, resulting in higher intensity measurements.

6.5.3 Reliability and precision parameters of the scans

This section will first discuss the *precision* of the scans obtained followed by discussions on the *reliability* and the *overall model.* In the end a conclusion will be given with respect to these three features.

The precision is examined by fitting a LSQ-plane through the scan points that represent one colour patch. All the residuals represent the *noise* of the measurements, which is used to express the precision of the scans. In order to gather insight in the spreading of the residuals the standard deviations (SD) [mm] of these residuals are computed (see table 6.1). Now, two conclusions with respect to the precision can be drawn:

1. one with respect to the performances of a laser scanner on different colours in general,
2. one with respect to the comparison of the performances of the two scanners.

Performances of a phase shift laser scanner with respect to colours in general

By looking at the SDs shown in table 6.2, different conclusions can be drawn. This section will discuss the red marked standard deviations of table 6.2 because these values are strikingly different.

Table 6.2: standard deviations [mm] of the residuals after a LSQ-plane was fitted through the scan points; per scanner per scan angle per colour patch; the red standard deviations are extreme values.

	White		**Yellow**		**Cyan**		**Green**		**Purple**		**Red**		**Blue**	
Scan angle	*IMA*	*FAR*	*IMA*	*FAR*	*IMA*	*FAR*	*IMA*	*FAR*	*IMA*	*FAR*	*IMA*	*FAR*	*IMA*	*FAR*
0[°]	*4.73*	2.31	0.87	2.11	1.01	2.53	1.02	2.70	0.62	*3.23*	0.91	*4.79*	0.79	*8.21*
20[°]	1.10	2.30	0.96	2.66	1.52	2.87	*2.17*	*4.44*	0.98	2.30	0.96	2.51	1.21	2.91
40[°]	1.33	2.75	1.05	2.90	1.42	3.19	*3.35*	*5.34*	1.06	2.50	1.17	2.50	1.26	2.88
60[°]	1.23	3.15	1.67	3.10	1.87	3.66	*4.21*	*6.52*	1.21	2.79	1.50	2.78	1.50	3.67

IMA = IMAGER 5003
FAR = FARO LS 880

White patch; IMAGER 5003; scan angle 0[°]

The SDs of the residuals for the IMAGER 5003 are in general < 2[mm]. However, for the white patch scanned with a scan angle of 0[°] a SD of 5.25[mm] is computed. This significant difference can be explained by looking at a visualization of the scan points of the white patch (figure 6.9a). The red circle in this figure indicates the source of the high SD. Further investigation let to insight in the problem; the test chart is located inside the angle measurement device with the white patch down. The top part of this device consists of shinny steel parts. It is most likely that these parts reflect the laser signals in a specular way. The specular reflected signal reaches the white patch and the laser signal reads the wrong distances. This effect is called *multi-path* and is visualized in figure 6.9b.

To see whether this problem also occurred for the FARO LS 880, the belonging scans are also researched. It is found out that the same problem occurred for the FARO LS 880 but less extreme, properly because of the interior selection. But this effect might explain the different behaviour of the *intensity – scan angle* curves of the white patch at a scan angle of 0[°].

A solution to this problem is to place black velvet on top of the shinny parts of the angular measurement device. This prevents the occurrence of specular reflection on top of the measurement device and therefore the multi-path effect.

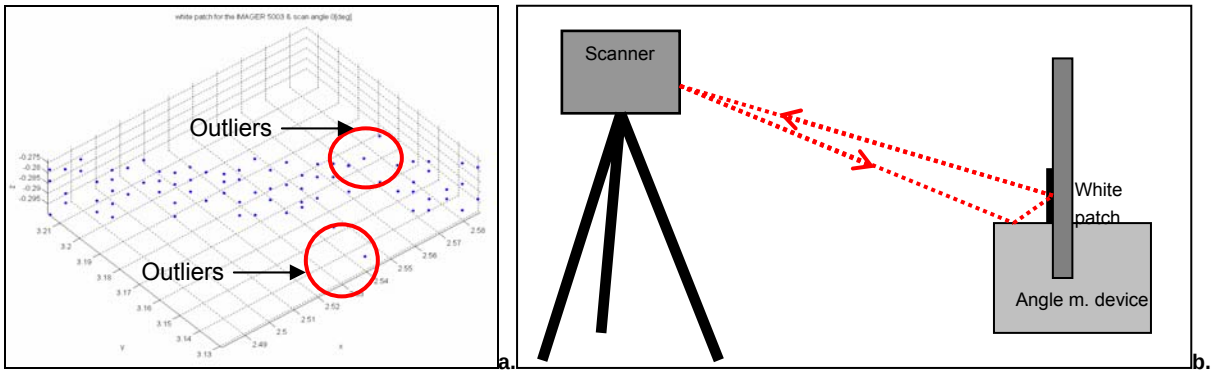

a. **b.**

Figure 6.9: **a.**: the visualization of the white patch selection scanned with the IMAGER 5003 for a scan angle of 0[°], the scan points in the red circles are the detected outliers, **b.**: a schematic overview of the multi-path effect, the laser signal is reflected by the angle measurement device to the white patch and reflected back to the scanner, causing another echo than the scanner expects.

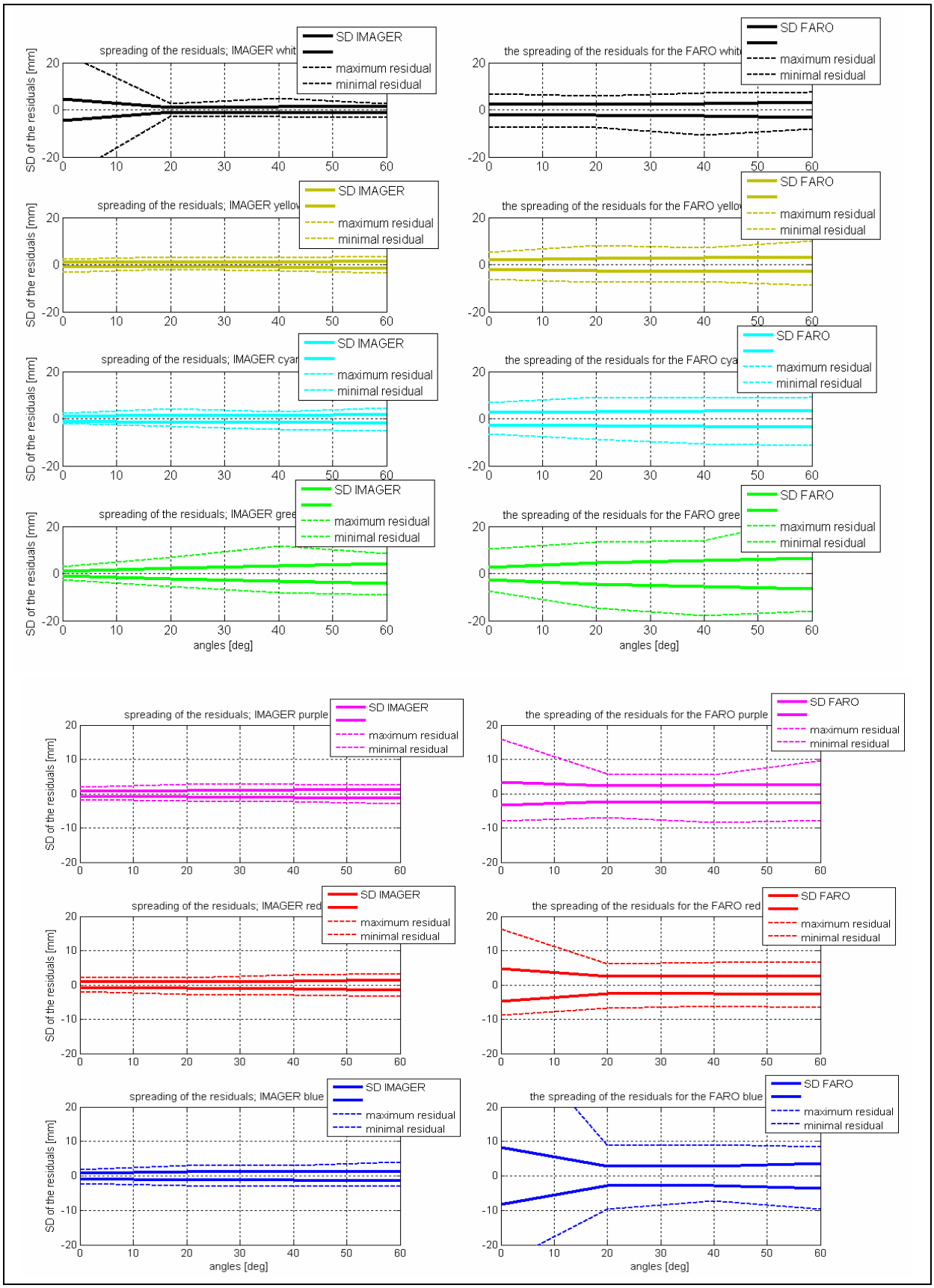

Figure 6.10: Visualization of the spreading features of the residuals by showing the trends of the standard deviation (SD), the minimum and the maximum residuals per scanner per colour patch per scan angle, 68% of the residuals are located within the bold lines of the figures as they represent the SD and 100% of the residuals are located within the dashed lines. *Left* the results obtained with the IMAGER 5003 and right the results obtained with the FARO LS per colour patch.

Purple, red and blue patches; FARO LS 880; scan angle 0[°]

The maximum and minimum residuals give additional information on the noise factor of the scans. They represent the range in which 100% of the residuals are located. Figure 6.10 shows the curves per colour patch of both scanners with two lines representing the SD of the residuals and two lines representing the maximum and minimum residual values.

It can be seen in this figure that not only the SD of the residuals of the purple, red and blue patch scanned with the FARO LS 880 are high, also the minimum and maximum residual values of these colours are extremely high, especially for the blue patch. Examination of the scans did not locate systematic errors or other strange behaviours. Therefore, it can be said that scanning a purple, red or blue surface with the FARO LS 880 at a scan angle of 0[°] does not give a precise scan.

However, an explanation of the effect on the blue patch can be given. It was mentioned in section 6.4.1 of this thesis that a lot of gaps occur on the blue patch scanned with the IMAGER 5003. These gaps are probably caused by the internal filter of the IMAGER 5003; the obtained results are so bad due to overloading the laser scanner that they are deleted from the scan. The FARO LS 880 however does not filter the points, which means that all the bad measurements are still present in the output scan.

Green patch; both laser scanners; scan angles ≥ 20[°]

It can be seen in table 6.2 that the computed SD for the green patch is for both scanners relatively high with respect to the other patches. This is as expected because green is the complementary colour of red and therefore, the green patch absorbs most of the incoming laser light which results in weaker echoes and less precise measurements.

Comparing the precision parameters of the two laser scanners

Figure 6.10 and table 6.2 can also be used to compare the *precision* of the two laser scanners. It follows from both sources that the output scans per colour obtained with the FARO LS 880 contain more noise than the output scans obtained with the IMAGER 5003. This mean that the output scan files obtained with the IMAGER 5003 are more precise then the output files obtained with the FARO LS 880.

Reliability of a phase shift laser scanner with respect to colours in general

The *reliability* of the scan is determined by comparing the measured scan angles with the true scan angles determined with the angle measurement device (see figure 6.11). By looking at graphs it can be seen that the computed scan angles of both laser scanners are located within the reliability of the angle measurement device. This means that based on this experiment it can be concluded that the colour does not influence the reliability of the scans obtained with both scanners.

The only exception on this conclusion is the measured scan angle for the blue patch scanned with the FARO LS 880.

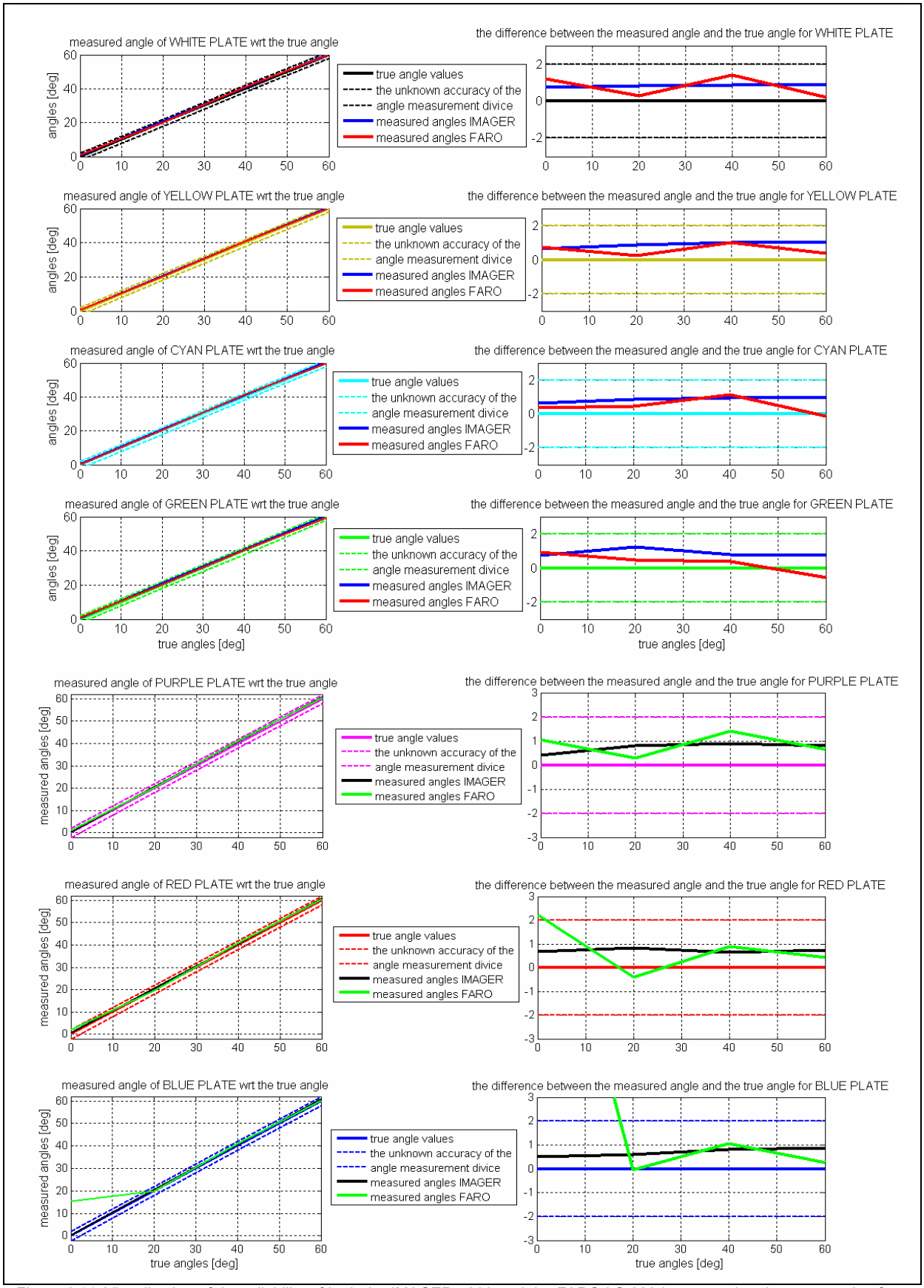

Figure 6.11: Visualization of the reliability of both the IMAGER 5003 and the FARO LS 880 by computing the scan angles from the scans obtained and their LSQ-plane and compare them with the true scan angles determined with the angle measurement device. The reliability of this device is assumed to be 2 [°]. *Left:* the *measured scan angle – true scan angle* curves for both laser scanners and right the difference between the true and the computed scan angles for both laser scanners.

Comparing the reliability parameters of the two laser scanners

Figure 6.11 is also used to compare the reliability of both laser scanners. It can be concluded that the measured scan angles per colour per scanner do not differ significantly apart from the blue patch. Therefore, in general it can be said that the obtained output scans with both scanners are evenly reliable with respect to the different colours.

The difference in the blue patch can be explained by the difference in filtering. The IMAGER 5003 filters the scan points which results in gaps in the scan while the FARO LS 880 'allows' the noisy data in the scan. This causes a less reliable scan points but without gaps.

As is also mentioned in the previous chapter, it is not 'fair' to compare the results of a non-filtered and a filtered scan, therefore, the conclusions drawn in this paragraph are only valid for the performances of the two scanners with respect to their output scans. The previous chapter also mentioned that Fugro-Inpark prefers to start interpreting and modelling the scans directly after the scanning phase and they require the highest accuracy for their models. Therefore, it can be concluded that, based on the colour experiment, the IMAGER 5003 is best to use as the data contains less noise which results in an overall model is the most accurate (see section 4.7.4).

6.5.4 Bias parameters

Section 3.2.6 of this thesis described an existing experiment set-up for the testing of laser scanners on surfaces with known colours. This existing experiment has a lot of similarities with the colour experiment of this research. One of the results obtained in the experiment of section 3.2.6 is offset or bias of the colour patches with respect to the average plane. This result gives insight in the systematic errors colours or grey values give in the measurements. For example it was shown that the black patch was located behind the average plane and the white patch was located in front of this average plane.

These offsets might indicate a systematic difference in the measured range that is unique or characteristic for the particular colour. In this section it is tried to give insight in these offsets for the colour patches.

Procedure of bias determination

In order to determine the biases of each colour patch first an average plane is estimated through the entire point cloud obtained. This estimation is based on the LSQ-principle and the same model of observation equations is used as discussed in section 4.6 of this thesis. Following the best fitting planes of the separate colour patches are subtracted from the average plane. This is done by placing a regular grid on top of both planes. These grid coordinates are the same for both planes and result in different range (y) values. These y-values can be compared in order to find the biases of each grid point. Next the mean, minimum and maximum of these biases is computed. Negative values correspond to colour patches of which the range is measured too long with respect to the average plate. Table 6.3 shows the mean biases per colour patch per scanner with respect to the average plane. Figure 6.12 shows the curves of these mean, minimum and maximum values. NOTE: the differences in the y-axis of this figure.

By looking at the results shown in figure 6.12 it can be concluded that not all patches are situated exactly parallel to the average plane. If the biases of the colour patches at a certain scan angle have a positive minimum value and a negative maximum value, the colour patch LSQ-plane intersects with the average plane. The reason for this is shown in figure 6.13 for a scan angle of 0[°] for both scanners.

Table 6.3: The mean values of the biases [mm] between the average plane through the point cloud and the planes through the different colour patches. Negative values represent patches that are located behind the average plane and positive values represent patches that are located in front of the average plane.

	White		**Yellow**		**Cyan**		**Green**		**Purple**		**Red**		**Blue**	
Scan angle	*IMA*	*FAR*	*IMA*	*FAR*	*IMA*	*FAR*	*IMA*	*FAR*	*IMA*	*FAR*	*IMA*	*FAR*	*IMA*	*FAR*
0[º]	-0.32	-3.82	0.05	-2.64	0.24	3.27	0.20	8.28	-0.64	-2.65	0.51	2.93	-0.19	-6.74
20[º]	0.35	-1.62	0.20	-0.66	0.20	2.19	-1.35	2.57	-0.19	-3.75	0.46	0.48	0.20	1.16
40[º]	0.34	0.17	0.24	-0.13	0.44	0.56	-1.26	1.17	-0.19	-3.63	0.56	0.51	0.02	0.07
60[º]	0.63	2.69	0.32	-0.94	0.09	0.98	-0.60	-0.18	-0.33	-3.44	0.38	-1.10	-0.14	1.81

These intersections are properly caused by the fact that the colour patches are relatively small and the redundancy is therefore small as well. This influences the accuracy of the fitted plane (see section 4.7.3). It would be better to invest the influence of the colours using larger patches.

This explanation can be combined with the knowledge obtained from figure 6.13. This figure visualizes a side view of the scans obtained of the colour test chart with the FARO LS 880 and the IMAGER 5003 at a scan angle of 0[º]. It can be seen in this figure that the points obtained with the FARO LS 880 are varying with an unknown pattern. Because the colour patches of the test chart are all connected to each other, it is imaginable that the points on the boundaries of the patches contain mixed information and cause the wave behaviour of the data. This problem was thought the be overcome by taking the interior selections of the patches but as figure 6.13 shows, this effect is larger then expected, especially for the blue patch of the FARO LS 880. The strange behaviour of the plane representing the blue patch (figure 6.12) can be explained by this theory, just like the non-parallelism of the patches with respect to the average plane because the mixed points influence the plane fitting.

This problem does occurs for the IMAGER 5003 as well but less extreme and this can be explained by the fact that the IMAGER 5003 filters or correct the data before the output is created. This means that the point vary less extreme for the IMAGER 5003 (see figure 6.13b). The difference is present but hardly visible. This results in more parallel plane fits but still intersections are present due to the size and the redundancy of the patches.

In general it can be seen that the purple patch is in all situations located behind the average plane. This is means that the distance measured by a laser scanner to a purple or magenta object will be measured too long. The cyan patch is always located in front of the average plane which means that the distance to an object of this colour is expected to be measured too short.

No general trend is seen in the rest of the colour patches, so additional research is recommended to gather insight in the characteristics of different colour with respect to measurements with laser scanners.

Furthermore, it can be seen in table 6.4 and the figures 6.12 and 6.13 that the biases of the IMAGER 5003 are very small; on sub-millimetre level in most situations. The biases of the FARO LS 880 vary more and they are within millimetre level. This is properly due to the more accurate models (see section 6.5.3) obtained for the IMAGER 5003 and this is connected to the filter properties of the IMAGER 5003.

Additional research is recommended on the characteristic bias determinations caused by colours because the procedure discussed in this section is based on an average plane determined through all colour patches. Taking an average plane on which the performances of laser scanners is known is thought to be better because the influence of one colour can be examined easier and exact. The second recommendation follows this statement as it is most likely better to examine one colour per scan to eliminate mixed colour information that can influence the results negatively.

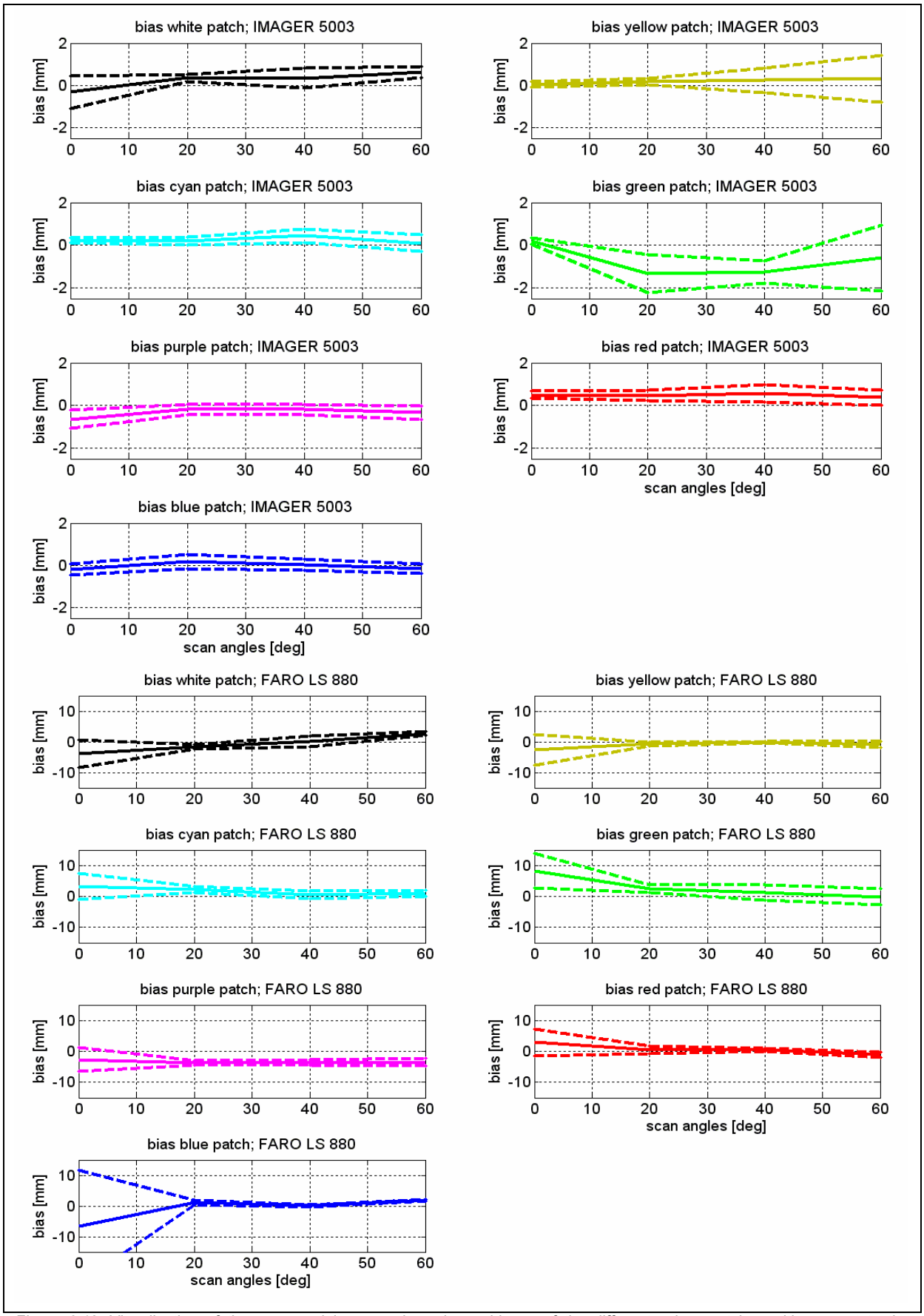

Figure 6.12: Visualization of the mean, minimum and maximum biases of the different colour patches with respect to the average plane through the point cloud per scanner. NOTE: the different y-axis of the top curves and the bottom curves!

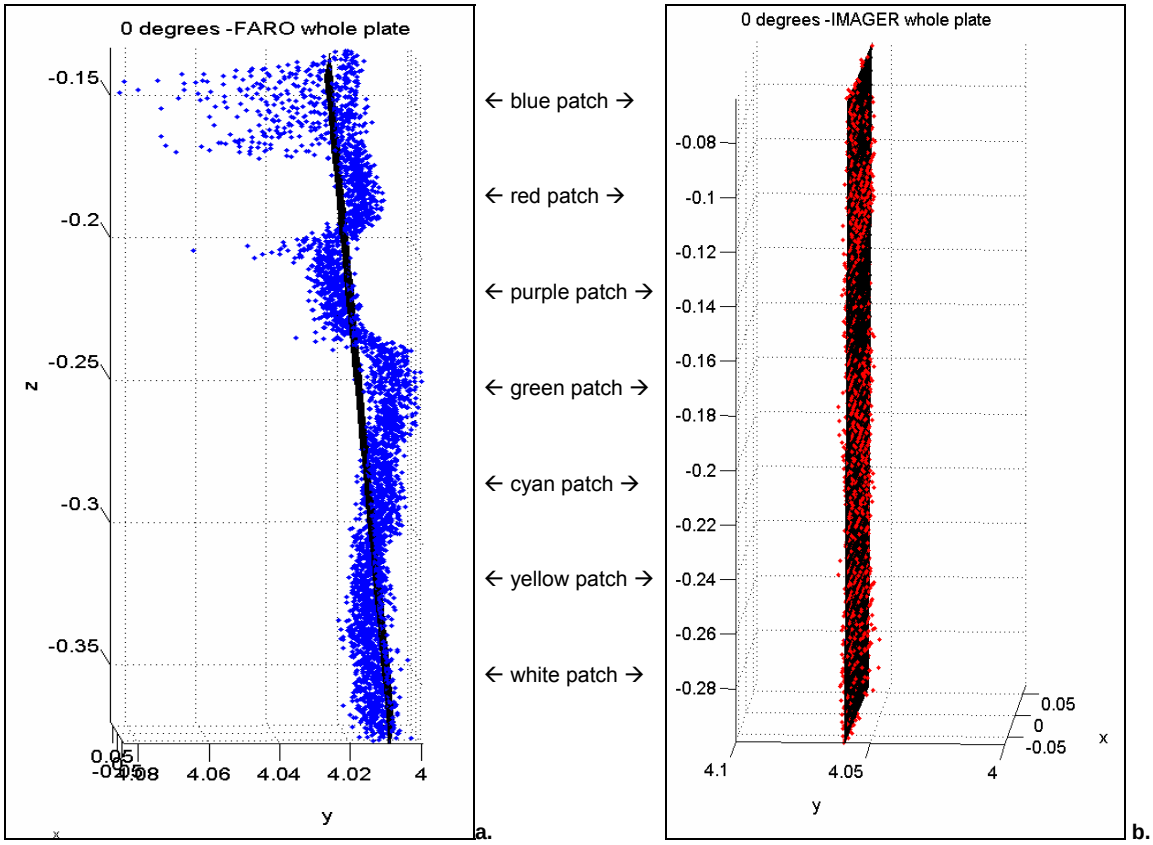

Figure 6.13: Two side views of the LSQ-plane of through the point cloud of the colour test chart at a scan angle of 0[º]. To remember: the test chart consists of the following colours from bottom to top: white, yellow, cyan, green, purple, red and blue. **a.** a side view of the scan obtained with the FARO LS 880 and the average plane, showing large variances in the data, influenced by the different colours. **b.** a side view of the scan obtained with the IMAGER 5003 and the average plane, showing almost no variances in the data, influenced by the different colours.

7 Reflectivity experiment

The feature of interest that will be discussed in this chapter is the reflectivity of the surface of an object. First a motivation for the implementation of this experiment will be given in paragraph 1, followed by the experiment set-up in paragraph 2. The expected results or hypotheses with respect to (1) the number of points scanned, (2) the intensity values and (3) the reliability and precision of the scans obtained are discussed in paragraph 3 and this chapter finishes with the results of the experiment in paragraph 4.

7.1 Motivation

Inside the scan areas in which laser scanning is used, numerous of different objects are present. These objects have different surface characteristics and these characteristics influence the absorption and reflectivity of the different objects. Knowledge on the behaviour of both scanners on surfaces with known reflectivity characteristics is useful to be able to predict the performance of the scanner in a particular situation.

7.2 Experiment set-up

The reflectivity experiment is closely connected to the colour experiment (see chapter 6). In this experiment however, not the effect of the colour is examined but the 'known' reflection characteristics of different grey value charts.

In this experiment also an 'Esser test chart' is used (see figure 7.1) [Digitalkamera, 2006]. The plate consists of two 5-graduated counter current grey scales that are arranged on a grey background. The reflectance features of the different patches are known and mentioned in table 7.1. In the middle of the two rows of grey values, a field of black velvet is located. The remission of this field is almost 0 (< 0.5[%]), meaning that it is expected that this velvet will absorb all of the incoming energy and nothing will be reflected back to the laser.

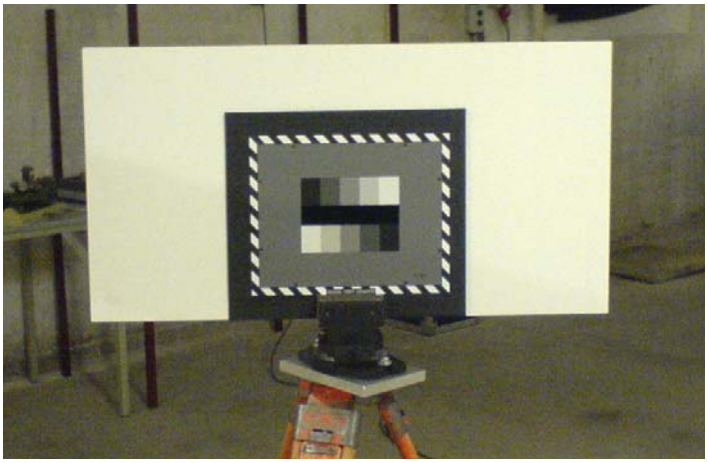

Figure 7.1: the 'Esser grey scale test Chart' (photo: Van Ree, 01-05-2006).

Table 7.1: the characteristics of the 5-graduated grey scales of the Esser grey scale test chart used in the reflectivity experiment

Step	Relative Brightness*	Remission [%]	Output voltage [%]
1 white	0.15	71	100
2	0.37	43	77.5
3	0.65	22	55
4	1.05	09	32.5
5 black	1.75	02	10

* the brightness values are determined relative to BaO_4S which is set 0. BaO_4S has a total reflection and is used in mirrors

The base set-up as shown in figure 4.1 will be used to create this experiment. The test chart is placed in front of the white plate. By rotating the plate with steps of 20[°] (clockwise), the influence of the scan angle on the known reflectivity is determined as well. The scan angle is varied from $0[°] \geq \alpha \geq 60[°]$ so a total of four scan angles are examined per resolution per scanner. This means that the whole experiment will result in sixteen scans of the test chart. Figure 7.2 shows two of the scans obtained, one obtained with each scanner, at a scan angle of 0[°] and the middle resolution.

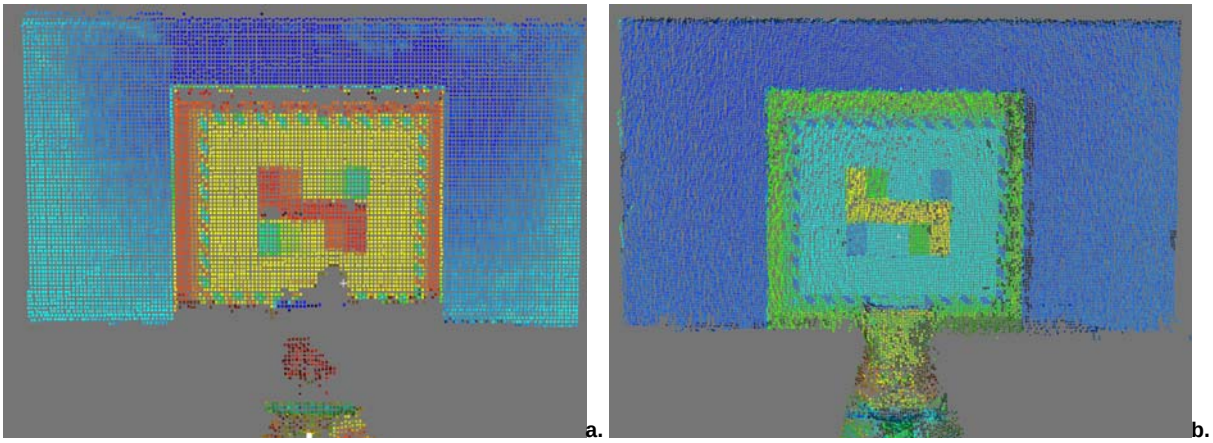

a. **b.**

Figure 7.2: Two scans achieved with the grey value experiment set-up, both scanned at the middle resolution and with a scan angle of 0 [°], **a.**; the scan achieved with the Leica HDS4500, **b.**; the scan achieved with the FARO LS 880.

The colours in figure 7.2 represent the intensity values measured. It can be seen that the intensity values are not the same for both scanners but as the middle patch of the scanned plate represents the black velvet, the colour of this patch represents a low intensity value. Despite the expectation that no points will be measured on the black velvet it can be seen that both scanners did measure some points.

In the discussion of this experiment the white and the black patches are referred to as white and black patches. The grey value patches in between there patches however are referred to as light-grey, middle-grey and dark-grey (from white to black).

7.3 Hypothesis

By combining the knowledge of the absorption and dispersion theories (see section 4.1.3) it is possible to create a number of hypotheses with respect to the influence of the surface reflectivity on the scans obtained. These hypotheses can also be used for the comparison of the obtained results.

This paragraph will discuss the expected results with respect to the following three features:

1. the number of points scanned,
2. the scanned intensity values,
3. the reliability and precision of the scans obtained.

7.3.1 The number of points scanned

The reflectivity characteristics of a surface determine the intensity. The intensity values of the echoes of dark and rough surfaces are expected to be low and there is a chance that they will not expand the threshold value. When the echo is not detected, this can cause gaps in the scan.

However, a smooth white surface absorbs less of the signal but reflects most of the signal in a specular way. In this situation also no echo will return to the scanner when the scan angle is > 0[°]. Both of these situations result in no echo returning to the scanner, which means that no measurement can be done and fewer points on the object will be scanned.

Concluding; this means that the surface characteristics of scanned objects are of importance for the total number of points scanned. Two *expectations* can be created, which are the following:

1. If the scan angle is > 0[°], more scanned points will be measured when a light and rough object is scanned. The worst results are expected on dark and/or smooth objects as they absorb most of the incoming signal and reflect it in a specular way.

2. If the scan angle is = 0[°], more points will be measured when a light and smooth object is scanned. The worst results are expected on dark and/or rough objects as they absorb most of the incoming signal and reflect it in a diffuse way.

7.3.2 Intensity values

Absorption characteristics are dependent on both the colour (see chapter 6.2) and the brightness of the surface. Darker objects absorb more of the incoming energy than lighter objects.

The reflectivity characteristics are responsible for the scatter pattern of the incoming signals. When the surface of an object is rough, most of the incoming signal strength will be reflected diffusely and when the surface is smooth the scatter pattern will be close to specular reflection.

A combination of both the brightness and reflectivity features will result in different situations. Figure 7.3 shows four extreme combinations.

It can be seen that in all situations only a part of the reflection returns to the scanner. In the situations where most of the signal strength is absorbed (figure 7.3b and d), the strength of all the reflections together is weaker. The echo returning to the scanner is even weaker, meaning less intensity is measured for that scanned point.

The situations shown in the figures a. and c. of figure 7.3 are totally different because less energy is being absorbed due to the bright colour of the surface. This means more of the incoming energy is reflected resulting in a higher overall reflection.

Figures 7.3a and b show that when the surface is smooth, most of the signal is reflected in the direction of the angle of reflection (see section 4.1.3). This results in high intensity values measured if the scan angle is 0[°] but they will decrease very fast when the scan angle becomes > 0[°].

However, if the surface is rough, the signal is reflected diffusely as is shown in the figures 7.3c and d. The measured intensity value will be lower for a scan angle of 0[°] then if the object will be smooth but the intensity values measured will decrease less when the scan angle is increased.

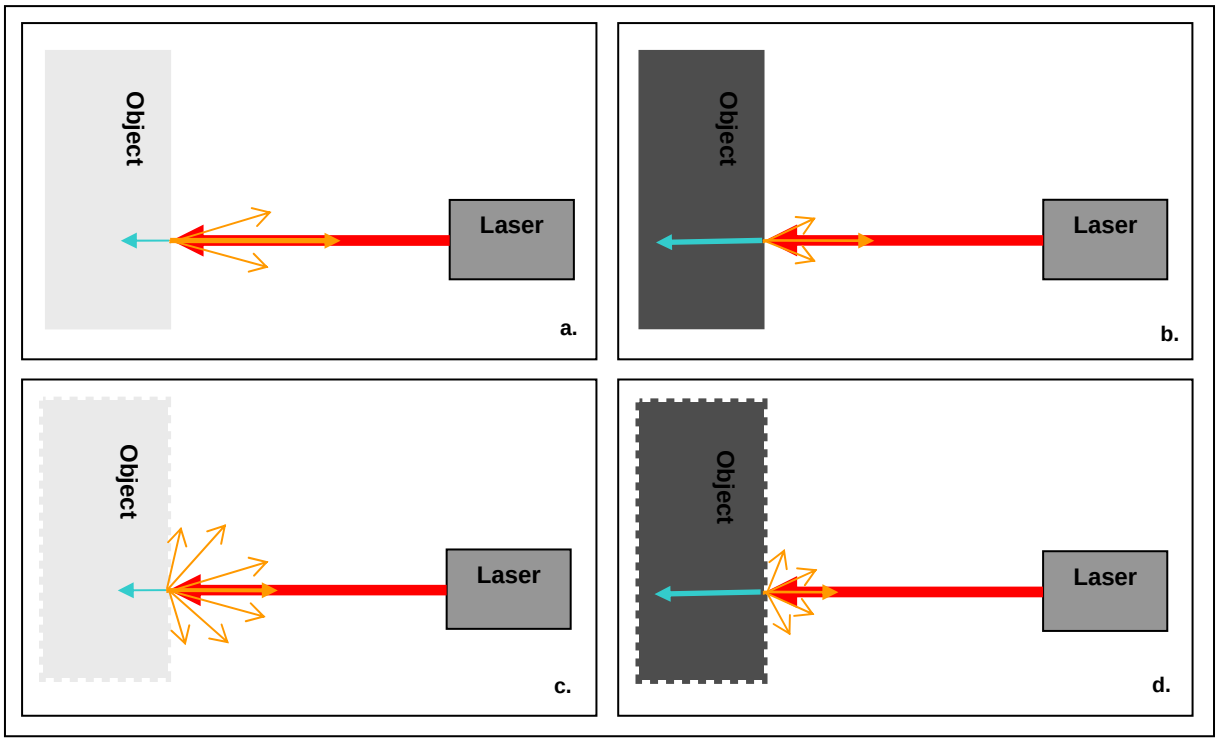

Figure 7.3: four combinations of absorption and reflection characteristics, the absorption is represented by the size and thickness of the blue arrows and the dispersion by the sizes and thickness of the orange arrows, **a.**; a light object with a smooth surface, **b.**; a dark object with a smooth surface, **c.**; a light object with a rough surface, **d.**; a dark object with a rough surface.

Concluding this means that two possible expectations are created:

1. When the scan angle is > 0[°], it is expected that the intensity values are high when a bright and rough object is scanned. The worst results are expected on dark and smooth objects as they absorb most of the incoming signal and reflect it in a specular way.

2. When the scan angle is 0[°], it is expected that the intensity values are high when a bright and smooth object is scanned. The worst results are expected on dark and rough objects as they absorb most of the incoming signal and reflect it in a diffuse way.

7.3.3 The reliability and precision of the scans

In the previous two sections it was explained that the surface characteristics of the scanned object have influences on: (1) the number of points scanned on an object and (2) the intensity values measured per scan

point. This resulted in two different hypotheses per section: one with respect to a scan angle of 0[°] and one with respect to a scan angle > 0[°] which resulted into two different hypotheses for the reliability and precision of the measurements as well.

1. If the scan angle is > 0[°], the *best* precision and reliability will most likely be achieved on a light and rough object because scanning an object with these characteristics results in a high number of points scanned with high intensity values.

   Smooth objects reflect the incoming signal in a specular way which results in very little measurements, resulting in a bad a precision and reliability of the measurements. When a rough object is dark however, most of the signal is absorbed and the weak reflected signal will be reflected diffusely. The echo that returns to the laser scanner is even weaker and might even not even extend the threshold value of the scanner. This results in no measurements at all or measurements with bad accuracies and precisions.

   Concluding, this means that the *worst* reliability and precision parameters can be expected for objects which are dark. These objects absorb most of the incoming signal and it is expected that the reflected echoes are not always detected.

2. If the scan angle is = 0[°], the number of points scanned and the intensity values will be high, when a light and smooth object is scanned. It is expected that this combination results in the *best* reliability and precision of the measurements. Furthermore it is expected that scans obtained on dark – smooth objects and light – rough objects will also have a *good* reliability and precision when the scan angle is 0[°]. *Lower* reliability and precision is expected for dark and/or rough objects as they absorb most of the incoming signal and reflect a weak signal in a diffuse way.

7.4 Results

The scanning phase of this experiment resulted in 8 scans obtained at the middle resolutions of the scanners. These scans are used for threefold analysis: (1) number of points scanned, (2) the intensity values and (3) the reliability and precision of the scans and the overall model parameters.

After implementing a couple of changes to the automatic selection interior program (chapter 4), the interiors of the patches are selected. Two examples of interior selections of the scans obtained at a scan angle of 20[°] are shown in figure 7.4. The different colours of the points inside the selections represent the intensity values measured.

NOTE: all results that are discussed in this paragraph are achieved on the Esser grey scale test chart at a scan range of approximately 4[m] and scanned with the middle resolution of both scanners.

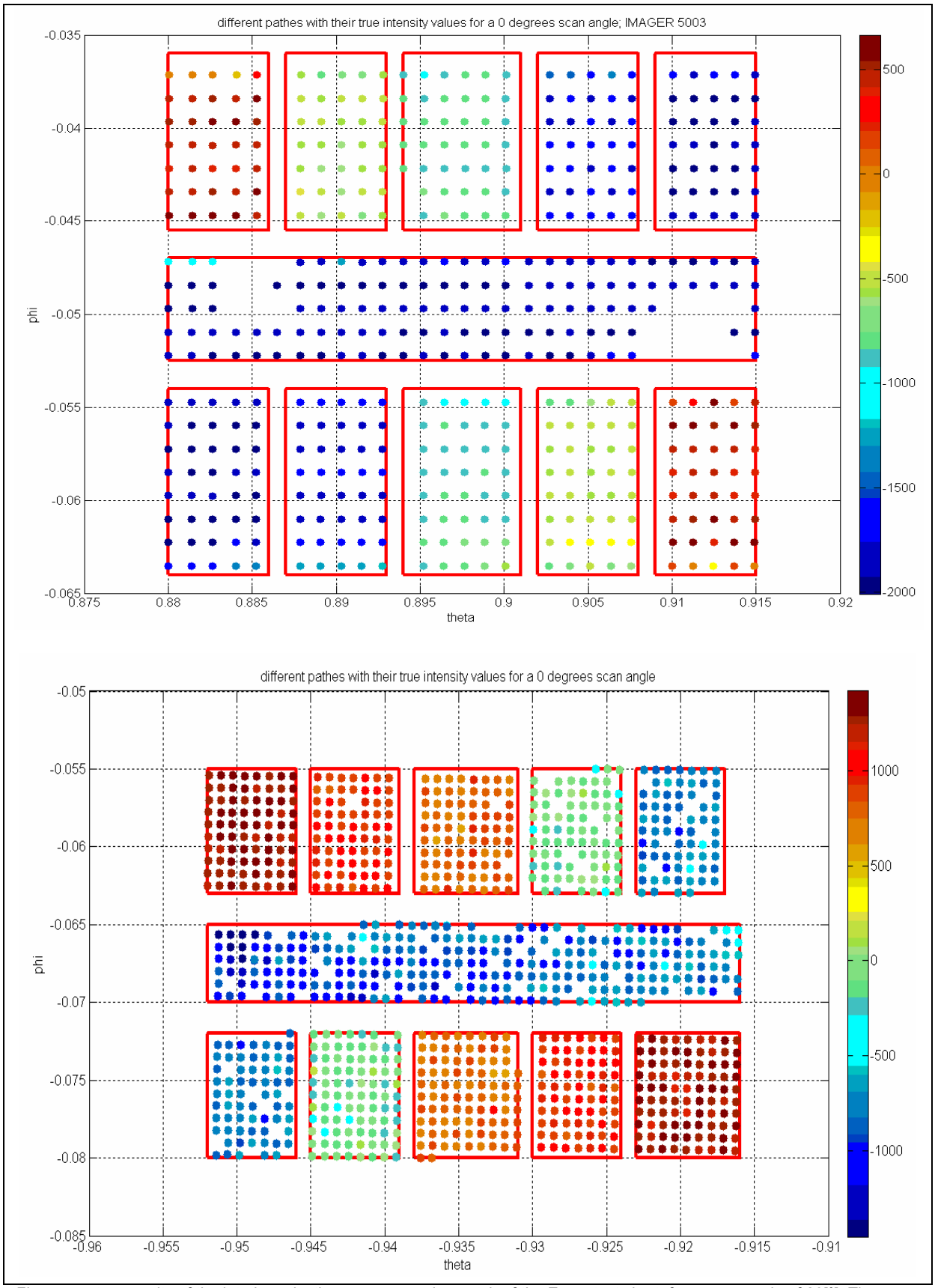

Figure 7.4: two results of the interior selections per grey value patch of the Esser test chart; for a scan angle of 20[°]. The areas on the bottom left and top right represent the white patches and the patch on the bottom right and top left represent the black patches. The middle area corresponds to the black velvet. *Top*: the results obtained with the IMAGER 5003 and *bottom:* the results obtained with the FARO LS 880.

7.4.1 Number of points scanned

Seven *number of points scanned – scan angle* curves per laser scanner are computed. Six of these curves represent the obtained number of points per [cm^2] per grey value patch and one curve represents the number of expected points per [cm^2] (see figure 7.5).

It can be seen that the curves computed for the IMAGER 5003 follow the expected *number of points – scan angle* curve closely up to a scan angle of 60[°] except for the black velvet. The number of points scanned on the black velvet is much less then the expected values. The bad result on the black velvet however, is as expected, because the remission characteristic of this patch is almost 0. In fact it is expected that no signal at all will return to the scanner but in fact quite a lot of measurements are obtained.

It can also be seen in figure 7.5 that the grey value patches scanned with the FARO LS 880 do follow the expected number of points-line very closely up to a scan angle of 40[°]. After this scan angle fewer points are scanned than expected in some situations. The curve corresponding to the black velvet patch also shows a deviation with respect to the other curves. This curve is also located lower then the other curves but not as significantly as with the IMAGER 5003. This again can be explained by automatic filtering build-in in the IMAGER 5003.

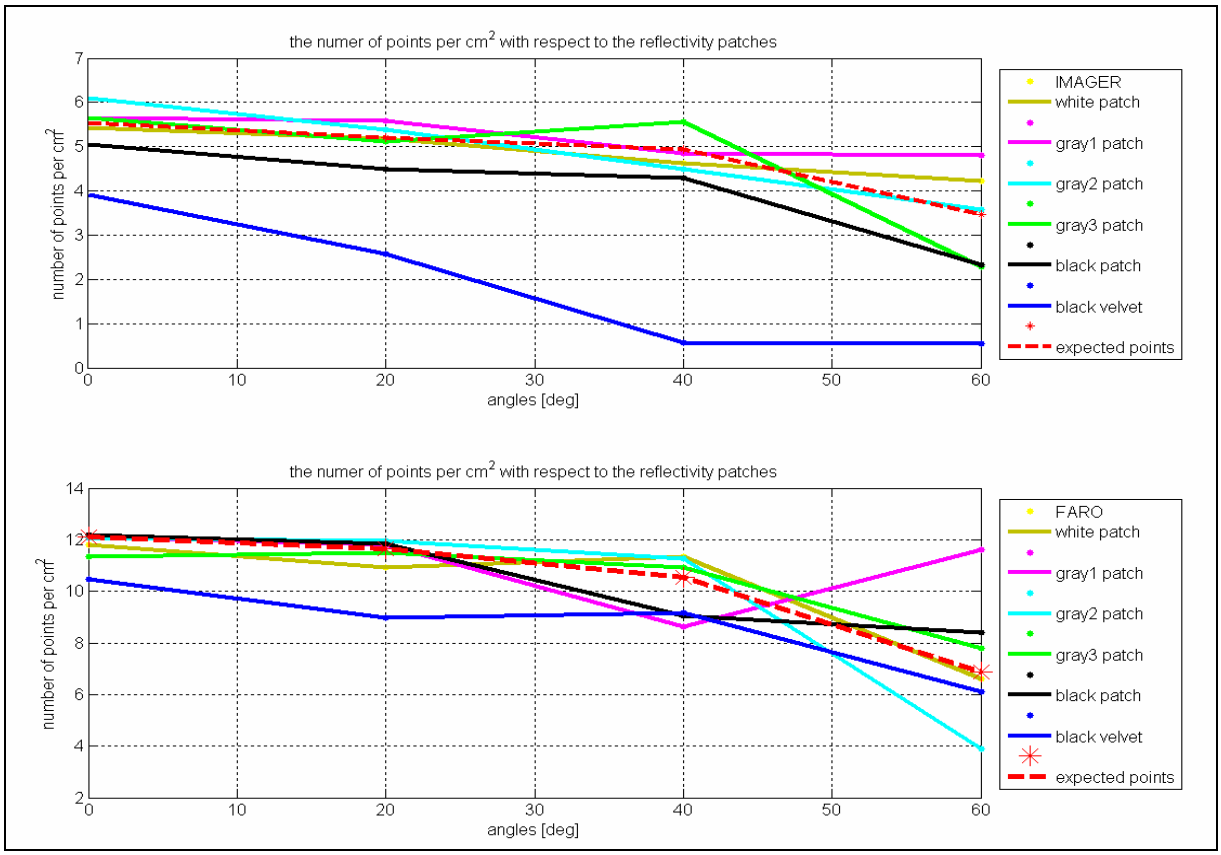

Figure 7.5: The *number of scanned and expected points – scan angle* curves per [cm^2] per scanner per grey value patch. *Top:* the curves for the patches scanned with the IMAGER 5003, *Bottom:* the curves for the patches scanned with the FARO LS 880.

The difference between the scanned and the expected number of points

The curves in figure 7.6 represent the difference between the number of points scanned and the number of expected points. The last is set as 100% so a negative percentage in this graph means that more points are

scanned than is expected. As mentioned in the chapter 5, fluctuations between approximately -5% and 5% are insuperable due to the criteria used for the interior selections.

With this knowledge it can be seen that, apart from the black velvet patch also the black patch extents this 5% threshold for the IMAGER 5003. This can be explained by the remission of 02, which is also very low (table 7.1). Furthermore, the number of points scanned shows an unexpected behaviour around the scan angle of 60[°]. The black velvet, black and dark-grey patches lose a lot of points at this angle which is expected. On the other hand, a scan angle of 60[°] on the white, light-grey and middle-grey patches result in more points then expected. No explanation can be given for this last part. The loss of points on the darker patches is due to the combination of the scan angle and their remission features.

The number of points scanned with the FARO LS 880 almost never extents the 5% threshold up to a scan angle of 40[°] apart from the black velvet. When the scan angle is increasing however, the number of points acts differently as expected, but there does not seem to be a relation with respect to the darker patches as is the case for the IMAGER 5003. At a scan angle of 60[°] the least points are scanned on the middle-grey patch whereas on the black velvet much more points are scanned. No direct explanation can be given for this occurrence.

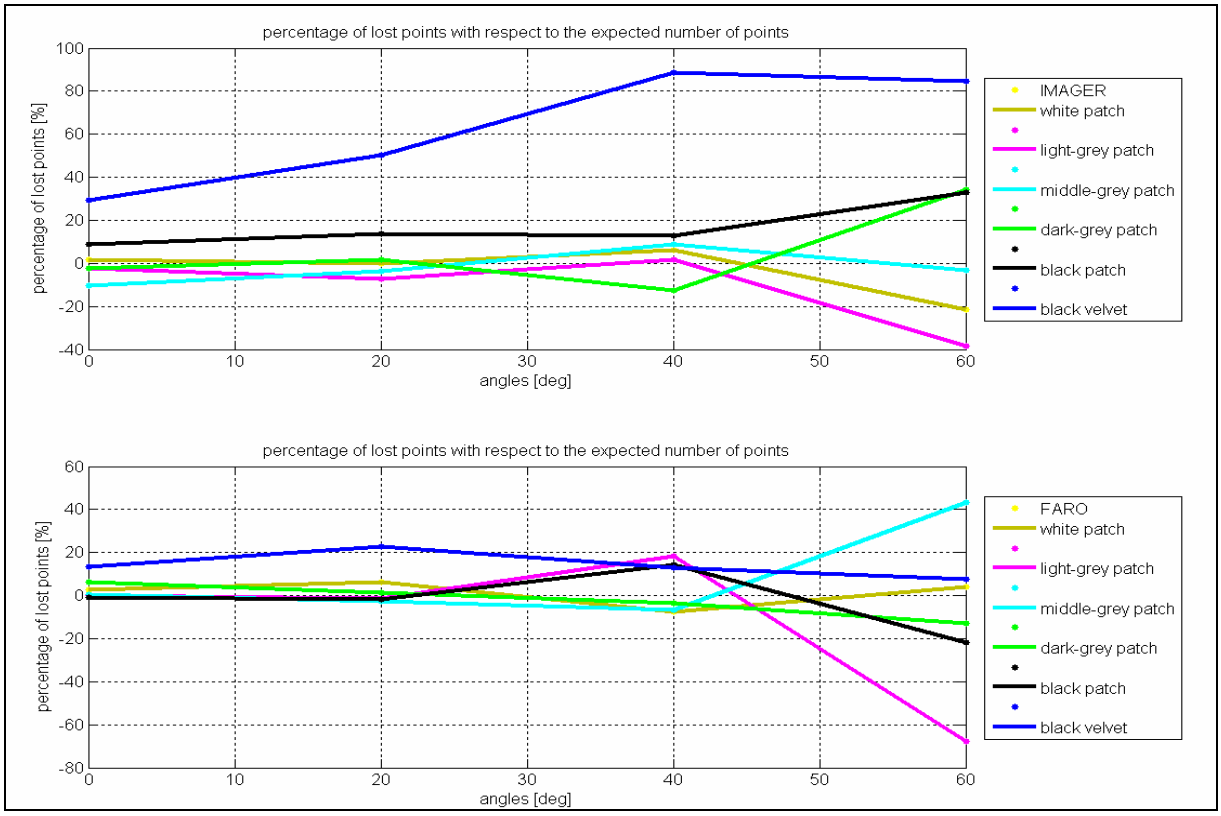

Figure 7.6: The curves showing the difference in percentages between the number of points scanned and the number of expected points for an increasing scan angle per grey value patch per scanner, *Top:* the curves for the patches scanned with the IMAGER 5003, *Bottom:* the curves for the patches scanned with the FARO LS 880.

7.4.2 Intensity values

The intensity values measured give insight in the amount of absorbed and reflected energy per grey value patch. The intensity values measured obtained with both laser scanners are normalized and compared. The resulting *intensity – scan angle* curves per grey value patch per scanner are shown in figure 7.7.

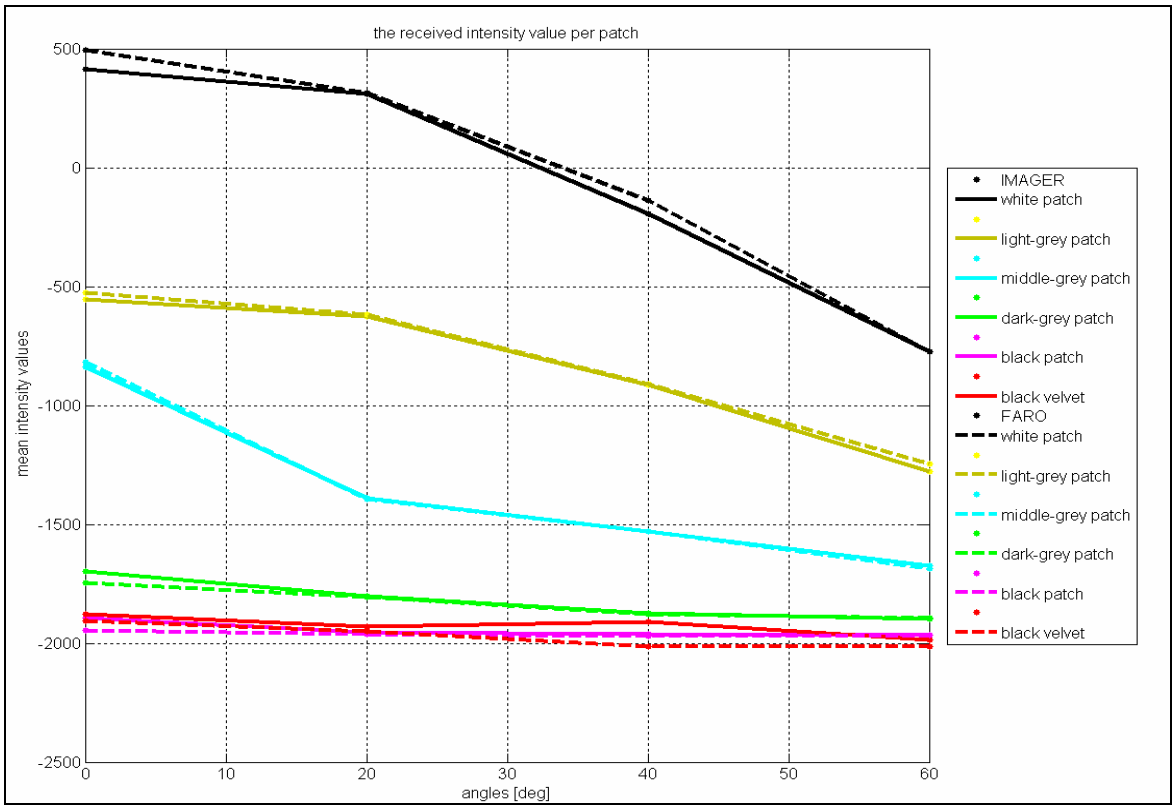

Figure 7.7: The resulting *intensity – scan angle* curves per grey value patch per scanner.

Scatter patterns

The middle-grey patch is the only curve that might be represented by a Minneart model which was the outcome of the previous two discussed experiments, the scan angle experiment (chapter 5) and the colour experiment (chapter 6).

The computed curves for the white and light-grey patches that are shown in figure 7.7 seem to represent the Lambertian scatter pattern (see paragraph 5.3). However, only four scan angles are researched in this experiment so before any conclusions can be drawn, it is recommended to do additional research.

The *scan angle* curves of the dark-grey, the black and the black velvet patches are located very low on the mean intensity axis which means that less intensity is measured for the points located within these patches. This is as expected because the remission values of these patches are very low (see table 7.1). As the shape of these curves is not steep, it is not easy to see which scatter pattern they represent. Further investigation showed a small specular trend. But as mentioned above, only four scan angles are investigated during this experiment. Therefore, additional research on more scan angles might give more information on the scatter patterns of these patches.

Comparison with scan angle and colour experiments

It is remarkable that the *intensity – scan angle* curves computed for this experiment do not show the same shape as the curves obtained for both the scan angle experiment (chapter 5) and the colour experiment (chapter 6) apart from the curve that represents the middle-grey patch. The scan angle experiment and the colour experiment are independent experiments that gave similar results with respect to the intensity values measured and the scan angles. However, the reflectivity characteristics are eliminated in both experiments because the surface features of the objects of interest were constant during the entire experiment. Therefore, it is possible that the objects

used in the scan angle and the colour experiments by accidence have the same remission characteristics. If this holds true, these characteristics are similar to the middle-grey patch remission characteristics because their *intensity - scan angle* curves show the same relation. Further research might result in an answer to this statement.

Absorption

The height of the curves on the y-axis (= mean intensity values) represents the strength of the returning signal. In this experiment the maximum intensity value that can be achieved is 2048 and the minimum intensity value is -2048. By looking at the overall heights of the curves, a list can be created which represents the grey values with the highest intensity values measured to the grey values with the lowest intensity values measured:

1. white patch;
2. light-grey patch;
3. middle-grey patch;
4. dark-grey patch;
5. black patch/black velvet.

This list follows the remission characteristics of the patches (see table 7.1). The white patch has the highest remission value, which means that it reflects most of the incoming signal strength with respect to the other patches. Therefore, the intensity values measured are higher for this patch, which is as expected. This confirmation of the expectations continues up to the dark-grey patch from the list.

At position 5 of the list both the black patch and the black velvet are mentioned. It follows from figure 7.7 that these curves do not differ a lot. Their remission values are both very low so the position of the curves on the y-axis is as expected. However, it was expected that the black velvet would perform even worse because almost no points would return to the scanner. As can be seen in section 7.4.1, there are some points scanned on the black velvet and their intensity values are similar to the black patch.

7.4.3 Reliability and precision of the scans

This section will first discuss the *precision* of the scans obtained followed by the *reliability.* In the end an overall conclusion will be given with respect to these two features.

The precision is examined by fitting a LSQ-plane through the scan points that represent one grey value patch. All the residuals together represent the *noise* of the measurements, which is used to express the precision of the scans. In order to gather insight in the spreading of the residuals the standard deviations (SD) [mm] of these residuals are computed (see table 7.2). Now, two conclusions with respect to the precision can be drawn:

1. one with respect to the performances of a laser scanner on different colours in general,
2. one with respect to the comparison of the performances of both scanners.

Performances of a phase shift laser scanner with respect to colours in general

By looking at the SDs shown in table 7.2 and the spreading curves of figure 7.8 and compare them with the remission features discussed in table 7.1, it can be seen that for both scanners the precision decreases when the remission of the grey value patch decreases as well. In other words this means that the scans of the white patch contain less noise followed by the light-grey patch up to the black velvet patch. This is as discussed in paragraph 7.3 and therefore the obtained results are as expected.

Table 7.2: standard deviations [mm] of the residuals after a LSQ-plane was fitted through the scan points; per scanner per scan angle per grey value patch; the red standard deviations are extreme values.

	White		**Light-grey**		**Middle-grey**		**Dark-grey**		**Black**		**Black Velvet**	
Scan angle	*IMA*	*FAR*	*IMA*	*FAR*	*IMA*	*FAR*	*IMA*	*FAR*	*IMA*	*FAR*	*IMA*	*FAR*
0[°]	0.90	2.34	1.03	2.81	1.33	2.42	3.27	5.76	7.07	7.85	9.85	10.20
20[°]	0.95	2.83	0.94	2.83	1.68	4.71	3.24	6.49	6.97	10.28	8.10	10.99
40[°]	0.98	2.61	1.37	3.10	1.82	4.81	3.68	6.36	7.13	11.90	*21.32*	*18.55*
60[°]	1.37	3.09	1.31	3.49	1.51	4.70	4.34	8.13	6.55	12.09	*28.85*	*19.67*

IMA = IMAGER 5003
FAR = FARO LS 880

It can also be seen that the SDs that belong to the black velvet patch are extremely high, especially when the scan angle is increased and this means that this patch contains a lot of noise. Therefore, it can be concluded that whenever it is possible, the scanning of dark and rough objects needs to be avoid in all situations because they have a very bad influence on the precision of the scans.

Furthermore, table 7.2 shows two main turnovers, for each scanner one. The precision of the FARO LS 880 is starting to decrease faster for the middle-grey patch at a scan angle of 20[°] onwards. This turnover point can also be seen for the IMAGER 5003. For this scanner the precision starts to decrease faster for the dark-grey patch at a scan angle of 0[°] onwards. This feature can also be seen in the reliability values of both scanners that will be discussed further on in this section.

Comparing the precision parameters of both laser scanners

Figure 7.8 and table 7.2 can also be used to compare the precision of both laser scanners. It can be seen that the scans obtained with IMAGER 5003 have a higher precision in almost all situations. The only exception is the black velvet patch at a scan angle of 40 and 60[°]. But the reliability of both scanners is very poor in this situation, so in general it can be said that the precision of the IMAGER 5003 with respect to different reflectivity features is better then the precision of the FARO LS 880. The reason for this difference again is due to the filtering differences between both scanners.

Reliability of a phase shift laser scanner with respect to grey values in general

As mentioned at the beginning of this section the reliability of the scan is also determined. This is done by comparing the measured scan angles with the true scan angles determined with the angle measurement device (see figure 7.9).

It can be seen in this figure that a high reliability is achieved for the white and light-grey patch with both scanners. The middle-grey patch shows still a high reliability for the scans obtained with the IMAGER 5003 but the reliability of the scan representing this patch obtained with the FARO LS 880 is decreasing fast with the scan angle. This is the same turnover point as followed from the precision determination. However, the accuracies of the dark-grey, black and black velvet patches are decreasing with both the reflectivity characteristics and the scan angle, which results in low accuracies for these patches in most situations.

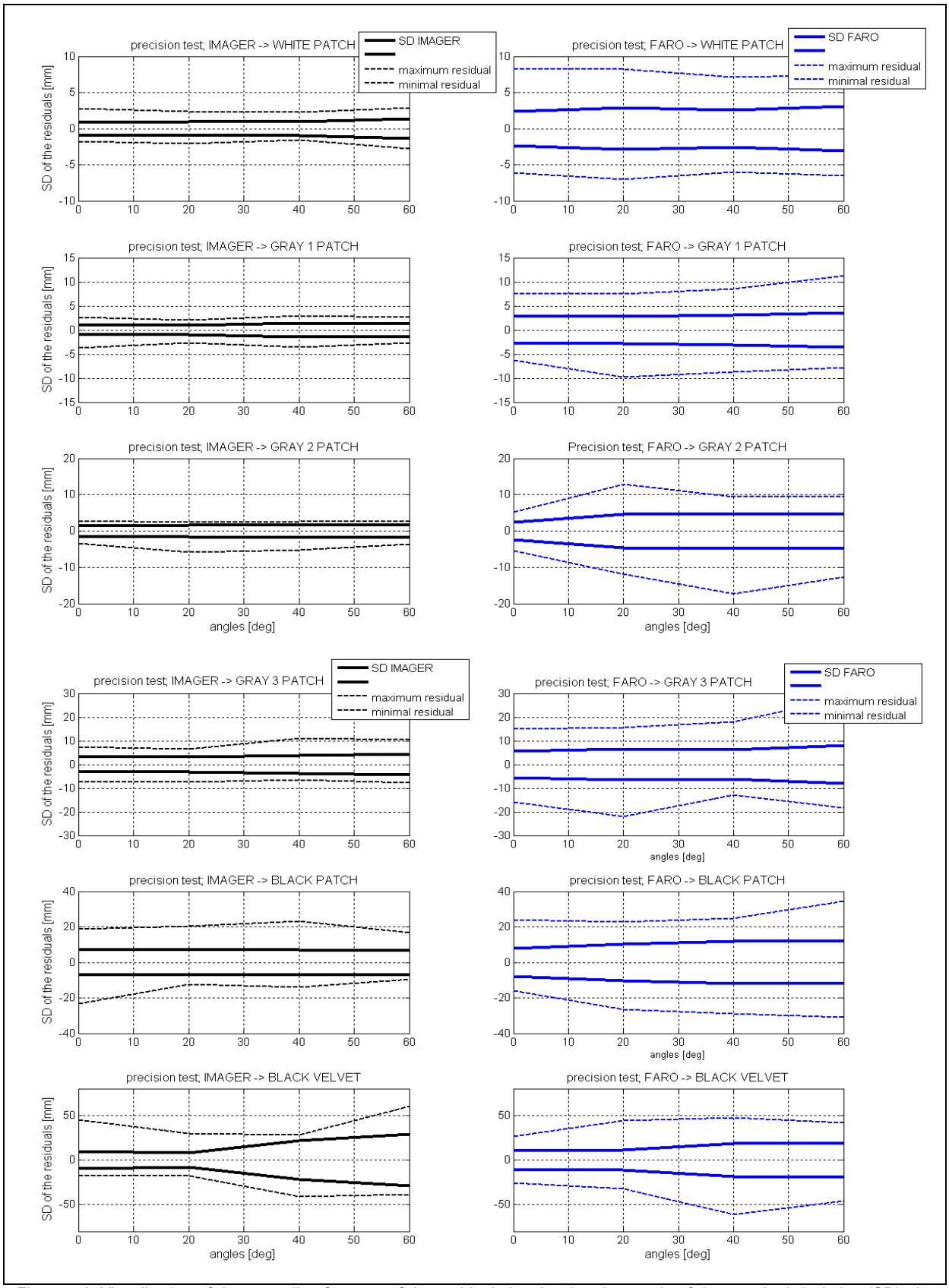

Figure 7.8: Visualization of the spreading features of the residuals by showing the trends of the standard deviation (SD), the minimum and the maximum residuals per scanner per grey value patch per scan angle, 68% of the residuals are located within the bold lines of the figures as they represent the SD and 100% of the residuals are located within the dashed lines. Left the results obtained with the IMAGER 5003 and right the results obtained with the FARO LS 880.

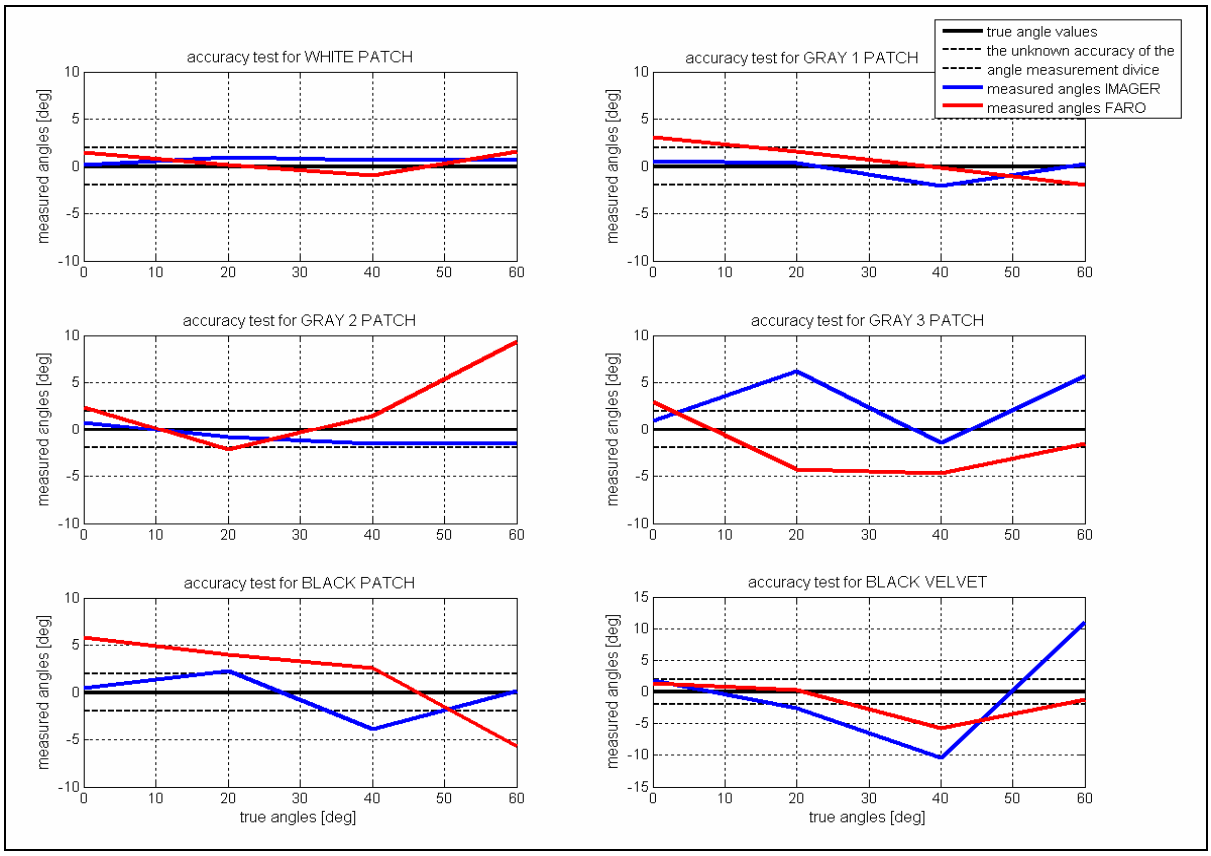

Figure 7.9: Visualization of the reliability of both the IMAGER 5003 and the FARO LS 880 by computing the scan angles from the scans obtained and their LSQ-plane and compare them with the true scan angles determined with the angle measurement device. The reliability curves for the white patch are located on the top left of this figure, the light-grey patch at the top right up to the black velvet on the bottom right. The blue lines represent the difference between measured and known scan angle for the IMAGER 5003 and the red line represents the same difference but then for the FARO LS 880.

Concluding this means that white and bright grey values are best to scan with a phase shift scanner in general. This is due to a high remission value of these patches, which results in higher intensity values measured. It is better to avoid scanning black and dark objects with a phase shift laser scanner, as the obtained results are not reliable enough for most companies. However, when it is unavoidable to scan dark objects, it is best to scan them with a scan angle of 0[°] because then the reliability is the highest and close to given specifications of the scanners. This conclusion is as expected.

Comparing the reliability parameters of the two laser scanners

Figure 7.9 is also used to compare the reliability of both laser scanners. It can be concluded that the measured scan angles per grey values patch per scanner do not differ significantly apart from the middle-grey patch. Therefore, in general it can be said that the output scans obtained with both scanners are evenly reliable (or unreliable) with respect to the different reflectivity characteristics.

As is also mentioned in chapter 5 and 6, it is not ‘fair’ to compare the results of a non-filtered and a filtered scan, therefore, the conclusions drawn in this paragraph are only valid for the performances of both scanners with respect to their output scans. Chapters 5 and 6 also mentioned that Fugro-Inpark prefers to start interpreting and modelling the scans directly after the scanning phase. Therefore, it can be concluded that, based on the reflectivity experiment, the IMAGER 5003 is best to use as the data is less noisy which results in an overall model is the most accurate.

On the other hand, it can be recommended that whenever it is possible it is best to avoid scanning dark (and rough) objects as the results with respect to these patches are bad for both scanners.

7.4.4 Bias parameters

Section 3.2.6 of this thesis described an existing experiment set-up for the testing of laser scanners on surfaces with known colours. This existing experiment has a lot of similarities with the colour and reflectivity experiment of this research. One of the results obtained in the experiment of section 3.2.6 is offset or bias of the patches with respect to the average plane. This result gives insight in the systematic errors grey values give in measurements. For example it was shown that the black patch was located behind the average plane and the white patch was located in front of this average plane.

These offsets might indicate a systematic difference in the measured range that is unique or characteristic for the particular grey value. In this section it is tried to give insight in these offsets for the grey value patches.

Table 6.3: The mean values of the biases [mm] between the average plane through the point cloud and the planes through the different grey value patches. Negative values represent patches that are located behind the average plane and positive values represent patches that are located in front of the average plane.

	White		**Light grey**		**Middle grey**		**Dark grey**		**Black**		**Black velvet**	
Scan angle	*IMA*	*FAR*	*IMA*	*FAR*	*IMA*	*FAR*	*IMA*	*FAR*	*IMA*	*FAR*	*IMA*	*FAR*
0[°]	1.04	-3.45	0.95	-0.47	0.78	-0.48	0.80	-1.36	-2.60	2.50	-6.26	0.94
20[°]	1.19	-2.30	0.74	-0.65	0.83	0.10	0.70	-2.05	-1.48	1.45	-15.83	3.92
40[°]	0.32	-1.79	1.74	-1.17	0.09	1.90	0.15	2.20	-4.40	3.28	-17.15	0.57
60[°]	1.15	-1.46	0.49	-3.14	2.07	-0.48	1.32	4.91	-2.11	2.68	-70.62	-11.77

Procedure of bias determination

In order to determine the biases of each grey patch first an average plane is estimated through the entire point cloud obtained. This estimation is based on the LSQ-principle and the same model of observation equations is used as discussed in section 4.6 of this thesis. Following the best fitting planes of the separate grey value patches are subtracted from the average plane. Next the mean, minimum and maximum of these biases are computed. Negative values correspond to colour patches of which the range is measure too long with respect to the average plate. Table 7.3 shows the mean biases per grey value patch per scanner with respect to the average plane. Figure 7.10 shows the curves of these mean, minimum and maximum values.

By looking at the results shown in figure 7.10 it can be concluded that not all patches are situated exactly parallel to the average plane. If the biases of the grey value patches at a certain scan angle have a positive minimum value and a negative maximum value, the grey patch plane intersects the average plane. This is shown in figure 7.11 for a scan angle of 0[°] for both scanners.

These intersections are properly caused by the fact that the grey patches are relatively small and the redundancy is therefore small as well. This influences the accuracy of the fitted plane (see section 4.7.4). It would be better to invest the influence of the reflectivity using larger patches.

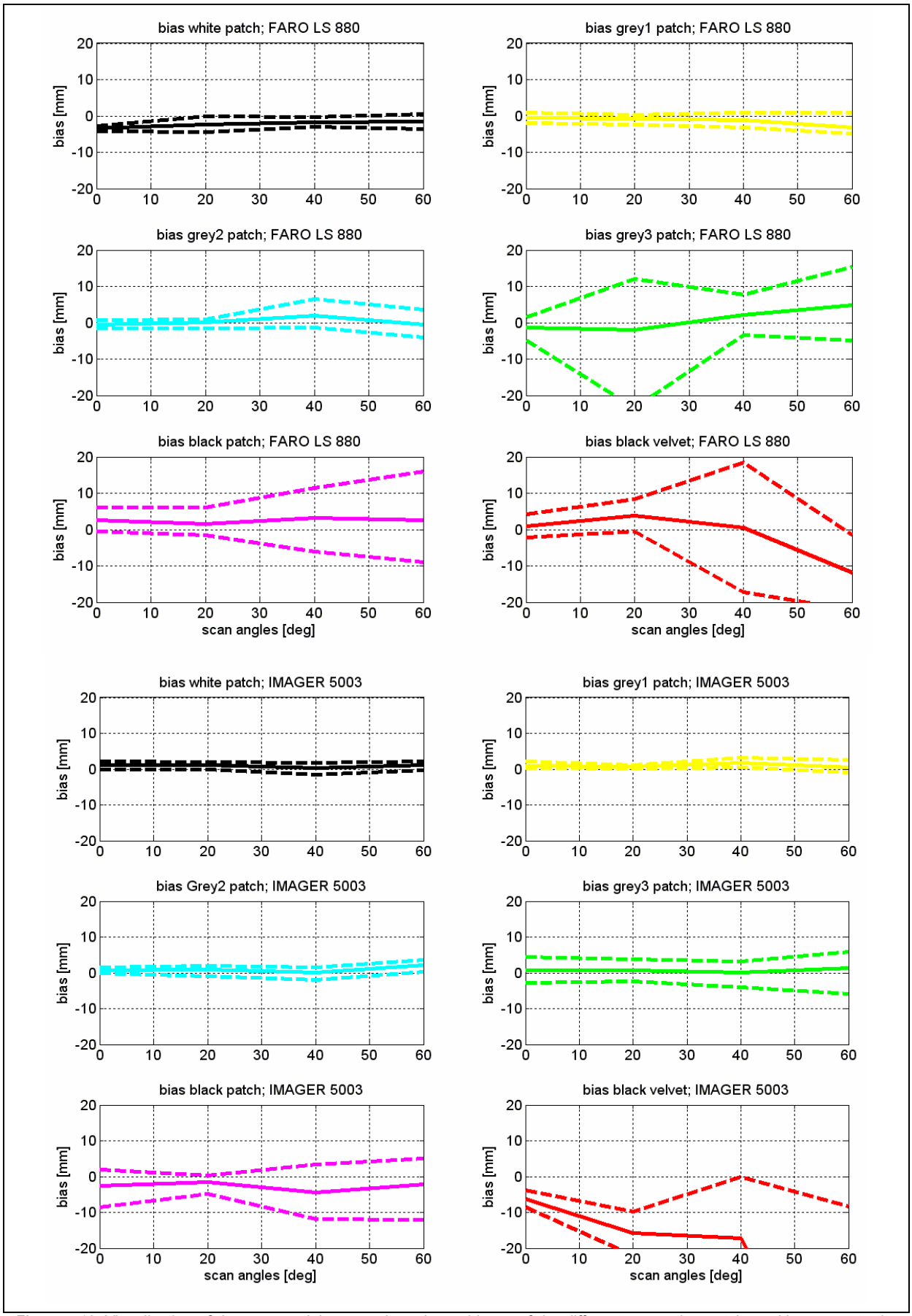

Figure 7.10: Visualization of the mean, minimum and maximum biases of the different grey value patches with respect to the average plane through the point cloud per scanner.

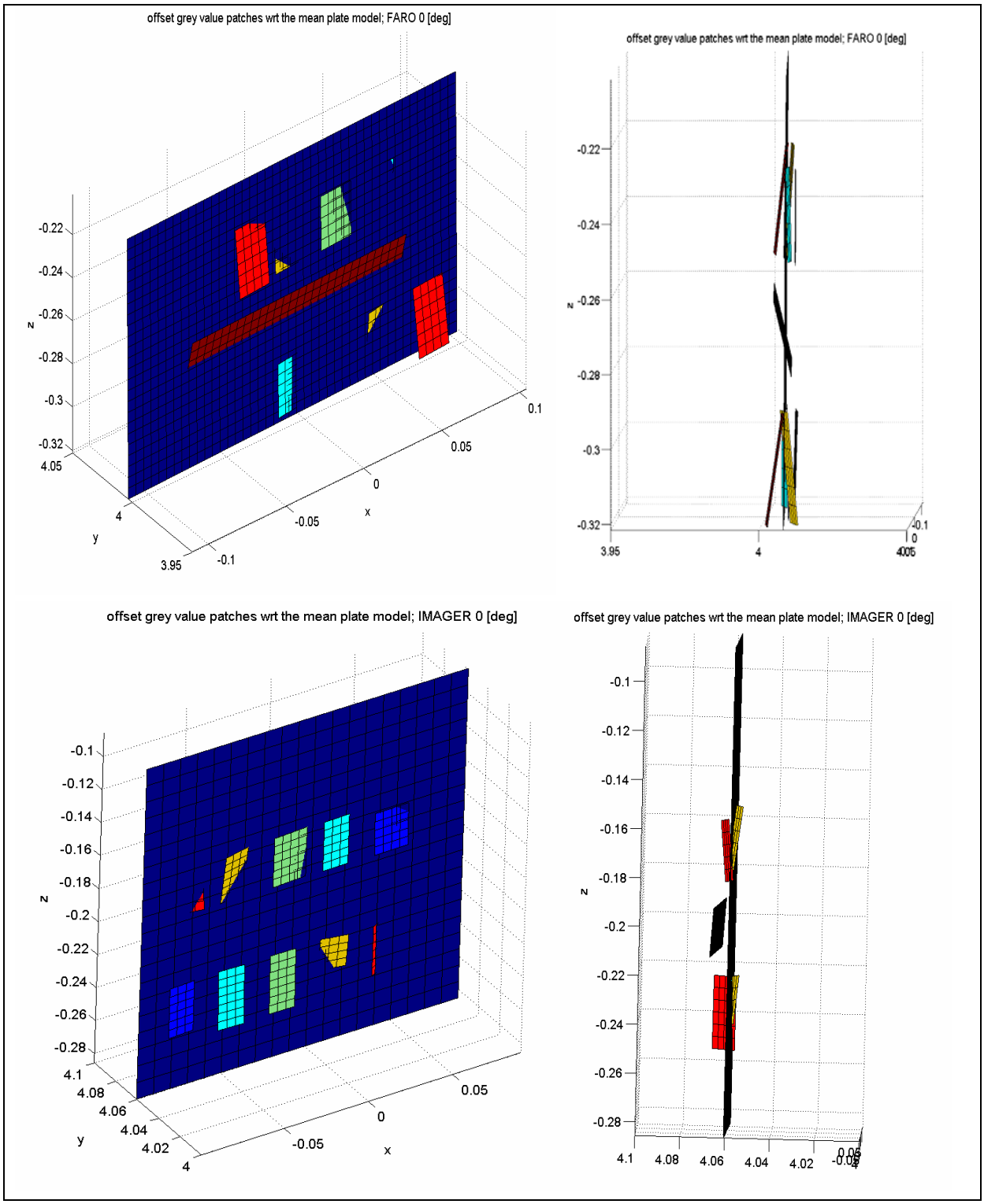

Figure 711: The location of the LSQ-planes of the grey value patches of the test chart wit respect to the average plane through these patches at a scan angle of 0[º]. To remember: the test chart consists of the following grey patches (from bottom left to bottom right): white, light grey, middle grey, dark grey and black. On the top exactly the other way around and they are separated by a large patch of black velvet. **a.** and **b.** the patches wrt the average plane determined for the FARO LS 880. **c.** and **d.** the patches wrt the average plane determined for the IMAGER 5003.

Te theory of the influences of the sizes of the patches can be combined with the knowledge obtained from figure 6.13b of the previous chapter. This figure visualizes a side view of the scan obtained of the colour test chart with the FARO LS 880 at a scan angle of 0[º]. It can be seen in this figure that the pattern of the points in the scan is

of an unknown pattern. This is most likely due to the mixed information at the boundaries of the patches. The patches of the grey value plate are also connected to each other. The non-parallelism of the patches with respect to the average plane can therefore most likely be explained by the mixed points that influence the plane fitting.

This problem occurs for the IMAGER 5003 as well but less extreme and this can be explained by the fact that the IMAGER 5003 filters or correct the data before the output is created. This feature results in more parallel plane fits but still intersections are present due to the size and the redundancy of the patches.

By looking at the figures 7.10 and 7.11 it can be seen that the two scanners obtain almost opposite results. The models of the darker patches obtained with the IMAGER 5003 are located behind the average plane in general. The brighter patches are most of the times located in front of the plane. The models of the dark patches obtained with the FARO LS 880 however are located in front of the average plane and the brighter patches behind this plane. This opposite behaviour was first explained by a programming error but after checking the bias program no error could be found. Therefore, it is not possible to give a general conclusion with respect to the offset features caused by differences in reflectivity characteristics. In order to get this information additional research is recommended to gather insight in the characteristics of different reflectivity characteristics with respect to measurements done with laser scanners.

Furthermore, it can be seen in table 7.3 and the figures 7.10 and 7.11 that the biases of the IMAGER 5003 are very small for the brighter patches; on sub-millimetre level in most situations. The biases of the FARO LS 880 vary more for these patches and they are within millimetre level. This is properly due to the more accurate models (see section 6.5.3) obtained for the IMAGER 5003 and this is connected to the filter properties of the IMAGER 5003. However, it can also be seen that the biases for the darker patches are smaller for the FARO LS 880.

Additional research is recommended on the characteristic bias determinations caused by reflectivity because the procedure discussed in this section is based on an average plane determined through all patches. Taking an average plane on which the performances of laser scanners is known is thought to be better because the influence of one grey value can be examined easier and exact. The second recommendation follows this statement as it is most likely better to examine one grey value per scan to eliminate mixed reflectivity information that can influence the results negatively. These recommendations are the same as the recommendations done in the previous chapter.

8 Range experiment

The feature of interest that will be discussed in this chapter is the influence of the scan range on the performance of the laser scanners. This feature is eliminated from the previous discussed experiments but it is obvious that different ranges are present in each set-up, as well as their influences on the accuracy of the scans obtained.

A motivation for the implementation this experiment will be given in paragraph 1 followed by the experiment set-up in paragraph 2. The hypotheses with respect to (1) the number of points scanned, (2) the intensity values measured and (3) the reliability and precision of the scans obtained are discussed in paragraph 3. Finally, the results will be discussed in paragraph 4.

8.1 Motivation

Section 3.1.5 already mentioned that the *distance – accuracy* curves of the different laser scanners are not known. Knowledge of these curves is required, to be able to subtract the curve from the scan to correct the data for range errors. If subtracting the curve from the dataset is not possible, it can help to limit a measurement set-up in the distance. Now a company can guarantee certain accuracies to be achieved within their scans.

8.2 Experiment set-up

The range experiment is done in a 29[m] long corridor. The same white plate as discussed in the scan angle experiment (chapter 5) is mounted on a tripod. The tripod is moved backwards with steps of approximately 1[m] till the distance of 29[m] is reached. The scanner is located on one position during the entire measurement session.

But as the used laser scanners do not allow forced centring, it was assumed that only distance differences could be measured in the first place. However, it was found out that both laser scanners can be placed on a ‘normal’ tripod, which means that the laser scanner can be placed on the same connection as a total station. The centring of both laser scanners and the total station are now redundant as their measurements are done from the same position. Therefore, the assumption is made that the middle point of the laser scanner is exactly in the middle of the device and on the same position as the middle point of the total station. This assumption makes it possible to measure the absolute distances as well. Therefore, five arbitrary points on the white plate are taken as a ground truth and these are measured with a Topcon total station, which has an accuracy of 3[mm] + 2ppm on a distance up to 25[m] [Topcon, 2006].

Figure 8.1 shows an overview of the experiment set-up and figure 8.2a shows a picture of the corridor in which the measurements are done. The plate is in this situation located at the far end of the corridor and the laser scanner used in this situation is the FARO LS 880. Figure 8.2b visualizes the approximate positions of the points measured with the Topcon on the white plate.

Unlike the previous discussed experiments the most important parameter that is tested in this experiment is the *range*. The experiment set-up as shown in figure 8.1 eliminates irrelevant parameters like the *scan angle* and *the surface characteristics* from the experiment.

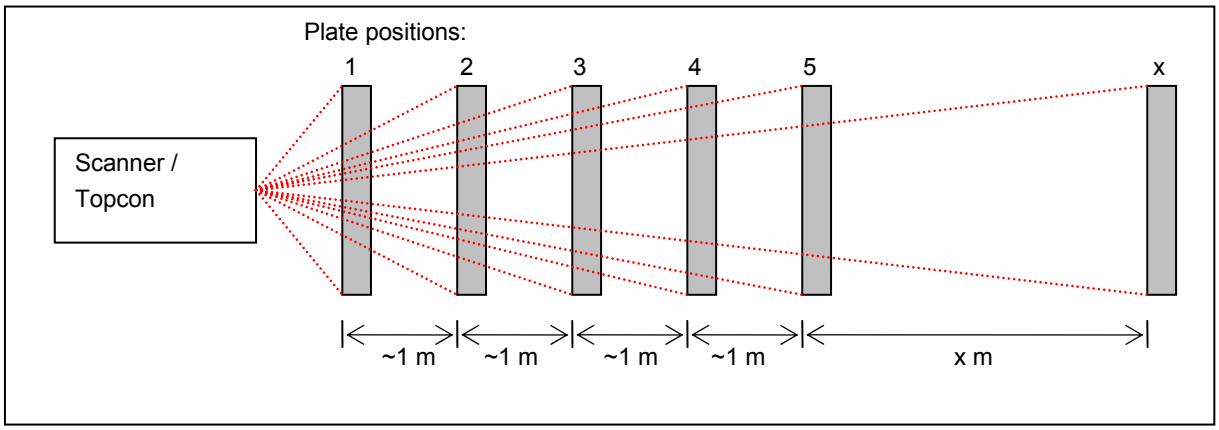

Figure 8.1: a top view of the range experiment set-up, the grey rectangles represent the white plate which is shifted with steps of 1 [m]. The tripod, on which both the laser scanner and the total station can be placed, is stable during one measurement session.

a.

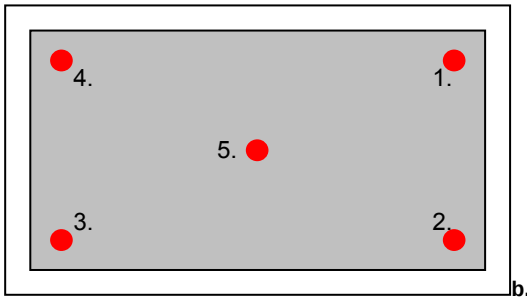

b.

Figure 8.2: **a.**: a picture of the range experiment done with the FARO LS 880, the white plate (= object) is located at the far end of the corridor (photo: Van Ree, 11-07-2006), **b.**: the approximate positions of the 5 points on the white plate measured with the Topcon.

During this experiment only the FARO LS 880 is used because the IMAGER 5003 was not available for this experiment within the time limit of this research. The middle resolution of the FARO LS 880 is used to reduce both the scan time and the obtained file sizes. The plate is shifted approximately 1[m] between two positions. After 21[m] the plate is shifted with steps of 2[m] up to a distance of 29[m]. Therefore, this experiment resulted in 25 scans.

8.3 Hypotheses

To gather insight in the influence of the range on the performance of both scanners, the relation between the *number of points* and the range is determined. Also the influence of the range on the intensity values and the reliability and precision parameters is determined. Before these relations are discussed, hypotheses with respect to these features are made.

8.3.1 Number of points scanned

The knowledge of the constant angle increments between two emitted laser signals results in the expectation that the number of points on an object decreases when the scan range is increased. This theory is shown in figure 8.3 schematically.

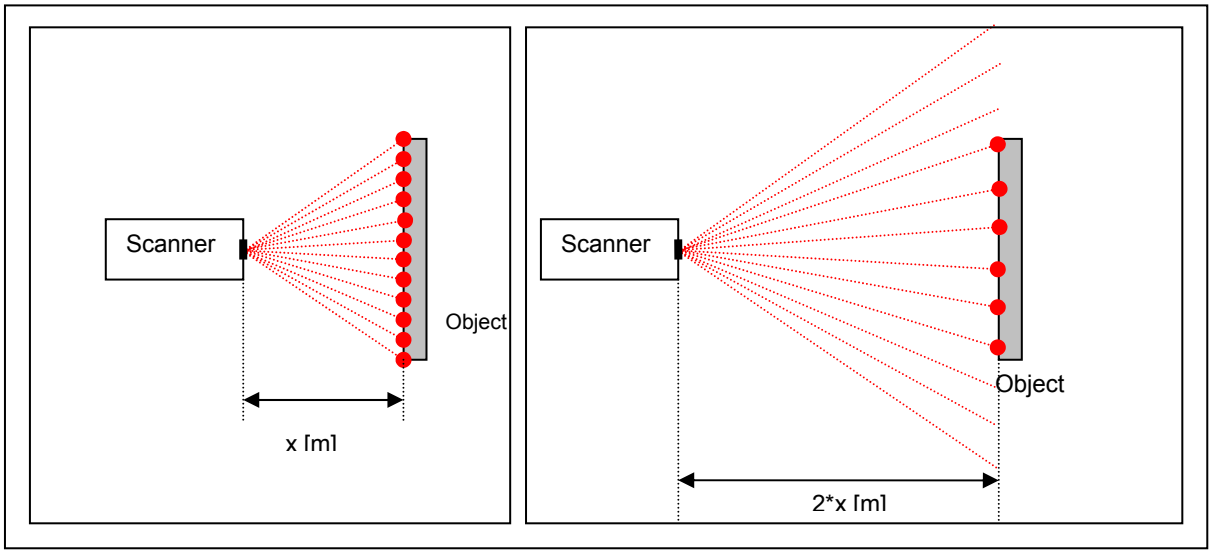

Figure 8.3: the influence of the range on the number of points scanned on an object, *left;* the distance is set at x[m] and *right* the distance is doubled, the angle increment between two scan lines is the same, so less points hit the objects surface when the range is increased.

The expected *number of points – range* curve is visualized in figure 8.4. Formula 4.4 is used for the computation of this curve, using a vertical and horizontal angle increment of 0.0025[°] and a plate of 1 by 1[m]. The effects of the travel time of the signal and the footprint size are not taken into account in the simulation of this curve. These two effects result in a decreasing intensity value which might not exceed the threshold value. Therefore, the expectation is that the number of points-range curve will decrease as shown in figure 8.4 but it might decrease even more, especially for larger ranges.

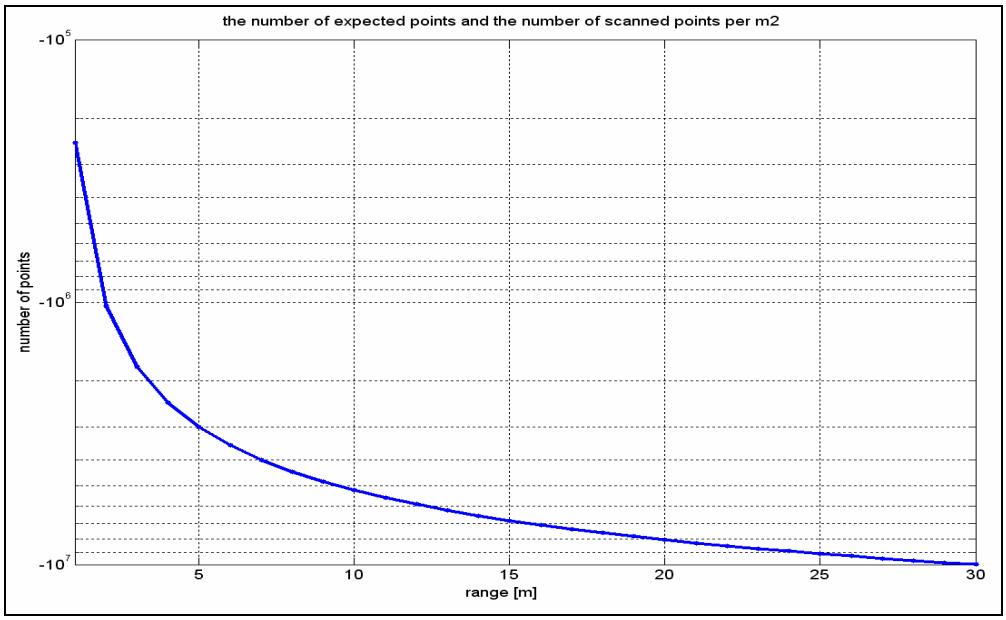

Figure 8.4: the expected number of points-range curve determined for a plate of 1[m^2] and an angle increment of 0.0025[°], the scan angle between scanner and plate is assumed 0[°].

8.3.2 The intensity values measured

If the range between an object and the scanner increases, the outgoing signal has to travel a longer period through the air. Lots of small particles are present in the air and they will absorb small parts of the energy of the travelling signal. The strength of the echo will therefore decrease with the travel time through air. In other words, when the range between the scanner and the object is increased, the intensity values measured will decrease.

The range also influences the size of the footprint of the laser signal on the object (section 3.1.4). This might also result in a loss of intensity because the strength of the emitted laser signal is spread over the entire footprint area which results in a weaker signal of one particular point in this footprint. *Concluding* this means that the intensity value is expected to decrease with the range due to the size of the footprint as well.

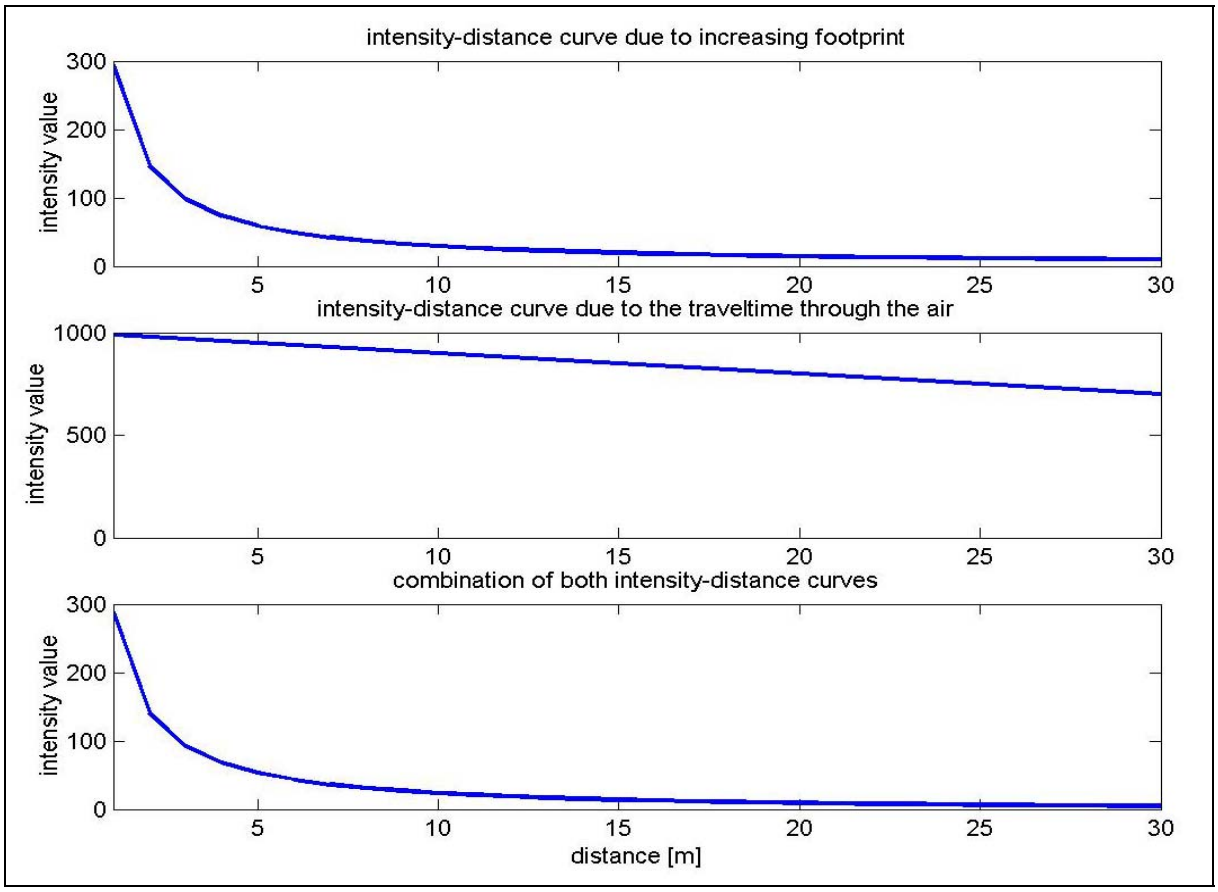

Figure 8.5: three *intensity-range curves* created by a simulation, *top;* the *intensity-range* curve that can be expected when only the effect of the increasing footprint is taken into account, *middle;* the curve that can be expected when only the travel time of the signal through the air was taken into account, *bottom;* the combined and therefore expected intensity-range curve of a laser scanner.

Figure 8.5 shows three *intensity – range* curves created by a simulation. Formula 3.4 is used for the determination of the top curve as this curve shows the relation if only the footprint effect on the intensity is taken into account. For this curve the total amount of incoming energy is divided by the footprint size at a particular range (8.1). It is assumed that the energy hitting the surface at one pulse is 100. Therefore, the top curve of 8.5 shows the expected intensity loss in percentages with respect to this incoming signal strength.

$$I_{fpr} = \frac{I_L}{F_i} \tag{8.1}$$

with:

I_{fpr} = the percentage of lost energy due to an increasing footprint
I_L = Incoming energy strength at the objects surface
F_i = Footprint size of the laser beam at distance *i* (see function 3.4)

The middle curve is created by only taking the influences of the travel time of the signal through the air into account. These atmospheric effects are assumed to be linear with the distance [Rees, 2006]. The combination of these two curves is shown in the bottom curve of figure 8.5. This curve shows that it is expected that the measured intensity value will be decreasing fast if the range between scanner and object is increased.

8.3.3 Reliability and precision of the scans

For the range measurements it is expected that the accuracy will decrease with the distance. The figures 8.4 and 8.5 show that the number of points scanned and the intensity values measured decrease with the range. The combination of these two hypotheses resulted in the conclusion that the accuracy must decrease fast with the range as well. The conceptual shape of the accuracy-range curve is shown in figure 8.6.

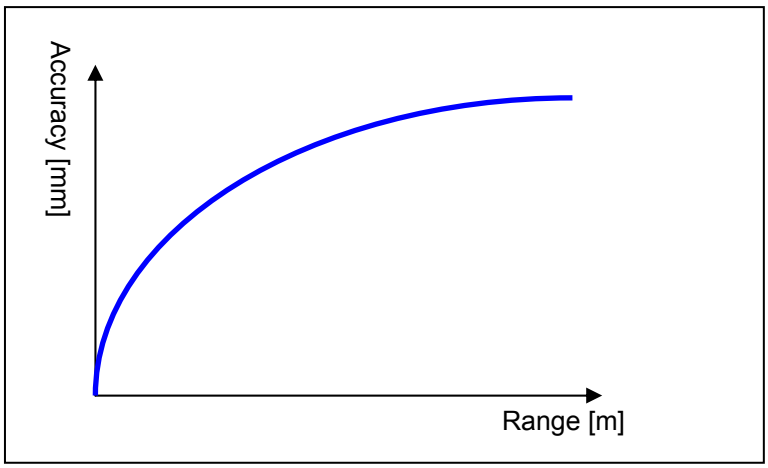

Figure 8.6: The expected shape of the accuracy-range curve based on the expectations of both the number of points scanned and the intensity values measured, it can be seen that the accuracy will decrease fast with the range.

8.4 Results

As mentioned in the beginning of this chapter, the results discussed in this section are therefore only obtained with the FARO LS 880 at the middle resolution. This analysis of the results is again divided into three parts: (1) number of points scanned, (2) the intensity values and (3) the reliability and precision of the scan.

8.4.1 Number of points scanned

Like in the previous three chapters the *number of points scanned – range* curve is determined for the scans obtained for this experiment as well. The curve is shown in figure 8.7a. By comparing this curve with the *number of points scanned – scan angle* curve discussed in hypotheses, it can be seen that the relation is indeed as expected.

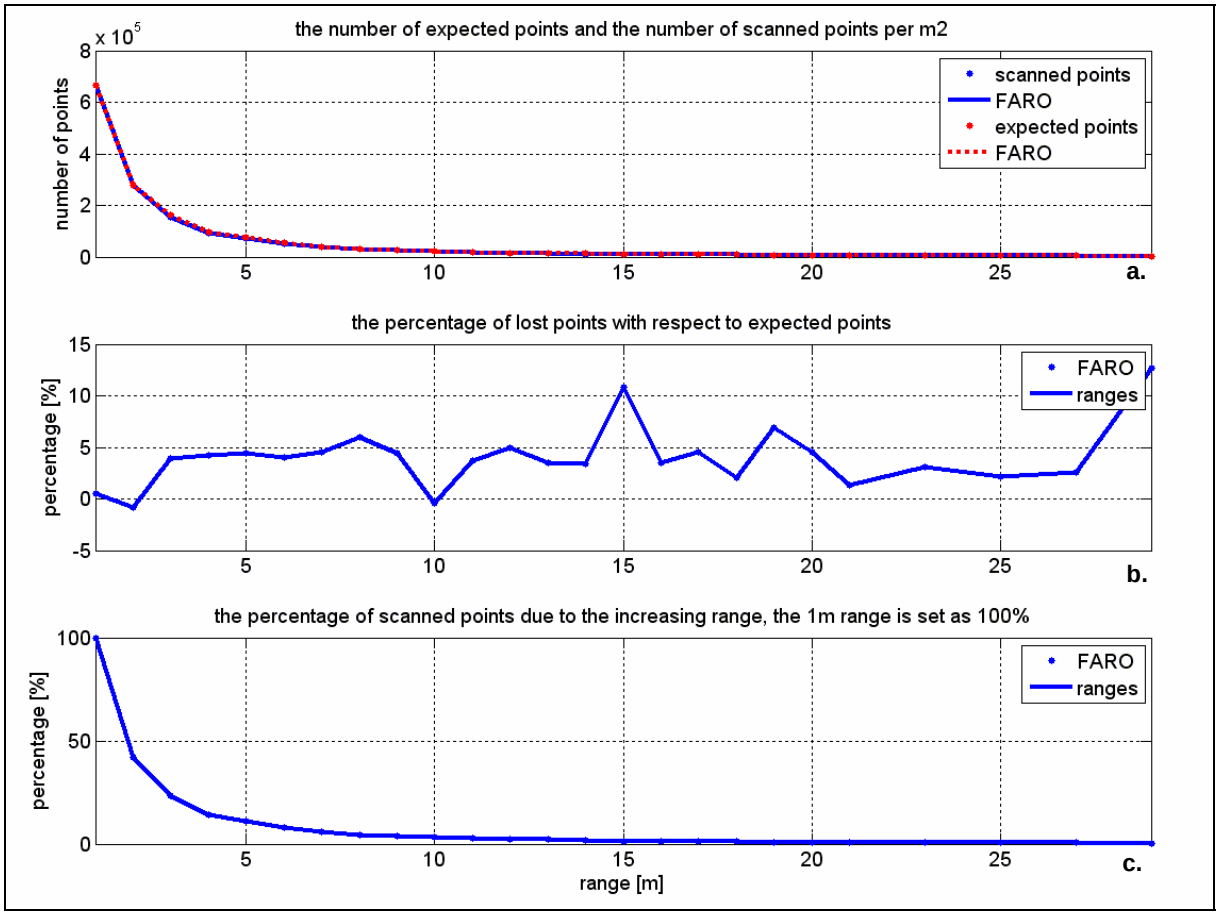

Figure 8.7: 3 curves showing the relation between the number of points scanned and the range, **a.**: the number of scanned and expected points per [m^2] for the FARO LS 880 at different ranges, **b.***:* the difference in percentages between the number of points scanned and the number of expected points, **c.***:* the relation between the range and the number of points scanned, the number of points on an object scanned with a range of 1 [m] is set as 100%.

Table 8.1 shows the exact values of the curves in figure 8.7 because they are difficult to compute from the curves exactly. Figure 8.7a is highlighted in figure 8.8 on a logarithmic scale for a better interpretation.

Figure 8.7b shows the percentage of lost points with respect to the expected number. The latter follows from the specifications. For this experiment the 5% threshold due to the interior selection is valid as well (see section 5.4.1). It can be concluded that specifications of the FARO LS 880 are true in almost all situations within this 5% threshold.

Large deviations with respect to the 5% threshold can be spotted at a range of 15[m] and 29[m]. No explicit reason can be given for this occurrence but it might be due to the frequency of one of the modelled carrier waves because it seems to occur with steps of approximately 15[m]. Further research is recommended to clarify this statement.

Table 8.1: the values used to compute the curves of figure 8.7.

Scan range [m]	Scanned points per [x10^5 m^2]	Expected points per [x10^5 m^2]	Percentage of lost points [%]	Percentage of scanned points [%] *
1	6.64	6.67	0.48	100.00
2	2.79	2.77	-0.83	42.06
3	1.56	1.62	3.93	23.44
4	0.93	0.97	4.24	13.97
5	0.73	0.77	4.44	11.02
6	0.52	0.54	3.99	7.85
7	0.39	0.40	4.51	5.81
8	0.29	0.31	5.94	4.40
9	0.26	0.27	4.46	3.89
10	0.22	0.22	-0.44	3.33
11	0.18	0.19	3.72	2.75
12	0.15	0.16	4.97	2.25
13	0.14	0.15	3.53	2.18
14	0.12	0.13	3.38	1.86
15	0.09	0.10	*10.87*	1.39
16	0.10	0.10	3.51	1.46
17	0.09	0.10	4.50	1.38
18	0.08	0.09	2.04	1.26
19	0.06	0.07	6.90	0.97
20	0.06	0.06	4.52	0.86
21	0.06	0.06	1.37	0.93
23	0.05	0.05	3.11	0.75
25	0.06	0.06	2.17	0.85
27	0.05	0.05	2.56	0.72
29	0.03	0.03	*12.68*	0.43

* the number of points on an object scanned with a range of 1 [m] is set as 100%

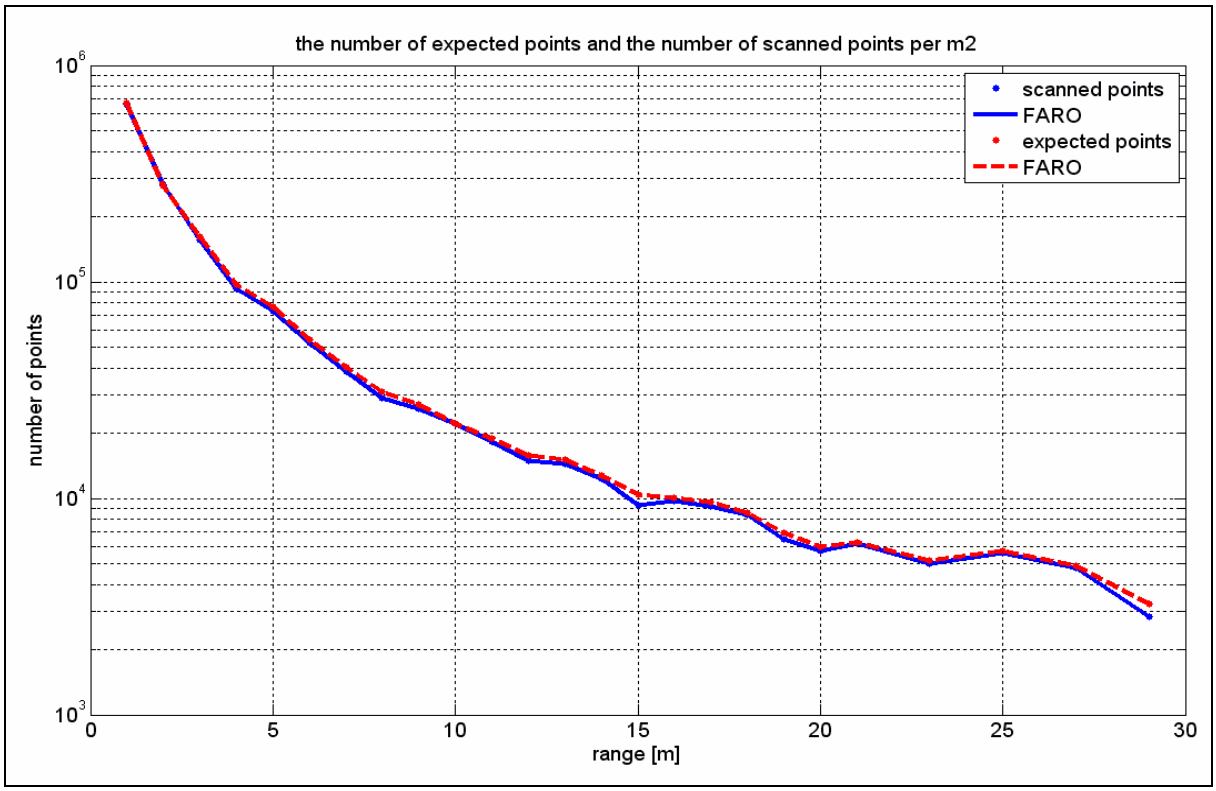

Figure 8.8: a visualization of the *number of points scanned – range* curve on a logarithmic scale in order to make the interpretation easier.

Figure 8.7c shows the percentage of scanned points with respect to a distance of 1[m]. This means that the number of points scanned at a distance of 1[m] is set as 100% and the results of other distances are relatively connected to this 100%. It follows from this figure and table 8.1 that more then 99% less points will be scanned on an object located at 20[m] from the scanner then on the same object located at a distance of 1[m] from the scanner. In other words this means only 1% of the points will be scanned on an object located at a distance of 20[m] compared to the number of points scanned at a scan range of 1[m].

8.4.2 Intensity values

Figure 8.8 shows the resulting *intensity – range* curve of the FARO LS 880 at middle resolution with respect to the scan range. It can be seen that the shape of this curve does not behave as expected (see figure 8.5). Apart from the ranges of 1 – 4 [m], the curve seems to behave linear, which indicates that the intensity values measured are most likely influenced by the atmosphere only (see section 8.3.2). This implies that the effect of the footprint, as discussed in section 8.3.2, does not influence the relation between the intensity and the range. Therefore, this theory might not be true. Further research is necessary to find the relation between the footprint resolution and the atmosphere on the intensity values measured.

As mentioned above, the *intensity – range* curve shows an unexpected behaviour in the ranges 1 – 4[m]. Instead of a decreasing trend, the curve shows an increasing trend at these ranges. Whether this is behaviour is a coincidence or a standard has to be clarified. Therefore further research is recommended on these short distances as well.

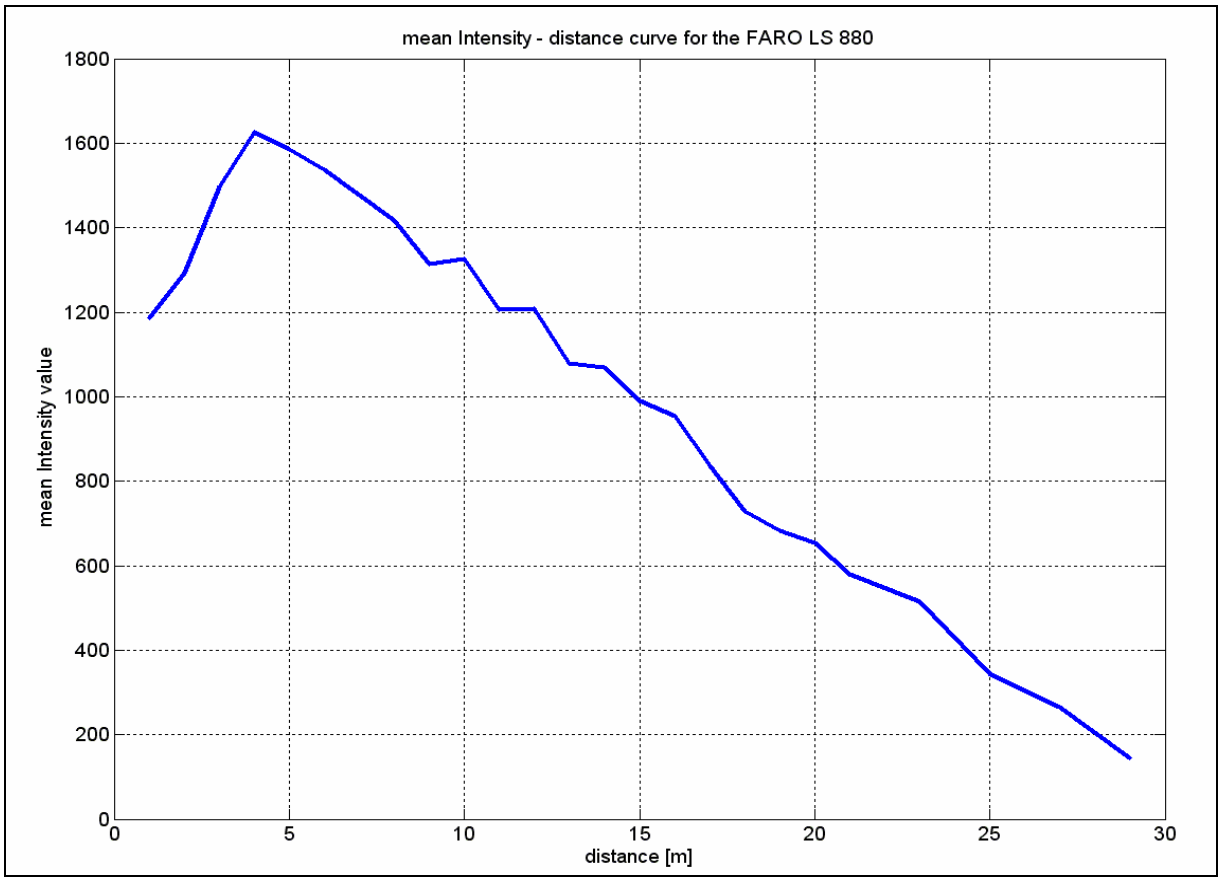

Figure 8.9: the obtained *mean intensity – range* curve for the FARO LS 880 at middle resolution.

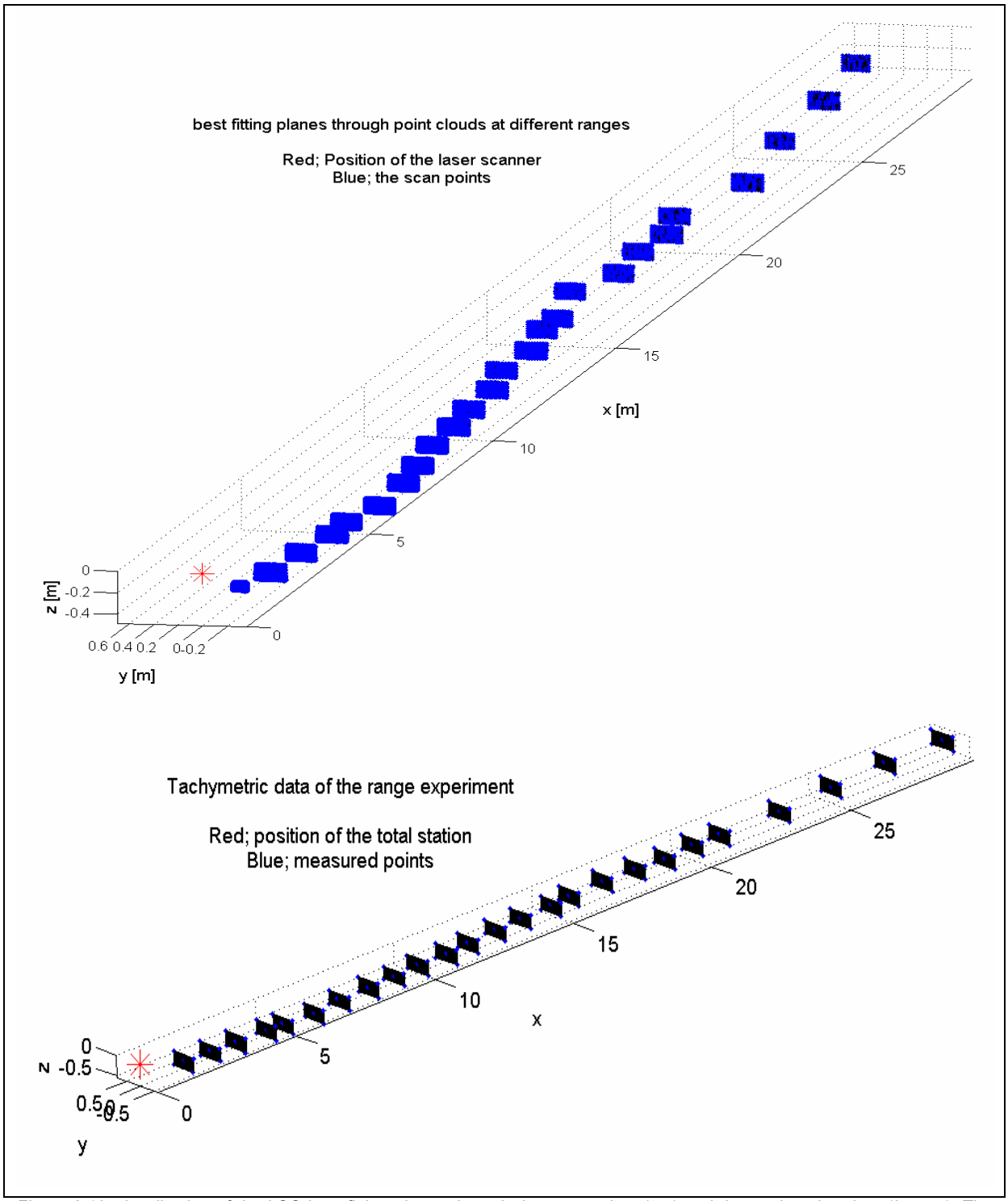

Figure 8.10: visualization of the LSQ-best fitting planes through the scan points (*top*) and the total station data (*bottom*). The blue dots in the top figure are the scan points and in the bottom figure they represent the five measured points on the white plate with the Topcon total station. The red star on the left of both figures represents the position of the tripod on which alternately the Topcon and the laser scanner is located.

8.4.3 Precision and reliability parameters of the scans

Like in the previous three chapters a LSQ-plane is fitted through the scan points obtained. A LSQ-plane is fitted through the ground truth points per plate per scan range measured with the Topcon total station as well. Figure

8.10 visualizes these plane fittings and the range direction is in the direction of the corridor in which the experiment is done. The red star indicates the position of the tripod on which the total station and the laser scanner are located alternately. Figure 8.11 shows two close-ups of fitted planes through the scan points.

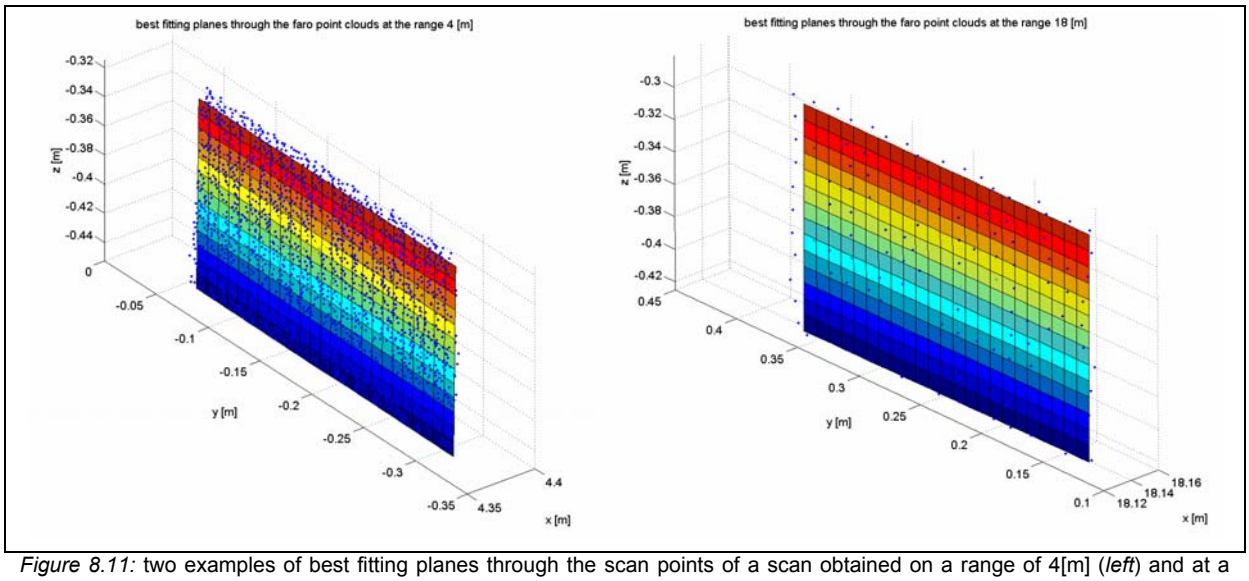

Figure 8.11: two examples of best fitting planes through the scan points of a scan obtained on a range of 4[m] (*left*) and at a range of 18[m] (*right*). Both scans are obtained with the FARO LS 880 at middle resolution.

The fits (or models of the plate) will be used for three purposes that all together determine the *reliability* and the *precision* of the laser scanner with respect to the range:

1. The residuals of the best fitting plane through the scans are used to gather insight in the level of noise, by determining the standard deviation (SD) of the residuals. The lower the value for the standard deviation, the less noise is present in a scan.
2. The distance differences between the plates determined with the laser scanner can be compared with the ground truth distance differences determined with the total station. The advantage of this approach is that systematic errors are eliminated from the results. In order to compare these results and those of the next step the overall model test values of both instruments are determined as well.
3. The difference between the best fitting plate through the scan points and the best fitting plane through the total station points on position *n* can be calculated. The latter is set as a ground truth for the corresponding distance. These three steps will be discussed individually next in this section.

Precision parameters of the FARO LS 880 with respect to the range

Like mentioned above, the SDs of the residuals are computed in order to gather insight into the noise factor of the scans obtained with the FARO LS 880 with respect to the range. Figure 8.12 and table 8.2 contain these SDs and it can be seen that they vary from 2 – 5[mm] up to a distance of 29[m]. This result is much better as expected because the expectation was that the scans become much noisier with the scan range. Figure 8.13 shows four histograms of the residuals and it can be seen that the normal distribution decreases slightly with the range because the width of the histograms increases. However, the decreasing trend of the SDs is less extreme as expected.

Figure 8.12 and table 8.2 also contain information on the spreading features and the SDs of the residuals of the total station data. It can be seen that these SDs are much smaller with respect to the SDs of the laser scan data. However, it must be noted that the redundancy of the two measurements sets is completely different. Whether this difference is of influence will be discussed in the next part of this section.

Table 8.2: standard deviations [mm] per scan range of the residuals after a LSQ-plane was fitted through the scan points for both the FARO LS 880 and the total station.

Standard deviations [mm]					
Range [m]	**FARO LS 880**	**Topcon**	**Range [m]**	**FARO LS 880**	**Topcon**
1	2.37	0.56	**14**	2.48	0.90
2	2.30	0.50	**15**	2.00	0.57
3	2.08	0.28	**16**	2.83	0.70
4	2.13	0.58	**17**	2.42	1.37
5	1.87	0.63	**18**	2.68	0.15
6	2.19	0.68	**19**	2.16	0.67
7	2.06	1.47	**20**	2.22	0.87
8	2.30	0.76	**21**	3.13	0.10
9	2.44	0.50	**23**	3.04	0.09
10	2.56	0.67	**25**	2.59	0.66
11	2.08	0.61	**27**	2.87	0.51
12	2.22	0.47	**29**	4.58	0.71
13	2.85	0.45			

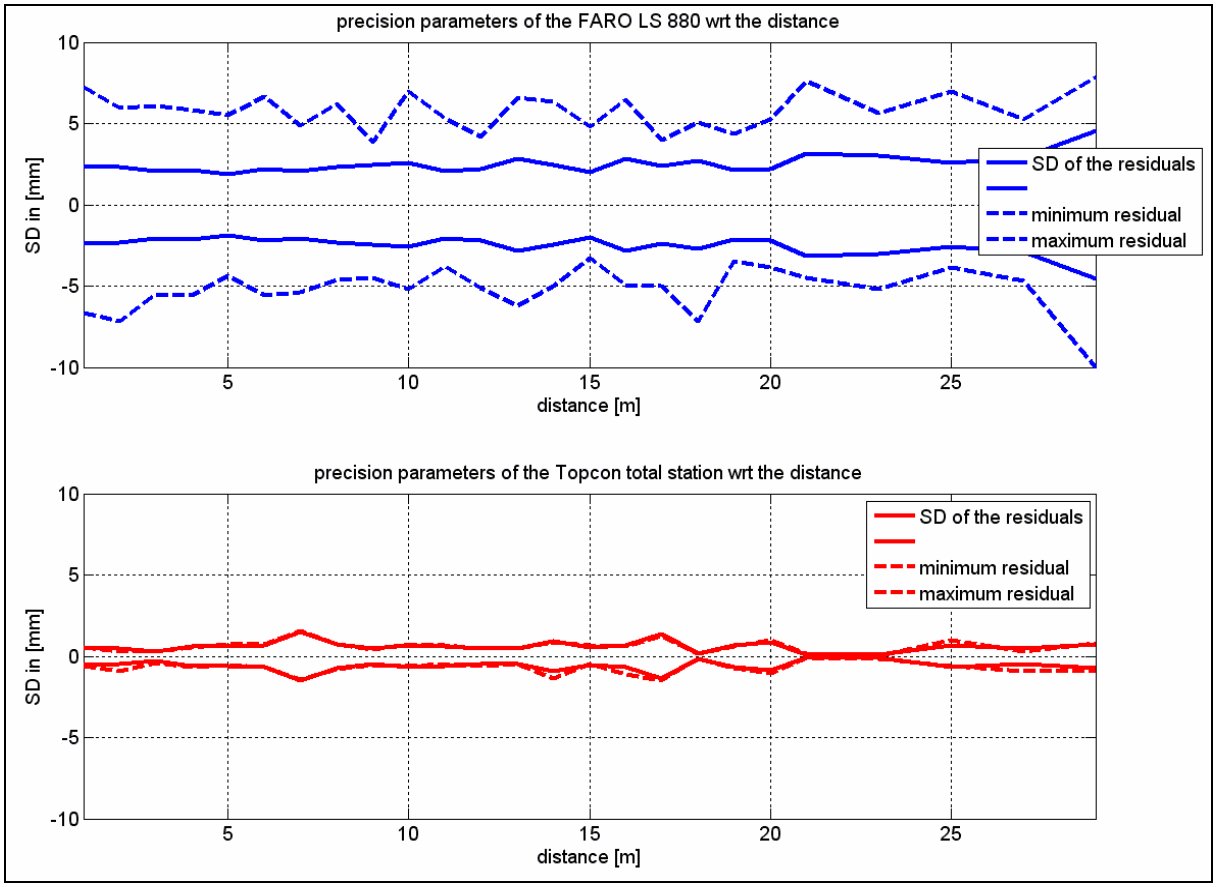

Figure 8.12: Visualization of the spreading features of the residuals by showing the trends of the standard deviation (SD), the minimum and the maximum residuals per measurement instrument per scan range, 68% of the residuals are located within the bold lines of the figure as they represent the SD and 100% of the residuals are located within the dashed lines. *Top:* the visualization of the spreading features of the FARO LS 880. *Bottom:* the visualization of the spreading features of the total station.

The difference in redundancy can clearly be seen in figure 8.12. The minimum and maximum residual curves are almost the same as the curve of the SD because 68% of 5 points is 3.4 points. This means that the minimum and maximum values represent just one point measured with the total station.

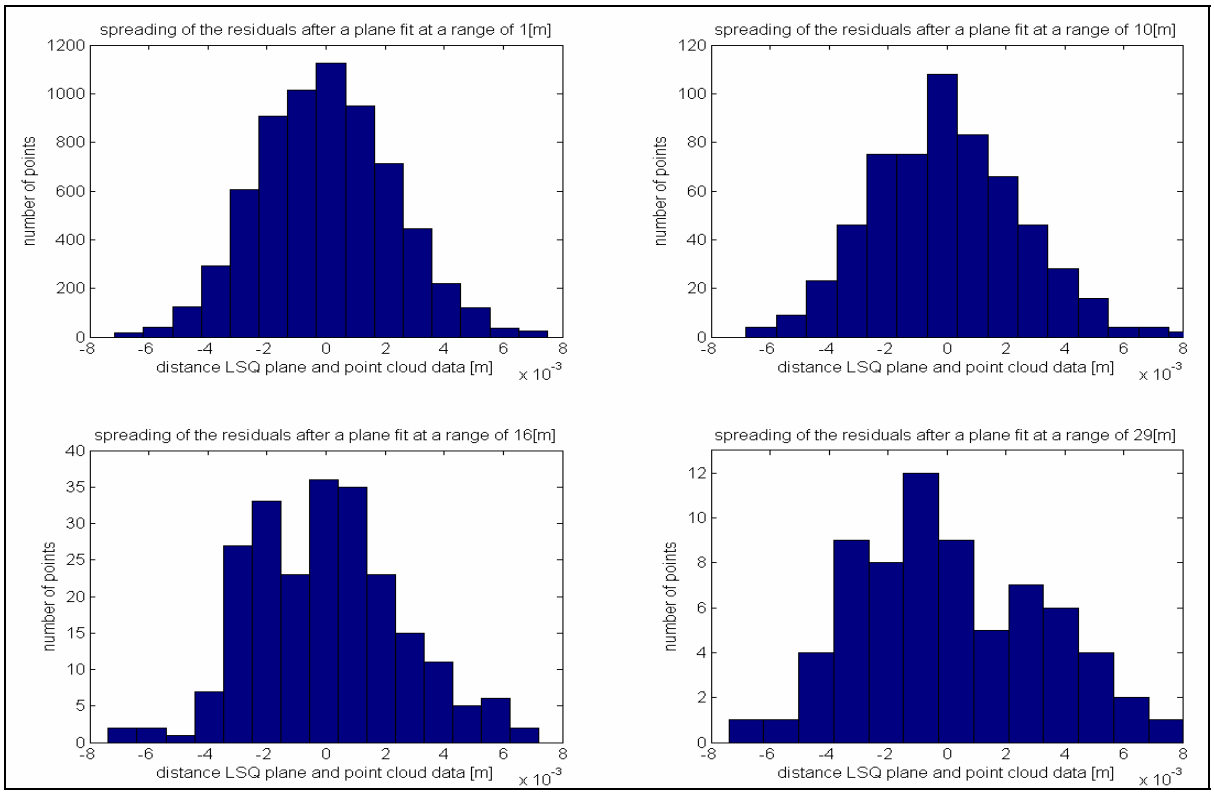

Figure 8.13: four examples of histograms of the residuals after a LSQ plane was fitted through the points of the scans obtained at the scan ranges of 1[m], 10[m], 16[m] and 29[m]. It can be seen that the normal distribution decreases very little with the range.

By taking the information of the figures 8.12 and 8.13 into account, it can be concluded that the precision of the scans obtained with the FARO LS 880 decreases minimally with the distance. Therefore, it can be mentioned that scanning objects up to 29[m] does not result in significant precision differences of the scans obtained.

Relative reliability parameters of the FARO LS 880 with respect to the range

As mentioned in the introduction of this section, the distance differences between the scanned plates are computed in order to determine the relative reliability parameters of the FARO LS 880 with respect to the range. In order to be able to compute these parameters, the relative distances between the plane models obtained for the scans are compared with relative distances computed with the total station. The latter is set as the ground truth. The advantage of this approach is that systematic errors are eliminated from the results.

Relative distance determination procedure

The results of the LSQ adjustments done are the three plane parameters that minimize the sum of the residuals between the measured points in the datasets. These parameters are obtained for both the laser scan data and the total station data and they represent an infinite plane in the 3D space (see section 6.4.1).

However, the laser scanner and the total station did not measure the coordinates of the exact same points but because all datasets obtained in this experiment are rotated so that the centre of gravity of all plates is located on the x-axis, the measured y- and z-values of the total station data are used because it is known that they are located on the object. Together with the plane parameters these y- and z-coordinates are used to determine the x-values of the total station plane and the laser scan plane respectively.

This approach resulted in five 3D-coordinates per instrument per scan range, which is a total of 250 3D-coordinates, 125 for the laser scanner and 125 of the total station. The distance differences between all 125

points representing the planes of one instrument are determined next. By subtracting the determined relative distances of the laser scan data from the relative distances determined with the total station, the difference between the measured relative distances with the total station and the laser scanner are computed. The result is shown in figure 8.14. The red line represents the mean difference between the relative distances determined with the total station and the laser scanner. Whenever this line or the blue dots represent a negative value, the relative distance measured with the laser scanner is measured too long with respect to the ground truth.

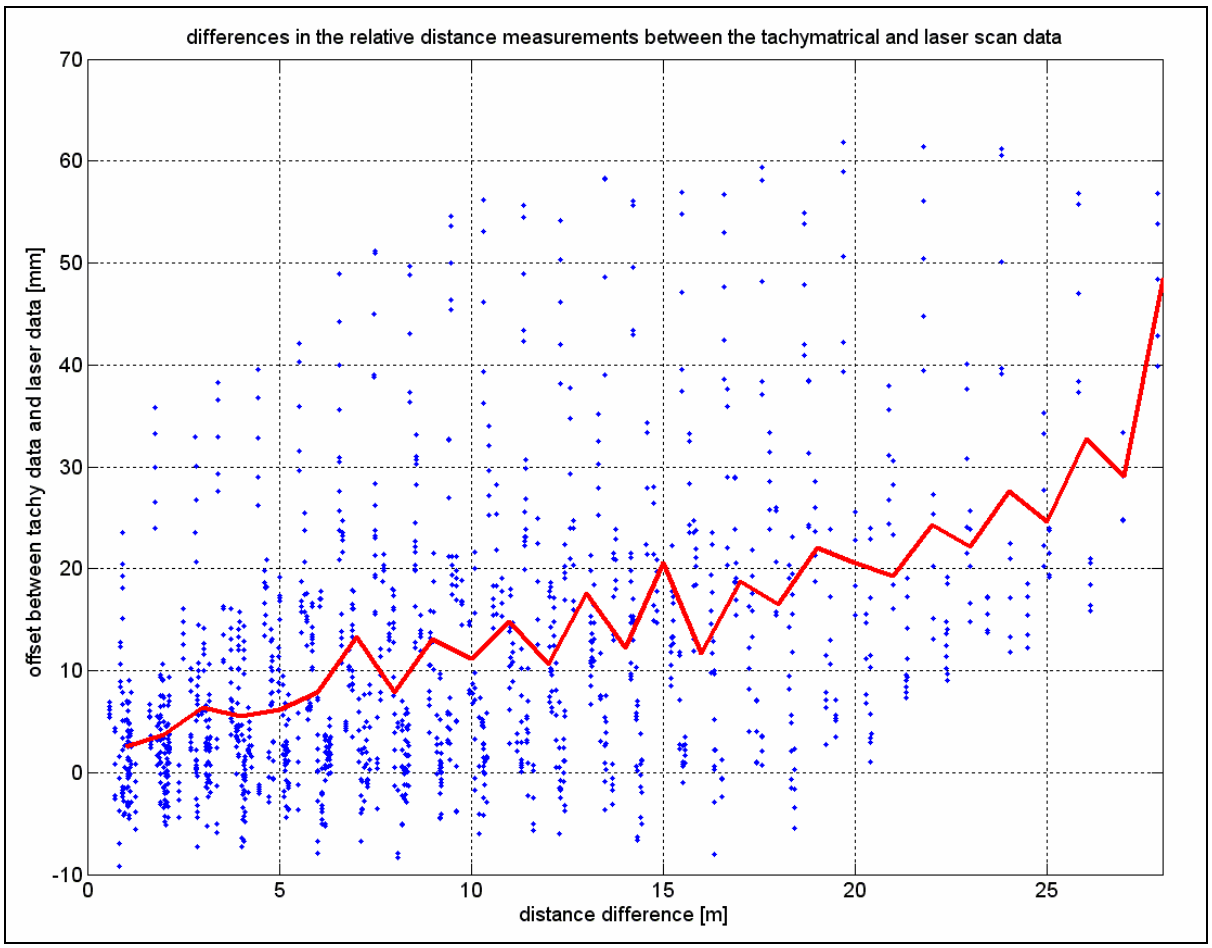

Figure 8.14: The resulting plot of the comparison of the relative distances measured with the total station and the laser scanner. The blue dots represent a ground truth distance difference (on the x-axis) and the difference between this ground truth and the laser scan data. The red line represents the mean values of the blue dots.

It can be concluded from this figure that the trend of the red line is going up. This means that if the relative distance between two points becomes larger, the reliability of this distance measured with the FARO LS 880 will decrease.

It can also be seen that the differences between the ground truth and the relative distances determined with the laser scanner are relatively large, in the order of centimetres. According to the specifications this difference has to be in the order of millimetres. This large difference might be due to the small redundancy of the total station data. It was explained in section 4.7.4 that the redundancy also influences the accuracy and therefore the reliability parameters of a measurement. The overall model test showed that in order to compute an unbiased estimator of the variance σ^2 the weighted sum-of-squares of the residuals need to be divided by the redundancy. Because the difference between the redundancy of the laser scan data and the total station data in this experiment is large, the overall model test might point out that the SD of the overall model of the laser scan data is better

than the SD of the overall model obtained for the total station data. In this situation the range experiment done is not valid.

Section 4.7.4 also mentioned that the chosen σ^2 does influence the outcome of the overall model test positively if the manufacturer gives an opportunistic variance value and the other way around. In order to determine the performances of different scanners with each other, this is unwanted. However, in this experiment not the performances of two different laser scanners are compared but the performances of a laser scanner on one hand and a total station on the other are compared. Because other information on the variances of these instruments is not known, the variances given in the specifications are used to compute the overall model tests for all models obtained (see table 8.3)

Table 8.3: The SD of the overall models of both the total station and the laser scan data.

	SD of the overall models [mm]			**SD of the overall models [mm]**	
Scan range [m]	*Topcon*	*FARO LS 880*	**Scan range [m]**	*Topcon*	**Scan range [m]**
1	0.27	0.79	**14**	0.42	0.85
2	0.24	0.77	**15**	0.27	0.69
3	0.13	0.70	**16**	0.33	0.98
4	0.27	0.71	**17**	0.65	0.85
5	0.30	0.63	**18**	0.07	0.94
6	0.32	0.74	**19**	0.32	0.75
7	0.69	0.69	**20**	0.41	0.77
8	0.36	0.78	**21**	0.05	1.10
9	0.24	0.83	**23**	0.04	1.07
10	0.32	0.87	**25**	0.31	0.93
11	0.29	0.71	**27**	0.24	1.03
12	0.22	0.76	**29**	0.33	1.64

It can be concluded from table 8.3 and figure 8.15 that the SDs of the overall models obtained with the total station data are smaller than the SDs of the models obtained with the laser scanner data despite the difference in redundancy. However, the difference between the SDs is not extremely large. It is wanted that the differences between the SDs are large because then the SDs of the overall model determined for the ground truth is much lower. In order to obtain this large difference it is recommended to use more targets in future experiments because then the difference between the standard deviations of the overall models will increases rapidly.

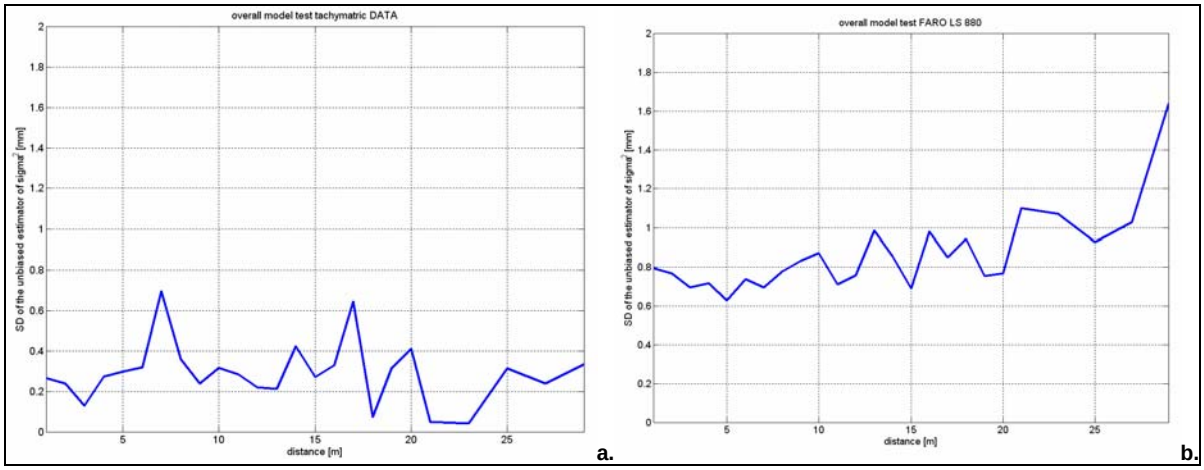

Figure 8.15: Visualization of the trend of the SDs of the overall models for the total station (*left*) and the FARO LS 880 (*right*)

However, for this research is can be concluded that based on the results of table 8.3 and figure 8.15, the residuals of the total station data are much smaller with respect to the residuals of the laser scanner and that the larger redundancy of the laser scanner does not result in more reliable models. Therefore the total station data can be used as a ground truth and the results of figure 8.14 hold true and additional research is recommended to explain the large offsets between the total station and the laser scan data.

Absolute reliability parameters of the FARO LS 880 with respect to the range

It followed from the previous section that it is valid to use the total station data as a ground truth. During this step the absolute reliability parameters of the FARO LS 880 will be determined with respect to the range and the ground truth used is obtained with the Topcon as well.

Absolute distance determination procedure

In order to determine the absolute distances between the object on position *n* and both instruments, the same five points are used as for the relative distance determination. Though, this time the distance between the middle point of the laser scanner (and total station) and the five points located on the plate are determined. The absolute distances determined with the laser scan data is subtracted from the absolute distances determined with the total station. The results are shown in figure 8.16 and negative values represent absolute distances determined with the laser scanner that are too long.

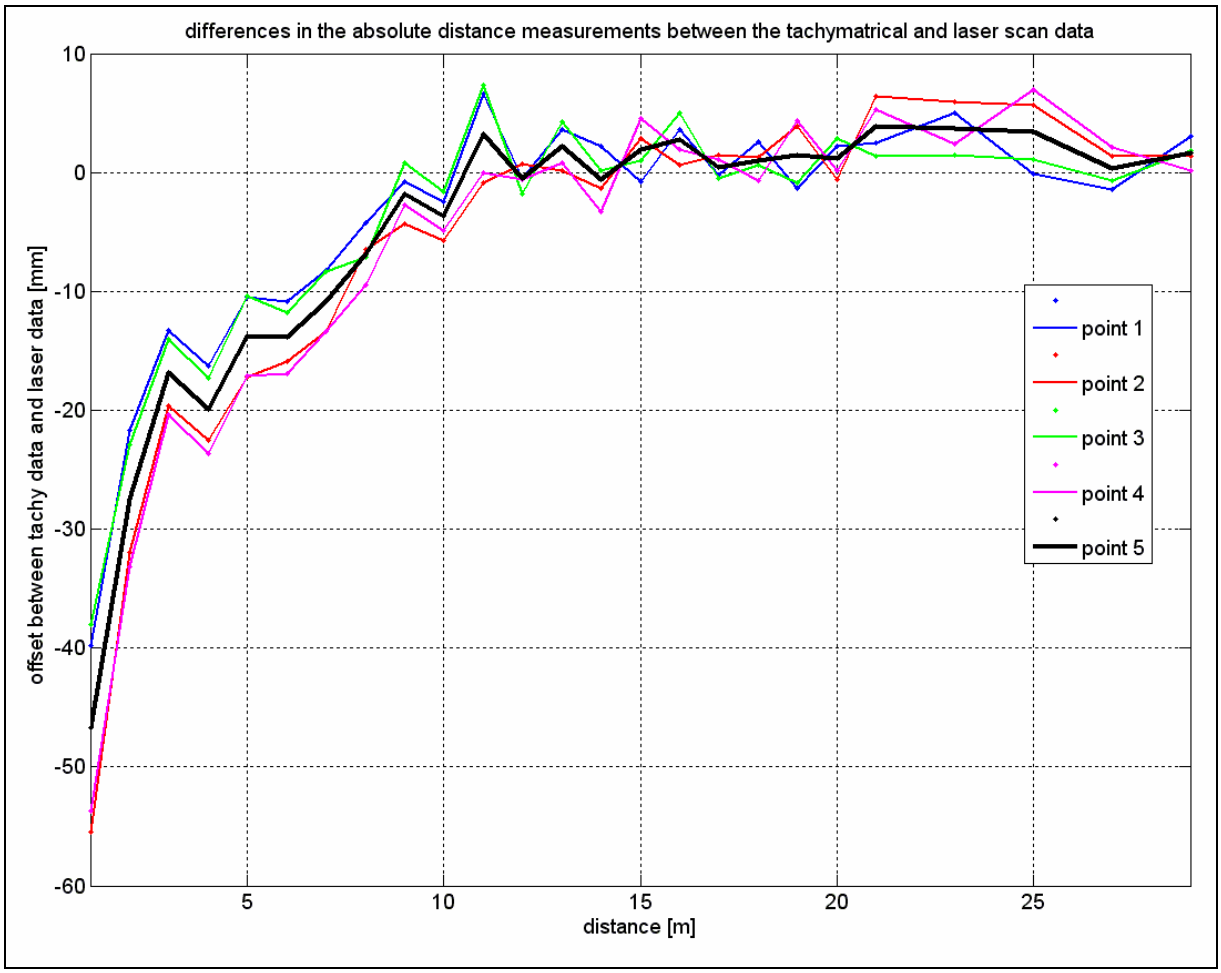

Figure 8.16: The curves that represent the offset between the absolute distances determined with the total station and the laser scanner. The distances of five points on the object are compared with each other and each curve represents one of these points.

The black line in figure 8.16 represents the mean offset between the ground truth and the total station data. It can be concluded from this figure that the offset between the absolute distances on the short ranges is extremely high, in the order of centimeters. However, after a scan range of 10[m] this offset becomes much smaller and in the order of millimeters.

Figure 8.17 shows four examples of the absolute distance difference between the ground truth and the plane determined with the laser scanner for the ranges of 3, 13, 23 and 29[m]. The colours represent the offset in the absolute distance for a part of the object (the scale of the colourbar is in [mm]). It can de seen that the offsets are indeed higher for the short scan range of 3[m] and not significantly different for the larger ranges. This result is exactly the opposite of what is expected and further research is recommended to give a suitable explanation.

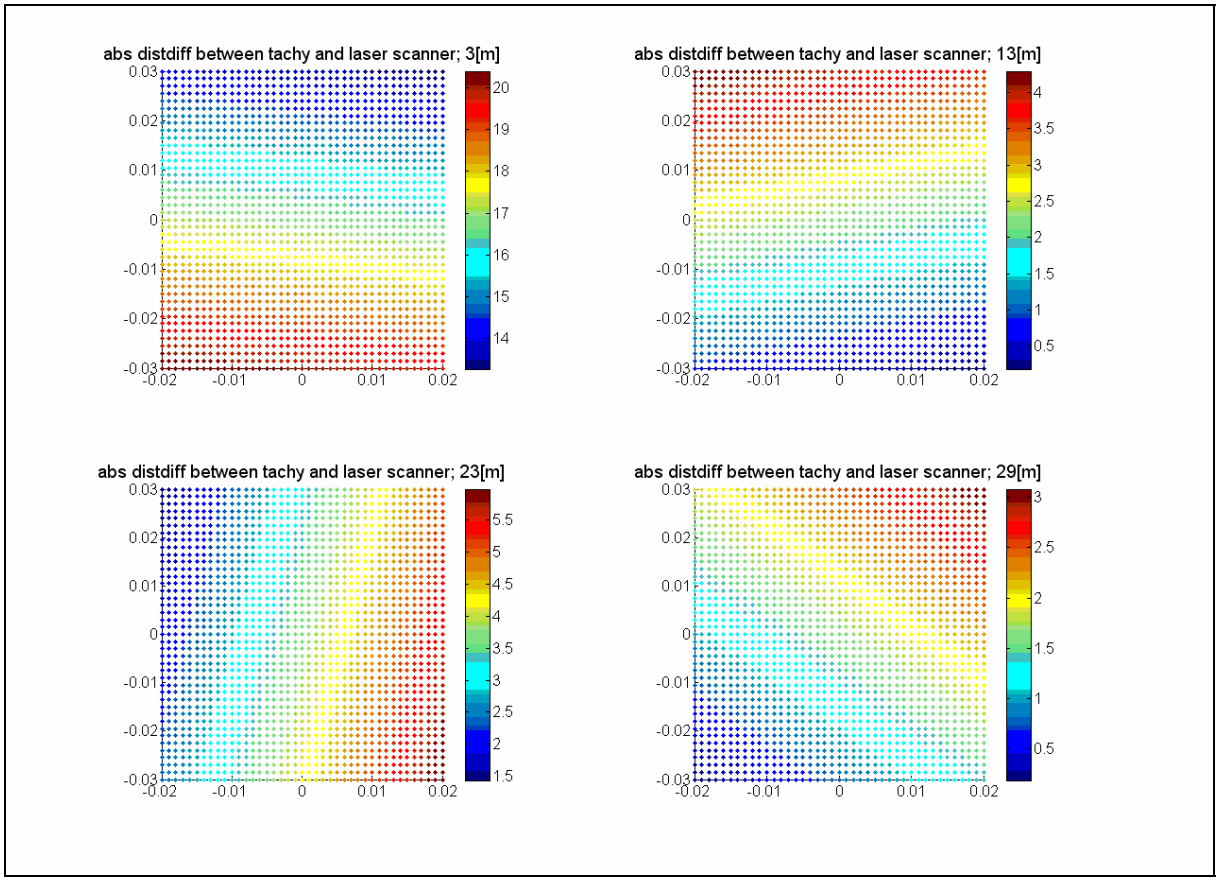

Figure 8.17: Visualization of the offset between the absolute distances determined with the laser scanner and the ground truth values determined with the total station. This figure shows the offset of a part of the object which is the white plate. *Top left:* the offsets at a scan range of 3[m]. *Top right:* the offset at a scan range of 13[m]. *Bottom left:* the offset at a scan range of 23[m] and *Bottom right:* the offset at a scan range of 29[m].

9 Conclusions and recommendations

This chapter discusses the conclusions and recommendations that can be made based on the results obtained in this research.

9.1 Conclusions

The conclusions drawn up in this paragraph are based on the results obtained and are divided into six categories, i.e.: conclusions with respect to (1) General findings of the experiment, (2) the number of points scanned, (3) the intensity values measured, (4) the precision parameters, (5) the reliability parameters, and (6) the created experiment set-up.

9.1.1 General findings of the experiment

The analyses have shown that *there is no large difference between the two scanners with respect to the number of points scanned and the intensity values measured*. The performances of the IMAGER 5003 are slightly better with respect to the number of points scanned.

A few exceptions to this statement hold good for extreme objects like a black velvet patch with a remission of only 0.5% and a blue patch. The FARO LS 880 loses almost no points on these difficult objects, whereas scans obtained with the help of the IMAGER 5003 show a lot of gaps.

There is a big difference when it concerns the precision parameters of both scanners. *The precision of the IMAGER 5003 is in almost all situations more than twice as good as the precision of the FARO LS 880*. Further research has shown that the IMAGER 5003 filters the data before an output file is created whereas the FARO LS 880 software allows manual filtering and does not filter the data beforehand. This is an explanation of the difference in precision but this knowledge was gained after the analyses and therefore the results of the two scanners are not really comparable in this research.

The reliability of the scans of both scanners is not significantly different. The reliability of the scans made by the IMAGER 5003 is in most situations slightly higher. This can also be explained by the difference in the filtering approach of both scanners.

The FARO LS 880 demands manual filtering after the scanning phase and the IMAGER 5003 filters automatically. Therefore, if a company wants to limit the post processing stage of the data processing*, the IMAGER 5003 is the better scanner for them to use*.

The FARO LS 880 is the better scanner to be used when difficult objects (like dark objects) have to be scanned. In this situation the IMAGER 5003 software filters the noisy data, which results in gaps in the scans. By using the FARO LS 880 at least some information on these objects is obtained, even though this information is noisy.

9.1.2 The number of points scanned

Due to an increasing scan angle fewer points will be scanned on an object. 85% less points will hit the surface of the object when it is scanned with a scan angle of 80[°] instead of 0[°].

The number of points scanned on a planar white object is within the bounds of what can be expected according to the specifications when the scan angle is increased.

Apart from the blue patch at a scan angle of 0[°], *the IMAGER 5003 acts as to be expected with respect to the number of points scanned on the different colours patches*. However, the number of points scanned with the FARO LS 880 exceeds the threshold of 5% occasionally. This means that in these situations fewer points are scanned than can be expected from the specifications.

The black velvet patch fails on the 5% threshold with respect to the number of points scanned with both the IMAGER 5003 and FARO LS 880 for all scan angles. This is as to be expected because the remission of this patch is less than 0.5%. When the scan angle is increasing, the performances of the other darker patches decrease as well with respect to the number of points scanned. This eventually results in an exceeding of the threshold value as well.

The range experiment has shown that *the performances of the FARO LS 880 with respect to the number of points scanned and an increasing scan range are within the bounds of the expectations.* The expectations are based on the specifications of the laser scanner.

It follows from the range experiment that 99% less points will be scanned on an object located at 20[m] from the scanner then on the same object located at a distance of 1[m] from the scanner. In other words this means only 1% of the points will be scanned on an object located at a distance of 20[m] compared to the number of points scanned at a scan range of 1[m].

9.1.3 The intensity values measured

The mean measured intensity value of an object scanned decreases with the scan angle in general. The resulting *intensity – scan angle* curve is used to gather insight into the scatter pattern of the scanned object. The scatter pattern of the white plate used for this research is most likely a Minneart scatter pattern in combination with either the Henyey-Greenstein model of forward scattering or a model close to a specular scatter pattern.

The scatter patterns of most colour patches for the scan angles between 20[°] and 80[°] can be represented by a Minnaert model as well.

The scatter patterns of the grey value patches are not identical. The middle-grey patch is the only curve that might be represented by a Minneart model. The scatter patterns of the other patches are unknown but it seems Lambertian for the white and light-grey patch and close to specular for the dark-grey, black and black velvet patches.

The colour range in intensity values measured from high to low: *(1) Purple (highest), (2) Yellow, (3) Red, (4) Blue, (5) Cyan and (6) Green (lowest).*

The obtained intensity values for the *green patch* are much lower than the intensity values for the other patches. This is as to be expected because green is the complementary colour of red.

The grey value range in intensity values measured from high to low with both scanners: *(1) white patch (highest), (2) light-grey patch, (3) middle-grey patch, (4), dark-grey patch and (5) black patch + black velvet (lowest)*. This list follows the remission characteristics of the patches.

The intensity – range curve of the FARO LS 880 at middle resolution does not behave as expected. Apart from the ranges of 1 – 4 [m], the curve seems to behave *linear* which indicates that the intensity values measured are most likely influence by the atmosphere only. This implies that the effect of the footprint does not influence the relation between the intensity and the range.

9.1.4 Precision parameters

All scans obtained contain more noise when the scan angle is increased. *It can therefore be concluded that in general the precision of the scans decreases with the scan angle.* This is as expected because fewer points are scanned when the scan angle is increased and the intensity values measured are decreasing with the scan angle as well.

The output scans obtained with the IMAGER 5003 have a higher precision than the output scans obtained with the FARO LS 880. This is due to the fact that the IMAGER filters the data before computing an output file.

The precision of the green patch is for both scanners relatively low in comparison with the other colour patches. This is as to be expected because green is the complementary colour of red so the green patch absorbs most of the incoming laser light because this is close to red light.

Bright objects are scanned with a higher precision than darker objects. This is as expected because less energy of the incoming signal is absorbed by brighter objects, which means that more energy can be reflected back to the scanner.

The precision of the FARO LS 880 does not significantly changes with the scan range. This precision parameter is in the order of 2 – 4.5[mm] up to a distance of 29[m].

9.1.5 Reliability parameters

The reliability of the output scan obtained with the IMAGER 5003 has a higher reliability then the output file obtained with the FARO LS 880. This is due to the different approach on the filtering of the scans.

In general colour does not influence the reliability of the scans obtained with the two scanners. The only exception to this is the reliability of the blue patch scanned with a scan angle of 0[º]. Because the FARO LS 880 does not filter the data the reliability of this patch at this scan angle is poor. On the other hand, the IMAGER 5003 loses a lot of points on the blue patch implying difficulties with this colour as well. *Therefore, it is best to avoid scanning a blue object with a scan angle of 0[º].*

Despite the poor precision of the green patch, the reliability of this patch is not different from the reliability of the other patches.

The output scans obtained with the two scanners are as reliable (or unreliable) when it concerns the different reflectivity characteristics. General findings with respect to the reflectivity characteristics are: (1) *Bright objects can be scanned best because of the precision and reliability.* If the scan angle is 0[°] the highest values for these parameters are obtained. When the scan angle increases the results are still precise and reliable. This counts for both scanners. (2) *Darker objects result in bad precision and reliability parameters.* These objects are best to be avoided during the scanning phase. However, when it is not possible to avoid the darker object inside a scan area, it is best to scan them with a scan angle of 0[°] because then the reliability is within accepted values or just beyond these values. Both statements are as expected.

If the relative distance between two points becomes larger, the reliability of this distance measured with the FARO LS 880 will decrease and becomes in the order of centimetres. According to the specifications this difference has to be in the order of millimetres and therefore, the specifications do not hold true.

This relative distance determined with the FARO LS 880 is compared with a ground truth obtained with a total station. It can be concluded from the results of the overall model test that the standard deviations of the overall models obtained with the total station data are smaller than the standard deviations of the models obtained with the laser scanner data, despite the difference in redundancy. *Therefore the total station data can be used as a ground truth*.

9.1.6 Created experiment set-up

The corridor in which all the experiments were done has approximate constant climatic conditions. Small deviations in temperature and atmospheric conditions could have occurred during the measurements and might have influenced the results. However, these influences are assumed to be minimal.

Because centring of both laser scanners is not possible, the distance between the scanner and the object of interest was set as approximately 4[m] each time the experiment set-up of the scan angle, the colour and the reflectivity experiment was rebuild. *This means that small deviations within in the distance between scanner and object are possible*. This makes the two sets of measurements not completely comparable, because of possible small range changes. However, these influences are assumed to be minimal.

This 'constant' scan range also means that all results obtained for these three experiments during this research are valid for a scan range of 4[m] only. The behaviour of the scanners with respect to the scan angle, the colour and the reflectivity on other ranges is not researched and therefore not known. It is expected however that comparable results are obtained for comparable range distances (=short ranges).

The accuracy of the angle measurement device which is used in the scan angle, the colour and the reflectivity experiment is not known exactly but assumed to be in the order of 2[°]. This assumption has an influence on the conclusions because when the accuracy of the device is better, the conclusions with respect to the scan angle would be 'harder' and when the accuracy is of the device is worse; the conclusions with respect to the scan angle would be less 'hard'. In the last case, the results might even be unsatisfying.

The object of interest during the scan angle and range experiment was the white plate. This plate is assumed to be a neutral object on which the influences of the range and scan angle could be examined best. *In reality lots of different objects are present in a scan area and the obtained results of this research are not automatically valid for all objects.*

The methods of analysis as programmed in Matlab can be used to evaluate the performances of different laser scanners on all planar objects. The analyses are based on (1) the number of points scanned, (2) the intensity values measured and (3) the precision and reliability parameters.

Due to the high number (about 120) of processed scans an interior selection was made in order to reduce the calculation time (and also the edge effects). *The automatic interior selection of the scans turned out to be a representative tool to reduce the total calculation time.*

During the range experiment, one tripod is used for the total station and the laser scanner. By placing the instruments on the same tripod it is assumed that they scan from the same position. However, the middle point of the laser scanner is said to be exactly in the middle but no prove for this statement is found yet. *Therefore, it might be possible that small changes in the results are present due to this difference. However, these differences are assumed to be minimal.*

9.2 Recommendations

In this paragraph recommendations for further research are given, first with respect to the results obtained during the research and second with respect to the test set-up in general.

9.2.1 Recommendations with respect to the results obtained

Further research is recommended on the difference in precision and reliability parameters after filtering the scans obtained with the FARO LS 880. Because the same filtering approach for both scanners is required, insight into the filters used by the IMAGER 5003 should be gained first. After this filtering the analyses need to be done again. This will make it possible to compare the scans of the two scanners and clarify which scanner is more precise and reliable.

During the data acquisition phase of the experiments both the middle and the second highest resolutions of the scanners were used to obtain scans. However, the results discussed in this thesis are only valid for the middle resolution because of the time limit of this research. *It is recommended to follow the same steps of analysis discussed in this thesis in order to gain an insight into the performances of the two laser scanners on the higher resolutions.* These results can also be compared with the results discussed in this thesis in order to see whether high resolutions indeed result in higher accuracies.

Every experiment resulted in a number of curves. *An investigation into the possibility of combining these curves has not been done during this research*. However, it can be expected that the information obtained from the scan angle experiment can be combined with the information obtained from, for example, the range experiment. It is to be expected that this combination will give an insight into the precision and reliability expectations of a situation in which an object is scanned at a certain range and with a certain scan angle. Whether this is possible has to be examined first. This can for example be done by creating the scan angle experiment again but now at a constant range of 8[m].

The experiments have shown that the scatter theory is different as expected. *Additional research is required to gain an insight into the scatter patterns of the scanned objects.* It is to be expected that the patterns of the colour

patches and the white plate follow the Minneart scatter model for the scan angles of 20 - 60[°]. The scatter pattern of the scan angles between 0 - 20[°] is expected to follow either the Henyey-Greenstein model of forward scattering or a close to specular scatter pattern. Insight into these patterns can be obtained by rotating the object of interest with smaller angle increments, for example increments of 1[°].

At the moment, the output intensity values measured with the two scanners are binary numbers. The meaning of these numbers is not known but it is assumed to be a percentage of the energy of the emitted signal. Whether this is true needs to be investigated and if it is true this knowledge can be used to get the absolute intensity values. *If the absolute intensity value is known, they can be used for numerous applications like the determination of the exact absorption of different colours and the scatter patterns of the scanned objects*. During this research all conclusions with respect to the intensity are relative.

One of the theories discussed in this research is based on the behaviour of colours on Near Infra Red (=NIR) signals. Because NIR can not be seen, it is not possible to give any expectations or conclusions with respect to this theory. *Therefore, it can be recommended to invest the test chart on the presence of NIR in order to be able to exclude or include this theory.*

The *intensity – range* curve shows an unexpected behaviour in the ranges 1 – 4[m]. Instead of a decreasing trend, the curve shows an increasing trend at these ranges. Whether this is behaviour is a coincidence or a standard has to be clarified. Therefore, additional research is recommended on these short distances.

The *intensity – range* for the larger distances, 5 – 29[m], also shows a different behaviour as expected. It is expected that the increasing footprint also affects the intensity values measured. This feature does not follow from the obtained curve and therefore *it further research is recommended on the effect of the laser footprint and the range. This in order to find the exact relation between the footprint resolution and the atmosphere on the intensity values measured*.

During the range experiment large offsets are detected for both the relative and absolute distances determined with the FARO LS 880. Because these differences are extremely different from the expectations, they are in the order of centimetres whereas millimetres were expected, it is recommended to perform an additional research. The datasets obtained might contain errors but it is also possible that these offsets are general. Therefore, it is recommended to perform a comparable experiment with other laser scanners and the FARO LS 880 and compare the results obtained with the results of this research.

Finally, additional research is required on the effect of blue colours scanned with a scan angle of 0[°]. Both scanners have problems with respect to this colour and it seems that the reason is overloading of the system because high intensity values are measured for the blue patch at this scan angle.

9.2.2 Recommendations with respect the test-set up in general

The object of interest during the scan angle and range experiment was the white plate. This plate is assumed to be a neutral object on which the influences of the range and scan angle could be examined best. In reality lots of different objects are present in a scan area and the obtained results of this research are not automatically valid for all objects. *Whether the results are valid for more objects should be investigated further in order to create a general statement.*

During this research Zoller und Fröhlich created a new scanner, the IMAGER 5004. It is said that this scanner is a big improvement on the IMAGER 5003, especially the hardware is improved. One of the improvements involves the possibility to centre this scanner above a known point. This is also said that this scanner is more accurate [Zoller + Fröhlich, 2006]. *It is recommended to invest the performance of the IMAGER 5004 in the future as well, because the IMAGER 5003 is not produced anymore.*

At the moment a permanent experiment set-up is created, it is recommended to create a fixed position on which the different laser scanners can be mounted. This position needs to be located on the beginning of a rail. It must be possible to mount different objects of interest on this rail in order to move them back and forward with known range increments with respect to the scanner. It is best if the connection between the object and the rail allows rotation of the object with known increments as well. Figure 9.1 visualizes a schematic overview of the recommended experiment set-up.

For the ground truth a total station needs to be implemented in the experiment as well. Therefore, a number of targets need to be located at fixed positions around the set-up but also on the object of interest. *It is recommended to use more then five targets on the object,* for example eight or nine targets. This research used five targets on the object of interest and the standard deviation of the overall model of the total station was indeed higher than the standard deviation of the overall model of the laser scanner but not much higher. This latter is however what is wanted and recommended and by measuring more then five targets on the object of interest, the difference between the standard deviation of the overall models increases rapidly.

By measuring these targets with both the laser scanner and the total station, the laser scan data can be transformed in the local coordinate system of the total station, or the other way around. This makes it possible to compare the results of the laser scanner with the total station, of which the accuracy is known. Other instruments of which the accuracy is known can be used as well.

It is also recommended to create the experiment set-up in a room or area in which the climate can be controlled exactly in order to be able to completely eliminate this influence. Furthermore, it must be possible to eliminate external light sources such as sunlight from the area in which the experiment set-up is created because they might affect the performances of the laser scanners.

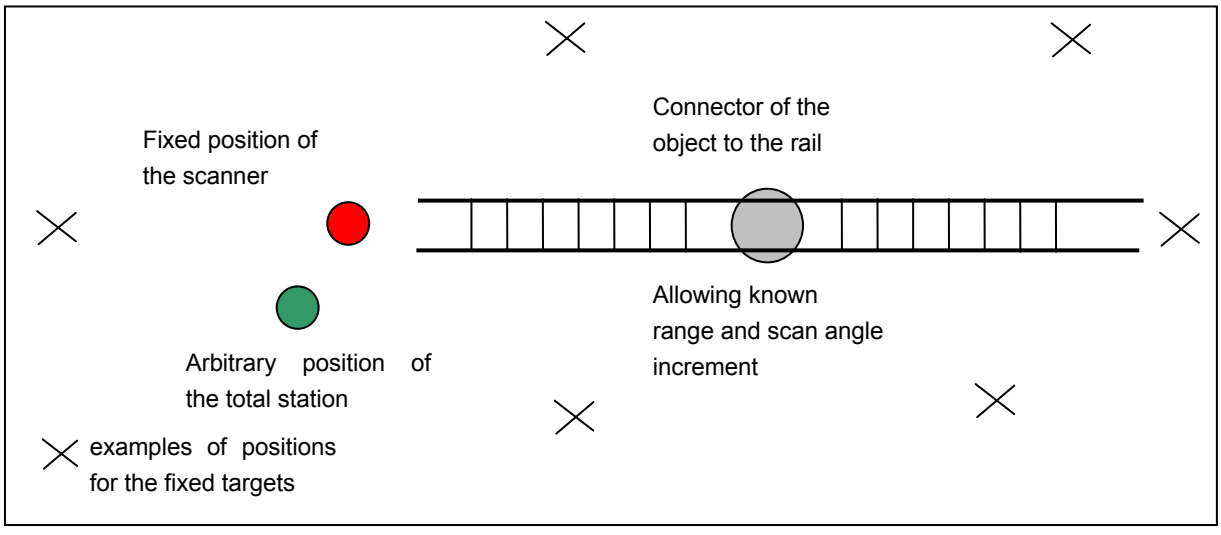

Figure 9.1: a schematic top view of the recommended experiment set-up.

References

Boehler, W. and A. Marbs, 2002. *3D scanning instruments,* Proceedings of the CIPA WG6 International Workshop on scanning for cultural heritage recording, ISPRS commission V, p. 9 – 12.

Boehler, W., et al, 2003. *Investigating laser scanner accuracy,* Proceedings of the XIXth CIPA Symposium, Antalya, Turkey.

Bucksch, A., *Personal comment,* 23rd of March 2006.

Claassen, E.P., 2003. *Registratie van airborne en terrestrische laserdata,* Master thesis, Delft University of Technology, Faculty of Civil engineering and Geosciences, Department Geodesy, Delft.

Claassen, E.P., *Personal comment,* 12th of January 2006.

Clark, J., and S. Robson, 2004. *Accuracy of measurements made with CYRAX 2500 laser scanner against surfaces of known colour*, Proceedings of the XXth Congress of ISPRS, Vol. XXXV, Istanbul, Turkey.

Gosliga, R. van, 2005. *Deformatie analyse van een geboorde tunnel met behulp van terrestrische laserscanning*, Master thesis, Delft University of Technology, Faculty of Aerospace engineering, Delft.

Lester, P.M., 2005. *Visual Communication, images with messages,* 4th edition, Thomson Wadsworth, Belmont, pp. 11.

Lichti, D.D., and M.G. Licht, 2006. *experiences with terrestrial laser scanner modelling and accuracy assessment,* ISPRS, Vol. XXXVI, Part 5, Dresden, Germany.

Lindenbergh, R.C., et al, 2005. *Accuracy analysis of the Leica HDS3000 and feasibility of tunnel deformation monitoring,* Proceedings of the ISPRS workshop Laser scanning 2005, Twente, The Netherlands.

Longhurst, R.S. 1957, *Geometrical and Physical Optics,* 2nd edition, Longman Group, London.

Pfeifer, N., 2005. *lecture notes Digital Terrain Modelling*, Delft University of Technology, Delft.

Sablerolle, S.A., 2006. *Automatic registration of laser scanning data and colour images,* Master thesis, Delft University of Technology, Faculty of Aerospace engineering, Delft.

Teunissen, P.J.G., 2000a. *Adjustment Theory, an introduction*, Delft University of Technology, Delft.

Teunissen, P.J.G., 2000b. *Testing theory, an introduction,* Delft University of Technology, Delft.

Rees, W.G., 2001. *Physical principles of Remote Sensing,* 2nd edition, Cambridge University Press, Cambridge.

Wehr, A. en U. Lohr, 1999. *Airborne laser scanning – an introduction and overview*. ISPRS 54, p.68-82.

Visited websites

All refer, Definition plane
http://reference.allrefer.com/encyclopedia/P/plane.html, last visited at: 15-08-2006

Brother, primary and secondary colour theory
http://www.brother.com/eu-printer/lcv/light1.html, last visited at: 30-10-2006

CIE, theory of the CIE-diagram
http://www.cie.co.at/frameaboutcie.html, last visited at 31-10-2006

Digitalkamera, 'Esser test charts.
http://digitalkamera.image-engineering.de/article.php/Testcharts, last visited at: 11-09-2006

Faro, hardware specifications FARO LS 880.
http://www.faro.com/content.aspx?ct=ho&content=pro&item=5, last visited at 26-09-2006

Fugro, Company profile.
http://www.fugro.com, last visited at: 30-05-2006

Fugro-Inpark, Company profile.
http://www.fugro-nederland.nl, last visited at: 28-05-2006

Gretagmacbeth, ColourChecker chart.
http://www.gretagmacbeth.com/index/products/, last visited at: 23-05-2006

Leica Geosystems, hardware specifications HDS 4500.
http://www.leica-geosystems.com/hds/en/lgs_5572.htm, last visited at 15-08-2006

Mathworld, definition Cartesian Coordinates.
http://mathworld.wolfram.com/CartesianCoordinates.html, 17-08-2006a

Mathworld, definition laws of sine and cosine.
http://mathworld.wolfram.com/LawofSine.htm, last visited at: 08-06-2006b

Mathworld, definition Spherical Coordinates.
http://mathworld.wolfram.com/SphericalCoordinates.html, 17-08-2006c

Mathworld, vector mathematics.
http://mathworld.wolfram.com/Vector.htm, last visited at: 08-06-2006d

Michaelharding, primary and secondary colour visualization
http://www.michaelharding.co.uk/colour-and-technique.php, last visited at: 30-10-2006

Optics, Specular Reflection.
http://electron9.phys.utk.edu/phys136d/modules/m10/geometrical.htm, last visited at: 08-05-2006

Riegl, picture interior scanner.
www.rieglusa.com/products/lms-z360/e_lms-z360.htm, last visited at: 27-04-2006

Topcon, total station information
http://www.topconeurope.com/index.asp, last visited at: 13-10-2006

Yorku, colour spectrum
http://www.yorku.ca/eye/spectru.htm, last visited at: 01-09-2006

Zoller + Fröhlich, hardware specifications IMAGER 5003.
http://www.zf-laser.com, last visited at: 26-09-2006

Used software

Cyclone. Version 5.4. Copyright 2000-2005, Leica Geosystems HDS LLC.

FARO Scene. Version 3.0.11.23 Copyright 2001-2006, FARO.

Matlab®, The Language of Technical Computing. Version 7.1.0.246 (R14) Service Pack 3, Copyright 1984-2005, The MathWorks, Inc, August 02, 2005.

Appendix I : FUGRO Inpark company profile

The research described in this thesis is done by order of Fugro-Inpark B.V. (FINP) which is a part of the worldwide company Fugro N.V. This appendix contains a brief outline about the company and a focus on the section of Geo Information services of FINP as this is the section for which this research is done.

Fugro N.V.

Fugro N.V. was founded in 1962. It has been listed on Euronext N.V. in Amsterdam since 1992 and has been included in the Amsterdam Midkap Index since March 2002. Fugro has over 8,500 staff permanently stationed in over 50 countries (Fugro, 2006).

Fugro N.V. operates around the world at sea, on land and from the air, using professional and highly specialised staff supported by advanced technologies and systems, many of which have been developed in-house. They collect, process and interpret data related to the earth's surface, the soils and the rocks beneath. Generally this is done to provide advice for purposes related to the oil and gas, the mining and the construction industry.

Fugro's objective is the occupation of a leading market position by providing high-quality services supported by technological developments. This requires a strong international and/or regional market position.

Organisation

Organisationally Fugro can be divided into the following three divisions (see figure A1.1):

1. geotechnical services;
2. survey services;
3. geoscience services.

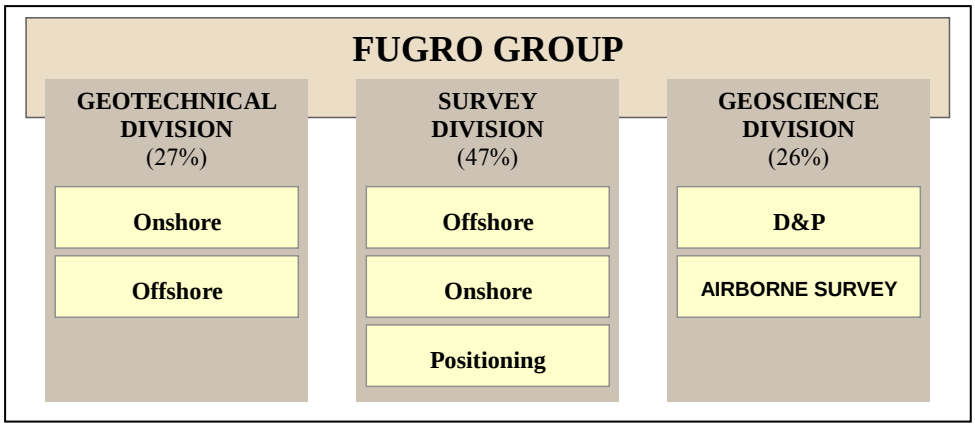

Figure A1.1: The organisation of Fugro N.V. represented in a schematically way (source: Fugro, 2006).

Geotechnical division

The geotechnical division creates mainly analytical models of the subsurface to provide the most complete understanding possible of the physical characteristics of the subsurface, its conditions and the interaction between manmade structures and the subsurface. As can be seen in figure A1.1, the geotechnical division of the

FUGRO GROUP can be subdivided into an onshore and an offshore subdivision. A summation of some main activities of both subdivisions will be given next.

Onshore activities

- probing[6], drilling and in-situ[7] measurements to collect data on certain areas,
- testing the availability and quality of constructing materials,
- performance of life time monitoring of different constructions,
- consultancy and design assignments related to foundations for buildings, infrastructure projects etc.

Offshore activities:

- seabed investigations using measurement techniques like sampling, coring[8] and in-situ testing,
- advising on foundations for offshore structures, tunnels, bridges and harbour constructions,
- collecting data of the seabed for the laying of underwater pipelines and cables,
- monitoring large structures like offshore platforms, bridges and tunnels.

Survey division

The survey division focuses mainly on precise positioning and geo-spatial data management services. Also mapping is part of this division, therefore topographical, hydrographical and geological maps are one of its main products. This all can be combined into supporting services for construction projects. Figure 2.1 shows that this division can be divided into 3 subdivisions: offshore, onshore and positioning. A summation of the activities of all three subdivisions will be given next:

Offshore activities:

- positioning services using GPS[9] and acoustic[10] systems,
- geophysical surveys to map shallow geological features and hazards,
- route and site investigations for underwater pipelines and cables,
- marine construction survey support,
- acoustic and visual pipeline inspections surveys,
- oceanographic and meteorology measurements and studies.

Onshore activities:

- cadastral, property, engineering, construction, mining and topographic surveys,
- digital topographic mapping and map revision,
- GPS control surveys,
- dimension control and structural monitoring,
- aerial imagery acquisition and processing,
- geo-spatial data registration and management, including the creation of GIS solutions,
- laser mapping (FLI-MAP)
- regulatory and ecological assessment surveys.

[6] Probing is the determination of the carrying-capacity of the soil, using drilling pipes to see the actual soils' structure

[7] In-situ measurements are done to measure the actual situation at a certain moment, like a bridge or fly-over

[8] Coring measurements are done to get insight in the interior of the bottom by using small drilling pipes

[9] GPS is the Global Positioning System

[10] acoustic systems are systems that measure underwater

Positioning activities:

- provision of wide area accurate satellite positioning at the decimetre accuracy level,
- promotion and development of high performance positioning services for the land, the airborne and the marine market,
- provision of vehicle tracking services and fixed asset monitoring,
- maintenance of a global infrastructure with more than 85 reference stations.

Geoscience division

The geoscience division is responsible for the gathering and the interpretation of geophysical and geological data. Furthermore they make quantitative and qualitative estimations of oil, gas, mineral and water resources. Their third task is to optimise the production of oil, gas and minerals. Also this division can be divided into 2 subdivisions i.e.: development & production and airborne survey. The activities of both subdivisions will be summed up next.

Development & Production:

- marine, seismic, gravity and magnetic data acquisition, processing and interpretation,
- exploration and reservoir services,
- non-exclusive surveys, reports and datasets,
- data management and GIS services.

Airborne survey:

- mineral and diamond exploration,
- location of aquifers for water, and saline layer detection for agriculture,
- structural mapping for oil and gas deposits, as well as shallow gas exploration,
- environmental and engineering surveys and shallow bathymetric mapping,
- collection of geophysical data to assist in the creation of geological maps.

Fugro-Inpark B.V.

Fugro Nederland is a dome organisation of the Dutch Fugro company's in the Netherlands, with Fugro-Inpark B.V. and Fugro Ingenieursbureau B.V. as major units. Fugro Nederland is on its turn a subsidiary company of the global company Fugro N.V. Within de Fugro group, FINP is operating in the Onshore Survey Division (see figure A1.1) and has approximately 250 employees [Fugro-Inpark, 2006].

FINP is an engineering specialist in data collection, processing, interpretation and management of geographical information. Due to their expertise in these processes, they also offer interim management services, advice and software solutions.

Organisation profile

The companies profile is shown in figure A1.2. From this figure it can be seen that FINP consists of 4 divisions:

1. ICT;
2. subsurface infrastructure and secondments;
3. Aerial Acquisition;
4. Geo-Information Services.

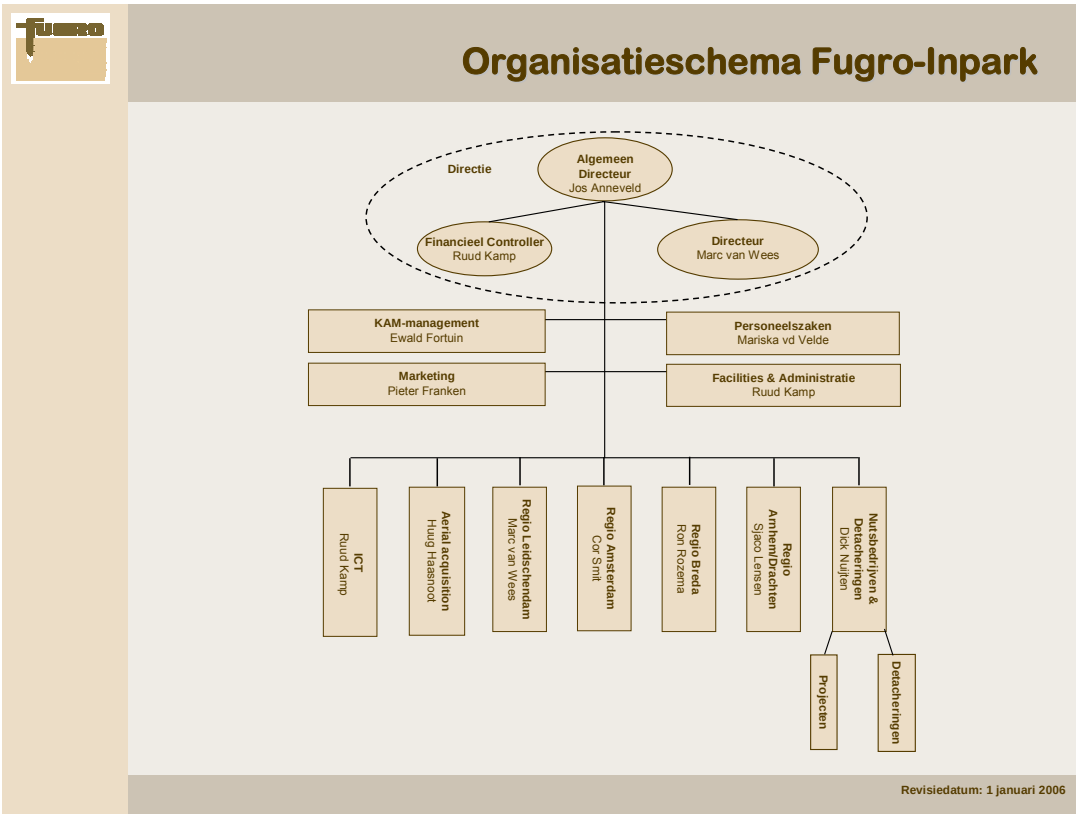

Figure A1.2: The Company profile of FUGRO-INPARK B.V.

ICT

This division manages the entire network and all digital data of FUGRO B.V. and FINP. They are also responsible for the purchasing of new soft- and hardware if this is desirable. Occasionally they develop their own software if a certain special specification is recommended by another division of FINP.

Subsurface infrastructure and secondments

The division of subsurface infrastructure and secondments (OIS) of FINP offers geo information related services and products with respect to the designing, construction and managing phases of cables and conduit-pipes. These divisions' activities are subdivided into four product-market combinations (PMC's):

- OIS rail: for all constructing phases related to cables and conduit-pipes in the railroad sector,
- OIS software and advise: software and independent advise for the designing and managing phases of cable and conduit-pipes data,
- Managing of the geographic data of OIS: maintenance and updating of the geographic data in OIS files,
- Secondments: FINP offers companies to hire their experienced personnel for a certain period.

Aerial Acquisition

The section of Aerial Acquisition of FINP offers Geo-information related services. This information acquisition is obtained from the air. Therefore, a number of advanced systems are used which are integrated in helicopters and airplanes. The products obtained from this acquisition are for example Digital terrain models and orthophotos. The activities of the division of Aerial acquisition can be subdivided into two main services:

FLI-MAP

FLI-MAP is a mapping system of FINP on board of a helicopter. FLI-MAP is able to measure and visualise long infrastructures like railroads and roads efficiently. The system integrates LIDAR and Photogrammetry with GPS and INS data to create a topographic file consisting of a continuously coverage of an area. The data can be used for a number of different applications like 3D mapping, Digital Height Models or Digital Elevation models.

Photogrammetry

A technique which measures certain objects in photos in order to create topographic and/or thematic maps and terrain models. In most situations, these photos are taken from an airplane also combining a image device with GPS and INS measurements.

Geo-information services

Geo-information services is the largest division of FINP and offers a lot of different services. Services offered are: (terrestrial) laser scanning, machine guidance, independent quality survey, Geo Information Systems (GIS) and the creation of high scale maps.

As the research described in this thesis is done by order of the FINP division geo information services and its section *laser scanning,* this section will be discussed shortly.

The laser scanning specialists

Laser scanning is a technique used to collect 3D data of a surrounding and can especially be used in areas which are hard to enter, for example, for the modulation of complex objects or the determination of the exact sizes of buildings.

FINP uses laser scanning for architecture, infrastructure and industrial plants. They support the whole process from collecting the geometric data until the actual modelling. Whenever it is necessary, laser scanning is combined with traditional instruments to achieve an even better efficiency.

The final result of each project can be different and will be defined at the beginning of each project. The final product can vary from a geometrical point cloud of the scanned area till a complete CAD model ready to be implemented in programs like AutoCAD and Micro Station. This way, the data can be used in the familiar way for a company. FINP makes sure that the laser scanners point cloud will be stored forever.

Appendix II : Terminology of mathematics

In section 6.6 of this thesis the methods of determining a plane are discussed. This section introduces a number of vector operations which will be discussed next. More information on vector mathematics can be found on [Mathworld, 2006d].

Vectors in a 3D space are often represented as a linear combination of the 3 perpendicular unit vectors. Typically these unit vectors correspond to the x, y and z directions of a Cartesian coordinate system. That is, any vector **a** in 3D can be written as $\mathbf{a} = a_1 x + a_2 y + a_3 z$ with real numbers for a_1, a_2 and a_3.

$$\mathbf{a} = \begin{bmatrix} a_1 \\ a_2 \\ a_3 \end{bmatrix} \tag{A21}$$

Length of a vector

The length of a vector is based on Pythagoras' theorem and can be determined by the following formula (A2.2):

$$\|\mathbf{a}\| = \sqrt{a_1^2 + a_2^2 + a_3^2} \tag{A2.2}$$

Vector addition

For a vector **a** and a vector **b** in 3D space, the sum of **a** and **b** becomes (A2.3):

$$\mathbf{a} + \mathbf{b} = (a_1 + b_1)x + (a_2 + b_2)y + (a_3 + b_3)z \tag{A2.3}$$

The addition can be represented graphically by 'the parallelogram rule'. Figure A2.1a visualises this rule. The principle is simple: by placing the start of the vector **b** at the tip of the vector **a**, and then drawing an arrow from the start of **a** to the tip of **b** results in a vector that represents vector **a** + **b**.

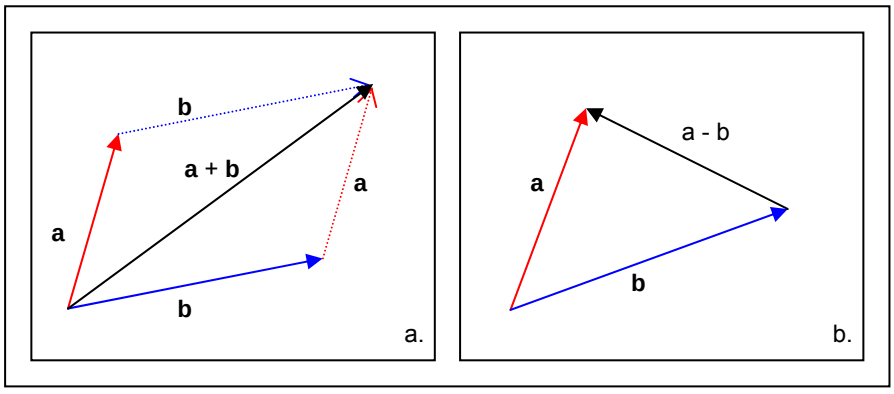

Figure A2.1: the visualization of the addition and subtraction of two vector in a 3D space, a.; the addition of two vectors **a** and **b**, b; the subtraction of two vectors **a** and **b**.

Vector subtraction

For a vector **a** and a vector **b** in a 3D space, the difference vector between **a** and **b** becomes (A2.4):

$$\mathbf{a} - \mathbf{b} = (a_1 - b_1)x + (a_2 - b_2)y + (a_3 - b_3)z \tag{A2.4}$$

Figure A2.3b visualizes the subtraction of the two vectors **a** and **b**. This is done by placing the beginnings of **a** and **b** at the same point, the vector that connects both tips represents the vector **a** − **b**.

Dot product

The dot or the inner product of two vectors **a** and **b** is denoted by **a** ⋅ **b** and is defined as (A2.5):

$$\mathbf{a} \bullet \mathbf{b} = \|a\| \cdot \|b\| \cdot \cos\theta \tag{A2.5}$$

with:

a, **b**	= the vectors a and b
$\|a\|, \|b\|$	= the lengths of the vectors a and b
θ	= the angle between vector a and b

Formula A2.7 shows that when two vectors are perpendicular (θ = 90 [°]) the dot product will be zero. This feature was used to determine which points are inside a plane. If the normal of a plane is perpendicular to the difference vector between point *P* on the plane and point *Q,* point *Q* is located on the plane (see paragraph 6.6). This is true when the dot product between the difference vector and the normal vector is zero.

The dot product can also be defined as the sum of the products of the components of each vector (A2.6):

$$\mathbf{a} \bullet \mathbf{b} = \left[a_1, a_2, a_3\right] \cdot \left[b_1, b_2, b_3\right]^T = a_1 b_1 + a_2 b_2 + a_3 b_3 \tag{A2.6}$$

Cross product

The cross or outer product differs from the dot product primarily in that the result of a cross product of two vectors is also a vector. The cross product is denoted as **a** × **b** and the result is a vector perpendicular to both **a** and **b** and is defined as (A2.7):

$$\mathbf{a} \times \mathbf{b} = \|\mathbf{a}\| \|\mathbf{b}\| \sin(\theta)\mathbf{n} \tag{A2.7}$$

with:

a, **b**	= the vectors a and b
$\|\mathbf{a}\|, \|\mathbf{b}\|$	= the lengths of the vectors a and b
θ	= the angle between vector a and b
n	= a unit vector perpendicular to both **a** and **b**

The problem with this definition is that there are two unit vectors perpendicular to both **a** and **b**. Which vector is the correct one depends upon the orientation of the vector space. Graphically the cross product can be represented by figure A2.2:

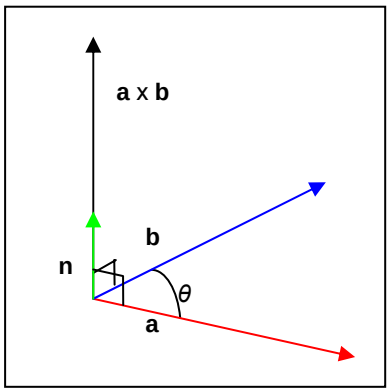

Figure A2.2: the visualization of the cross product between two vectors **a** and **b**, the cross product is perpendicular to both vectors **a** and **b**.

This feature was used to determine the normal vector of a plane (paragraph 6.6). The normal of a plane can be determined by taking the cross product of two vectors that are located on the plane.

The cross product can also be expressed by using the vector coefficients (A2.8):

$$\mathbf{a} \times \mathbf{b} = (a_2 b_3 - a_3 b_2 \ , \ a_3 b_1 - a_1 b_3 \ , \ a_1 b_2 - a_2 b_1) \qquad \text{(A2.8)}$$

Appendix III : Histogram equalization

In section 6.4 it was mentioned that the storage of the intensity values of the two different laser scanners is not the same. To be able to compare the results with respect to the intensity, the intensity values of the FARO LS 880 need to be spread over the same domain the IMAGER 5003 uses for the intensity storage. This spreading is done by using the technique of histogram equalisation and the principle is discussed in this appendix.

Histogram spreading is mostly used for processing images as it improves the contrast and the brightness of the images. The intensities of the image pixels are organised in 256 bins. Figure A4.1a shows a histogram of the intensity values in an image. In this case most of the pixels are in the low intensity region and the image does not use the full available range of grey values; 0 - 255. Therefore an image can have a low brightness (many pixels in lower grey values) or a bad contrast (all pixels in a small range). When histogram equalization is used to improve these properties, the following steps are performed [Rees, 2001]:

1. calculate the histogram H for the input image,
2. normalize the histogram,
3. compute H' integral of the histogram,
4. transform the image using H' as a look-up table.

In *step 1* all pixels are counted for every intensity bin of the image (256 grey values) and put in the histogram. *Step 2* normalizes the resulting histogram of step 1. Normalizing means that the number of pixels in one bin is divided by the total number of pixels, so that the sum of all bins becomes 255:

$$NH(i) = \frac{\#\ pixels\ with\ Intensity\ (i)}{Total\ \#\ pixels} \qquad with:\ i = 0,\ldots,255 \tag{A3.1}$$

In *step 3* the integral of the normalized histogram is computed:

$$H'(i) = \int_0^i NH(j) \cdot dj \qquad with:\ i = 0,\ldots,255 \tag{A3.2}$$

The discrete version of equation A3.2 is needed for digital images:

$$H'(i) = \sum_{j=0}^{j=i} NH(j) \qquad with:\ i = 0,\ldots,255 \tag{A3.3}$$

Finally in *step 4* the transformation takes place as the new position of a point is selected from the integral of the normalized histogram. The histogram of the output image is shown in figure A3.1b.

In this thesis instead of digital images scans are used. But the scans also contain intensity values for each point so the process of histogram equalization remains the same.

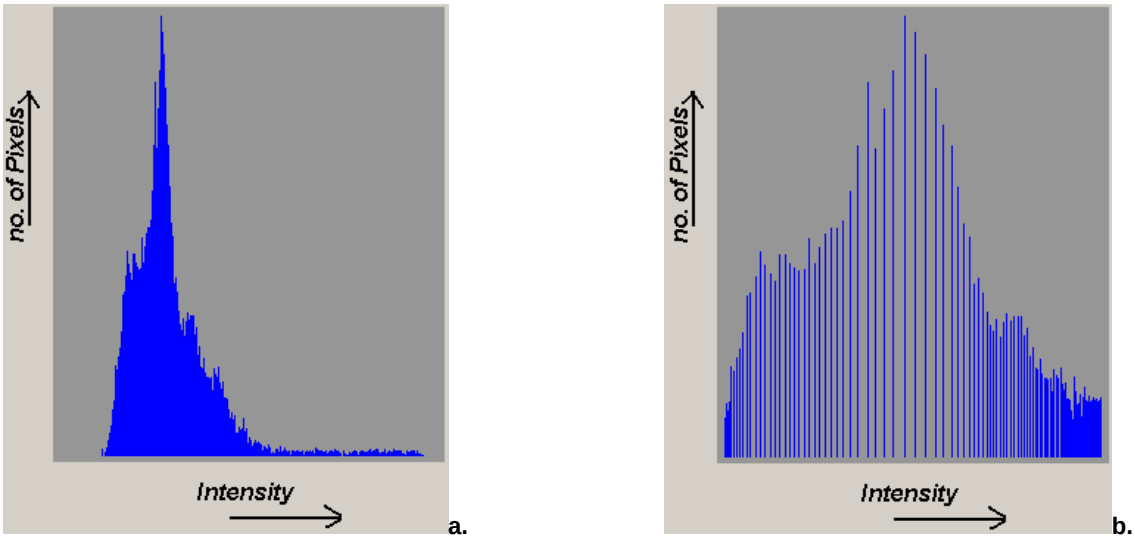

Figure A3.1: An example of histogram equalization, a; the image histogram before equalization, b; the image histogram after equalization.

Appendix IV : The CIE-diagram

In the study of the perception of colour one of the first mathematically defined colour spaces was the CIE XYZ colour space (also known as CIE 1931 colour space), created by the International Commission on Illumination in 1931 [CIE, 2006]. This appendix gives a short overview of the CIE-diagram and theory, for more information refer to [CIE, 2006].

The human eye has receptors for short (S), middle (M), and long (L) wavelengths, also known as blue, green, and red receptors. That means that one, in principle, needs three parameters to describe a colour sensation. A specific method for associating three numbers (or tristimulus values) with each colour is called a colour space. The CIE XYZ colour space is one such spaces but the CIE XYZ colour space is special, because it is based on direct measurements of the human eye, and serves as the basis from which many other colour spaces are defined.

The CIE XYZ colour space was derived from a series of experiments done in the late 1920s by W. David Wright and John Guild [CIE, 2006]. Their experimental results were combined into the specification of the CIE RGB colour space, from which the CIE XYZ colour space was derived.

In the CIE XYZ colour space, the tristimulus values are not the S, M, and L stimuli of the human eye, but rather a set of tristimulus values called X, Y, and Z, which are close to red, green and blue, respectively. Two light sources may be made up of different mixtures of various colours, but it is possible that they have the same apparent colour, This means that have the same tristimulus values, no matter what different mixtures of light were used to produce them.

Since the human eye has three types of colour sensors that respond to different ranges of wavelengths, a full plot of all visible colours would be a three-dimensional figure. However, the concept of colour can be divided into two parts: *brightness* and *chromaticity*. For example, the colour white is a bright colour, while the colour grey is considered to be a less bright version of that same white. In other words, the chromaticity of white and grey are the same while their brightness differs.

The CIE XYZ colour space is designed so that the Y parameter is a measure of the brightness of a colour. The chromaticity of a colour was then specified by the two derived parameters x and y which are functions of all three tristimulus values X, Y, and Z (A4.1):

$$x = \frac{X}{X+Y+Z}$$

$$y = \frac{Y}{X+Y+Z} \qquad \text{(A4.1)}$$

The X and Z tristimulus values can be calculated back from the chromaticity values x and y and the Y tristimulus value (A4.2):

$$X = \frac{Y}{y}x$$

$$Z = \frac{Y}{y}(1-x-y) \qquad \text{(A4.2)}$$

Figure A4.1 shows the related chromaticity diagram. The outer curved boundary is the visible part of the electromagnetic spectrum, with wavelengths shown in [nm]. NOTE: the chromaticity diagram is a tool to specify how the human eye will experience light with a given spectrum. It cannot specify colours of objects since the chromaticity observed depends on the light source as well while looking at an object.

Mathematically, x and y are projective coordinates and the colours of the chromaticity diagram occupy a region of the real projective plane.

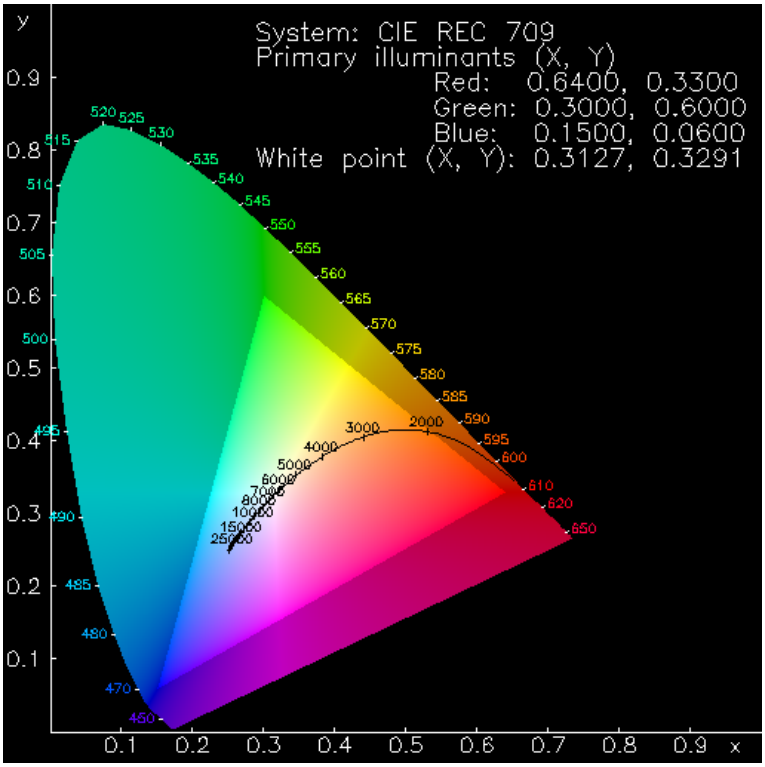

Figure A4.1: The CIE 1931 colour space chromaticity diagram. The outer curved portion is the spectral locus, with wavelengths shown in [nm].

The chromaticity diagram illustrates a number of interesting properties of the CIE XYZ colour space:

1. The diagram represents all of the chromaticities visible to the average person. These are shown in colour and this region is called the gamut of human vision. The gamut of all visible chromaticities on the CIE plot is the tongue-shaped or horseshoe-shaped figure shown in colour. The curved edge of the gamut is called the spectral locus and corresponds to monochromatic light, with wavelengths listed in [nm]. The straight edge on the lower part of the gamut is called the purple line. These colours, although they are on the border of the gamut, have no counterpart in monochromatic light. Less saturated colours appear in the interior of the figure with white at the centre.
2. It is seen that all visible chromaticities correspond to positive values of x and y (and therefore to positive values of X, Y, and Z).
3. If one chooses any two points on the chromaticity diagram, then all colours that can be formed by mixing these two colours lie between those two points on the straight line connecting them. It follows that the gamut of colours must be convex in shape. All colours that can be formed by mixing three sources are found inside the triangle formed by the source points on the chromaticity.
4. The mixture of two equally bright colours will not generally lie on the midpoint of that line segment. In more general terms, a distance on the xy chromaticity diagram does not correspond to the degree of difference between two colours. Other colour spaces (CIELuv and CIELab in particular) have been designed to meet this problem.

Appendix V : Procedure of performing an experiment

This appendix contains the used and recommended procedure of performing an experiment with different laser scanners. Figure A5.1 gives a schematic overview of the procedure and every step will be explained in this appendix.

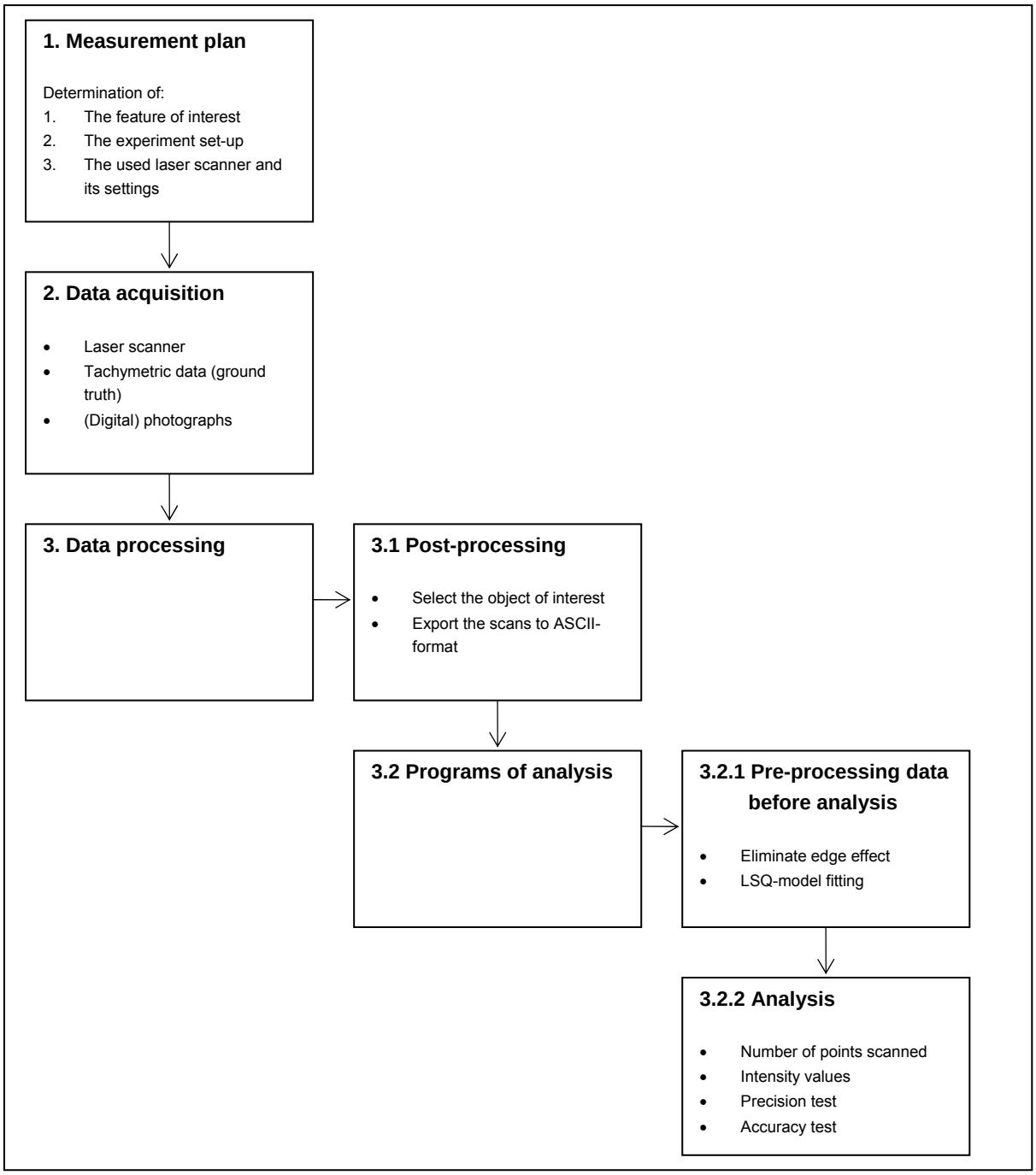

Figure A5.1: A schematic overview of the procedure for performing an experiment with laser scanners.

Step 1: Measurement plan

The measurement plan that will be created before creating and scanning an experiment needs to contain:

1. A description of the feature of interest or in other words: the feature that is going to be examined during the experiment.
2. The eliminated parameters and the created set-up; because to be able to examine the feature of interest all other influences need to be eliminated (or set constant when the performances of two or more scanners will be compared). This can be achieved by eliminating the influences in the experiment set-up.
3. A description of the selected laser scanner(s) and the settings of the laser scanner(s) that are going to be used during the experiment.

A time schedule can also be implemented if the scanners are available for a limited time or more then one experiment is done.

Step 2: Data acquisition

Obviously the experiment set-up will be scanned with a laser scanner. One of the results of the data acquisition step will therefore be different scans obtained with the used laser scanner(s) of the object of interest. To influence the scan time and therefore the duration of the data acquisition, only the area in which the object of interest is located can be selected and scanned with the laser scanner(s).

If the experiment requires an accuracy determination, a comparison of the obtained results with an instrument of which the accuracy is known can be required. In this situation a total station measurement can be added to the experiment. The accuracy of most total stations on short ranges is known to be a few [mm].

Another reason to use a total station is when the scans need to be connected to a known coordinate system. This can be achieved by scanning some prominent points (for example manually placed targets) and measure them with a total station as well. By measuring some known points with the total station, the scan obtained with the laser scanner can be transformed to the known coordinate system.

Digital photographs are used to register the situation during the acquisition phase of the experiment. They can be used to retrieve the situation during the analyzing steps of the procedure and to give additional information in the coverage of the experiment.

Step 3: Data processing

The first step of this phase is the post-processing of the scans obtained followed by the creation of the programs of analysis. These steps will be discussed next.

Step 3.1: Post-processing

Even though the obtained scan only contains the area in which the object of interest is located, a lot of redundant information can be present in this scan. Therefore, the software of the laser scanner will be used to select the object of interest or, in other words, delete the external points. The main advantage is that the size of the scans will be reduced.

During this research it was found out that not all laser scanners filter their data automatically. These laser scanners allow manual filtering, which is implemented in their software packages. It is recommended to perform this filtering if either two laser scanners need to be compared and one of the laser scanners filters the data automatically, or when the goal is to gather insight in the ‘best’ performance of the laser scanner is a particular situation.

Next, the software of the laser scanner will be used to export the scans to ASCII files, which means that they now can be imported in other software packages that are used for the analysis.

Step 3.2: Programs of analysis

The remaining scans of the post-processing are still not entirely ready to use. Therefore, the data needs to be pre-processed before the analyzing steps can be preformed. Both the pre-processing and the analysis will be discussed next.

Step 3.2.1: Pre-processing the data before analysis

In most cases, the file sizes of the remaining scans will be too large to handle on a 'normal' computer and edge effects will still present. These problems can be solved by selecting only a part of the object of interest or the interior of the object. The last is possible in case the object of interest is planar.

After the interior selection of the object of interest, the object in the scan needs to be represented by a model in order to be able to analyze the results. The Least Square theory can be used to determine the best fitting model through the scan points. Examples of models are: planes, cylinders or cubes (only after registering a number of scans). In case the equations of the models are not linear, linearization is necessary [Teunissen, 200a]. The least squares adjustment results in the model parameters that fit the points in the scan best.

Step 3.2.2: Analysis

Now the interior of the object of interest is determined and represented by a model, the final analysis can be done. The goal of the analysis is to determine the performance of the selected laser scanner with respect to a particular feature. This performance can be split into four analyses:

1. *The number of points scanned*; the true number of measured points per [cm^2] are compared with the expected number of points per [cm^2] based on the specifications. This is for example done to gather insight in the trueness of the specifications.
2. *The mean intensity values;* this analysis is done to gather insight in the influence of the feature of interest on the intensity values measured. It can be assumed that when low intensity values are measured, the object of interest is most likely scanned with a low precision and accuracy.

   If the intensity values of two different scanners need to be compared a histogram equalization can be used to make the results comparable.
3. *The precision test;* subtracting the scan points from the best fitting model results in the residuals. These residuals determine whether the model fits the scan points closely or not and are used to express the precision of the laser data. The standard deviation of the residuals is used to express the precision. The maximum and minimum residuals are also computed because they give insight in the spreading features of the scan and thus the precision.
4. *The accuracy test;* the reliability of the obtained results can be researched by comparing the model features with the true features. This for example means, comparing the measured scan angle with the true scan angle or comparing the measured distance with the true distance. The difference between the true values and the measured values determine the reliability of the scan and therefore the laser scanner.

Appendix VI: Matlab scripts

In this appendix the created Matlab functions are shown. The main programs, in which all functions per experiment are invoked, are not assimilated in this thesis. These programs can be found on the attached CD. The following functions are applied on every dataset, in chronological order:

A. Cartesian to spherical coordinates
B. Interior and corner selection
C. Spherical to Cartesian coordinates
D. Number of points scanned determination
E. Intensity values and histogram equalization
F. Rotation
G. Bias determination
H. Plane fitting and precision test
I. Reliability test

A. Cartesian to spherical coordinates

```
% this function determines the spherical
% coordinates

% INPUT     = 1. dataset/point cloud containing
%       of 4 columns

% OUTPUT    = 1. the spherical coordinates of the
%       dataset (phi,theta,R,intensity)

function
[sphdataset]=cartesian2spherical(dataset)

x=dataset(:,1);
y=dataset(:,2);
z=dataset(:,3);
Int=dataset(:,4);

[theta,phi,R]=cart2sph(x,y,z);

sphdataset=[theta phi R Int];
```

B. Interior and corner selection

```
% this function determines the interior selection
% of the point clouds

% INPUT     = 1. dataset/ point cloud containing
%       of 4 columns with spherical
%       coordinates
%           = 2.& 3. the grid size
%
% OUTPUT    = 1. the coordinates of the points %
        located in the interior
%           = 2. the corner points of the
%       interior selection

function
[interior,cornerpoints]=interiorselection(dataset
,scanner,k,s1)

x=dataset(:,1);
y=dataset(:,2);
z=dataset(:,3);
Int=dataset(:,4);

% the interior selection is done by 6 steps:
%   1- fit a grid through the original datapoints
%   2- determine the grid middle points
%   3- determine the closest grid point for each
%      datapoint
%   4- determine the middle point of the entire
%      grid
%   5- decide the size of the selection manually
%      (horz and vert grid points)
%   6- transform the grid points back to the
%      original datapoints
%%%%% step 1:
c1=x;
c2=y;
c3=z;

minc1=min(c1);
maxc1=max(c1);
minc2=min(c2);
maxc2=max(c2);

m=60;
[X,Y]=meshgrid((minc1):...
        ((maxc1-minc1)/k):(maxc1),...
        (minc2):((maxc2-minc2)/m):(maxc2));

%all x values are in the first row of matrix X
%all y values are in the first column of matrix Y
xx=X(1,:)';
yy=Y(:,1);

%%%%% step 2:
gridpnt=[];
for i=1:length(xx)-1
    for j=1:length(yy)-1
        gridpnt=[gridpnt;
        (xx(i)+xx(i+1))/2 (yy(j)+yy(j+1))/2];
    end
end
```

```
%%%%%% step 3:
matrix=[];

for h=1:(k)
    for j=1:(m)
        matrix=[matrix; j h];
    end
end

grpnt=[];
grpnt=[matrix(:,1) matrix(:,2) gridpnt(:,1)
gridpnt(:,2)];


z=100;
ii=0;
jj=0;
M=[];
for i=1:length(c1)
    for j=1:length(grpnt)
        d=sqrt(((c1(i)-grpnt(j,3))^2)+ ...
         ((c2(i)-grpnt(j,4))^2));
        if d < z
           z=d;
           ii=i;
           jj=j;
       end
   end
   M=[M; grpnt(jj,1)  grpnt(jj,2) c1(ii) c2(ii)
        grpnt(jj,3) grpnt(jj,4) c3(ii) Int(ii)];
   z=100;
end


%%%%% step 4:
q=round(k/2);
z=round(m/2);
midgrx=0;
midgry=0;
for i=1:size(grpnt,1)
    if grpnt(i,1) == z & grpnt(i,2) == q
       midgrx=grpnt(i,3);
       midgry=grpnt(i,4);
    end
end


%%%%% step 5 and 6:
s2=s1;
selgrid=[];
for i=1:size(grpnt,1)
    if grpnt(i,1)>=(z-s2)& grpnt(i,1)<=(z+s2)
        & grpnt(i,2)>=(q-s1) & grpnt(i,2)<=(q+s1)
       selgrid=[selgrid; grpnt(i,:)];
    end
end

interior=[];
for i=1:size(M,1)
    if M(i,1)>=(z-s2) & M(i,1)<=(z+s2)
        & M(i,2)>=(q-s1) & M(i,2)<=(q+s1)
       interior=[interior; M(i,:)];
    end
end
```

```
%%% Determination of the cornerpoints of the
interior selection

minrow=min(selgrid(:,1));
maxrow=max(selgrid(:,1));

mincol=min(selgrid(:,2));
maxcol=max(selgrid(:,2));

corner=[];
for i=1:size(selgrid,1)
    if selgrid(i,1) == minrow &
        selgrid(i,2) == mincol
       corner(1,:)=[selgrid(i,:)];
    elseif selgrid(i,1) == minrow &
            selgrid(i,2) == maxcol
        corner(2,:)=[selgrid(i,:)];
    elseif selgrid(i,1) == maxrow &
            selgrid(i,2) == mincol
        corner(3,:)=[selgrid(i,:)];
    elseif selgrid(i,1) == maxrow &
            selgrid(i,2) == maxcol
        corner(4,:)=[selgrid(i,:)];
    end
end

plot(corner(:,3),corner(:,4),'k.','MarkerSize',5)

z=100;
ii=0;
cornerpoints=[];
for j=1:4;
    for i=1:size(interior,1)
       d=sqrt(((interior(i,3)-corner(j,3))^2)+...
             ((interior(i,4)-corner(j,4))^2));
        if d <  z
            z=d;
            ii=i;
        end
    end
    cornerpoints(j,:)=[interior(ii,:)];
    z=100;
    ii=0;
end

figure
plot(M(:,3),M(:,4),'r.','MarkerSize',10)
hold on
plot(interior(:,3),interior(:,4),'g.')
plot(cornerpoints(:,3),cornerpoints(:,4),'k.','Ma
rkerSize',15)


%%%% uitvoer

interior=[interior(:,3) interior(:,4)
interior(:,7) interior(:,8)];
cornerpoints=[cornerpoints(:,3) cornerpoints(:,4)
cornerpoints(:,7) cornerpoints(:,8)];
```

C. Spherical to Cartesian coordinates

```
% this function transforms the spherical
% coordinates back to Cartesian coordinates

% INPUT     = 1. sphdataset/point cloud
%       containing of 4 columns
%       (theta,phi,R,intensity)

% OUTPUT    = 1. the cartesian coordinates of the
%       dataset (x,y,z,intensity)
```

```
function
[dataset]=spherical2cartesian(sphdataset)

theta=sphdataset(:,1);
phi=sphdataset(:,2);
R=sphdataset(:,3);
Int=sphdataset(:,4);

[x,y,z]=sph2cart(theta,phi,R);

dataset=[x y z Int];
```

D. Number of points scanned determination

```
% this is the points function

% INPUT     = 1. dataset/ point cloud containing
%       of 4 columns (after interior
%       selection)
%           = 2. the corner points of the
%       interior selection, used to
%       determine the surface area
%           = 3. the vertical and horizontal
%       angle increment according to
%               the specifications of the
%       manufacturer

% OUTPUT    = 1. the number of points per cm2
%           = 2. the number of expected points
%       per cm2
%           = 3. the percentage of lost points
%-----------------------------------------------

function
[p,ep,percnt]=points(dataset,cornerp,vincr,hincr)

x=dataset(:,1);
y=dataset(:,2);
z=dataset(:,3);
Int=dataset(:,4);

%-----------------------------------------------
% 1. number of points per cm2 = p
%-----------------------------------------------

p=size(x,1);

len1=sqrt(((cornerp(1,1)-cornerp(2,1))^2)+ ...
         ((cornerp(1,2)-cornerp(2,2))^2)+...
         ((cornerp(1,3)-cornerp(2,3))^2));
len2=sqrt(((cornerp(1,1)-cornerp(3,1))^2)+ ...
         ((cornerp(1,2)-cornerp(3,2))^2)+...
        ((cornerp(1,3)-cornerp(3,3))^2));
area=(len1*len2)*10000;
p=p/area;

%-----------------------------------------------
% 2. number of expected points in the selected
%      interior of the dataset is determined by %
%      taking the distance between the scanner
%      and the lower 2 corner points →
%      horizontal and vertical #points

%-----------------------------------------------

dist1=sqrt(cornerp(1,1)^2+cornerp(1,2)^2+...
         cornerp(1,3)^2);
dist2=sqrt(cornerp(2,1)^2+cornerp(2,2)^2+...
         cornerp(2,3)^2);

% determine the angle between these 2 distances
% using the law of cosine
% 2*a*c*cos(betha)=a^2+c^2-b^2

d=2*dist1*dist2;
e=dist1^2+dist2^2-len1^2;
csb=e/d;
bethah=acos(csb);
bethah=(bethah*360)/(2*pi);

% dividing the angle by the horizontal increment
% of the used scanner at that resolution

ph=(bethah/hincr)+1;

% the same is done for the vertical situation

dist3=sqrt(cornerp(1,1)^2+cornerp(1,2)^2+...
         cornerp(1,3)^2);
dist4=sqrt(cornerp(3,1)^2+cornerp(3,2)^2+...
         cornerp(3,3)^2);
d=2*dist3*dist4;
e=dist3^2+dist4^2-len2^2;
csb=e/d;
bethav=acos(csb);
bethav=(bethav*360)/(2*pi);
pv=(bethav/vincr)+1;

% the expected number of points per cm2 now
% becomes:

ep=ph*pv;
ep=ep/area;

%-----------------------------------------------
% 3. determine the percentage of lost points per
% scanner = percnt
%-----------------------------------------------

percnt=(100*p)/ep;
percnt=100-percnt;
```

E. Intensity values and histogram equalization

1. Intensity determination IMAGER 5003

```
% this function determines the mean intensity
% values for the IMAGER 5003 data

% INPUT =   1. interior selection of a dataset
%       achieved with the IMAGER

% OUTPUT =  1. meanInt => mean intensity value
%       for the interior of the object
%        =  2. SDInt => the Standard deviation of
%       the intensity values measured,
%       gives insight in the spreading
%       of the intensity values

function [meanInt,SDInt]=intens(dataset)

x=dataset(:,1);
y=dataset(:,2);
z=dataset(:,3);
Int=dataset(:,4);

meanInt=mean(Int);
SDInt=std(Int);
```

2. Histogram equalization and intensity determination FARO LS 880

```
% this function uses histogram equalization to
% make the results of both scanners comparable

% INPUT     = 1. dataset/ point cloud containing
%       of 4 columns
%           = 2. bin = the dataset of the IMAGER
%       achieved under the same
%       circumstances

% OUTPUT    = 1. the mean intensity of the
%       FARO dataset after hist equaliza
%           = 2. the Standard deviation of the
%       intensity

function [meanInt,SDInt]=histogrameq(dataset,bin)

x=dataset(:,1);
y=dataset(:,2);
z=dataset(:,3);
Int=dataset(:,4);

range=bin(:,4);
```

```
minbin=min(range);
maxbin=max(range);

%-------------------------------------------------
% the histogram equalization is done in four
% steps:
%   1- counting the number of points per
%      intensity value and make a histogram
%   2- normalize the histogram by p=ni/n, with ni
%      is Int at interval i and n is total
%      #points
%   3- compute the cumulative histogram of all
%      the p values
%   4- use the cumulative histogram as a look-up
%      table
%-------------------------------------------------

%-------------------------------------------------
% step 1:  counting the number of points per
% intensity value and make a histogram
%-------------------------------------------------

minInt=min(Int);
maxInt=max(Int);
n=0;
h=[];

for j=minInt:maxInt
    for i=1:size(Int,1)
        if Int(i) == j
           n=n+1;
        end
   end
   h=[h; j n];
   n=0;
end

n=size(Int,1);

%-------------------------------------------------
% step 2:  normalize the histogram by p=ni/n,
% with ni is Int at interval i and n is total
% #points
%-------------------------------------------------

for i=1:size(h,1)
    p=h(i,2)/n;
    h(i,3)=p;
end

%-------------------------------------------------
% step 3:  compute the cumulative histogram of
% all the p values
%-------------------------------------------------

cul=0;
for i=1:size(h,1)
    for j=1:i
        cul=cul+h(j,3);
    end
    h(i,4)=cul;
    cul=0;
end

%-------------------------------------------------
% step 4:  use the cumulative histogram as a
%look-up table
%-------------------------------------------------

bin=maxbin-minbin;
nInt=0;
for i=1:size(h,1)
    nInt=(h(i,4)*bin)+minbin;
    h(i,5)=nInt;
    nInt=0;
end

%plot of a histogram
a=0;
vec=[];
v=[];
for i=1:size(h,1)
    a=h(i,2);
    for j=1:a
        v(j,1)=h(i,5);
    end
    vec=[vec;v];
    a=0;
    v=[];
end

figure
hist(vec,bin)
figure
plot(h(:,5),h(:,2))

%-------------------------------------------------
% uitvoer
%-------------------------------------------------

meanInt=mean(h(:,5));
SDInt=std(h(:,5));
```

F. Rotation

```
% this function determines the rotation angle
% around the z and x-axis of the entire dataset
% in order to create a 'constant' x- and z- value
% for the dataset, the y-value becomes the only
% unknown and will be used in the LSQ-plane fit.

% INPUT  =  1. interior selection of a dataset
%        =  2. used scanner; IMAGER=1 and FARO=2

% OUTPUT =  1. the rotated dataset, using
%              rotation matrices

function
[rotateddataset]=rotation(dataset,scanner)

x=dataset(:,1);
y=dataset(:,2);
z=dataset(:,3);
Int=dataset(:,4);

CoG=[mean(x) mean(y) mean(z) mean(Int)];

if scanner == 1;
    alpha=atan(CoG(1)/CoG(2));
elseif scanner == 2;
    alpha=(.5*pi)-atan(CoG(2)/CoG(1));
end

rot=[cos(alpha) (-1)*sin(alpha) 0;
        sin(alpha) cos(alpha) 0;
        0 0 1];

rotateddataset=[];
for i=1:size(x,1)
    rotateddataset=[rotateddataset;
    rot(1,:)*[x(i) y(i) z(i)]'
    rot(2,:)*[x(i) y(i) z(i)]'
    rot(3,:)*[x(i) y(i) z(i)]'
    Int(i)];
end

x=rotateddataset(:,1);
y=rotateddataset(:,2);
z=rotateddataset(:,3);
Int=rotateddataset(:,4);

CoG=[mean(x) mean(y) mean(z) mean(Int)];

gamma=atan(CoG(3)/CoG(2));
gamma=(-1)*gamma;

rot=[1 0 0;
        0 cos(gamma) (-1)*sin(gamma);
        0 sin(gamma) cos(gamma)];

rotateddataset=[];
```

```
for i=1:size(x,1)
    rotateddataset=[rotateddataset;
        rot(1,:)*[x(i) y(i) z(i)]'
        rot(2,:)*[x(i) y(i) z(i)]'
                rot(3,:)*[x(i) y(i) z(i)]'
        Int(i)];
end
```

```
figure
plot(rotateddataset(:,1),rotateddataset(:,3),'.r'
)
title('rotated dataset used for analysing steps')
xlabel('x')
ylabel('z')
```

G. Bias determination

```
function
[gembias,minbias,maxbias]=
        bias(dataset,xhatdataset,colour,
                xhatcolour,fact);

% INPUT = 1. the dataset of the mean plate
%                through all patches
%         2. estimated plane parameters of the
%                mean plate
%         3. the dataset of the colourpatch
%         4. estimated plane parameters of the
%                colour

%OUTPUT = 1. mean value of the offset between the
%                colourpatch and the mean
%                plate
%         2. minimal distance between the mean
%                plate and the colourpatch
%         3. maximal distance between the mean
%                plate and the colourpatch

minx=min(colour(:,1));
maxx=max(colour(:,1));
miny=min(colour(:,2));
maxy=max(colour(:,2));
minz=min(colour(:,3));
maxz=max(colour(:,3));
```

```
dataset1=[];
for i=1:size(dataset,1)
    if dataset(i,1) < maxx &&
        dataset(i,1) > minx &&
        dataset(i,3) < maxz &&
        dataset(i,3) > minz
        dataset1=[dataset1; dataset(i,:)];
    end
end

[Xc,Zc]=meshgrid(minx:.005:maxx,minz:.005:maxz);

yc=xhatcolor(1)*Xc+xhatcolor(2)*Zc+xhatcolor(3);
Cc=fact*ones(size(Xc));

surf(Xc,yc,Zc,Cc)
hold on

y=xhatdataset(1)*Xc+xhatdataset(2)*Zc+
        xhatdataset(3);

bias=(y-yc);
gembias=mean(bias);
gembias=(mean(gembias))*1000;
minbias=min(bias);
minbias=(min(minbias))*1000;
maxbias=max(bias);
maxbias=(max(maxbias))*1000;
```

H. Plane fitting and precision test

```
% this function determines the best fitting plane
% through the data points after rotation. The y-
% value is the unknown in this situation. After
% the plane fit, the standard deviation of the
% residuals is determined in order to get insight
% in the precision of the scan

% INPUT  =  1. interior selection of a dataset
%       = 2. the sigma of the measurements
%            according to the manufacturer

% OUTPUT  =  1. xhat → estimators of the unknown
%        plane parameters
%          =  2. Qxhat → insight in the fit
%       =  3. ehat → residuals
%       =  4. SD → standard deviation of the
%             residuals [mm]; gives insight in
%             the precision
%       =  5. new → scan of the plane

function
[xhat Qxhat ehat SD new]=plane(dataset,sigma)

% after rotation around the z-axis; the y-axis is
% now the distance vector and unknown; the x and
% z values are said to be the observations.

x=dataset(:,1);
y=dataset(:,2);
z=dataset(:,3);

%the LSQ plane formula is [x z 1]*[a b c]'=y

one=ones(length(x));
A=[x z one(:,1)];
```

```
% Qy=(sigma^2)*eye(size(A,1));this matrix is too
% big for the computer but because the matrix is
% an identity matrix it can be computed
% differently

Qy=sigma^2;
y=[y];

xhat=(inv(A'*inv(Qy)*A))*A'*inv(Qy)*y;
yhat=A*xhat;
ehat=(y-A*xhat);

plot3(x,y,z,'.')
hold on
grid on
xlabel('x')
ylabel('y')
zlabel('z')

X=0;
Z=0;
[X,Z]=meshgrid(min(x):.005:max(x),...
        min(z):.005:max(z));
yy=xhat(1)*X+xhat(2)*Z+xhat(3);

new=[x yhat z];
surf(X,yy,Z);
axis([-0.1 0.1 3.8 4.2 -0.25 -0.1])

SD=std(ehat);
SD=SD*1000; %SD in [mm]

Qxhat=inv(A'*inv(Qy)*A);
```

I. Reliability test

1. Scan angle reliability test

```
% This function tests the reliability of the
% obtained scan by:
% Comparing the scan angle it with the reality so
% determined the scan angle using the fitted
% plane and compare this with the true angle
% measured with the angle measurement device (z-
% value is set constant)

% INPUT  =  1. interior selection of a dataset
%      = 2. the LSQ determined estimators of
%           the unknown parameters

% OUTPUT  =  1. alpha → the determined scan
%            angle of the dataset, using the
%            LSQ plane fit

function [alpha]=truetest(dataset,xhat)

x=dataset(:,1);
y=dataset(:,2);
z=dataset(:,3);
Int=dataset(:,4);

minx=min(x);
maxx=max(x);

miny=minx*xhat(1)+0*xhat(2)+xhat(3);
maxy=maxx*xhat(1)+0*xhat(2)+xhat(3);

x=maxx-minx;
y=maxy-miny;

alpha=atand(y/x);
alpha=abs(alpha);
```

2. Range; absolute reliability test

```
% This function tests the absolute reliability of
% the obtained scan by:
% Comparing the ground truth distances between
% the distances measured with the laser scanner

% INPUT  = 1. plane parameters of every scan
%        range of the ground truth datasets
%        = 2. plane parameters of every scan range
%        of the laser scan datasets

% OUTPUT  =  1. distdiff → a matrix containing
% the offset between the absolute distances
%                determined with the total
%                station and the absolute
%                distances determined with the
%                laser scanner.

function [distdiff]=absdist(xhattachy,xhatlaser)

y=[0.02;0.02;-0.02;-0.02;0];
z=[0.03;-0.03;0.03;-0.03;0];

dist=[(1:21)';23;25;27;29];
distdiff=[];
for i=1:size(xhattachy,1)
    for j=1:5
       xt=y(j)*xhattachy(i,1)+
         z(j)*(xhattachy(i,2))+xhattachy(i,3);
       x=y(j)*xhatlaser(i,1)+
         z(j)*(xhatlaser(i,2))+xhatlaser(i,3);
       dt=sqrt(xt^2+y(j)^2+z(j)^2);
       d=sqrt(x^2+y(j)^2+z(j)^2);
       distdiff=[distdiff;dist(i) j (dt-d)*1000];
    end
end

[Y,Z]=meshgrid(-0.02:0.001:0.02,
                -0.03:0.0015:0.03);

Y1=[];
Z1=[];
for i=1:size(Y,1)
    Y1=[Y1; Y(:,i)];
    Z1=[Z1; Z(:,i)];
end

X3t=xhattachy(3,1)*Y1+
       xhattachy(3,2)*Z1+xhattachy(3,3);

X3l=xhatlaser(3,1)*Y1+
       xhatlaser(3,2)*Z1+xhatlaser(3,3);

d=[];
for i=1:size(X3t,1)
    d(i)=(sqrt((X3t(i)-X3l(i))^2))*1000;
end

figure
subplot(2,2,1),
scatter(Y1,Z1,20,d,'filled')
title('abs distdiff between
       tachy and laser scanner; 3[m]')
colorbar

X13t=xhattachy(13,1)*Y1+
       xhattachy(13,2)*Z1+xhattachy(13,3);
X13l=xhatlaser(13,1)*Y1+
       xhatlaser(13,2)*Z1+xhatlaser(13,3);

d=[];
for i=1:size(X13t,1)
    d(i)=sqrt(((X13t(i)-X13l(i))^2))*1000;
end

subplot(2,2,2),
scatter(Y1,Z1,20,d,'filled')
title('abs distdiff between
       tachy and laser scanner; 13[m]')
colorbar

X23t=xhattachy(22,1)*Y1+
       xhattachy(22,2)*Z1+xhattachy(22,3);
X23l=xhatlaser(22,1)*Y1+
       xhatlaser(22,2)*Z1+xhatlaser(22,3);

d=[];
for i=1:size(X23t,1)
    d(i)=sqrt(((X23t(i)-X23l(i))^2))*1000;
end

subplot(2,2,3),
scatter(Y1,Z1,20,d,'filled')
title('abs distdiff between
        tachy and laser scanner; 23[m]')
```

```
X29t=xhattachy(25,1)*Y1+
       xhattachy(25,2)*Z1+xhattachy(25,3);
X29l=xhatlaser(25,1)*Y1+
       xhatlaser(25,2)*Z1+xhatlaser(25,3);
d=[];
for i=1:size(X29t,1)
    d(i)=sqrt(((X29t(i)-X29l(i))^2))*1000;
end

subplot(2,2,4),
scatter(Y1,Z1,20,d,'filled')
title('abs distdiff between
       tachy and laser scanner; 29[m]')


colorbar
```

3. Range; relative reliability test

```
% This function tests the relative reliability of
% the obtained scan by:
% Comparing the ground truth distances between
% the distances measured with the laser scanner

% INPUT  = 1. plane parameters of every scan
%        range of the ground truth datasets
%        = 2. plane parameters of every scan range
%        of the laser scan datasets

% OUTPUT  =  1. A → a matrix containing
%               the relative distances for the
%               ground truth data, the relative
%               distances for the laser scan
%               data and the offset between
%               these two distances.
%            2. meann → the mean values of the
%               offsets determined per
%               corresponding distance
%               differences.

function [A meann]=reldist(xhattachy,xhatlaser)

y=[0.02;0.02;-0.02;-0.02;0];
z=[0.03;-0.03;0.03;-0.03;0];

A=[];
for i=1:size(xhattachy,1)-1
    for j=i+1:size(xhattachy,1)
        for k=1:5
         dt=(xhattachy(j,1)*y(k)+
             xhattachy(j,2)*z(k)+xhattachy(j,3))-
            (xhattachy(i,1)*y(k)+
             xhattachy(i,2)*z(k)+xhattachy(i,3));
         dl=(xhatlaser(j,1)*y(k)+
             xhatlaser(j,2)*z(k)+xhatlaser(j,3))-
            (xhatlaser(i,1)*y(k)+
             xhatlaser(i,2)*z(k)+xhatlaser(i,3));
         A=[A; round(dt) dt dl (dt-dl)*1000];
         dt=0;
         dl=0;

        end
    end
end

m=[];
meann=[];
for j=1:29
    for i=1:size(A,1)
        if A(i,1) == j
            m=[m;A(i,4)];
        end
    end
    if size(m,1)== 0;
       meann(j)=0;
    elseif size(m,1) > 0
       meann(j)=mean(m);
    end
    m=[];
end
```